Computational Wear Simulations in Total Knee Replacements with Consideration for Energy Dissipation and Colloid-Mediated Boundary Lubrication

By

Sean Tyler O'Brien

A thesis submitted to the Faculty of Graduate Studies
in partial fulfilment of the requirements for the degree of

Doctor of Philosophy

Department of Mechanical Engineering
Faculty of Engineering
University of Manitoba
Winnipeg, Manitoba, Canada

August 18, 2016

August 18, 2016

Abstract

The cost and time efficiency of computational wear simulations may enable the optimization of total knee replacements for the reduction of polyethylene wear, thereby potentially improving the long term success of total knee replacements. However, previously existing computational wear models have only demonstrated weak correlations (R^2<0.65) in comparison to knee simulator wear tests. This thesis presents the development and verification of new computational models for the simulation of polyethylene wear in total knee replacements. Finite element and multibody dynamic simulation models were implemented for the prediction of total knee replacement contact mechanics. A new wear model was developed, based on a time dependent cross shear and energy dissipation approach, and was evaluated for the prediction of total knee replacement wear. The effects of contact pressure on polyethylene wear were investigated through both computational and *in vitro* experiments. This verified computational wear model was further advanced through the development and addition of a lubrication model, which provided consideration for the colloidal protein mediated boundary lubrication of total knee replacements. Finally, the predictability of the newly developed computational model was evaluated through the prediction of a broad range of pin-on-disk and knee simulator wear test experiments. The time dependent – energy dissipation – colloidal boundary lubrication model developed in this thesis resulted in greatly

improved correlation strength for the prediction of pin-on-disk (R^2=0.85) and knee simulator wear test (R^2=0.96) results compared with previously published wear models such as Archard's wear law (R^2=0.12), time independent cross shear wear models (R^2=0.60) and other time dependent wear models (R^2=0.65). The computational wear simulation models developed in this thesis have demonstrated sufficient predictive accuracy (Validation Metric: 0.85) to enable the optimization of total knee replacements for the reduction of wear, which may improve the long term success of these necessary clinical devices.

Acknowledgments

Firstly, I would like to thank my advisor Dr. Jan-M Brandt and my co-advisor Dr. Yunhua Luo. I greatly appreciate their guidance and support throughout my studies. Their extensive knowledge and mentorship have been a great benefit to this research.

The financial support of the Natural Sciences and Engineering Research Council of Canada (NSERC) through my Postgraduate Scholarship (Doctorial) has helped enable this research. The NSERC Discovery Grant of my advisor (Dr. Jan-M. Brandt) has also greatly benefited this research. Additionally, I would like to thank DePuy-Synthes (Warsaw, IN) for providing manufacturing drawings and Computer Aided Design models of the AMK and PFC-Sigma total knee replacements. These models have made it possible to verify the accuracy of the computational models developed in this thesis in comparison to a broad range of knee simulator wear test results.

I would like to thank my parents, Shirl and Gord O'Brien, for all their support and encouragement throughout my education, as well as my parent in-laws Gail and Laurie Hall for their encouragement in my research. Lastly I would like to thank my wife and best friend, Laura O'Brien, for her outstanding encouragement and support as I completed this PhD research.

Dedication

To Laura O'Brien

Contents

List of Tables

List of Figures

List of Abbreviations

TKR	Total Knee Replacement
CoCr	Cobalt Chromium Alloy
Ti6Al4v	Titanium Alloy
PE	Ultra High Molecular Weight Polyethylene
XPE	Crosslinked Ultra High Molecular Weight Polyethylene
FE	Finite Element
MBD	Multibody Dynamic
R^2	Coefficient of Determination
ρ	Spearman's Rank Correlation Coefficients
ISO	International Standardization Organization
ASME	American Society Mechanical Engineers Standards
POD	Pin-on-Disk
EF	Elastic Foundation
PO	Pressure Overclosure
TD-ED	Time Dependent Cross Shear – Energy Dissipation Wear Model
TD-ED-TR	TD-ED Wear Model with Consideration for Tractive Rolling
CPI	Contact Pressure Independent Wear Model

ED	Shortened Abbreviation for the TD-ED-TR Wear Model (ED model does not include the Energy Rate Factor)
CBL	Colloidal Boundary Lubrication Wear Model
MC	Million Cycles
CAD	Computer-Aided-Design

List of Symbols

F	Force
μ	Coefficient of Friction
L	Load
F_a	The Force Required to Shear Adheared Asperities
F_d	The Force Required for the Deformation of Asperities
V_{wear}	Wear Volume
k	Wear Factor
S	Sliding Distance
H	The Hardness of a Surface
I	Proportionality Factor
F_N	Normal Force
P	Contact Pressure
E	Young's Modulus of Elasticity
v_p	Poisson's Ratio
h	Thickness
d	The Deflection or Displacement of an Elastic Foundation Spring
W_{depth}	Wear Depth
CS	Cross Shear

C_w	Current Work
A	Area
CS_e	Cross Shear at the End of a Time Step
B_w	The Theoretical Work Required to Reach the CS at the Initiation of the Current Time Interval
M_{mc}	The Mobility of the Molecular Chain
CS_i	The Cross Shear at the Initiation of the Time Interval
R_w	The Materials Resistance to Wear
v	Sliding Velocity
ERF	Energy Rate Factor
EDR	Energy Dissipation Rate
y_i	A Known or Experimental Value
$\overline{y}$	The Average Value of the Known or Experimental Values
f_i	A Predicted or Modeled Value
Denatured Fraction	The percent (%) of proteins in the fully denatured state
t	Time
F_{aby}	Fraction of β-globulin and γ-globulin Proteins Compared to the Total Mass of all Proteins
F_s	Shear Force
L_{Vol}	Lubricant Volume
Γ	The Amount of Protein Adsorbed Per Unit Surface Area
Γ_{max}	The Maximum Adsorption Capacity of the Adsorbent
c	Protein Concentration of the Lubricant

K_L	The Ratio of Desorption to Adsorption Rate Constants
C_l	The Relative Strength of Adsorption Bonds
P_{Native}	The Magnitude of Native Adsorbed Proteins
$P_{Denatured}$	The Magnitude of Denatured Adsorbed Proteins
L_F	The Effect of Lubrication on the Wear Performance

Chapter 1

Introduction

1.1 Total Knee Replacements

Total knee replacements (TKRs) are used to replace the articulating surfaces of the human knee (Figure 1), which may have become damaged as a result of trauma, disorders or diseases such as arthritis. Damaged articular cartilage may cause pain and limit the mobility of the individual. Therefore, a TKR may be implemented to alleviate pain and restore mobility to the patient. In 2005 there were approximately 450,000 primary TKR surgeries performed within the United States [1] and over 60,000 performed in Canada [2]. The number of primary TKR procedures has been projected to increase greatly over the following years and exceed 4 million per a year within the United States by 2030 [1], with a similarly proportional increase being expected in Canada. The combination of an aging population, as well as increased acceptance of TKRs, are both expected to have contributed to the trend of the greatly increasing implementation of TKRs [1].

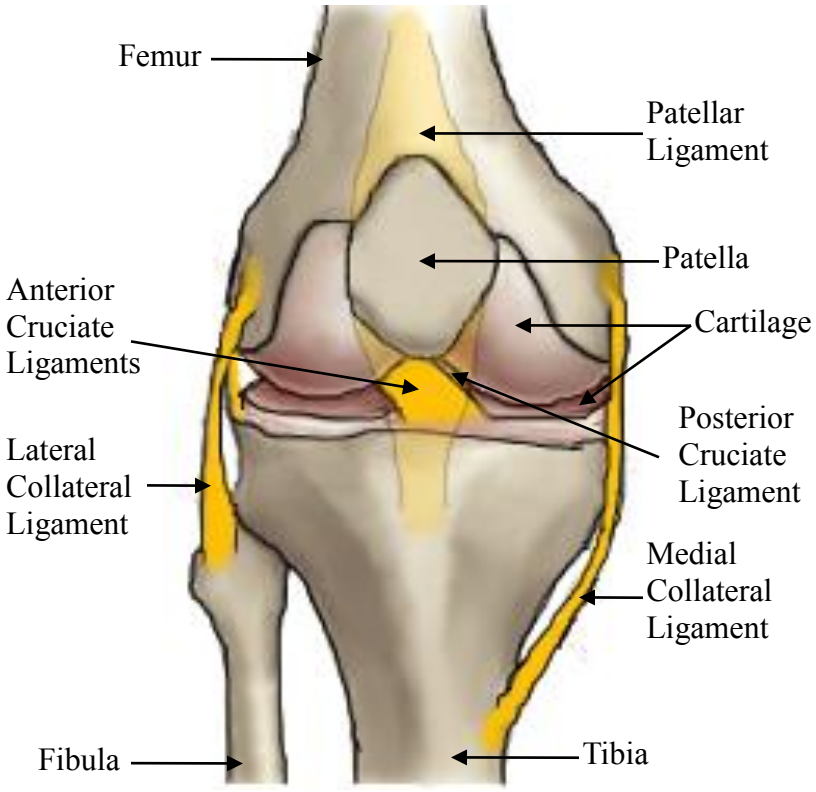

Figure 1: The human knee: including the femur, tibia, fibula, patella, cartilage and ligaments.

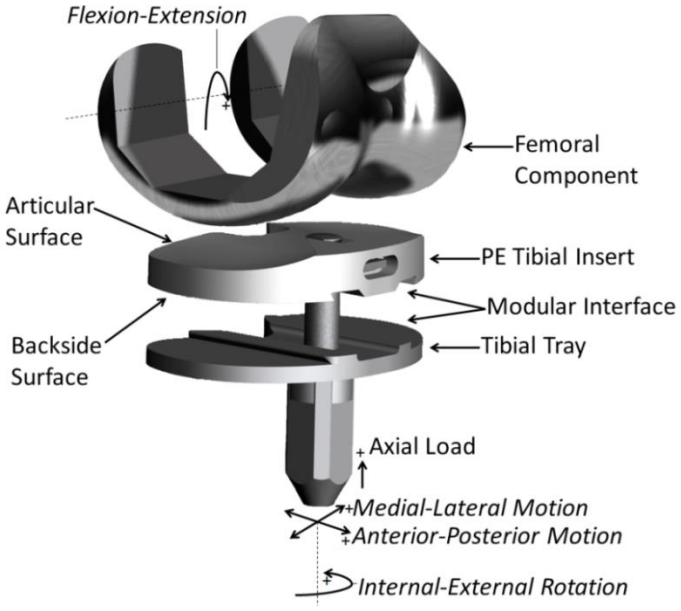

Figure 2: Modular fixed bearing total knee replacement (Anatomical Modular Knee ®, DePuy-Synthes Inc., Warsaw, IN).

Different types of knee replacement systems exist, each of which has exhibited different advantages and disadvantages. The range of available knee replacement systems includes modular and non-modular designs, fixed bearing and mobile bearing, cruciate retaining and posterior stabilized, partial and total [3]. Of the available knee replacement types, the modular fixed bearing TKR has been the most commonly and widely implemented type of knee replacement system [3].

Modular TKRs include a femoral component, tibial insert, tibial tray and may also include a patella resurfacing component (Figure 2). The femoral component is used to resurface the articular surface of the human femur and is typically comprised of a cobalt chromium molybdenum alloy (CoCr, ASTM-F75) [3]. Alternatively, other materials such as Oxinium (oxidized zirconium) may be used for the femoral component [4]. The tibial insert is comprised of either conventional non-crosslinked or crosslinked ultra high molecular weight polyethylene (PE) [3]. Modular fixed bearing tibial inserts are attached to the tibial tray by means of a mechanical locking mechanism. The tibial tray is used to resurface the tibia and is typically comprised of either CoCr alloy or a titanium alloy (Ti, Ti6Al4V) [3]. The patella resurfacing component is typically comprised of PE and articulates along the patellar groove of the femoral component.

The components may be attached to the bone by using bone cement, or by including porous surfaces to encourage bone ingrowth (cementless fixation) [5]. Cemented fixation has been the most commonly implemented approach, with 78% of all knee replacement surgeries in Canada from 2013 to 2014 having been implanted using bone cement [6].

Non-modular TKRs typically consist of the same components as modular systems with the exception that the functions of the tibial insert and tibial tray are fulfilled by a single component. Examples of non-modular tibial components include both metal backed PE, as well as all PE tibial components [3]. Non-modular TKRs eliminate the issue of wear at the tibial insert – tibial tray interface (backside wear) [7-11]. However, modular TKRs offer the advantage of enabling the easy replacement of the tibial insert during revision surgery, while leaving a well fixed tibial tray attached to the patients tibia [3]. In comparison, non-modular TKRs would require the full detachment of the tibial component from the patient's tibia. Hinge joints also exist, which utilize a simple hinge to provide the flexion/extension motion of the knee [3]. However, the natural human knee is subject to complex kinematics, including flexion, anterior-posterior translation, medial-lateral translation, internal-external rotation, and abduction-adduction (Figure 2) [3]. The hinge joint is unable to replicate the complex kinematics of the knee and therefore its implementation is typically only utilized for the treatment of severe bone or tissue loss [12].

Mobile bearing knee replacements differ from fixed bearings by permitting movement between the tibial insert and tibial tray [13-15]. This relative movement is typically either internal-external rotation, anterior-posterior translation or both [3]. Internal-external rotation of the tibial insert, relative to the tibial tray, may result in unidirectional sliding and reduced wear [16] (unidirectional sliding will be discussed further in Section 2.3.1).

Another knee replacement design variation involves the decision to preserve or resect the posterior cruciate ligament (Figure 1). Designs which preserve the posterior cruciate

ligament are referred to as cruciate retaining, and designs which require the removal of the posterior cruciate ligament are referred to as posterior stabilized [3]. Maintaining the posterior cruciate ligament by using a cruciate retaining design retains the anatomical conditions of the human knee to a greater extent in comparison to the posterior stabilized design [3, 17, 18]. As a result, well functioning cruciate ligaments can provide additional constraint and may result in more natural kinematics [3, 17, 18]. However, cruciate ligaments are not always functional in elderly patients, or due to previous trauma, and as a result the posterior stabilized design may provide improved kinematics over the cruciate retaining design [3].

Partial knee replacements include unicondylar, hemiarthroplasty and partial-hemiarthroplasty. Unicondylar knee replacements can be used to replace only one condyle of the knee and may be used for patients which have damage to only one condyle [19, 20]. Hemiarthroplasty involves resurfacing only one side of the articulation [3]. For instance femoral components have been implemented to replace damaged femoral condyles, while leaving the tibial side of the joint unaltered. Meanwhile, partial-hemiarthroplasty is even more anatomically sparing and may be used to replace only part of the area that would be resurfaced by a hemiarthroplasty component [3]. Partial knees have the advantage of preserving a greater portion of patient anatomy in comparison to TKRs. However, since most patients typically experience damage to more than one area of the knee, either immediately or in the long term, TKRs are far more common than partial knee replacements [3]. Of the knee replacement surgeries performed in Canada from 2013 to 2014, only 0.6% were partial knees [6].

Although there are many different types of knee replacement systems, the modular fixed bearing TKR is by far the most common [3, 6]. Therefore, the research of this thesis is primarily focused on the modular fixed bearing TKR. However, the research of this thesis may also be equally applicable to the other knee replacement systems (apart from hinged, hemiarthroplasty and partial-hemiarthroplasty as they do not consist of a CoCr-on-PE articulation).

1.2 Polyethylene Wear

The relative sliding between TKR components results in wear. Tibial insert wear occurs at the articular (topside) surface [3, 17], the distal (backside) surface of modular designs [7, 21-25], the post of posterior stabilized designs [26] and at the articular surface of patella resurfacing components [3]. PE wear particles, released from the tibial insert and the patella resurfacing components, can initiate a cascade of adverse tissue responses leading to osteolysis [27]. Osteolysis, caused by the immunological response to the PE wear particles, can cause the resorption of bone by osteoclasts leading to the loosening of the TKR components [27]. The loosening or disassociation of the TKR components from the patient's bone requires revision surgery to replace the TKR components [24, 25, 28-31]. TKR failures due to wear not only necessitate costly revision surgeries, but also expose patients to additional risk of infection and pain. Furthermore, morbidity increases when revision surgery is necessary for patients of increased age [3].

According to the Canadian Joint Replacement Registry [6] up to 30% of all revisions during the 2013-2014 period may have been caused by PE wear related issues (aseptic loosening, wear and osteolysis). Recently, new bearing materials have been developed in order to reduce the risk of PE wear particle induced osteolysis (bone resorption). The introduction of crosslinked PE (XPE) to TKRs, as well as new sterilization methods and changes to reduce the oxidization potential of PE components has led to a reduction in PE wear particle generation and improved *in vivo* wear performance [32-34]. However, TKRs are also becoming increasingly prevalent among younger, heavier and more active patients [1], resulting in increased tribological demand. Additionally, with the objective

of longer implantation periods, PE wear may continue to limit the long term success of TKRs.

Although the greatest volume of PE wear particles are released from the articular surface of the PE tibial insert (as well as from the post of posterior stabilized designs), the distal surface of the modular PE tibial insert is also a very important source of clinically relevant PE wear particles as they may be smaller and may have increased osteolytic potential [7, 11, 21-25, 31, 35, 36]. Therefore, it is very important to consider both articular and backside wear in the design and evaluation of TKRs.

The design of TKRs with improved wear resistance may greatly improve the long term success of TKRs. TKRs with improved wear resistance may reduce the number of required revision surgeries, thereby reducing health care costs and improving patient care [3, 6, 37]. However, the limitations of the current methods for TKR design may prevent the optimization of TKRs for the reduction of wear. Currently, wear is evaluated by producing prototypes of a design and testing the prototypes using *in vitro* knee simulators [38]. Unfortunately, due to the high cost and time requirements of performing knee simulator wear tests [3, 38], it may only be possible to test a small number of design variables, across a small range of conditions. Therefore, there is great need for an efficient wear assessment method which could be used to analyze a broad range of design variables, in addition to a broad range of test conditions [38].

Computational wear simulations have demonstrated greatly increased time and cost efficiency over the use of knee simulator wear tests [38]. Additionally, computational wear simulations can be easily adapted to include consideration for additional objectives such as kinematics. Therefore, the ideal TKR development process may include

computational simulations to optimize a design based on specific objectives and conditions, followed by knee simulator wear tests of the final design for the precise verification of the computational results. However, despite the attractive efficiency of computational wear simulations [38], the level of accuracy of currently available computational wear simulation models has been insufficient to enable the optimization of TKRs for the reduction of wear [39, 40]. Previously existing computational wear models have typically provided coefficient of determination (R^2) values of 0.65 or less when utilized to predict multiple knee simulator wear test results [39, 40]. The unsatisfactory predictive accuracy of previously available computational wear models may be attributed to greatly over-simplified representations of wear within their formulas, as well as the complete omission of consideration for the lubrication of TKRs.

1.3 Thesis Objectives

The development of efficient and accurate computational models for TKR wear simulations could enable a broader range of TKR designs to be evaluated and across a wider range of operating conditions. Therefore, the development of accurate computational wear simulation models may enable the design optimization of TKRs for the reduction of wear. However, previously existing computational wear simulations have demonstrated insufficient accuracy to enable the design optimization of TKRs for the reduction of wear [39, 40].

The overall objective of this thesis research was to develop computational models for the prediction of wear which would be highly correlated with knee simulator wear test experiments (R^2>0.85), to enable the wear optimization of TKR designs. Six supporting research objectives contributed towards the overall objective of this research. The first supporting research objective was to develop models for the accurate prediction of TKR contact mechanics (Section 3.2). This first research objective was essential, as the evaluation of TKR contact mechanics would be required for the prediction of wear. The second research objective was to implement an existing computational wear model, along with the contact mechanics prediction from the first research objective, for the prediction of TKR wear (Section 3.3). However, the limited accuracy of previously existing computational wear models required the development of a new computational wear model in order to enable the improved prediction of TKR wear. Therefore, the third research objective was to develop an entirely new computational wear model with improved relevance to PE and XPE wear theory which would lead to the improved

predictability of TKR wear (Section 3.4). Since the effects of contact pressure on PE and XPE wear in TKRs was not well understood and widely debated in the literature, it was necessary to further investigate this variable and evaluate whether the newly developed computational wear model could accurately predict its effects. Knee simulator wear testing and computational wear simulations, incorporating the contact mechanics models and the new computational wear model, were conducted for the fourth research objective of investigating the effects of contact pressure on wear (Section 3.5). The fifth research objective was to include consideration for the effects of the lubricant on TKR wear and included the development of a new colloid boundary lubrication model (Section 3.6). Finally, the last research objective was to evaluate the predictability of the newly developed models and consider their suitability for the wear optimization of TKR designs (Section 3.7).

Chapter 2

Literature Review

2.1 Introductory Remarks

The research of this thesis is concerned with the development of computational models for the accurate prediction of TKR wear. Therefore, the present chapter provides a review of the relevant literature to both general and TKR tribology. First a brief review of general tribology is presented. The characterization and interactions of surfaces is discussed, as understanding surface interactions is essential to understanding the mechanisms of wear (Section 2.2.1). These surface interactions are responsible for the force of friction and the dissipation of energy between articulating interfaces (Section 2.2.2), as well as being responsible for wear (Section 2.2.3). General lubrication is discussed, with a particular focus on boundary lubrication (Section 2.2.4). The general computational simulation of wear is also reviewed (Section 2.2.5). Secondly, the tribology of TKRs specifically is considered, which builds upon the review of general tribology. The variables affecting PE wear are reviewed, TKR lubrication is discussed

and several design and clinical implementation variables of TKRs are discussed (Section 2.3). Lastly, the available methods for evaluating TKR wear are considered, including *in vivo*, *in vitro* and *in silico* wear evaluation methods (Section 2.4). This chapter provides the foundation of knowledge necessary for the research of this thesis, as well as identifies the areas in need of further research.

2.2 General Tribology

Tribology is concerned with the study of interacting surfaces in relative motion (under dry or lubricated conditions) [41]. The term tribology was first introduced in a report by Jost for the British Department of Education and Science in 1966 [42]. The term was derived from the Greek word tribos, meaning to rub [41]. Although the term tribology has been somewhat recently introduced, the study of interacting surfaces in relative motion does appear to predate recorded history [43, 44]. Many great researchers have contributed to the field of tribology throughout history [43, 45-48]. Interest in tribology research has grown over time, as recognition of the importance of relative motion in machines, as well as in the natural world, has increased.

2.2.1 Surface Interactions

An understanding of the interacting surfaces is essential to tribology. Solid surfaces consist of several zones (Figure 3) which each have different physico-chemical properties [49-51]. Surfaces may generally include a physisorbed layer on the order of 0.3-3nm in thickness, a chemisorbed layer of approximately 0.3 nm, a chemically reacted layer of 10-100nm, a heavily deformed layer of 1-10um, a lightly deformed layer of 10-100um and finally the base material [52].

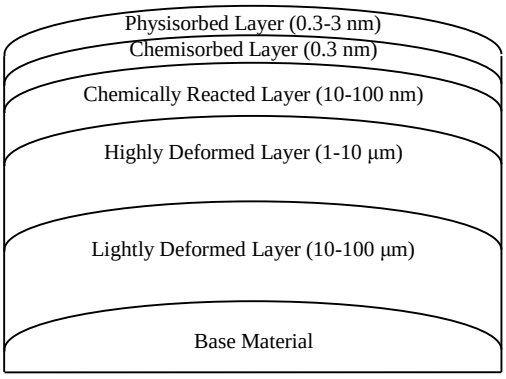

Figure 3: Typical surface layers or zones.

A deformed (or work hardened) layer may be formed on a metal, alloy, ceramic, or polymer as a result of the manufacturing processes used in the production of the part [53-55]. Additionally, a deformed layer may be formed during any tribological process, including during the parts intended use, through contact with other surfaces [56]. The amount of energy utilized for the deformation process and the nature of the material both affect the size of the deformed layer, as well as the extent of material changes of the deformed layer relative to the bulk material [44, 51].

Chemically reacted layers may be formed due to the interaction of the material with its environment. A common example, would be the formation of oxide layers on a metal or alloy by reacting with oxygen when exposed to air [57].

A chemisorbed layer may also be formed due to the interaction of a surface with its environment. Chemisorption involves the sharing or interchange of electrons through covalent bonding and consequently more energy is required for the removal of a chemisorbed layer compared to a physisorbed layer [58]. Chemisorbed layers are monomolecular layers, unlike chemically reacted layers [58]. Once a chemisorbed

monolayer has been formed and remains in place, chemisorption ceases and any subsequent layer formation can only occur through physisorption or chemical reaction.

A physisorbed layer may be formed due to the interaction of a material with its environment. Absorbate layers formed from molecules of water, oxygen and hydrocarbons are some common examples [50]. Physisorption does not involve the exchange of electrons between the adsorbate and adsorbent, instead the process typically involves van der Waals forces [50]. Therefore, the physisorbed layer can generally be removed with very little energy. The physisorbed layer can be either a monomolecular or polymolecular.

Surface layers may greatly influence the surface interactions and wear of materials [52] and are highly relevant to TKRs. Deformed layers are present in CoCr alloy femoral components, as well as the CoCr alloy or Ti64Al4v alloy tibial tray components [3]. These deformed layers are largely due to the manufacturing processes by which the components were produced [52]. PE components also develop deformed layers during manufacturing and the deformed layers continue to be altered through the articulation of the PE components with the femoral and tibial tray components [59-61]. PE may also oxidize over time and develop chemically reacted oxidized layers [62, 63]. CoCr alloy and Ti6Al4v alloy components may corrode to similarly form chemically reacted layers [64-68]. Lastly, all of the TKR components may also form chemisorbed and physisorbed layers through the adsorption of the constituents of the synovial fluid [32, 33, 69-73]. These aspects of TKR surfaces will be further discussed in Section 2.3.

Surface texture is another important characteristic of a surface which has great influence on its tribological properties. Surface roughness, waviness, lay and flaws are all

a part of surface texture [52]. Roughness refers to the surface fluctuations of a short wavelength and is characterized by local maixma (asperities) and local minima (valleys) of varying amplitudes and spacing (Figure 4). Various metrics for surface roughness have been specified by organization such as the International Standardization Organization (ISO) [74] and the American Society Mechanical Engineers Standards (ASME) [75]. Waviness is the surface irregularity of longer wavelengths, relative to roughness, and may result from causes such as workpiece vibration and deflection during machining. Lay refers to the direction of the predominant surface pattern and may be caused by the manufacturing processes used to create the surface. Flaws refer to non-deliberate interruptions in the surface texture.

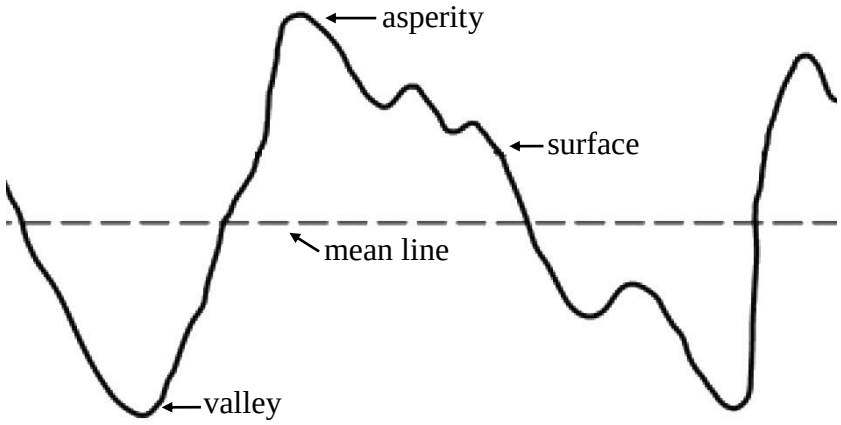

Figure 4: Two dimensional representation of a surface roughness profile.

As a result of surface texture, the true contact area between two interacting surfaces is much less than the apparent (nominal) area of contact (Figure 5). This is because contact would occur at discrete locations as a result of the local maxima (asperities). The true contact area is dependent on the surface texture, material properties and loading conditions. As the load is increased between two surfaces in contact, additional material deformation may occur, leading to contact between additional asperities and an increase in true contact area [76, 77].

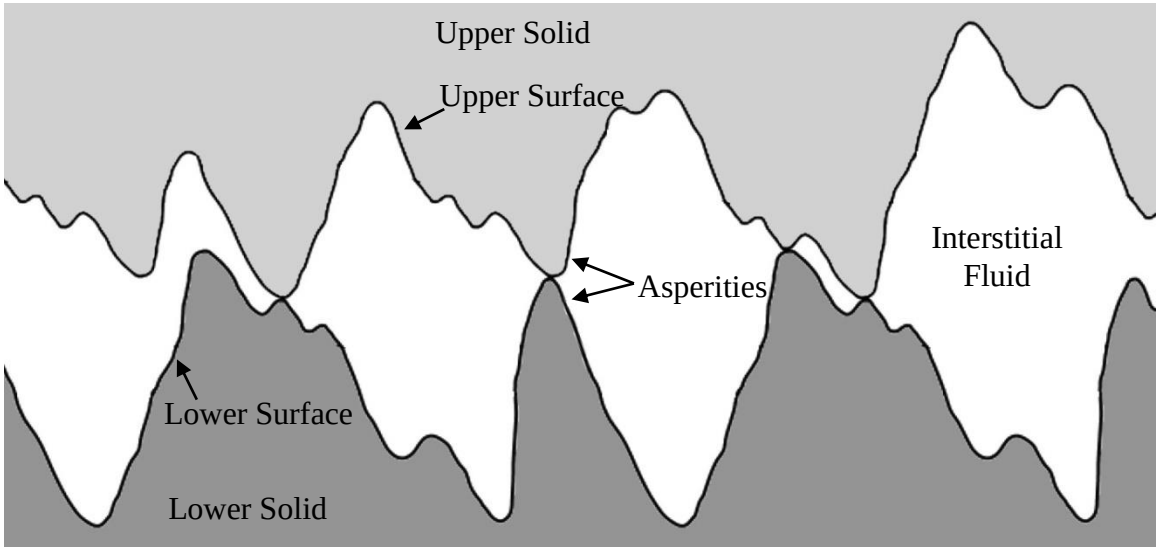

Figure 5: Two dimensional representation of the contacting asperities of two opposing surfaces.

Adhesion can occur between two solid surfaces when they are brought into contact. As a result, a force (adhesive force) would exist between the two surfaces. Adhesion can occur for dissimilar or identical materials, and can occur even in the presence of an interposed fluid. When two surfaces in contact undergo relative sliding, there is typically

an increase in the true area in contact due to plastic deformation, as well as an increase in the adhesive force [78, 79]. Adhesion can occur through the formation of covalent bonds [52], ionic [80, 81] or electrostatic bonds [82-86], metallic bonds [80, 81, 87], hydrogen bonds [54, 88], and van der Waals bonds [89-91]. In addition to the adhesion between contacting asperities, the relative contact also results in the elastic and possibly plastic deformation of the asperities. Interactions between contacting asperities are further discussed in Sections 2.2.2 and 2.2.3.

2.2.2 Friction Force and Energy Dissipation

Friction force is the resistance to motion which can be observed when two contacting solid surfaces undergo relative motion or sliding (under dry or lubricated conditions). Guillaume Amontons [45], was the first researcher to publish the observation that friction force (F) may be directly dependent on the nominal load (L) [45]:

$$F=\mu L \tag{1}$$

where μ is the coefficient of friction. Amontons also reported that the friction force was independent of apparent area of contact between the contacting surfaces [45]. These two observations became known as Amontons Equations, Amontons Rules or Amontons Laws [52]. Later, Charles Coulomb [46], confirmed these findings and also reported the kinetic coefficient of friction to be independent of sliding velocity once the motion starts. It was also recognized that prior to the start of the sliding motion a higher coefficient of

friction was observed, referred to as the static coefficient of friction. The observation of the independence of the kinetic coefficient of friction on sliding velocity became known as Coulombs Rule or Coulombs Law [52].

These three rules can be demonstrated to be generally true for many systems, however it should be noted that these rules are entirely empirical observations. These rules are not based in theory and many physical experiments have demonstrated results which contradict these three rules. Experiments have demonstrated increasing load to have the effect of increasing the coefficient of friction in some cases [52, 92, 93], and decreasing the coefficient of friction in other systems [93, 94]. Furthermore, in some cases the force of friction has been observed to be proportional to the apparent area of contact, particularly in the case of polymers [52]. The kinetic coefficient of friction has also been demonstrated to depend on sliding velocity in many systems [95, 96]. Additionally, since sliding velocity would result in changes to the shear rate, the mechanical properties of the materials in contact may be altered at high sliding velocities [97, 98]. Although the rules of Amontons and Coulomb can be true under some specific circumstances, the interactions between surfaces in dry and lubricated contact are far more complex than what is represented by these rules and the equation above. Therefore in order to accurately predict the force of friction, a more sophisticated representation of the mechanisms responsible must be considered.

Coulomb proposed the mechanism of friction to be due to the action of wedge shaped asperities causing the surfaces to move apart and together again as wedge shaped asperities pass over each other [46]. The process of moving the surfaces apart as the wedges pass over each other was believed to result in potential energy, thereby

explaining the necessity of adding energy to a system to cause one surface to slide against another compared to what would occur in the absence of friction [52]. However, the explanation of potential energy is not fitting, as the potential energy would be recovered once the tips of the wedge shaped asperities of each surface had passed each other and the surfaces began to move closer together once more. This mechanical interaction theory was later abandoned, as friction had been shown to be a dissipative process and the mechanical interaction theory did not represent an energy dissipation mechanism [52]. Alternatively, Bowden and Tabor [96, 99, 100] proposed that the mechanism of friction was due to the interfacial adhesion between asperities and the energy required to cause the microscale deformation of the asperities during relative motion. As a result, the force of friction for an unlubricated contact interaction could be written as [96]:

$$F = F_a + F_d \tag{2}$$

where F_a is the force required to shear adheared junctions and F_d is the force required to supply the energy to deform asperities. Today this model is still widely accepted and applied [52]. It is important to note that the force F_a may relate to the adhesive force between asperities in contact (leading to the breaking of adhesive bonds), or it may refer to the cohesive force required to separate an asperity from the solid material (resulting in wear). The force F_d includes the forces used to elastically deform asperities, as well as the forces used to plastically deform asperities and fracture asperities (resulting in wear). The plastic deformation of asperities, including ultimate fracture, has been indicated as a dominant mechanism of energy dissipation for metals, with elastic deformation

accounting for a much smaller fraction of the energy dissipation [101]. For increasingly rigid and brittle materials, such as ceramic materials, the energy dissipated through the ultimate fracture of contacting asperities may become far more substantial than any energy dissipated through elastic deformation. Meanwhile, energy dissipation due to elastic deformation can account for a large portion of energy dissipation in viscoelastic materials as a result of elastic hysteresis losses [102-104].

As a result of the interactions between surface asperities, such as plastic deformation and hysteresis losses due to elastic deformation, the temperature at asperity contacts can become much higher than the bulk temperature of the system [105]. This localized increase in temperatures can be very significant, since many of the surface effects are temperature dependent, such as material properties and chemical reactions. Polymers generally result in relatively high interface temperatures due to their low thermal conductivity. Under some conditions, interface temperatures may generally be proportional to the pressure and velocity of the articulation [106, 107]. Hip simulator wear tests have demonstrated localized interface temperatures as high as 60^{o}C and 100^{o}C for PE articulating against CoCr alloy and ceramic femoral heads, respectively [108]. Although similar experiments have not been reported for knee simulator wear tests, high localized interfacial temperatures are also expected to occur for TKRs [108]. These increased temperatures may affect the surface interactions and wear of TKR components, as will be discussed further in Section 2.3.2. The mechanism of friction proposed by Bowden and Tabor [96, 99, 100] may also be expanded to explain the wear of materials, as will be discussed in the following section (Section 2.2.3), as well as Section 2.3.1.

2.2.3 Wear

Generally, wear refers to the removal of material from a solid surface in either dry or lubricated conditions. The wear of a single solid surface may occur through material transfer to the opposing surface, or through the release of wear particles. Wear is not a material property; it is a system response and is highly dependent on the operating conditions of the system. Although it has been sometimes assumed that high friction systems will result in high wear, this is an inaccurate assumption. For example, polytetrafluoroethylene can exhibit very low friction and relatively high wear, meanwhile ceramics may exhibit moderate friction and extremely low wear [52]. Wear may occur through six main distinct mechanisms: adhesive, abrasive, fatigue, impact, chemical and electrical [52]. In addition to these distinct wear mechanisms, in many cases wear may proceed through the combination of multiple mechanisms. Adhesive and abrasive wear mechanisms have been estimated to be responsible for two-thirds of all wear encountered in industrial situations [52]. Additionally, adhesive and abrasive wear are also the dominant wear mechanisms for the PE and XPE tibial inserts of modern TKRs [3, 15, 109, 110].

2.2.3.1. Adhesive Wear

Adhesive wear occurs due to the adhesive bonding between the contacting asperities of surfaces, as previously discussed in Sections 2.2.1 and 2.2.2. Relative sliding between the asperities of two surfaces requires that either the adhesive bonds between the

asperities must be broken, or the cohesive bonds of either solid material must be broken so that an asperity is released from the solid material, resulting in wear to that surface [111]. A released asperity may then remain attached to the opposing solid and contribute to the forming of a transfer film, the released asperity may later be transfer back to the initial surface from which it separated, or separate from both surfaces and be released as a wear particle. In the articulation of dissimilar material combinations, more wear particles of the softer material are generally formed. However, wear particles of the harder material may also be formed because local regions of low strength exist due to defects and cracks within the harder material that may come into contact with local regions of high strength of the softer material [52].

2.2.3.2. Abrasive Wear

Abrasive wear occurs as a result of plastic deformation or fracture. This wear may be due to contact between two solid bodies in relative motion (referred to as two-body abrasion), or may result from contact with particles trapped between the two surfaces (referred to as third body abrasion) [112, 113]. Frequently, abrasive wear may be recognized by the appearance of a series of grooves running parallel to the direction of sliding. Abrasion can cause the plastic flow of a material, where material is displaced to form a groove by moving material to the edges of the groove to create ridges [112]. This mode of abrasion may or may not involve material removal and may only involve material displacement. However, with repeated cycles the deformed material may fracture through the low cycle fatigue mechanism [114]. The plastic deformation may

also contribute to subsurface plastic deformation and the formation of subsurface cracks [107]. Through fatigue mechanisms these subsurface cracks may propagate parallel to the surface and lead to the delamination of the material and the release of thin wear platelets. Instead of displacing all material to the sides of the groove, the abrasion may lead to the formation of a wedge ahead of the contact, or the release of ribbon like wear particles [107].

Under certain conditions for pure metals, two body abrasion may be generally proportional to the normal load, sliding distance and inversely proportional to the hardness of the material subjected to abrasion [115-119]. However, for many other materials, such as alloys, these general observations between abrasive wear, load, sliding and hardness are not observed [115, 116]. The abrasive medium must also generally be harder than the abraded material in order for abrasive wear to occur [120-123]. In general, abrasive wear requires the ultimate failure of the material through plastic deformation, or in some cases abrasion results in the plastic deformation of material which does not immediately disassociate from the bulk solid, but is more easily removed later as a result of its altered material properties and geometry [107].

2.2.3.3. Fatigue Wear

Both repeated rolling and sliding have been observed to result in fatigue wear [107]. Commonly observed damage due to fatigue wear includes pitting and delamination. The cyclic loading, resulting from the contact between surfaces, can cause the propagation of subsurface or surface cracks [107]. Unlike wear resulting from other mechanisms, fatigue

wear does not occur through the gradual release of wear particles over time, but occurs through the accumulation of damage over time, followed by a rapid release of wear particles. As a result of the rapid nature with which fatigue wear progresses after having exceeded a threshold, fatigue wear is usually not quantified based on the volume of material lost, but the number of cycles which can be completed prior to the initiation of the release of particles through fatigue wear [107, 124-131]. In addition to the mechanical causes of fatigue wear, chemical reactions can also lead to the fatigue wear of solids [132].

2.2.3.4. Additional Wear Mechanisms

In addition to adhesive, abrasive and fatigue, wear may also occur due to impact. Impact wear may be caused by erosion due to the impingement of solid particles [133], or from the impact of a liquid [134], or due to the cavitation of a liquid at the surface of the solid material [135, 136]. Impact wear may also be caused by percussion as a result of repetitive solid body impact [137]. Chemical wear (also referred to as tribochemical wear) is another main wear mechanism, in which wear may proceed as a result of chemical reactions, such as the corrosion of interacting surfaces in relative motion [138, 139]. Electrical-arc-induced wear is caused by the arcing of electrical current between surfaces [140].

Various combinations of the above main wear mechanisms also exist. For example tribocorrosion is an important area of study which investigates the progression of wear through both relative sliding as well as corrosion chemical reactions [139]. Fretting

occurs when the relative sliding between two contacting surfaces is of a very low amplitude, generally less than a few tens of microns [107, 141]. Fretting is primarily a form of adhesive and abrasive wear occurring over small sliding distances [107].

Adhesive and abrasive wear have been demonstrated to be the dominant wear mechanisms of the PE and XPE tibial inserts of modern TKR bearing materials [3, 15, 109, 110]. In the past, the oxidization potential of XPE tibial inserts also led to significant fatigue and tribochemical wear [3, 142]. However, as a result of recent changes to XPE tibial insert manufacturing and sterilization processes, the fatigue and tribochemical wear of XPE tibial inserts is no longer a major concern [3]. The adhesive and abrasive wear of PE and XPE tibial inserts, specifically, will therefore be discussed further in Section 2.3.1.

In summary, wear is the removal of material from a solid surface. Wear is not a material property but depends on the operating conditions which make up the tribological system. The presence of a solid or liquid lubricant can have a great effect on the contact interaction, friction and wear, and will be discussed in the following section (Section 2.2.4).

2.2.4 Lubrication

Lubricants can reduce friction and wear in a tribological system. Both solids and fluids have been utilized for lubrication in the past, however, this section will focus on fluid lubrication. The various regimes of lubrication can be observed through the Stribeck

curve [143] (Figure 6), which investigates the effect of lubricant viscosity, velocity and load on the coefficient of friction.

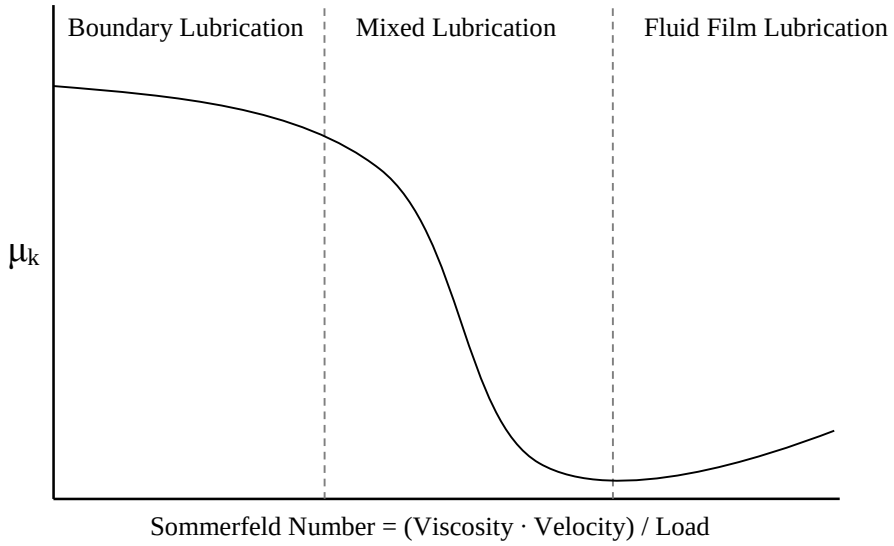

Figure 6: Relationship between the kinetic coefficient of friction and the Sommerfeld Number.

In a lubricated interaction between two surfaces, it can be observed that increasing the Sommerfeld Number [144] will result in vastly different kinetic coefficient of friction values (Figure 6). Each region corresponds to a different regime of lubrication. Under high Sommerfeld Numbers for highly conforming surfaces, the lubricating fluid is drawn between the two surfaces as a result of viscous entrainment. The fluid is then compressed between the two surfaces and fully supports the load applied between the two surfaces with no direct contact of solid asperities to provide what is known as fluid film lubrication [145-155]. Therefore, fluid film lubrication is considered ideal in many applications requiring low friction and low wear, since the lack of contact between the

two solids greatly reduces the potential for wear as well as reduces the friction losses. The trend of slightly increasing kinetic coefficient of friction with increasing Sommerfeld Number in the fluid film range is due to the viscous drag. It should also be noted that for bearings designed to operate in the fluid film lubrication regime, solid-solid contact will still occur during start-stop operations when the velocity is below the required value for the given combination of lubricant viscosity and load.

For low Sommerfeld Numbers (Figure 6), the regime of boundary lubrication may be experienced in which the load is supported through interactions between the monomolecular or multimolecular films of lubricants adsorbed to the surfaces, as well as through the contact of solid asperities [99, 148, 155-159]. For boundary lubrication no portion of the load between the surfaces is supported by the bulk fluid, as occurs fully in fluid film lubrication. Therefore, the viscosity of the lubricant is relatively unimportant in the boundary lubrication regime [52]. The boundary lubrication film may be formed through physical adsorption, chemical adsorption and or chemical reaction, corresponding to the physisorbed, chemisorbed and chemically reacted layers discussed previously (Figure 3). The stability and durability of boundary lubrication films generally increases in the order of physisorbed, chemisorbed and chemical reaction films [52]. Increased stability and durability of the boundary lubrication film will improve the films ability to prevent adhesion during the contact interactions of asperities. The adsorbed molecules can greatly reduce wear through preventing direct contact between the asperities of opposing surfaces. However, as a result of the limited strength of the bonds between the adsorbed molecules and the surface, adsorbed molecules may be continually being removed and replaced during relative sliding between opposing surfaces [52].

Lastly, between the regimes of fluid film and boundary lubrication, the region of mixed lubrication exists (Figure 6). The mixed lubrication regime exists as a combination of boundary and fluid film lubrication where a portion of the load is supported by the fluid film, while some load is also supported through asperity contact. Based on the Stribeck curve [143] (Figure 6) it can be observed that increasing the velocity of the surfaces, increasing the viscosity of the lubricant or decreasing the load would all lead to an increased Sommerfeld Number, thereby moving towards the fluid film lubrication regime. Additionally, it should be noted that in some industrial applications, hydrostatic lubrication is implemented in which an external pressure source such as a pump is used to pressurize the fluid, rather than relying on the relative velocity of the moving surfaces to draw the lubricant between the surfaces.

2.2.4.1. Colloidal Boundary Lubrication

Further attention must also be given to the case of colloid mediated boundary lubrication [160-163], as it has been deemed highly relevant to the lubrication of TKRs [164]. Colloidal suspensions are homogeneous mixtures which consist of two phases, evenly dispersed insoluble particles and a continuous solvent [165]. Colloidal suspensions can be distinguished from solutions through the existence of more than one phase, since unlike colloidal suspensions, solutions consist of a solute and solvent of only one phase. Synovial fluid may be considered a colloidal suspension [164, 166], and therefore the boundary lubrication of surfaces by a colloidal lubricant is particularly relevant.

Using a surface force apparatus, Georges et al. [160, 163] observed a heterogeneous layer of colloidal particles (calcium carbonate) to have adsorbed onto the solid surfaces and to influence the interaction of the surfaces. Both contact pressure and the materials used for the sphere-on-disk articulation pair were found to affect the force required for the movement of the sphere relative to the disk in the presence of calcium carbonate colloids [161]. Increasing the normal load between the sphere and disk was found to require increased tangential force for the movement of the sphere relative to the plate and it was suggested that this phenomenon may occur due to molecular entanglement [161]. Polyisoprene colloids were also found to adsorb to many different solid surfaces such as mica, cobalt, gold, platinum and steel [167]. The structure and size of the adsorbed film was found to depend on the structure of the adsorbed colloids and be independent of the roughness of the solid [167].

The influence of adsorbed polybutadiene on the contact interaction of a sphere-on-disk articulation was clearly demonstrated through the investigation of the reaction forces during axial oscillations. As the distance between the sphere and disk was reduced, the reaction forces were initially found to be proportional to the viscous flow of the bulk lubricant as it was squeezed out of the articulation [167, 168]. However, as the separation distances were reduced to less than the combined thickness of the adsorbed films, repulsive forces between the surfaces were observed with behaviour that was distinctly different from the viscous behaviour of the bulk lubricant [168-170]. This confirms the presence of adsorbed films which do not flow out of the articulation with the bulk lubricant but remain in the articulation (Figure 7) [168]. Once the separation distances were reduced to less than the combined thickness of the adsorbed films, a sharp transition

in the reaction forces between the surfaces was observed (Figure 8), with repulsion forces based on the structure of the adsorbed colloids [168]. The adsorbed film of colloidal particles was found to behave as a viscoelastic solid, and the concentration of the colloid particles in the colloidal suspension was found to affect the compression modulus of the adsorbed film [168]. In contrast to the repulsive forces observed during the compression of the adsorbed films, attractive forces were observed during the separation of the surfaces and were suggested to be due to bridging effects resulting from the penetration of the adsorbed polymer chains through the adsorbed film of the other surface, as well as possibly through polymer entanglement [168].

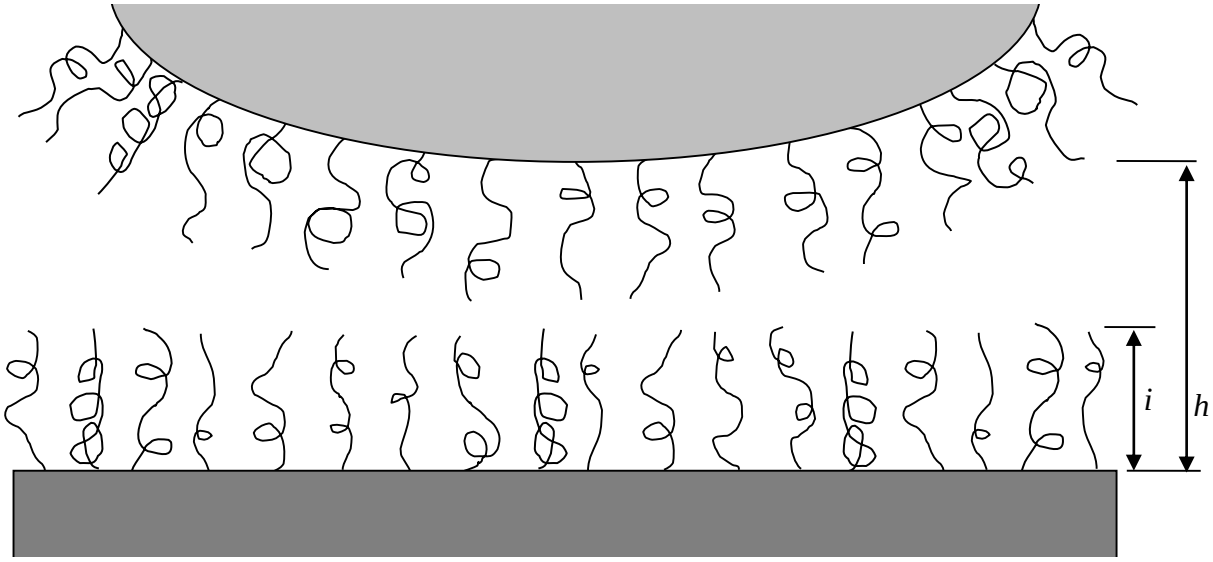

Figure 7: Schematic representation of polymer chains adsorbed to each articular surface, with the adsorbed film thickness *i* and the surface separation distance *h*.

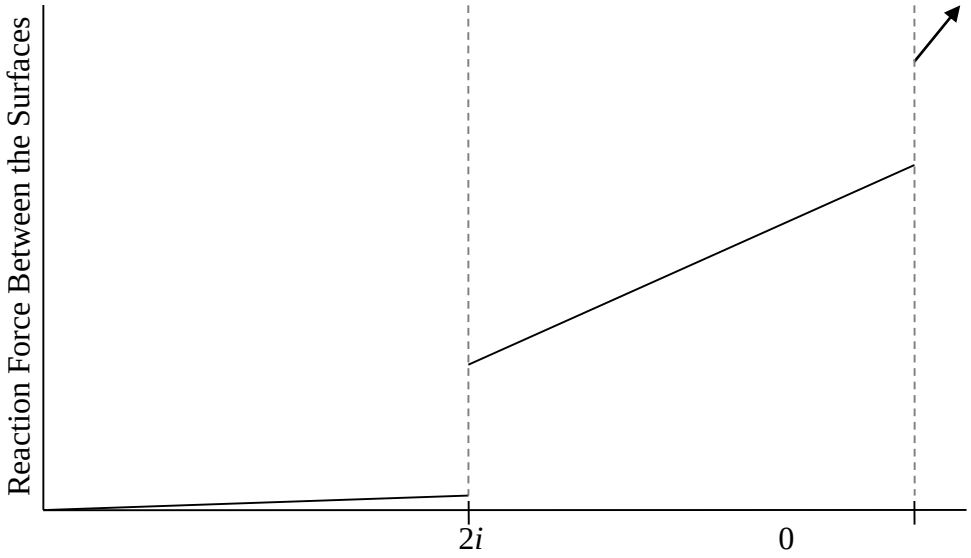

Figure 8: Simplified representation of the reaction force between two surfaces with adsorbed films as the separation distance (h) is decreased. Initially ($h>2i$), a small reaction force is observed due to the viscous forces of the bulk lubricant as it is forced from the articulation area, followed by a sharp increase in reaction force as the absorbed films come into contact ($2i>h>0$) and finally a second sharp increase in reaction force as the solid bodies come into contact.

Similarly, the colloidal proteins within synovial fluid and calf serum may adsorb to the surfaces of TKR components and alter the contact interaction between the TKR components. This colloidal boundary lubrication may affect the friction and wear of the TKR surfaces and will be discussed further in Section 2.3.2.

2.2.5 Computational Wear Simulation

Computational wear simulations can be used to predict the wear of a tribosystem. Computational wear simulations generally exhibit improved time and cost efficiency over

physical experiments [38]. Therefore, computational wear simulations have great potential to aid in the design and optimization of tribosystems for the reduction of wear. In addition to the implementation of computational wear simulations for the analysis of TKR wear, computational wear simulations have generally found the greatest implementation into the simulation of wear for drivetrains [171-175], linkage systems [176], and manufacturing processes [177, 178]. These computational wear simulations have generally involved the prediction of contact mechanics through a method such as finite element (FE) simulation, followed by the prediction of wear through the implementation of a wear model. The following sections provide an overview of computational wear simulations in general, computational wear simulations specific to the TKR will be discussed in Section 2.4.3.

2.2.5.1. Contact Mechanics Prediction

The computational prediction of wear requires the accurate prediction of contact mechanics such as contact pressure and sliding displacement vectors. Computational wear simulations in the past have generally predicted the contact mechanics of the tribological system through FE simulation [171-178]. In some cases multibody dynamic (MBD) simulations have also been implemented [179, 180]. Implementations of each of these methods for the evaluation of TKR contact mechanics will be discussed further in Section 2.3.3. Following the prediction of contact mechanics, the results are implemented in a wear model for the prediction of wear. It is important that the contact mechanics be predicted at regular intervals throughout the wear simulation, since wear will cause

changes to the geometry of the articulating surfaces which will affect the contact mechanics.

2.2.5.2. Wear Models

To enable the design of components with improved wear resistance, a mathematical formulation for predicting wear is of great interest. The wear of modern TKRs may occur dominantly through adhesive and abrasive wear [3] and therefore only adhesive and abrasive wear models will be considered. One of the earliest mathematical models for wear prediction was that presented by Holm [181]:

$$V_{wear} = kLS/H \tag{3}$$

where V_{wear} is the wear volume, k is a wear factor which is dependent on the materials in contact, L is the applied load, S is the sliding distance and H is the hardness of the surface which is subject to wear. Later, Archard [111] presented theoretical justification for this equation and it became known as Archard's wear law. Other variants of this equation also exist and one common representation is [111]:

$$V_{wear} = kLS \tag{4}$$

since material hardness could be accommodated within the wear factor k, and also because there is generally a poor correlation between material hardness and the wear rate

of a tribological system [107, 182]. Many variants of Archard's wear law have been developed [183]. Some variants have specified wear to be proportional to time in service rather than sliding distance [184, 185]. Other variants have attempted to add mechanisms to account for break-in behavior, generally by modifying the sliding distance representation in Archard's wear law [186, 187]. Yet in other variants, a nonlinear relationship for load has been specified, which is generally accomplished by specifying an empirically determined exponent value for the load term L [188-194]. Exponents have also been specified for other parameters of Archard's wear law based on empirical observations [185]. Additional variations of Archard's wear law have been developed specifically for the field of orthopaedics and will be discussed further in Section 2.4.3.2.

Archard's wear law, as well as most of the variants of Archard's wear law, are highly analogous to Amontons' rules of friction [45], where wear is assumed to be independent of the apparent area of contact and directly proportional to the applied load. Furthermore, Archard's wear law assumes wear to be independent of sliding velocity, similar to Coulombs friction rule [46]. As previously discussed, although the three friction rules may be true in some cases, many cases exist where these empirically observed trends are not true. Therefore, wear models based on these friction rules are unlikely to be sufficient for a unified wear model which can be used to predict wear if a change to the tribological system were to occur.

As previously discussed, Bowden and Tabor [99] proposed that the energy being dissipated through friction was caused by the combination of two mechanisms, the adhesion between asperities and the deformation of asperities. Each of these mechanisms of friction does not fully result in wear, but partially contributes towards the generation of

wear particles. Based on the theory that a portion of the frictional work is used to produce wear particles, Fleischer [195] specified a wear model in which the wear volume was equal to the product of frictional work and a proportionality factor (I), where the frictional work is the product of the normal force (F_N), the coefficient of friction (μ) and the sliding distance (S) [195].

$$V_{wear} = I \cdot (F_N \cdot \mu \cdot S) \tag{5}$$

This model has since been implemented in the literature to predict wear [196]. Other models have also been developed based on work or energy, such as the frictional power intensity approach [197], energy pulse [198], and cumulative dissipated energy [199-202]. Compared to Archard's wear law, these energy or work models added consideration for the coefficient of friction, which may be effective in providing some additional representation of the contact conditions beyond Archard's wear law, such as lubrication conditions. However, the inclusion of the coefficient of friction adds the additional requirement that the coefficient of friction of the system must be known in order to implement an energy or work model to predict wear. Another challenge with this approach is the specification of a static proportionality factor. The intention of the proportionality factor is to represent the proportion of dissipated energy which contributes to producing wear. However, since this factor is static it may be considered analogous to the wear coefficient of Archard's wear model, since a change in the tribological system (such as a change in material properties) will require a new proportionality constant to be determined.

Of the available wear models, Archard's wear law [111] and its closely related variants have been by far the most widely implemented models for the prediction of wear in the literature [171-178]. Archard's wear law has been applied to drivetrains such as gears [171-174] and clutches [175], linkage components such as pin joints [176], and manufacturing processes such as warm forging dies [177, 178].

Although it would be convenient to be able to select a wear coefficient for a given material to calculate wear, as is done for Archard's wear law, this would only be valid if wear were a material property rather than a system response. Wear has been demonstrated to be a system response which is dependent on a far greater range of variables than those specified by any of the models currently available in the literature [52, 183]. Therefore, further research must be done to provide consideration for additional variables which influence wear, in order to develop wear models which are more generally applicable beyond a narrow range of conditions for which a wear coefficient has been determined. The complex lubricated interactions between TKR components, as well as the complex material behavior of PE and XPE greatly increases the complexity of TKR wear prediction. The contact interaction between TKR components and the variables affecting TKR wear will be discussed further in Section 2.3. Computational wear models which have previously been investigated for the prediction of TKR wear will be discussed in Section 2.4.3.2.

2.2.5.3. Lubrication Prediction

Since lubrication can greatly influence wear [52], it is also necessary to predict the lubrication conditions as part of computational wear simulations. To the author's best knowledge, previous computational TKR wear simulations have not simulated the lubrication conditions of the TKR. However, the computational simulation of the lubrication conditions has previously been undertaken for other applications. A wide variety of methods [52, 203, 204] have been developed for the prediction of fluid film lubrication for both hydrodynamic and elastohydrodynamic conditions. However, research into the development of predictive methods to analyze boundary lubrication and its effects on wear are underdeveloped in comparison to the methods available for fluid film lubrication [52]. Since TKR lubrication has been shown to occur mainly in the boundary lubrication regime [70], methods for boundary lubrication prediction and analysis are particularly relevant. Aspects of boundary lubrication have previously been investigated through the utilization of molecular dynamics simulations [205-208], which can be used to study the physical and chemical interactions of a small number of boundary lubricating molecules and the surface. Further research is needed to expand the applicability of boundary lubrication simulations in general, especially with regard to analyzing the effect of adsorbed molecules on preventing the release of wear particles [52].

2.3 Total Knee Replacement Tribology

The tibial insert and patella resurfacing components of TKRs are comprised of PE. PE is a unique polymer with physical and chemical properties which make it well suited for use in TKRs [3]. PE is a linear homopolymer consisting of a long backbone of covalently linked carbon atoms with a pair of hydrogen atoms attached to each carbon atom (Figure 9) [209]. The chain ends of PE are typically terminated by methyl groups [209]. Ultra high molecular weight polyethylene is required to have a molecular weight exceeding 1 x 10^6 g/mol, which distinguishes it from low density and high density polyethylene [3]. PE is a partial crystalline polymer. The molecular chain of PE forms regions of both crystalline and amorphous structures (Figure 10). PE crystalline lamellae are formed through the rotation of the molecular chain about C-C bonds. Through the mobility of the molecular chain, PE is subject to directional strain hardening (Figure 10) [3]. Based on the loading conditions imposed upon the PE material, the molecular orientation of the crystalline lamellae may reorientate itself. The directional strain hardening of PE results in the increased resistance to wear in the direction of the molecular orientation, but reduced wear resistance (due to orientation softening) in the perpendicular direction to the molecular orientation [210]. The angle between the molecular orientation and the direction of relative sliding displacement is typically referred to as cross shear. Therefore, larger cross shear angles result in greater wear volume.

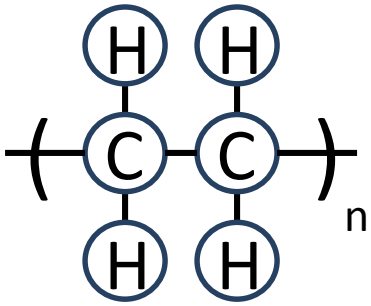

Figure 9: Chemical structure of polyethylene (n denotes repetition of structure).

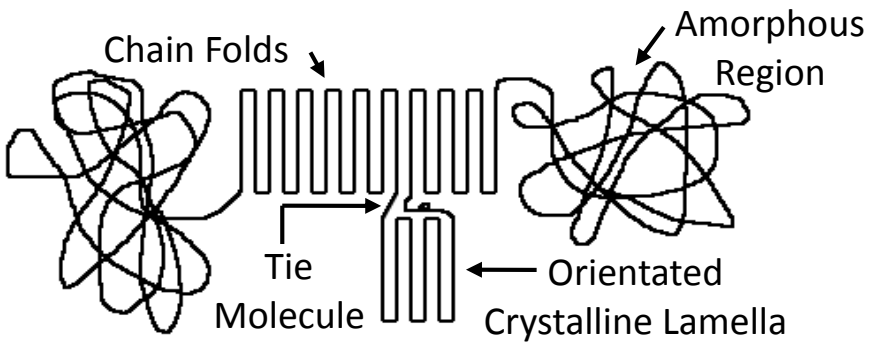

Figure 10: Polyethylene morphological features.

Over the past two decades, new bearing materials have been developed in order to reduce the risk of PE wear particle induced osteolysis [32-34, 211]. PE irradiation can be performed to crosslink PE (to form XPE), which increases the density of the C-C bonds between adjacent molecular chains. PE irradiation has been shown to improve wear resistance, but also to be accompanied by a reduction in material properties, including fatigue crack propagation resistance [212-215]. Additionally, it is of great importance that the irradiation occurs in an oxygen free, or oxygen reduced environment in order to reduce the likelihood of oxidative chain scission and the subsequent degradation of the

material both during storage, as well as in the body [3]. The introduction of moderately and highly crosslinked XPE to TKRs, as well as new sterilization methods and changes to reduce the oxidation potential of the XPE components, has led to a significant reduction in wear particle generation and increased implant longevity [32-34, 211]. However, despite the recent advancements in TKR bearing materials, the tribological demand placed upon TKRs is expected to increase as TKRs are implemented in younger, heavier and more active patients [1]. Thus, the development of methods which would enable the optimization of TKR designs for the reduction of wear are still of great interest, as they may enable the long term success of TKRs to be improved.

2.3.1 Polyethylene Wear

This section expands upon the general tribology theory presented in Section 2.2, but with the specific focus on PE and XPE wear in TKRs. For modern PE and XPE bearing materials with minimal oxidization potential, wear has been demonstrated to occur mainly through adhesive and abrasive wear mechanisms [3, 15, 109, 110] (Figure 11). Previously, XPE wear also occurred through fatigue and tribochemical wear due to the irradiation and storage or implementation of XPE in an oxygen rich environment [3, 142]. However, due to changes in the irradiation and sterilization practices of XPE, tribochemical and fatigue wear are no longer a major concern. The adhesive and abrasive wear of TKR PE and XPE depends upon many variables, and due to the complex interactions between these variables, the design of TKRs for the reduction of wear is

highly complex. In the following paragraphs the conditions and variables known to influence TKR wear are briefly summarized.

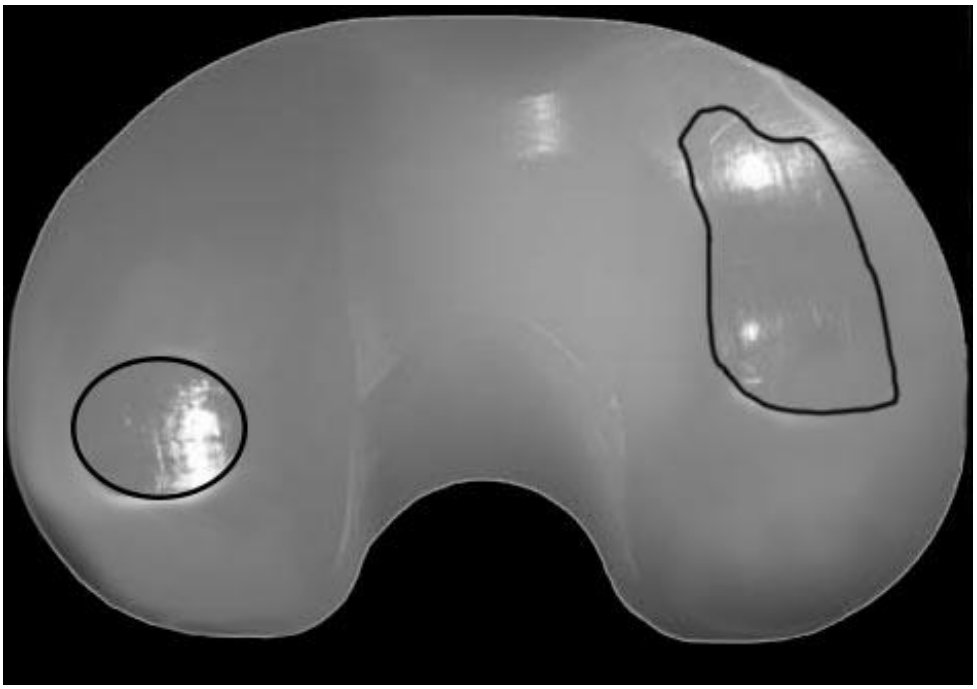

Figure 11: PE tibial insert which has been subjected to adhesive and abrasive wear (worn areas are circled).

PE and XPE wear has been demonstrated to be affected by sliding distances, with increased sliding distances generally resulting in increased PE wear [210]. Increased sliding distances would tend to increase both adhesive and abrasive wear. However, due to the directional strain hardening of PE and XPE, wear does not linearly increase with increasing sliding distances [60, 216]. As discussed previously in Section 2.3, PE and XPE are subject to directional strain hardening. As a result of the loading and sliding conditions the PE or XPE material has been subjected to, deformed layers (Figure 3) will

have developed in which the crystalline lamellae will have become orientated towards the direction of loading or sliding (Figure 10). The reorientation of the crystalline lamellae is a time dependent process. If sliding were initiated in a direction perpendicular to the molecular orientation of the crystalline lamellae (cross shear angle of 90 degrees), the sliding would initially result in high wear. However, with continued sliding in the consistent direction, the molecular chains of the crystalline lamellae would eventually become aligned in the direction of sliding and the wear rate would approach a negligible value [59].

Tractive rolling has been demonstrated to increase PE wear [217]. Tractive rolling may result in the transition to a static coefficient of friction at the interface which may be substantially higher than the dynamic coefficient of friction, leading to increased energy dissipation, adhesion, and wear [217]. Sliding velocity may also affect PE wear, with increased velocities resulting in increased wear [218]. Sliding velocity may influence wear rates as a result of the strain rate dependent material response of PE and XPE, or through the effect of the sliding velocity on the lubrication of the contact interaction [218].

The properties of the surfaces opposing the PE or XPE material have been demonstrated to affect PE wear. Increasing the material hardness of the opposing surface has been shown to reduce PE wear [17, 219]. The hydrophilicity-hydrophobicity of the opposing surface has been demonstrated to affect PE wear [17, 70, 219]. The hydrophilicity-hydrophobicity of the opposing surface likely influences wear rates by affecting protein adsorption and thereby affecting the colloidal boundary lubrication of the articulation [70]. Meanwhile, increasing the surface roughness of the opposing

surface has been shown to increase PE and XPE wear [220]. Increased surface roughness would tend to increase the abrasive wear of PE and XPE [220].

The material properties of the PE or XPE material also greatly affects wear. Increasing XPE crosslink density has been shown to greatly decrease wear [61, 211]. The increased density of C-C bonds between adjacent molecular chains may increase the cohesive strength of the XPE material [61]. Increasing PE or XPE molecular density may also decrease wear through improving the cohesive strength of the material [3]. The material properties of PE and XPE with increased oxidation potential may degrade over time, with the progression of oxidation, leading to greatly increased fatigue wear [32]. Manufacturing methods which result in decreased material properties have also been associated with increased PE wear [221].

PE and XPE wear has also been demonstrated to be dependent upon contact pressure [210, 222]. Increasing contact pressure has been shown to have the effect of initially increasing wear, but then decreasing wear once a threshold is exceeded by Pin-on-Disk (POD) tests (Figure 12) [210, 222]. The POD tests involved the articulation of a PE or XPE pin against a CoCr alloy disk in the presence of a lubricant. POD tests are discussed further in Section 2.4.2.1.

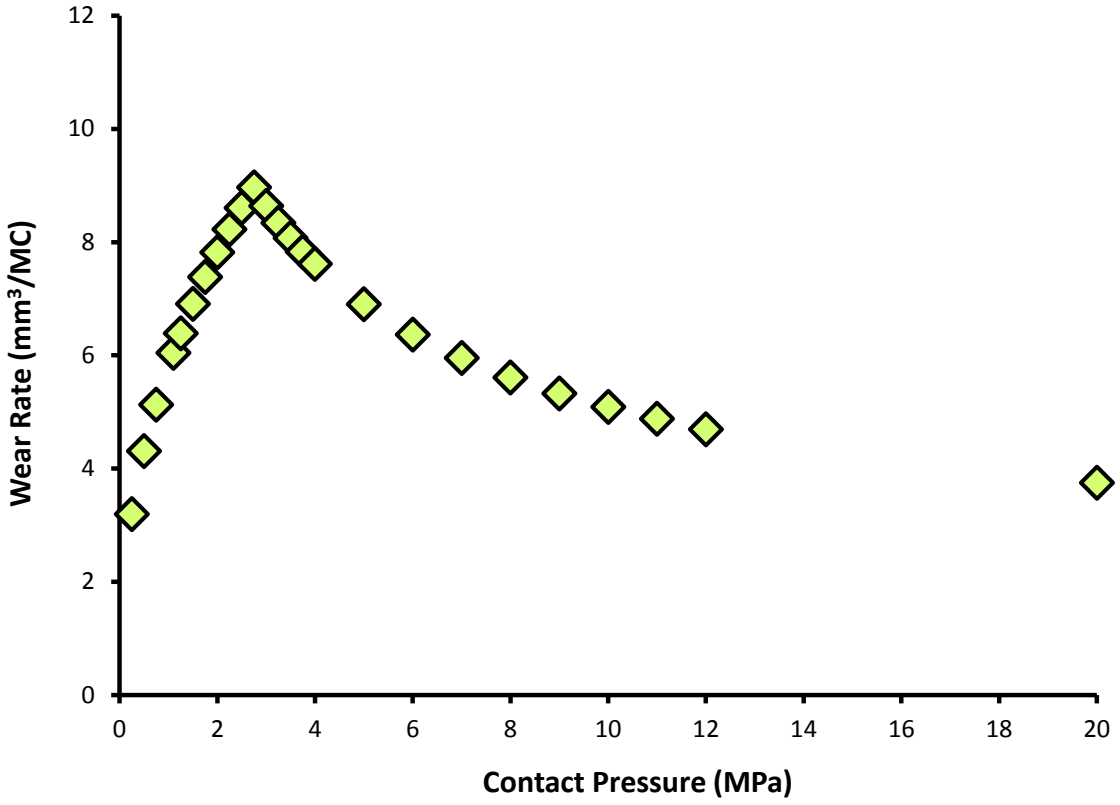

Figure 12: The effect of contact pressure on XPE wear as demonstrated by Saikko [222].

The wear rate trend demonstrated by POD tests under varying contact pressure [210, 222] is not immediately intuitive and does not agree with Archard's wear law which would predict consistently increasing wear under increasing load (and correspondingly contact pressure). Although this trend has been demonstrated for POD tests, the contact and lubrication conditions of POD tests are different than those of a TKR (as will be discussed further in Section 2.4.2.1). Therefore, it remains unknown whether these POD contact pressure trends are directly applicable to TKRs. The direct investigation of the effects of contact pressure on the wear of a TKR in a knee simulator would be of great value. However, to the author's best knowledge, knee simulator wear tests conducted

under a reference and increased vertical load, while keeping all other variables and kinematics constant, are not available in the literature. Clinical results regarding the effect of contact pressure on PE and XPE wear appear to be inconclusive. Several studies have suggested that increased body mass index may have a negative impact on clinical outcome [223-225], while other studies suggest that increased body mass does not negatively affect the clinical outcome [226-228]. Unfortunately, the effect of load and contact pressure on clinical wear is difficult to assess directly, as patients of increased body mass index may also have decreased levels of activity [229]. Furthermore, additional confounding clinical variables also exist, as patients of a higher mass typically utilize TKR components of greater size and of varying tibial insert thicknesses [229]. Therefore, there is a great need for further research into the effects of contact pressure on PE and XPE wear to understand the mechanism responsible for the complex behaviour demonstrated by POD tests [210, 222], as well as to understand whether the same behaviour would occur in a TKR.

The lubrication of TKRs also greatly influences TKR wear and is discussed in Section 2.3.2. In Sections 2.2.2 and 2.2.3, it was introduced that (for adhesive and abrasive wear) the energy dissipated at a contact interaction may be dissipated as a result of overcoming the adhesive forces between contacting asperities, as well as through the deformation of asperities. The adhesive bonding between contacting asperities in motion requires that the adhesive bond between the contacting asperities be broken (resulting in no wear), or the cohesive bond between the asperity and its base material to be broken (resulting in adhesive wear). Meanwhile the energy dissipated through the deformation of asperities may occur through elastic deformation (resulting in no wear), or may occur

through plastic deformation (possibly resulting in abrasive wear). Based on this energy dissipation wear theory approach, wear could be fully understood and predicted through having the full knowledge of the asperity contact conditions, adhesive bond strength, cohesive bond strength, and material deformation mechanics. All of the variables discussed in this section can be demonstrated to influence one or more of these energy dissipation variables, thus affecting wear.

2.3.2 Lubrication of Total Knee Replacements

The wear of PE and XPE materials in TKRs is greatly influenced by the lubrication [164]. The human knee is encapsulated by the synovium and contains up to approximately 10ml of synovial fluid which is continually renewed through biological processes [211]. Synovial fluid is an aqueous solution containing proteins, lipids, hyaluronic acid and lubricin [34, 164, 211, 213]. Alterations to the lubricant composition and relative concentrations have been demonstrated to greatly affect PE and XPE wear [164].

Synovial fluid may be regarded as a colloidal lubricant, with both a liquid phase and a solid phase which includes proteins. TKRs have been suggested to operate mainly under the boundary lubrication regime [32, 33, 70, 73, 211, 230, 231]. The lubrication and wear of TKRs has been demonstrated to be highly dependent on the proteins suspended in the lubricant [10, 70, 164, 232] and the proteins have been proposed as the main boundary lubrication molecules of synovial fluid [70]. Human synovial fluid for osteoarthritic patients (the most common type of TKR patient) typically includes an

average protein concentration of approximately 30 g/l [34, 212, 233]. The protein composition of synovial fluid includes albumin (71%), α-1-globulin (2%), α-2-globulin (6%), β-globulin (11%), and γ-globulin (10%) [34, 212, 233]. Albumin has been shown to be the most abundant protein in synovial fluid, accounting for approximately 71% of the total protein concentration [214, 233]. Serum albumin consists of 585 amino acids with a molecular mass of 65 kDa [215, 234]. The secondary structure of albumin consists of a high α-helical content without any β-sheet structure [215, 234]. Albumin, as well as the other proteins in synovial fluid, can become denatured based on thermal, chemical and mechanical conditions [32, 70, 72, 73]. Thermal denaturation conditions may include elevated bulk temperatures, as well as localized elevated temperatures through the energy dissipated between the asperities of multiple surfaces [72]. Protein chemical denaturation can occur through methods such as enzymatic digestion [235] or guanidine hydrochloride and urea chemical unfolding [236]. Mechanical conditions of protein denaturation may include both shear and agitation conditions [70, 237, 238]. The denaturation of a protein may be related to the enthalpy, or absorbed energy, during denaturation and can be obtained as the area under a differential scanning calorimetry curve [34, 72, 164, 233].

Molecular dynamics simulations have suggested the progressive denaturation of albumin to cause the linearly increasing exposure of hydrophobic amino acid side chains [33]. This finding is in agreement with the experimental observations of protein aggregation and adsorption. Shear has experimentally been shown to cause hydrophobic areas of the protein to be exposed, leading to protein aggregation [237, 239]. The exposure of hydrophobic areas would also tend to increase the adsorption of the protein to hydrophobic surfaces [33, 70, 237]. The denaturation of albumin has been

demonstrated to result in a compact, unfolded, and hydrophobic structure which preferentially adsorbs to the surfaces of TKR components over native albumin [33, 71]. The denatured albumin more strongly adheres to the surfaces of TKR components over native albumin, providing improved wear resistance [33, 240], yet also results in an increased coefficient of friction due to its more compact structure [70, 71]. Adsorbed proteins have been suggested to form a monomolecular layer based on quartz crystal microbalance with dissipation and atomic force microscopy measurements [73]. The adsorption of both denatured and native proteins are of great importance to the wear of TKRs [32, 70, 71, 73]. It should also be noted that because proteins are constantly being renewed through biological processes *in vivo*, protein denaturation may have a greater effect on *in vitro* knee simulator wear tests than would occur *in vivo* [70].

Lubricin and superficial zone protein have also been indicated to influence the lubrication of healthy knee joints [241]. However, patients suffering from arthritis have been demonstrated to have reduced levels of these proteins compared to healthy knee joints and the role of these proteins in TKRs is uncertain [242]. Hyaluronic acid has been suggested to affect wear rates [34, 213] and occurs with an approximate concentration of 1.5 g/l in human synovial fluid for osteoarthritic patients with a molecular weight of 1.8 MDa [212, 213, 233]. The hyaluronic acid of synovial fluid has been demonstrated to influence the viscosity of synovial fluid [213, 243]. However within the boundary lubrication regime, the viscosity of the bulk fluid has been demonstrated to have a negligible effect on lubrication [52], as previously discussed in Section 2.2.4. Hyaluronic acid has been demonstrated to have comparatively very low adsorption onto TKR component surfaces in comparison to albumin [32, 73], and may not independently make

a large contribution to TKR lubrication [244-246]. However, hyaluronic acid may substantially influence the lubrication of synovial fluid and calf serum through its interaction with proteins. Previously, proteins were assumed to bind irreversibly to hyaluronic acid [247, 248]. However, it has more recently been demonstrated that the direct binding of hyaluronic acid and proteins may only occur at very low ph values (ph<5) [243, 249]. Instead, proteins may entangle with hyaluronic acid at physiologically relevant ph values and the presence of hyaluronic acid may lead to increased structure formation [237]. Proteins have been suggested to interact with hyaluronic acid in the formation of aggregate structures [237]. However the adhesion forces of adsorbed albumin on the surface of PE has been indicated to be independent of the presence of hyaluronic acid in the solution [32, 73]. Phospholipids may also influence TKR wear [34]. However the concentrations of phospholipids in osteoarthritic patients are typically about 0.5 g/l and are therefore very low in comparison to the proteins [34].

During POD and knee simulator wear testing, synovial fluid is typically represented by calf serum. The relative protein concentrations and trace elements of calf serums typically used in solutions for simulating human synovial fluid for *in vitro* testing are summarized in Table 1 below. The serum are typically diluted to 17 g/l [250]. Of the commonly implemented calf sera, alpha calf serum most closely matches the relative protein constituent fractions of human synovial fluid [164]. The differences between calf serum and synovial fluid lubricants in terms of protein concentration, protein constituent fractions, level of osmolality, trace element concentrations, hyaluronic acid concentration and protein stability against denaturation may all influence the resulting PE or XPE wear. Therefore, it is important that the simulated lubricants of *in vitro* knee simulator wear

tests provide the closest representation of human synovial fluid as is practical in order to maintain the clinical relevance of the tests [4, 34, 164, 251-253].

Table 1: Composition of common calf sera used in POD and knee simulator wear test experiments [164].

		BCS	**NCS**	**ACS**
Albumin	[%]	51.7	40	71.7
α-1-globulin	[%]	3	11.2	3.8
α -2-globulin	[%]	12.7	22.8	8.4
β-globulin	[%]	20.4	14.2	15.8
γ-globulin	[%]	12.2	11.8	0.3
Total polypeptide concentration	[g/L]	69	52	42
Fe	[mmol/L]	0.0065	0.0157	0.0085
Ca	[mmol/L]	2.78	2.7	0.5
Inorganic P	[mmol/L]	3.16	2.82	0.2
Mg	[mmol/L]	1.02	1.06	0.06
pH		7.29	7.49	7.65
Osmolality	[mmol/kg]	301	290	291

2.3.3 Clinical Implementation and Design Variables

As discussed in the preceding sections (Sections 2.3.1 and 2.3.2), a wide range of variables directly impact the wear performance of TKRs. Consideration must also be provided for important clinical implementation and design variables such as articular conformity, tibial insert modularity and insert thickness.

The conformity between the femoral component and PE or XPE tibial insert is an important design variable which may greatly influence TKR kinematics and wear [254-257]. Increasing conformity may lead to increased contact area, decreased peak contact pressure and increased constraint of kinematics [256]. Increased conformity may therefore have a complex effect on TKR wear. Greater kinematic constraint has the potential to either increase or decrease wear depending on the specific kinematic input [3]. Increased contact area would tend to increase wear [3]. Meanwhile, as discussed in Section 2.3.1, the effects of contact pressure on wear were previously unknown prior to the research of the present thesis. Increased contact pressure had previously been suggested to increase [258-260], decrease [210] or to have no effect on wear [254, 261]. Further research must be conducted to improve our understanding of wear in order to design TKRs with the appropriate conformity to ensure proper kinematics and wear performance.

The design of the modular tibial interface (PE or XPE tibial insert and tibial tray interaction) also greatly affects TKR wear and osteolysis [7, 21-25]. The forces and displacements which are imparted on the tibial insert by the femoral component have been shown to cause the relative movement (micromotion) between the distal (backside) surface of the PE or XPE insert and the tibial tray of modular TKR's [8, 30]. Although wear particles from the modular interface represent only a small fraction of the total volume of wear particles for modern TKR designs, the particles originating from this interface may have increased biological activity and osteolytic potential [7, 11, 21-25, 30, 31, 35, 36, 262, 263]. Backside wear has been demonstrated to make a significant contribution to osteolysis [8, 24, 25, 31]. The surface finish of the tibial tray and the

locking mechanism of the modular interface are considered critically important design variables affecting backside wear [7, 8, 21-25, 31]. Thus, it is important that TKR design and evaluation methods are available not only for articular wear, but also for the analysis of backside wear.

Tibial insert thickness has also previously been demonstrated to affect TKR wear [15, 109, 264-266]. The availability of a wide range of insert thicknesses is necessary to enable the surgical balancing of soft tissues in the operating room. A significant source of TKR patient dissatisfaction may be caused by improperly balanced soft tissue [72, 73, 232, 267]. Stiffness and instability caused by improperly balanced soft tissue has also been demonstrated to be a significant reason for TKR revision surgery [17, 18]. Relatively small changes in soft tissue balance and component positioning can compromise postoperative performance [72, 73, 267]. Not only must the medial-lateral soft tissue balance be correct, but the correct PE or XPE insert thickness must also be selected. The implementation of an insufficiently thick insert may result in excessive laxity, instability and patient dissatisfaction [254]. Conversely, the implementation of an excessively thick insert may result in knee stiffness, limited range of motion and patient dissatisfaction [254]. Therefore, the availability of a wide range of insert thickness is important to ensure that proper soft tissue tension is achievable. For these reasons, it is important to understand the range of permissible insert thicknesses which will still result in sufficient wear performance, as well as understand how changes in insert thickness may generally affect insert wear.

Retrieval studies have previously demonstrated that insert thickness has an effect on the surface damage of tibial inserts. Several implant retrieval studies have demonstrated

that articular insert wear and damage increases for thinner inserts [15, 109, 264-266]. The effects of insert thickness on the articular surface has previously been investigated using static, linear and bi-linear elastic, FE simulations by Bartel et al. [256, 257]. These simulations have revealed that the von-Mises stresses within PE or XPE inserts increase greatly with decreasing insert thickness below 8mm due to the limited elastic deformation of the surrounding material [256, 257]. Therefore, the recommendation was made that inserts should be at least 8mm in thickness [256, 257]. The United States Food and Drug Administration [230] similarly specified that inserts must be 6mm or more in thickness. Although insufficient insert thickness has caused the failure of many gamma-air irradiated [264-266] and heat pressing formed inserts [221], the effects of insert thickness on the wear performance of modern, oxidation resistant PE and XPE bearing materials has not been as thoroughly investigated.

Insert thickness may affect backside (distal) insert wear as well as articular wear [8, 24, 25, 30, 31]. Recently, Brandt et al. [7] showed that backside damage may be greater for thick inserts than for thin inserts of the same design (Figure 13). It was anticipated that thinner inserts experienced increased engagement of the peripheral locking mechanism, resulting in decreased backside damage [7]. However, proof from mechanical *in vitro* tests to verify this suggestion has not been performed to date.

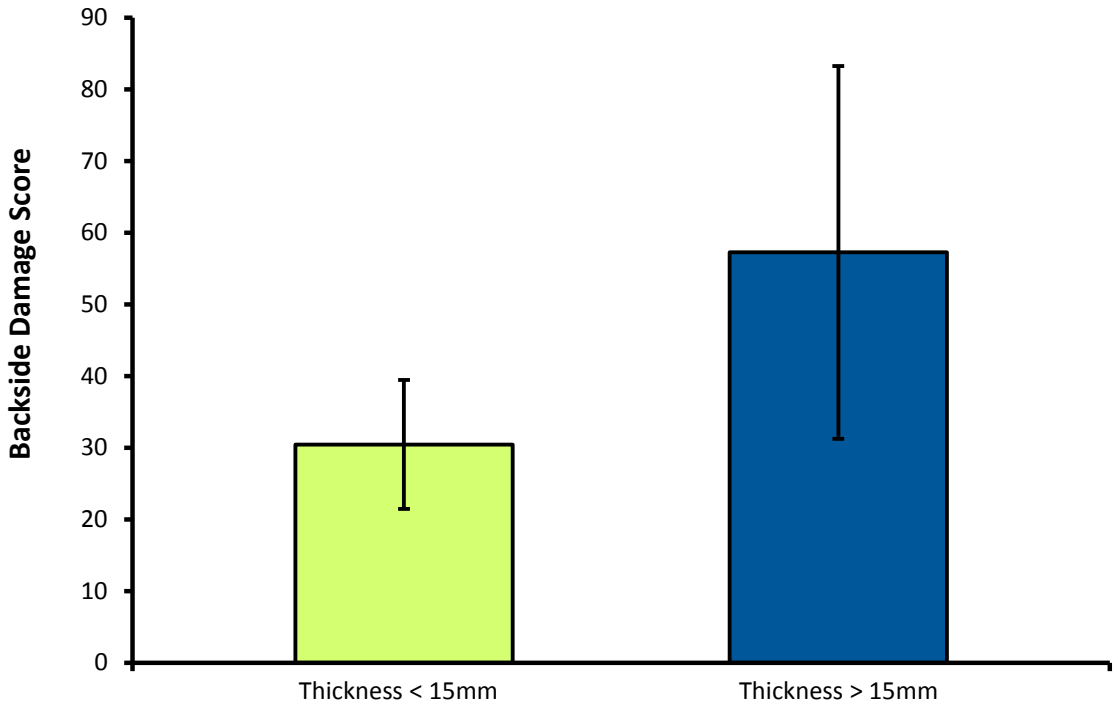

Figure 13: Backside damage score for retrieved tibial inserts with thicknesses of 15 mm or less and greater than 15 mm [7].

Static FE simulations have previously been performed for the articular surface [256, 257] of inserts. However, the author is not aware of any computational simulations investigating the effects of insert thickness on the backside surface or on insert wear. Dynamic FE simulations of the TKR during a gait cycle, combined with computational wear simulations, could enable the effects of insert thickness on contact pressure, sliding distances and wear to be more precisely analyzed than has been done previously. Therefore, further research must be done to further investigate the effects of insert thickness on contact pressure, sliding displacements and wear for both the articular and backside surfaces of PE and XPE tibial inserts.

2.4 Total Knee Replacement Polyethylene Wear Performance

Due to the importance of TKR wear performance on the long term success of TKRs, it is essential that methods are available for the evaluation of TKR wear performance. The wear performance of implanted TKRs can be monitored through radiographic methods, database review analyses, and implant retrieval analyses to directly evaluate the *in vivo* wear performance of TKRs. Alternatively, *in vitro* testing could be conducted to evaluate the wear performance of TKRs in a laboratory environment. Or finally, *in silico* simulations could be conducted to evaluate the wear performance of TKRs through computer simulations. The following sections (Sections 2.4.1 - 2.4.3) briefly discuss the various means of assessing TKR wear, as well as the practicality of utilizing such approaches to inform TKR design.

2.4.1 *In Vivo* Total Knee Replacement Polyethylene Wear

In vivo wear analyses provide the most relevant approach to evaluating the wear performance of a given TKR design in patients. TKR *in vivo* wear performance has been investigated mainly through radiographic methods, database review analyses, and implant retrieval analyses. The requirements for the accurate radiographic measurement of TKR wear are far more complex than those required for total hip replacements due to the increased degrees of freedom of the knee joint in comparison to the hip [268]. Thus, the simple and well established radiographic wear measurement methods developed for total

hip replacements cannot be directly applied to TKRs [3]. Although single plane radiographs cannot be used to accurately obtain quantitative measurements of TKR wear, radiographs are still regularly reviewed by surgeons for signs of excessive wear or osteolysis [3]. Radiosteriometeric analysis methods have been developed [269] to enable the quantitative evaluation of wear by utilizing biplanar radiographs to analyze the relative 3D positions of components and tantalum marker beads [268, 270-289]. Through the analysis of the relative position measurements of TKR components at various flexion angles, positions or loading, the wear of TKRs may be inferred [268, 270, 271, 274, 275, 278, 280, 281, 285, 287].

Database review studies have been used to analyze the general survivorship and reasons for revision of TKR designs [3]. Databases coordinated between multiple institutions such as the Canadian Joint Replacement Registry [6] and the Swedish Knee Arthroplasty Registry [290] have been very beneficial in enabling research to be conducted on larger sample sizes of data. Database review studies have proven to be very beneficial for the identification of general trends across large patient populations [3, 291-299].

Finally, implant retrieval studies can be conducted to analyze the wear and damage of TKR components after they have been retrieved from the patient. TKR components may be retrieved upon revision surgery or post-mortem [3]. The accurate and direct measurement of wear magnitude for retrieved components is not generally possible because the implant starting geometry and mass are not known and can vary within a product line [300]. Additionally, the fluid adsorption and material creep could not be accurately accounted for in TKR retrievals [3]. Therefore, instead of the direct

measurement of wear, the surface damage is analyzed with the assumption that damage would be correlated with wear. The damage of retrieved implant components are assessed using damage scoring methods to provide a consistent and reproducible means of quantifying damage [301-303]. Damage scores are specified based on the extent of the damage and the area of damage for various damage features. The total damage score is then calculated as the sum of all damage scores. The most frequently implemented damage scoring method has been that of Hood [301]. Many modified versions of the Hood method have also been developed and implemented for the assessment of TKR damage [4, 7, 262, 302, 303]. Implant retrieval analyses have proven to be very beneficial to understanding the clinical performance of TKRs *in vivo* [3].

In vivo wear and damage assessment methods are very beneficial for identifying the performance of TKRs *in vivo* and will therefore continue to be essential methods of monitoring TKR performance in the future. However, the direct and precise analysis of the effects of various design variables on wear is often not possible using *in vivo* wear and damage assessment methods due to large variations in patient anatomy, surgical alignment and patient activity [3]. Furthermore, *in vivo* wear and damage assessment methods cannot fully satisfy the wear assessment requirements necessary for the design of TKRs optimized for the reduction of wear. The optimization of TKRs for the reduction of wear would require the time efficient analysis of wear across a very large range of design variables and operating conditions (Section 2.3). Therefore, other methods are needed which can be used to evaluate TKR wear in a more time and cost efficient manner for design purposes.

2.4.2 *In Vitro* Simulation of Polyethylene Wear

In vitro methods have been developed to evaluate the wear of TKRs, and TKR materials, under carefully controlled laboratory conditions. In comparison to *in vivo* wear analysis methods, *in vitro* wear testing methods remove the limitation of unknown patient variability by enabling the accurate control of the operating conditions. *In vitro* wear testing methods also reduce the total time required for the analysis by removing or reducing the rest time TKRs would experience *in vivo* [3]. However, *in vitro* wear testing methods also tend to have reduced clinical relevance, as *in vitro* testing requires many simplifications of the *in vivo* conditions. Currently, the most widely used *in vitro* wear testing methods for the design of TKRs are pin-on-disk (POD) tests and knee simulator wear tests. Both POD (Section 2.4.2.1) and knee simulator wear tests (Section 2.4.2.2) are discussed in the following sections.

2.4.2.1. Pin-on-Disk Tests

The POD wear testing apparatus is used for conducting basic tribological tests by articulating a pin against a disk. POD testing relevant to TKRs typically utilizes a PE or XPE pin against an opposing counterface such as a CoCr alloy disk (Figure 14). The contact conditions of this basic tribological test are far simpler than those of knee simulator wear tests. As a result, POD tests are very useful to investigate the basic wear response of a tribological system. However, because of the large differences in operating conditions between POD tests and *in vivo* TKRs, POD tests should not be expected to

demonstrate clinically relevant wear rates, but are rather utilized for evaluating the wear response of simplified tribological systems which can be accurately controlled.

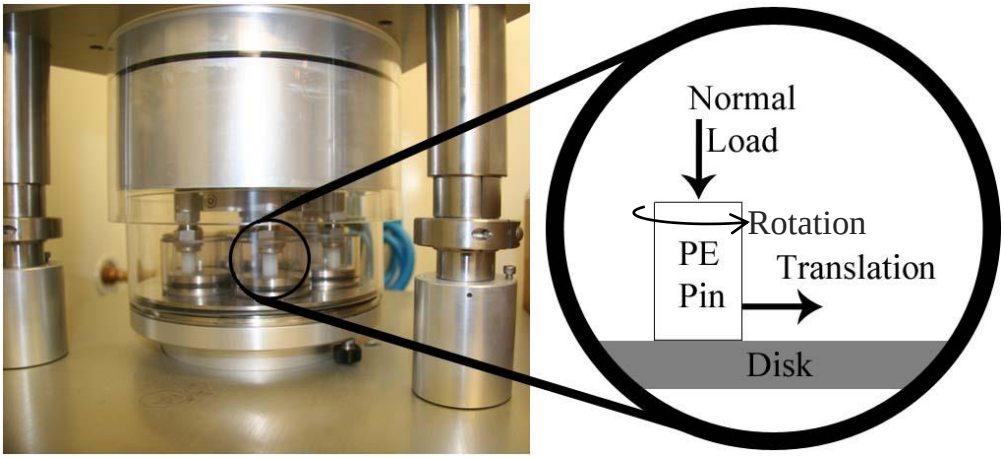

Figure 14: Pin-on-Disk Testing Apparatus (AMTI Orthopod, AMTI, Waltham, MA).

Currently, ASTM F732-00 [304] is the only available standard pertaining to the POD testing of TKR materials. ASTM F732-00 [304] provides only general guidance on POD testing and generally does not restrict a wide range of loading, displacement and lubrication conditions from being investigated. A wide range of pin paths have been utilized including linearly reciprocating [305-307], rectangular [59, 60, 308-311], elliptical [220, 222, 232, 312-316], translating-rotating [210, 216, 317, 318], and many others [319]. Wide ranges of loading conditions have also been applied to POD tests. Both static [59, 60, 210, 216, 220, 222, 232, 309-311, 317, 318, 320, 321] and dynamic loads [308, 313, 322] have been investigated.

The simplicity of POD testing, as well as the ability to precisely control the tribological conditions, make POD testing very useful to investigating tribological

systems. The ability of POD tests to somewhat isolate specific variables and analyze their influence on wear has enabled POD tests to be used for the development of computational wear models and to advance our general understanding of wear [38, 59-61, 210]. However, POD tests cannot be expected to provide the clinically relevant wear rate for a TKR design, since the operating conditions of the POD test do not reflect the complex operating conditions TKRs experience *in vivo*.

2.4.2.2. Knee Simulator Wear Tests

Knee simulator wear tests have been developed with the objective of simulating the conditions the TKRs will be subjected to *in vivo* (Figure 15). Current knee simulators feature 6-degrees of freedom (3 displacements and 3 rotations of the femoral component relative to the tibial component), and utilize provisions for the inclusion of a heated lubricant to surround the TKR. Knee simulators are utilized to conduct wear tests, either according to the ISO standards for displacement controlled (ISO 14243-3) [250] or force controlled testing (ISO 14243-1) [323], or under other specific wear conditions. Both ISO standards [250, 323] specify the flexion angle and axial loading of the TKR over the gait cycle (Figure 16 and Figure 17). The gait cycle begins with the initial heel strike, and ends after the swing phase before the foot contacts the ground again. The ISO standard for displacement controlled knee simulator wear testing specifies the anterior-posterior translation (Figure 18) and internal-external rotation (Figure 19) over the gait cycle in terms of displacements, while the ISO standard for force control specifies the values in terms of force (Figure 20) and moment (Figure 21). Both ISO standards also specify a

lubricant of diluted calf serum for the simulation of human synovial fluid [250, 323], which as discussed previously (Section 2.3.2) may greatly influence the wear test results.

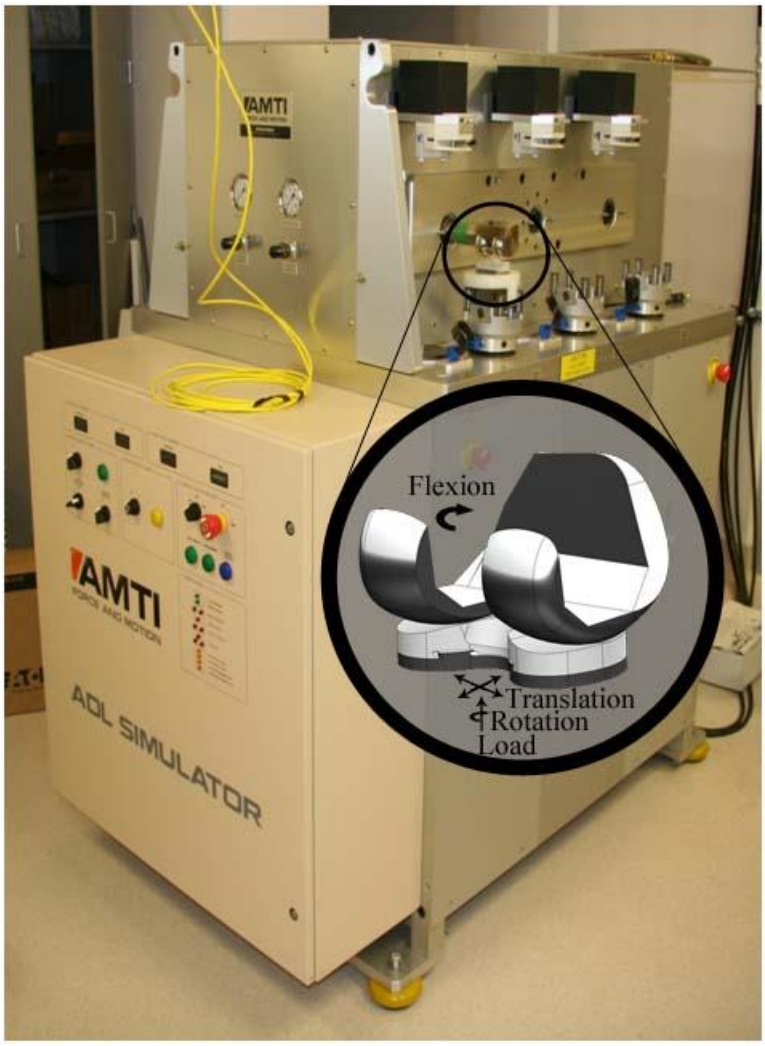

Figure 15: Six station knee simulator (AMTI, Waltham, MA).

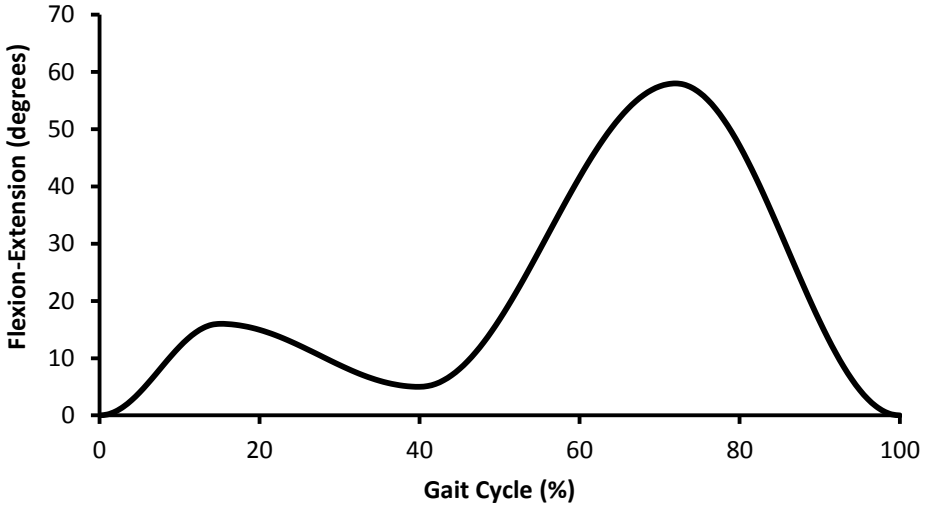

Figure 16: ISO 14243 standard flexion-extension angle over the gait cycle.

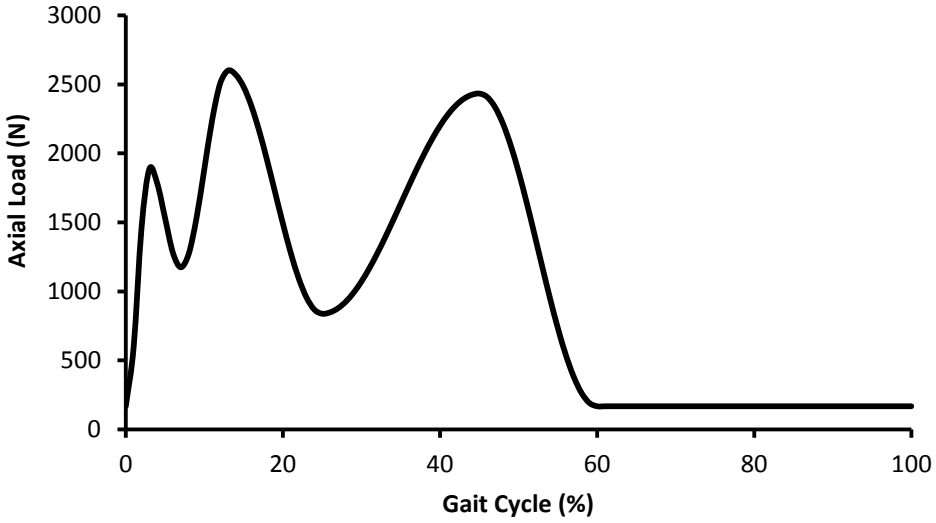

Figure 17: ISO 14243 standard axial loading over the gait cycle.

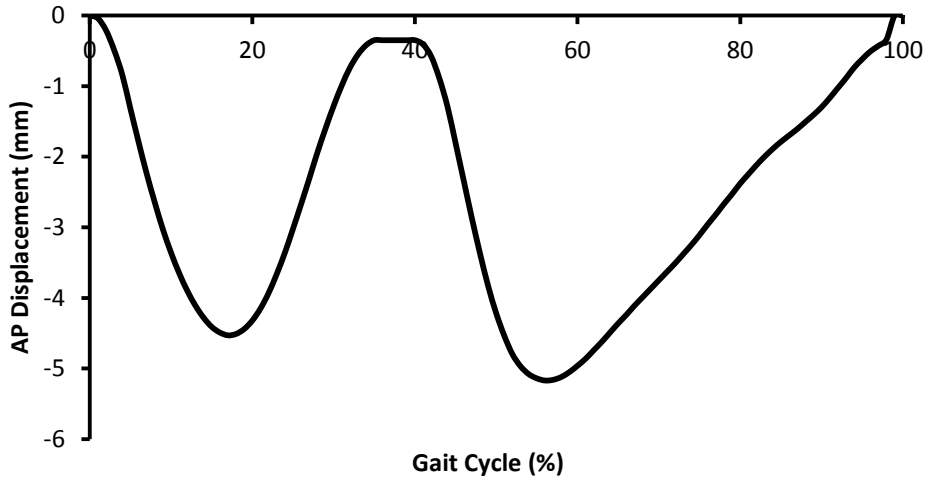

Figure 18: ISO 14243-3 standard anterior-posterior (AP) displacement over the gait cycle for displacement controlled testing.

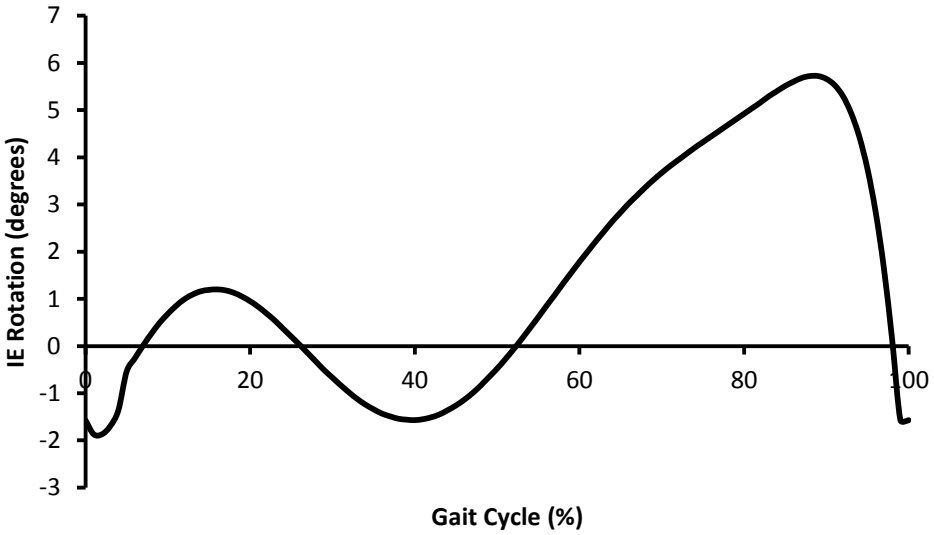

Figure 19: ISO 14243-3 standard internal-external (IE) rotation over the gait cycle for displacement controlled testing.

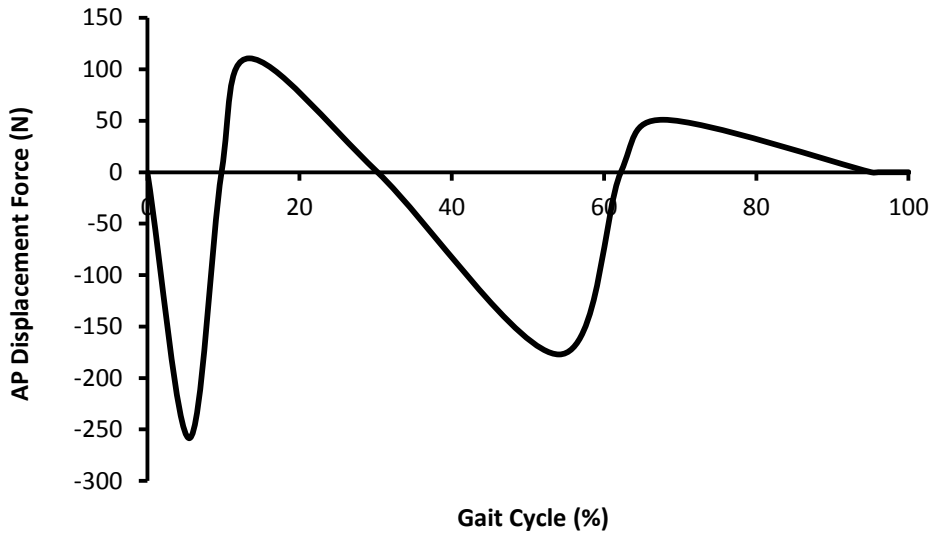

Figure 20: ISO 14243-1 standard anterior-posterior (AP) force over the gait cycle for force controlled testing.

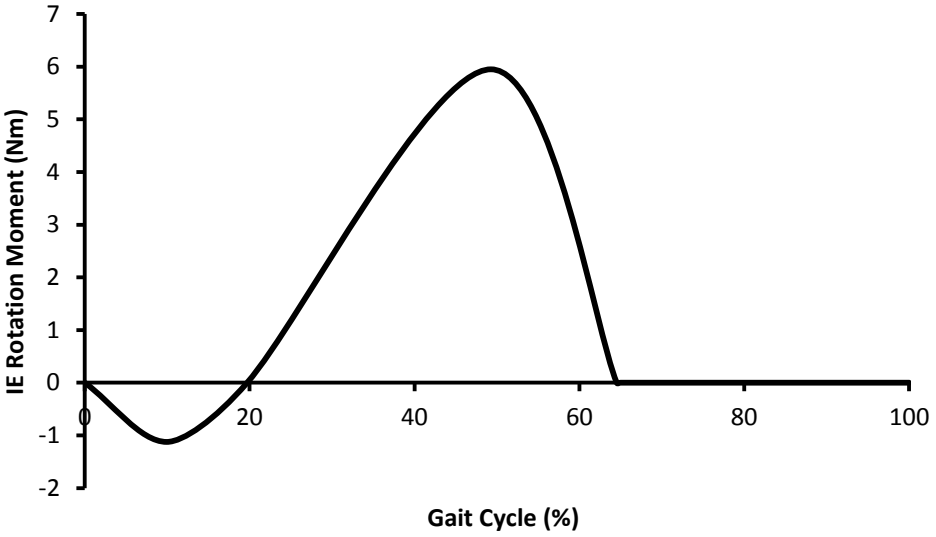

Figure 21: ISO 14243-1 standard internal-external (IE) moment over the gait cycle for force controlled testing.

The kinematics and loading conditions of the ISO standards [250, 323] have been developed with the intention of representing the conditions the TKR would experience *in vivo*. The specification of displacement controlled kinematics may generally offer greater reproducibility of the results, as small changes in the tribological system (such as changes to the lubricant) will not lead to different kinematic displacements, as may occur for force controlled knee simulator wear tests [3]. Additionally, the complexity of representing the laxity of the human knee in force controlled knee simulator wear testing may also be associated with a reduction in the reproducibility of the results [3, 324, 325]. On the other hand, force controlled knee simulator wear testing can be used to analyze any TKR design, even designs which highly restrict kinematic displacements [3]. Therefore, the increased robustness of the displacement controlled method may make it a more favourable method for the knee simulator wear testing of less kinematically restrictive designs, such as low to moderate conforming cruciate retaining fixed bearing TKR designs and mobile bearing TKR designs. Meanwhile the force controlled method may be favourable for more kinematically restrictive designs, such as highly conforming and posterior stabilized TKR designs. The same kinematic controls implemented for knee simulator wear testing can also be implemented in computational wear simulations. Furthermore, the ability to computationally replicate the conditions of POD and knee simulator wear tests provide an ideal means for verifying computational wear simulations.

Knee simulator wear testing is the current standard for the evaluation of TKR wear during the design and development of new TKRs. Knee simulator wear testing enables new designs to be evaluated prior to any clinical testing, thereby improving patient

safety. Knee simulator wear testing also generally enables the precise control of operating conditions in comparison to *in vivo* wear analyses. However, the simplifications of the knee simulator wear testing methods (such as calf serum lubrication and simplified kinematics) may somewhat reduce the clinical relevance of knee simulator wear testing. Although knee simulator wear testing is an essentially valuable method for the evaluation of TKR wear, the time and cost requirements of knee simulator wear testing may greatly limit the range of design variables and operating conditions which can be considered [38]. As a result of the many design variables, operating conditions, and the complex interactions amongst tribological variables, the optimization of TKRs for the reduction of wear through knee simulator wear testing may not be generally possible. Therefore, the need exists for additional methods with improved cost and time efficiency over knee simulator wear testing which may enable the design optimization of TKR designs for the reduction of wear.

2.4.3 *In Silico* Simulation of Polyethylene Wear

The excellent cost and time efficiency of computational simulations may enable computational wear simulations to be used for the optimization of TKRs for the reduction of wear [38]. However, computational wear simulations must first demonstrate a high level of predictive accuracy in order to verify the clinical relevance of such simulations. Computational wear simulations generally require the simulation of contact mechanics to evaluate the contact pressure, contact area, and sliding displacement vectors at the wear surface, followed by the implementation of a computational wear model for the

prediction of wear based on the contact mechanics results [259]. This process is then typically repeated at regular intervals throughout the wear simulation to account for the geometric changes from previous wear intervals in current wear interval predictions [259]. The following sections will discuss the methods and models for the prediction of TKR contact mechanics (Section 2.4.3.1) and computational wear models for the simulation of wear (Section 2.4.3.2).

2.4.3.1. Contact Mechanics Simulation

The *in silico* computational wear simulation of PE and XPE TKR wear first requires the accurate prediction of TKR contact mechanics. The contact mechanics of a TKR design are of great importance to the performance and success of the device overall. TKR contact mechanics greatly influences both the wear and kinematics of TKRs. PE and XPE wear has been demonstrated to be proportional to the contact pressure [326] and sliding distance [59, 111, 315] at the contact interaction. The kinematics of the TKR are also dependent on the contact mechanics [327-330]. Furthermore, the patients' perception of how similar the TKR's kinematics are to that of the natural knee may be essential to ensuring patient satisfaction [331-333]. Therefore, appropriate contact mechanics are vital to the design of TKRs. The computational simulation of contact mechanics is a crucial component to both computational wear simulations and computational kinematic predictions.

Computational wear simulations require the prediction of TKR contact mechanics as an input to the computational wear model for the prediction of PE or XPE wear.

Computational kinematic prediction analyses also require the evaluation of TKR contact mechanics. The reaction forces at the articular surface of the PE or XPE tibial insert, along with the human anatomy, determine the kinematics of the TKR [327-330]. The development of TKRs with kinematics similar to those of the natural human knee is of great interest, as unnatural kinematics may lead to patient dissatisfaction [331-333]. Therefore, the computational simulation of TKR contact mechanics is an important component to the design of TKRs for both improved performance and patient satisfaction.

TKR contact mechanics have typically been predicted by FE simulation [37, 38, 259, 261, 334, 335] or through the use of MBD simulations [39, 40, 260, 328, 336-338]. The simulation of the mechanical behaviour of PE and XPE is complex, as it exhibits a complicated nonlinear response to external loads. PE and XPE behave viscoelastically at small deformations, followed by distributed yielding, viscoplastic flow, strain hardening at large deformations and finally ultimate failure [3]. Therefore, FE and MBD simulations require accurate material models in order to provide accurate predictions of contact pressure, area and sliding distance.

Linear elasticity, hyperelasticity, linear viscoelasticity and the J_2-plasticity model are among the most commonly implemented material models used in deformable FE simulations [3, 339]. Linear elastic models offer simplicity as well as computational efficiency and have been previously implemented in TKR wear simulations [260, 340]. Linear elastic models only require the specification of Young's modulus and Poisson's ratio. However, the applicability of the linear elastic model is limited, as it has been shown to be unable to describe the characteristics of PE and XPE for medium to large

strain values [3]. The hyperelasticity model is also limited, as the lack of Drucker-stability in the computational solution may lead to inaccurate results at higher strain rates [341]. The descending branch of the PE and XPE stress-strain curve requires the prediction of increasing strain with decreasing stress, thereby violating the Drucker-stability postulate, which requires that a stress increase causes a strain increase to result in positive work and provide a stable computational solution [341]. The linear viscoelasticity model enables the prediction of time-dependence and viscoelastic flow. However, the viscoelastic model may provide inaccurate results at medium to high strain values, and the strain values in tibial inserts under ISO loading have been shown to reach levels higher than the yield strain of the material [3]. The J_2-plasticity model is typically represented by a modulus of elasticity and a set of tabular stress-strain values obtained from experiments. Piecewise linear interpolation is conducted between these stress-strain data points. The J_2-plasticity model has been demonstrated to accurately predict PE material behaviour in comparison to experiments conducted under small, intermediate, and large monotonic deformation, as well as cyclic loading; in addition to demonstrating high correlation strength R^2=0.87 [339]. FE simulations with the J_2-plasticity model have also been demonstrated to provide accurate results for the prediction of TKR contact mechanics, even for the backside (insert – tibial tray) interface [335]. The prediction of sliding distances and contact pressure at the backside interface is a highly complex task as it requires the accurate assessment of the complex contact interactions of each surface and the accurate prediction of the nonlinear material response to deformation. The author of this thesis has previously investigated the accuracy of deformable FE simulations, for the prediction of backside sliding distances, using the three most commonly implemented

PE and XPE material models, linear elasticity, viscoelasticity, and the elastic-plastic J_2-plasticity model [335]. The FE simulations were conducted according to the loading and displacement conditions of ISO 14243-3 [250] and were compared to experimental knee simulator wear tests conducted under the same standard [10, 11, 342, 343]. The linear elastic and viscoelastic models were found to provide inaccurate results compared to the knee simulator wear test results. Yet the J_2-plasticity model predicted very similar micromotion to the knee simulator results, further demonstrating the capabilities of FE simulations with the J_2-plasticity model for the prediction of TKR contact mechanics.

MBD simulations are an alternative method for the evaluation of TKR contact mechanics [39, 40, 260, 328, 336-338]. MBD simulations may offer greatly improved computational efficiency over deformable FE simulations [328]. However, the simplifications of this method may also lead to an associated decrease in prediction accuracy. Previous TKR MBD simulations have consisted of rigid femoral and tibial insert components. The deformation of the PE or XPE material is simulated by the utilization of elastic foundation (EF) theory [260, 344-346] or pressure-overclosure (PO) relationships [39, 40, 328, 347], which permit the penetration of the femoral component into the rigid body PE or XPE tibial insert. The EF theory includes the theoretical representation of the PE or XPE insert by a set of distributed elastic components “bed of springs” [260], where the contact pressure and deformation of each spring is independent of its neighbouring springs. The contact pressure (P) for each spring may be calculated using the equation [260]:

$$P = \frac{(1-v_p)E}{(1+v_p)(1-2v_p)}\frac{d}{h} \quad (6)$$

where E is the Young's modulus of PE or XPE, v_p is Poisson's ratio, d is the springs deflection or displacement and h is the thickness of the component. PO relationships similarly specify each node of the model to be associated with a spring, but unlike EF theory, each spring is considered to be of zero length in its non-deformed state [328]. With deformation, the stretching of PO relationship springs is defined by the specified linear or non-linear spring rate. Both EF theory and PO relationship MBD simulations support the use of linear and nonlinear elastic models [328]. The advantage of implementing MBD simulations is the greatly increased computational efficiency over fully deformable models. The MBD models can reduce computational time to just 2% of the time required for deformable models [328]. However, the assumption that each node is unaffected by the displacement of neighbouring nodes does not represent true material behaviour and may lead to a decrease in predictive accuracy. The independence of the displacement of neighbouring nodes also prevents this method from predicting the contact mechanics of the backside surface of the tibial insert of TKRs. Although the articular surface may be the source of the greatest volume of PE or XPE wear particles, particles originating from the backside surface may be of greater osteolytic potential due to their smaller size [8, 24, 25, 30, 31, 35, 36, 262, 263]. Therefore, the wear of both the articular and backside surfaces of the tibial insert are of interest when conducting computational wear simulations and during the TKR design process. However, MBD

simulations may still be of interest for the prediction of contact mechanics at the articular surface of PE and XPE tibial inserts.

Computational wear simulations and kinematics predictions in the literature which have utilized MBD simulations have typically implemented either the PO relationship [39, 40, 330, 348] previously developed by Halloran et al. [328], or the EF model [260, 337, 338, 344] previously developed by Fregly et al. [345]. Despite the implementation of EF and PO models in the literature [39, 40, 260, 328, 330, 337, 338, 344, 348], the accuracy of these models has not been extensively tested across a broad range of possible contact conditions [328, 345]. EF and PO model accuracy would likely vary for TKRs of differing conformity and therefore the comparison of EF and PO results to the results of a verified FE model for greatly varying TKR contact conditions has been deemed necessary. The contact pressure and contact area predictions of MBD simulations must be found to be in good agreement with either physical testing, or a verified deformable FE model, across a wide range of conditions, before the method can be considered to be accurate for the analysis of TKRs. Therefore, further verification of the accuracy of MBD simulations for the prediction of articular contact mechanics would be of great benefit.

2.4.3.2. Computational Wear Modeling of Polyethylene

As discussed previously, PE and XPE wear depends upon a large number of variables and conditions (Section 2.3). Thus, the development of a computational wear model is a complex task, as the model must be capable of accurately predicting PE or XPE wear for a wide range of designs and conditions. Computational wear models require knowledge

of the contact mechanics for the prediction of wear, which can be evaluated through FE and MBD simulations as discussed in Section 2.4.3.1. Previously existing computational wear models for TKR simulations can be grouped into three main categories based on the variables included in their formulation. These three groups include contact pressure and sliding distance dependent wear models (Section 2.4.3.2.1), time independent cross shear wear models (Section 2.4.3.2.2) and time dependent cross shear wear models (Section 2.4.3.2.3). Previously existing computational wear models are discussed in the following sections (Sections 2.4.3.2.1 - 2.4.3.2.3), followed by a discussion of variables requiring further consideration for the improved predictive accuracy of computational wear simulations (Section 2.4.3.2.4).

2.4.3.2.1. Contact Pressure and Sliding Distance

The wear of materials has generally been demonstrated to depend upon sliding distance and contact pressure [111]. Archard's wear law has previously been developed to model the wear of materials based on contact pressure, sliding distances and a wear factor or wear constant [111]. This model has proven to be very beneficial in other areas of tribology and was therefore also one of the first models to be applied to TKRs. Archard's wear law specifies that the wear depth is proportional to a wear factor (k) multiplied by the contact pressure (P) and the sliding distance (S) [111].

$$W_{depth} = k \cdot P \cdot S \tag{7}$$

The majority of TKR wear simulations [38, 260, 337, 338, 348-353], have been based upon Archard's wear law [111] with a wear factor obtained from POD testing. There are a wide range of published POD test derived wear factors intended for TKR wear, ranging from 5.0×10^{-8} to 1.8×10^{-6} mm^3/Nm [319]. The majority of previously developed Archard's wear law models were only applied to one implant, or resulted in poor predictability when the wear of TKRs with different geometries was predicted [40].

Despite the widespread implementation of Archard's wear law in the literature, Archard's wear law has demonstrated poor predictability for PE and XPE wear [40]. One of the reasons for the limited applicability of Archard's wear law to PE and XPE wear is because Archard's wear law does not account for the directional strain hardening of PE and XPE due to cross shear. As a result of this limitation, other computational wear models have been developed to include consideration for cross shear.

2.4.3.2.2. Time Independent Cross Shear

PE or XPE, as a thermoplastic material, is subject to directional strain hardening. In response to loading and relative sliding between components, the molecular chains can become mobile and form highly oriented crystalline lamellae aligned with the direction of loading or sliding. The direction of the crystalline lamellae is referred to as molecular orientation, and the materials wear resistance is increased in the direction of the molecular orientation, and decreased in the direction perpendicular to the molecular orientation (as discussed in Section 2.3.1). The strong dependence of wear on multidirectional motion (or cross shear) became apparent through the results of POD tests

[60], and knee simulator wear tests [354]. Therefore, more recent wear models have been developed to include the effect of cross shear on wear, a relationship also usually derived from POD test results [60, 210]. The majority of wear models have been built upon the existing foundation of Archard's wear law, by specifying the wear factor (k) to be a function of the cross shear, or by appending a cross shear term to the original equation [40, 60, 210, 216, 254, 261, 318, 355, 356].

2.4.3.2.3. Time Dependent Cross Shear

The majority of cross shear dependent wear models [40, 60, 210, 216, 254, 261, 318, 355, 356] have been time independent. Therefore, the molecular orientation of the PE or XPE crystalline lamellae remained fixed in a single direction over time, which may not be a clinically relevant representation of PE and XPE wear [59]. POD tests have demonstrated that with continued sliding in a consistent direction the molecular orientation may eventually become orientated in the direction of sliding, and the wear rate may drop to a near zero wear rate [59]. Thus, for large sliding distances in two directions separated by an angle of 90 degrees, a time independent wear model would predict a consistent wear rate proportional to a cross shear angle of 45 degrees and greatly over-predict wear. Conversely a time dependent wear model would predict a high initial wear rate, followed by a greatly reduced wear rate once the molecular orientation has become aligned with the direction of sliding (Figure 22).

Petrella et al. [336], developed a time dependent cross shear wear model by defining an incremental weight factor for material memory in a wear model based on a modified

version of Archard's wear law. The model maintained memory of the sliding direction from recent previous time increments (generally, 2 or 3 past time increments), to provide consideration of the cross shear experienced. Meanwhile, Strickland and Taylor [39] also developed a time dependent wear model based on a modified version of Archard's wear law, in which the sliding distance was represented by an exponential expression to compensate for the effects of time dependent cross shear. The model of Strickland and Taylor [39] was demonstrated to result in an additional increase in correlation strength (R^2=0.65) over several previously available time independent cross shear wear models (R^2=0.60). However, it should be noted that this time dependent wear model was contact pressure independent and was only dependent on sliding distances, cross shear and contact area.

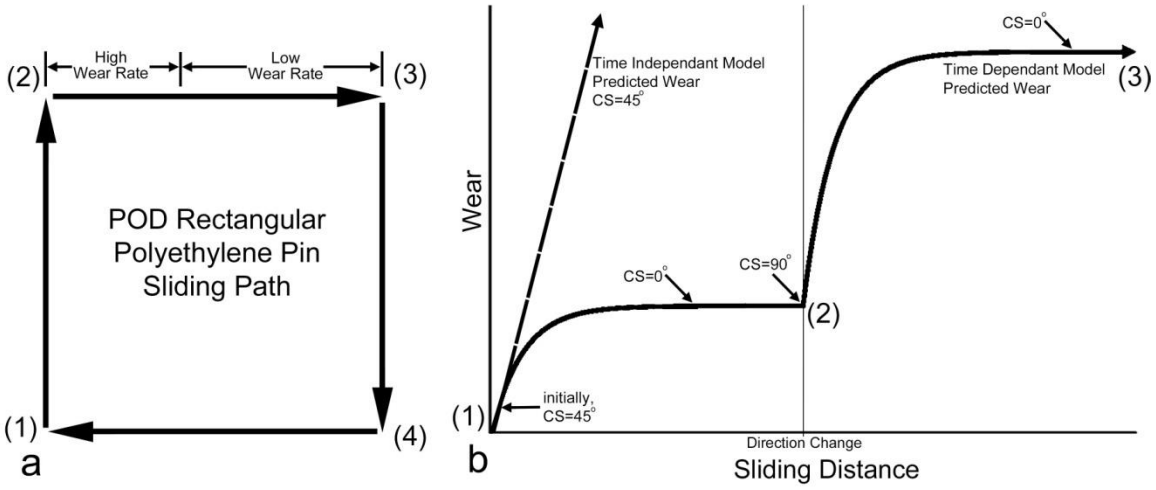

Figure 22: Time dependent and independent wear modeling: (a) square polyethylene sliding path of a pin-on-disk test: a change in direction results in a high initial wear rate followed by a greatly reduced wear rate, (b) relationship between wear and sliding distance for the time dependent and independent wear models (based on the sliding path indicated in "a") demonstrating that only time dependent wear models can predict the behaviour shown by POD tests.

2.4.3.2.4. Variables Requiring Further Consideration

Despite the large number of variables which have been shown to experimentally affect wear (as discussed in Section 2.3), current TKR computational wear models have only accounted for very few, mainly sliding distance, in some cases contact pressure, and in some cases either time independent or time dependent cross shear. Sliding distance and time dependent cross shear should certainly be represented in the formulation as the influence of each of these variables on wear has been well demonstrated [111, 210, 216, 315, 318]. The inclusion of contact pressure in the formulation of computational wear models is currently under debate, and some of the most recent wear models have been developed to be contact pressure independent [39, 40, 261, 357]. The reason for this controversy is that although wear does appear to be contact pressure dependent in POD tests, its influence is either non-linear, or confounding variables are present in the tests. POD tests have demonstrated increasing contact pressure to have the effect of initially increasing wear, but then decreasing wear once a threshold is exceeded [210, 216, 222, 318]. Therefore, POD tests have revealed the increase in contact pressure to result in a downward parabolic trend on PE and XPE wear. In response to this complex trend, many of the most recently developed computational wear models have been developed as contact pressure independent [39, 40, 261, 357]. Yet wear does appear to be influenced by contact pressure, even if the relationship is not of a simple linear form.

Tractive rolling has also been demonstrated to affect PE wear rates [217]. The majority of previous wear models [38-40, 259-261, 337, 356] have not implemented any

mechanism to account for the presence of tractive rolling, yet accounting for this variable might result in an increase in predictive accuracy.

To the author's best knowledge, all previous TKR computational wear simulations have neglected to model the effect of the lubricant on wear. In previous models, the lubricant was assumed to have a consistent effect under all conditions and has not been investigated. However, human synovial fluid is a complex colloidal lubricant, with both a liquid phase and a suspended solid phase consisting of proteins, which may exhibit complicated lubrication behaviour [70]. The composition of the lubricant has previously been demonstrated to have a substantial affect on TKR wear [164]. However, recent research suggests that not only does a change in lubricant composition affect TKR wear, but the conditions of the contact interaction may also cause changes to the lubrication and greatly affect wear. Protein denaturation and adsorption [70] studies suggest that changes to the contact interaction conditions may result in substantially different lubricant behaviour and thus wear. The lubricant has been shown to have a great effect on the PE and XPE wear of TKRs and the omission of the lubricant in computational wear simulations may be one of the greatest limitations to current TKR computational wear simulations.

Therefore, further research is needed to evaluate and develop the models used in TKR computational wear simulations. First, the predictive accuracy of TKR contact mechanics simulations must be evaluated to determine whether MBD simulations can accurately predict TKR contact mechanics, or whether the previously verified FE simulations should continue to be utilized. Next, computational wear model development research must be undertaken to develop a computational wear model with improved predictive accuracy.

2.5 Concluding Remarks

The long-term success of TKRs may be limited due to the wear of PE or XPE components. Therefore, there has been ongoing interest in improving our understanding of TKR wear, as well as to develop tools for the evaluation of wear which may enable the design optimization of TKRs for the reduction of wear. In general, the prediction of the wear of tribological systems is highly complex due to the complex interactions between the many variables which influence wear. Surface characteristics and interactions are very important to understanding wear (Figure 23). Physical and chemical interactions may result in the formation of various layers near the surface of a solid and each layer may have unique tribological properties (Section 2.2.1). Additionally, the surfaces of solids exhibit a surface texture which may be characterized by surface roughness, waviness, lay and flaws. An understanding of surfaces, including the presence of asperities and valleys is essential to understanding the wear process and wear mechanisms. It has been observed that solid surfaces in contact may require a force to be applied to cause relative motion between the solids (Section 2.2.2). The observed friction force has been suggested to be caused by a combination of the force required to overcome the adhesive forces between contacting asperities and the force required for the elastic deformation, plastic deformation and ultimate fracture of contacting asperities. These forces are therefore also affected by the surface layers and surface texture present, among other factors. A portion of the energy dissipated through friction may result in wear due to the adhesion of contacting asperities (adhesive wear) or the deformation and ultimate fracture of material (abrasive wear) through asperity contact (Section 2.2.3).

Additionally, wear may occur through fatigue, impact, chemical, electrical or through any combination of mechanisms. Since the wear of modern TKRs has been demonstrated to occur mainly through adhesive and abrasive wear, these wear mechanisms are particularly relevant to the present thesis. The wear of materials and the interactions of asperities are greatly affected by lubrication. Fluid film, mixed, boundary and specifically colloidal boundary lubrication regimes were discussed (Section 2.2.4).

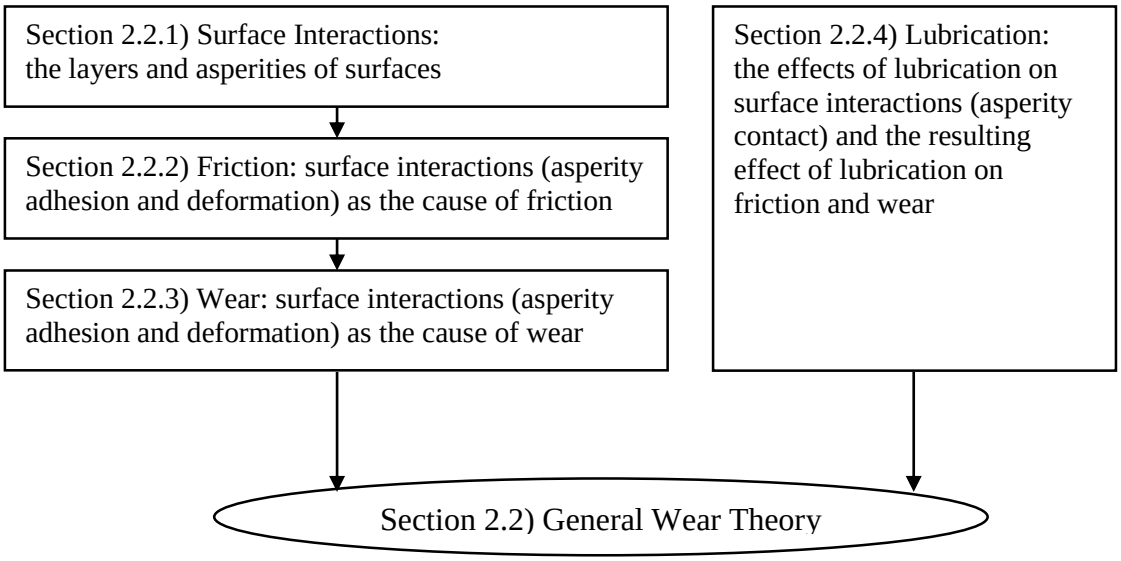

Figure 23: Relationships between the topics of the literature review for general wear theory.

Based on the general wear theory presented in Sections 2.2.1 - 2.2.4 the strengths and weaknesses of various methods and models for the general computational simulation of wear were discussed (Section 2.2.5) (Figure 24).

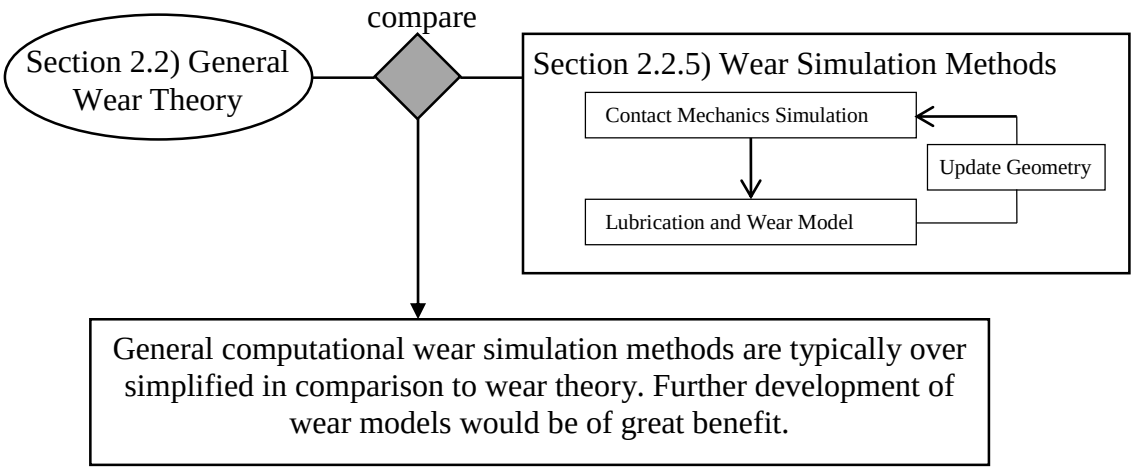

Figure 24: Consideration of general computational wear simulation methods compared to general wear theory.

The wear of TKRs specifically, was discussed in Section 2.3, based on the general tribological knowledge and theory presented in Section 2.2. The various factors known to influence PE and XPE wear were reviewed (Section 2.3.1) and discussed in terms of the energy dissipation theory of wear, which specifies wear to be proportional to the energy dissipated due to asperity adhesion and asperity deformation. The uncertainty as to the effects of contact pressure on TKR wear was also identified. The lubrication of TKRs and the effect of lubrication on asperity adhesion and deformation was also discussed (Section 2.3.2). Lastly, the importance of several clinical implementation and design variables was discussed, including TKR articular conformity, modularity and backside wear, as well as insert thickness (Section 2.3.3) (Figure 25).

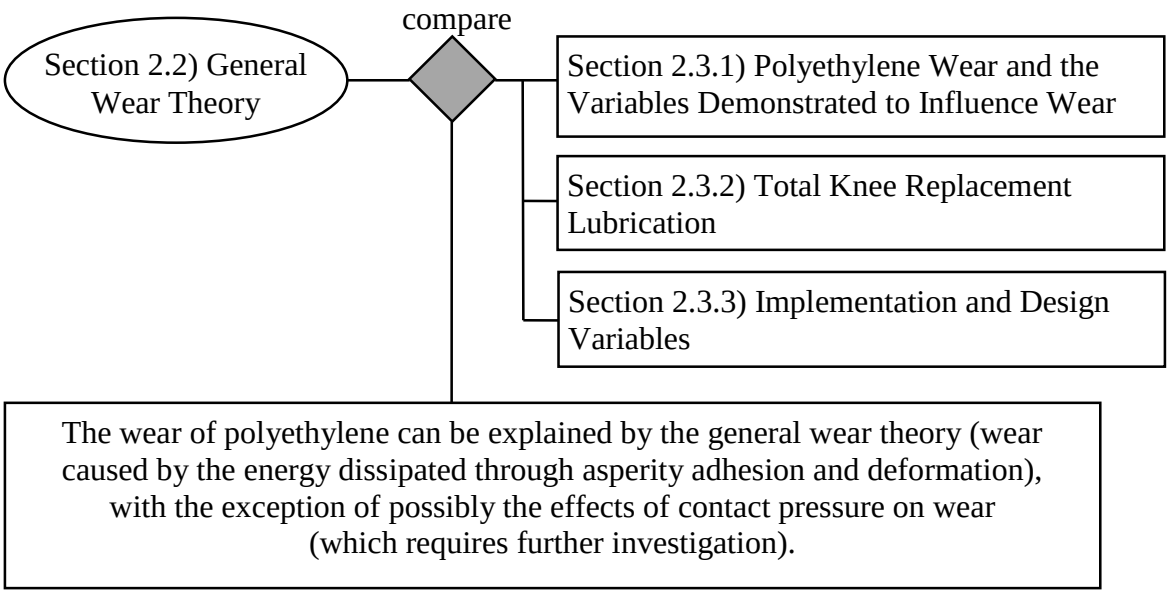

Figure 25: TKR wear theory literature review.

The currently available methods for the evaluation of TKR wear were reviewed, including *in vivo, in vitro* and *in silico* methods (Section 2.4). *In vivo* wear assessment methods are of great value because they have the greatest clinical relevance to how the TKR will perform in a patient (Section 2.4.1). *In vivo* wear assessment methods are very useful for indicating general trends and for confirming the general success or issues of a TKR, but does not provide sufficient information or control to enable the optimization of TKR designs for the reduction of wear. *In vitro* wear testing methods are very beneficial for verifying the wear performance of a design and enable increased control of the test conditions in comparison to *in vivo* wear assessment methods (Section 2.4.2). However, *in vitro* wear testing methods lack the time and cost efficiency necessary to conduct the wear optimization of TKR designs. *In silico* computational wear simulations have

previously demonstrated the necessary cost and time efficiency suitable for the wear optimization of TKRs, yet have demonstrated insufficient correlation strength for the prediction of TKR wear (R^2<0.65, Section 2.4.3). Therefore, the predictive accuracy of computational wear simulations must be improved in order to enable TKRs to be optimized for the reduction of wear through computational wear simulation. Computational wear simulations can utilize FE simulations for the accurate prediction of TKR contact mechanics (2.4.3.1). MBD simulations predict TKR contact mechanics with improved computational efficiency over FE simulations, however the accuracy of MBD simulations requires further investigation before such simulations be used as part of TKR computational wear simulations. Various computational wear models have been developed for TKRs (Section 2.4.3.2), yet all of the available models lack the sufficient level of accuracy to enable the wear optimization of TKRs.

Further research must be conducted to determine whether MBD simulations are sufficiently accurate for the simulation of contact mechanics, or whether the previously verified FE simulation methods should be utilized. Additionally, the influence of insert thickness, an important clinical implementation variable, on wear should be analyzed. To overcome the limited accuracy of existing computational wear models, a new computational wear model must be developed in order to improve the predictive accuracy of computational wear simulations. Since the effects of contact pressure on wear are currently unknown, contact pressure must be investigated to improve our understanding of wear and enable more accurate computational wear simulation models to be developed. A lubrication model for TKRs must be developed for computational wear simulations to improve their predictive accuracy. Finally, the developed models must be

evaluated by comparison to *in vitro* wear testing methods to evaluate the accuracy and correlation strength of the predictive models. The following chapter (Chapter 3) will discuss the methods utilized to achieve these research objectives.

Chapter 3

Methods

3.1 Introductory Remarks

Research was conducted to develop computational models for the prediction of TKR wear. First, the computational simulation of TKR contact mechanics was investigated (Section 3.2). Next, the contact mechanics simulation model was implemented, along with an existing computational wear model, for the computational wear simulation of TKRs with varying tibial insert thickness (Section 3.3). Unfortunately, the limited accuracy and insufficient correlation strength (R^2<0.65) of existing computational wear models limits the potential benefits of TKR computational wear simulations. Therefore, a new computational wear model was developed and verified by comparison to POD and knee simulator wear tests (Section 3.4). Knee simulator wear tests and computational wear simulations, using the newly developed computational wear model, were conducted to investigate the effects of contact pressure on wear and evaluate the predictive capabilities of the newly developed wear model under varying contact pressure

conditions (Section 3.5). Next, a lubrication model was developed in order to account for the effects of the lubricant on wear (Section 3.6). Lastly, the computational models developed within this thesis were assessed by comparison to POD and knee simulator wear test results (Section 3.7).

3.2 Simulation of Contact Mechanics

The computational simulation of wear first requires the accurate evaluation of contact mechanics. Therefore, research was first conducted to develop TKR contact mechanics models and evaluate the methods for the simulation of TKR contact mechanics. The contact mechanics simulation method demonstrated to provide the greatest computational efficiency and predictive capabilities would then be implemented for all future research on computational wear simulations.

Both FE and MBD simulations have previously been utilized in the literature for the prediction of contact mechanics (Section 2.4.3.1). The author of this thesis [259, 335] has previously established the accuracy of FE simulations for the prediction of TKR contact mechanics. The predictive accuracy of MBD computational wear simulations, however, has not been previously evaluated across a very broad range of conformity and loading conditions. Therefore, this section first presents a protocol previously developed and verified by the author [259, 335] for the prediction of TKR contact mechanics through FE simulation, followed by the development and evaluation of an optimized MBD simulation PO relationship for the prediction of TKR articular contact mechanics.

3.2.1 Finite Element Simulation

The FE simulations of the present research were developed and performed according to a protocol previously developed by the author [335]. The protocol has even been previously demonstrated by the author to accurately predict the backside micromotion of

TKR tibial inserts [335]. In each case, the models were developed using Abaqus/Explicit (Abaqus 6.131, Simulia Inc., Providence, RI), as the explicit integration method was required to solve the dynamics and nonlinearity of the problem. FE models were developed in the present thesis for several TKR product designs, which were simulated under a wide range of operating conditions. The TKR product designs included two commercial TKR products (Sections 3.2-3.7), as well as several parameterized TKR designs (Section 3.2).

The two commercial TKR products included the Anatomic Modular Knee (AMK) as well as the PFC-Sigma (DePuy-Synthes Inc., Warsaw, IN). Manufacturing drawings of the AMK, as well as the computer aided design models of the PFC-Sigma, were provided directly by DePuy-Synthes. The AMK drawings were of a size 3 femoral component and tibial tray, along with a size 3-4, 10 mm nominal thickness tibial insert. The computer aided design models were then created by the author using Solidworks (Solidworks, Simulia Inc., Providence, RI) based on the manufacturing drawings. The PFC-Sigma models were of a size 3 femoral component and tibial tray, as well as of a size 3-4, 10 mm nominal thickness tibial insert.

Computer aided design models of simple parameterized TKR components were also developed and utilized in the research of this thesis. Parameterized TKR components were utilized to represent TKR components of varying conformity and contact conditions. The computer aided design models of all parameterized components were created by the author using Solidworks. The geometry of all parameterized components is stated in the following sections of the present thesis for each study in which the parameterized components were implemented. POD studies were also simulated in the

present thesis to replicate POD experiments which had previously been performed and published. For each POD study, the geometry of the pin and disk were modeled in Solidworks according to the POD geometry of the experiment as specified by each publication.

For all simulations, the computer aided design geometry of the TKR and POD components were directly imported into Abaqus. The femoral and tibial tray components of TKRs, as well as the disks of POD tests, were modeled as rigid bodies for computational efficiency. This simplification enabled improved computational efficiency and was deemed appropriate since the modulus of elasticity of the CoCr alloy components is approximately 350-times greater than that of the PE or XPE material [3]. The PE or XPE material was always modeled as a deformable body with a density of 0.936 mm^3/kg. The PE or XPE material model utilized the J_2-plasticity model parameters developed by Bergström et al. [339] (Table 2). As discussed in Section 2.4.3.1, this J_2-plasticity material model has previously been demonstrated by the author to provide accurate results for the simulation of PE and XPE in TKRs. The modulus of elasticity was specified to be 1051 and 1216 MPa for the PE and XPE materials, respectively [3, 339]. Penalty contact was defined for the contact interactions between the contacting components. The CoCr-on-PE contact interactions were modeled using Coulomb-friction, including a coefficient of friction of 0.04 and this value was in agreement with experimental POD tests [329, 334, 340].

Table 2: Non-linear stress (σ_y) - strain (ε^p) values of the J_2-plasticity model.

Strain ε^p (%)	0.0	0.03	0.11	0.55	0.98	1.09	1.34
Stress σ_y (MPa)	12.1	21.4	23.8	44.0	92.4	135.0	515.0

The femoral and tibial tray components of TKRs, as well as the disks of POD tests, were modeled as analytical rigid surfaces when the geometry was compatible, or discrete rigid surfaces when the component geometry could not be modeled as an analytical surface. Components which were modeled as discrete rigid surfaces included only the necessary surfaces which would contact the PE or XPE tibial insert. Discrete rigid surfaces included a mixed mesh dominated by quadrilateral elements (for their speed of convergence), as well as triangle elements (for their flexibility in dealing with complex geometry). The PE or XPE components were modeled using a mixed mesh dominated by hexahedral elements (for their speed of convergence) and also including tetrahedral elements (to handle complex geometry). For all simulations, convergence studies were performed in order to limit discretization error. The convergence criteria required that double the mesh density must result in less than a 5% change to the key output variables (which included contact pressure, contact area and sliding vectors).

Loading and boundary conditions were applied directly to the rigid body components (Figure 26). TKR simulations included vertical loading, anterior-posterior displacements or loading, and internal-external rotation or moment applied to the tibial tray. The tibial tray was also specified to permit unconstrained varus-valgus rotation and medial-lateral

translation. The flexion-extension of the TKR was specified for the femoral component. Meanwhile for the POD simulations, the vertical loading was applied to the analytical rigid disk and the pin's lateral displacements and rotations were applied to the upper (non-articulating) surface of the pin. The loading and displacement conditions for both the TKR and POD simulations were specified to replicate the specific conditions of each *in-vitro* test being simulated.

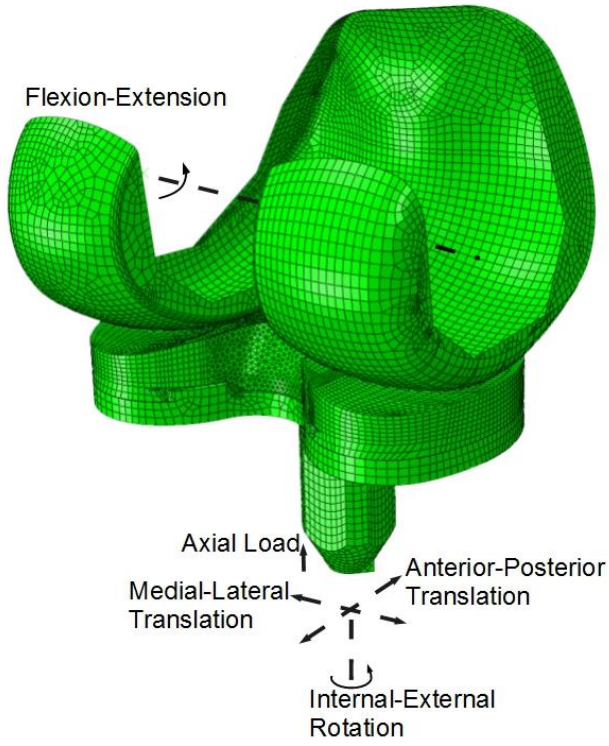

Figure 26: Meshed FE model of a TKR (AMK).

3.2.2 Multibody Dynamic Simulation

The PO relationship of a MBD simulation must be valid for a wide range of conformity and loading conditions to be relevant for all conditions that may be encountered by a TKR. Therefore, the development of an optimized PO relationship required a series of simulation scenarios which represented the range of contact conditions which may be encountered by the TKR. The optimization of the PO relationship based on the results of a single TKR simulation would lead to improved results for that single TKR design, yet may provide inaccurate results for situations outside of the conditions for which the model has been optimized. In order to optimize across a wide range of conditions, many simplified axis-symmetric simulations were conducted.

The axis-symmetric simulations were conducted under varying load and conformity (Table 3). The radius of the femoral component was specified to be 35 mm for all axis-symmetric simulations and this radius was specified to be similar to the sagittal radius of modern TKRs. The radius of the PE component varied from 36 mm to a completely flat component to provide consideration for highly conforming to minimally-conforming designs. The load was varied from 50 N to 4000 N to account for the wide range of loading conditions which may be experienced by the TKR components [259, 335], with a maximum value of approximately 1.5 times greater than the peak load of the ISO 14243-3 gait cycle (Figure 27) [250]. The 4 conformity scenarios, combined with the 8 loading conditions, provided a total of 32 simulation scenarios.

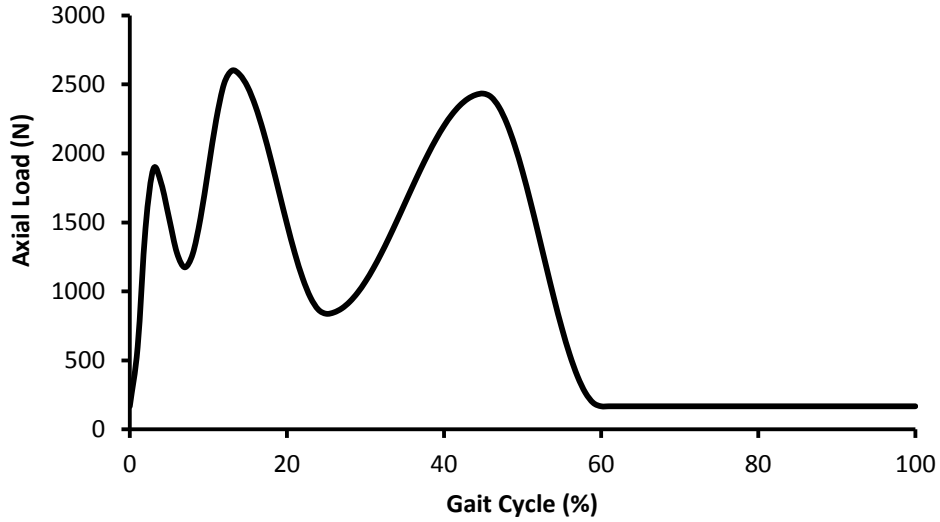

Figure 27: Axial loading over the gait cycle for the knee simulator wear testing standard ISO 14243.

Table 3: Axis-symmetric simulation parameters and conditions.

Femoral Radius (mm)	35							
PE Radius (mm)	36	45	72	Flat				
Load (N)	50	150	300	450	600	1000	2000	4000

The axis-symmetric cases were first evaluated by FE simulation (according to Section 3.2.1). A python script (Stichting Mathematish Centrum, Amsterdam, Netherlands) was written by the author to automatically conduct the FE simulations, MBD calculations, compare the results and optimize a MBD PO relationship based on the results. The python script was used to prepare the FE simulations and submit the simulation jobs for analysis to Abaqus/Explicit. The python script then analyzed the contact area, contact

pressure (P) and location of each node on the surface of the PE component. The necessary displacement (x) at each node in the corresponding MBD simulation was then calculated by the python script to match the contact area of each of the FE simulations. The displacement (overclosure) of each node required for the MBD simulations were then plotted against the contact pressure values of each corresponding node from the FE simulations. The python script was then used to implement least squares minimization curve fitting techniques to determine the optimized parameters (a, b) for the fit of a natural logarithmic equation to the data (Equation 8). The coefficient of determination of the fitted curve was then finally calculated by the python script.

$$P = a \cdot \ln(x) + b \tag{8}$$

Following the completion of the axis-symmetric simulations and the development of the optimized PO relationship, a series of three dimensional FE and MBD simulations were conducted to evaluate the optimized PO relationship. First, a series of static simulations were conducted using parameterized TKR components with varying geometric parameters to control the conformity of the design (Table 4). The conformity combinations corresponded to a highly conforming TKR design with high conformity in the sagittal and coronal planes, a medium conforming TKR design which was highly conforming in the coronal plane only, and a low conforming TKR design consisting of a flat PE insert. The component dimensions were based upon the approximate measurements from many existing TKR designs of high, medium and low conformity (Table 4). The simulations were conducted under multiple loading conditions including

170, 1300 and 2600 N, corresponding to the loading during the swing phase, moderate loading and peak loading of the ISO 14243-3 gait cycle [250], respectively. The 3 sets of geometric conformity and 3 sets of loading conditions provided a total of 9 static simulation scenarios. The predictive accuracy of MBD simulations with the optimized PO relationship was assessed by comparison to the results of the previously verified FE simulation method with the J_2-plasticity material model. The femoral components were once again modeled as analytical rigid surfaces. The FE simulations utilized deformable first order hexahedral elements, while the MBD simulations utilized rigid first order quadrilateral elements for the PE components. Mesh densities were once again determined by convergence analyses.

Table 4: Geometric parameters for static TKR simulations.

	Sagittal Radius (mm)	**Coronal Radius (mm)**
Femoral Component	38.0	25.5
PE Insert (High Conformity)	45.0	27.0
PE Insert (Medium Conformity)	Flat	27.0
PE Insert (Low Conformity)	Flat	Flat

As a final comparison, a TKR was simulated during a dynamic gait cycle according to ISO 14243-3 [250]. The Anatomic Modular Knee (AMK®, DePuy-Synthes Orthopaedics Inc., Warsaw, IN) was selected for the analysis. The AMK was selected as it was previously estimated to hold a large percentage of the TKR market [335, 342].

Additionally, the AMK was selected because the low conforming design of the AMK was expected to be challenging for the accurate prediction of TKR contact mechanics. The geometric models of a size 3, 10 mm nominal thickness, cruciate retaining tibial insert, and a size 3 femoral component, were supplied by DePuy-Synthes Orthopaedics (Warsaw, IN). The contact pressures and contact area of the PE tibial insert articular surface were recorded throughout the simulations for both the MBD and FE simulations.

Through this research, an optimized PO relationship was developed using axis-symmetric paired MBD and FE simulations. The accuracy of the optimized PO relationship for the prediction of TKR contact mechanics using MBD simulations was then evaluated through paired comparisons of the MBD simulation predictions to the results of FE simulations following the previously verified protocol (Section 3.2.1). Acceptance criteria for the MBD simulation method was specified to permit no more than 15% absolute maximum deviation between the MBD and FE simulation results for contact pressure and contact area predictions during the TKR contact mechanics verification simulations. The ability of the MBD simulation to meet this acceptance criterion would support the implementation of MBD simulations for future computational wear simulation research. Meanwhile, if the acceptance criterion was not met, then all further research in this thesis would utilize FE simulations, rather than MBD simulations, for the prediction of contact mechanics. Additionally, the general recommendation would be made for researchers to implement FE simulations instead of MBD simulations for the prediction of TKR contact mechanics if the acceptance criterion was not met by the MBD simulations.

3.3 Computational Investigation of the Effects of Insert Thickness on Wear

Computational wear simulations typically involve the prediction of TKR contact mechanics, followed by the utilization of those contact mechanics results in a computational wear model for the prediction of wear. In the previous section (Section 3.2) a method was selected for the prediction of TKR contact mechanics. In the present section, the TKR contact mechanics simulations were combined with an existing computational wear model for the prediction of TKR wear. These computational wear simulations were performed to investigate the effects of an important clinical implementation variable, insert thickness, on wear. An understanding of how insert thickness may affect wear performance is essential, as a large range of insert thicknesses are necessary to enable surgeons to appropriately balance the soft tissue around the TKR [254]. However, the insert must still also provide appropriate long term wear performance.

Computational simulations were performed to analyze the effects of insert thickness on contact pressures, sliding distances and wear. Simulations were performed for both PE and XPE bearing materials with low oxidation potentials to represent modern bearing materials. The XPE material was represented as a 10 MRad, highly crosslinked, material so that the PE and XPE materials would represent the two extremes of non-crosslinked and highly crosslinked materials. Five insert thicknesses were considered, 5, 10, 15, 20, and 25mm in order to investigate how the contact pressure, sliding distances and wear would vary across a range of tibial insert thicknesses. The PFC-Sigma (DePuy-Synthes

Inc., Warsaw, IN) was selected for the simulations to represent the design of a modern TKR. All TKR components were of size 3. A CAD model of each component was provided by DePuy-Synthes and the geometry of the tibial insert was modified in Solidworks to create the various thicknesses without modifying any dimension apart from thickness.

Cumulative backside sliding distances and wear have been shown to be affected by the interference fit between the tibial insert and the tibial tray locking mechanism [335]. Interference fit, or press-fit, refers to the amount of geometrical overlap between two components. To investigate the effects of interference fit on backside sliding distances and wear, a second set of FE simulations were conducted utilizing inserts with peripheral dimensions increased by 0.254 mm in the region of the locking mechanism. Therefore, the total number of simulated conditions was twenty (2 materials x 5 thicknesses x 2 levels of interference fit).

The FE simulations for the evaluation of TKR contact mechanics were conducted in Abaqus/Explicit according to the previously discussed protocol (Section 3.2.1). The TKR was simulated under the displacement and loading conditions of ISO 14243-3; 2009 [250]. The thoroughly established and evaluated wear model of Turell et al. [60] was selected for the computational PE wear model. The model was applied according to the implementation of Strickland and Taylor [40]:

$$W_{depth} = k \cdot CS \cdot P \cdot S \tag{9}$$

where H is the wear depth, k is the wear constant, CS is the cross shear, P is the contact pressure and S is the sliding distance during the current time increment. The model of Turell et al. [60] has been demonstrated to have improved predictive power (R^2=0.60) over the historical standard of Archard's wear law (R^2=0.12) [40], which has been commonly implemented in the past [38, 111, 259, 260, 337, 348, 349]. The time dependent cross shear and energy dissipation wear model discussed later in this thesis (Section 3.4) has since been established to have improved correlation strength for the prediction of TKR wear over the wear model of Turell et al. [60]. However, the present research was conducted prior to the development of a new computational wear model. Furthermore, the wear model of Turell et al. [60] was still expected to provide valuable insight into the effects of insert thickness on wear, despite its limitations of only providing consideration for contact, pressure, sliding distances and time independent cross shear. The alterations in insert thickness were mainly expected to influence articular and backside contact pressure, as well as backside sliding distances, all of which are considered by the wear model of Turell et al. [60]. Based on the specific and limited needs of the present research, the model of Turell et al. [60] was expected to provide meaningful results. Therefore, the previously existing wear model of Turell et al. [60] was implemented for the research of the effects of insert thickness on wear. For the Turell et al. wear model [60], articular wear constants of k=$3.3\cdot10^{-6}$ [40], and $1.65\cdot10^{-6}$ were implemented for the PE and XPE respectively. The articular wear constant for the XPE material was calculated proportional to the published PE value [40] based on published POD test wear rates for 10 MRad XPE compared to PE [355]. Backside wear constants were equal to the articular wear constant for the respective material multiplied by the

Mode-Mechanism factor of $2.36 \cdot 10^{-3}$ as determined by O'Brien et al. [259], which has been used to account for the differences in wear mode and wear mechanisms between the articular and backside surfaces. The computational wear model was implemented as a custom Python script written by the author to interface directly with Abaqus. A second, custom Python script was also written by the author to efficiently measure and report the peak contact pressures of the articular and backside surfaces, as well as the peak cumulative sliding distances of the backside surface. The peak contact pressure was defined as the maximum instantaneous contact pressure value for that particular surface at the particular time instant of 10% of the gait cycle. Cumulative sliding distances of the backside surface were defined as the sum of all sliding distances, in all directions, for a single node of the FE mesh over a single gait cycle. Peak backside cumulative sliding distance therefore refers to the greatest cumulative sliding distance value out of all the nodes on the backside surface.

The computational wear simulation predicted values and trends were then compared to clinical, knee simulator and independent FE simulation results. For the articular surface, the trends of the present computational wear simulation were compared to the trends of the static FE simulations of Bartel et al. [256, 257] and the implant retrieval study of Kilgus et al. [221]. For the backside surface, the wear trends predicted by the computational wear simulations were compared to the implant retrieval trends of Brandt et al. [7]. Finally, the overall wear rate predictions of the computational wear simulations were compared to knee simulator wear tests [16] and implant retrieval wear depth results [358]. The conditions of the ISO 14243-3 standard were intended to represent typical

patient kinematics and conditions. Therefore, the computational wear simulation results were expected to be somewhat relevant to the clinical results.

The results were analyzed regarding the effects of insert thickness on contact pressure, sliding displacements and wear for both the articular and backside surfaces of non-crosslinked PE and XPE tibial inserts. The effects of locking mechanism interference fit on backside sliding distances and wear was also analyzed for inserts of various thicknesses. The results of the present study were intended to provide the surgeon and engineer with an improved understanding of how insert thickness could affect insert wear, in order to ensure the longevity of TKRs *in vivo*.

3.4 Development of a Time Dependent Cross Shear and Energy Dissipation Wear Model

The previous sections have established the methods for the accurate evaluation of TKR contact mechanics (Section 3.2), as well as implemented a previously existing computational wear model for the computational simulation of TKR wear (Section 3.3). The implementation of a simple computational wear model may be beneficial to gain insight into the effects of small relative changes to TKRs, such as insert thickness (Section 3.3). However, the previously existing computational wear models have not demonstrated sufficient accuracy to enable the optimization of TKRs for the reduction of wear [40]. Therefore, the development of a new computational wear model was undertaken. The present research of this section proposes an energy dissipation wear model, which considers the time dependent molecular behaviour of PE, aspects of tractive rolling and contact pressure. This time dependent – energy dissipation wear model was evaluated, along with several other wear models, by comparison to pin-on-disk results, knee simulator wear test results under various kinematic conditions and knee simulator wear test results that were performed following the ISO 14243-3 standard.

3.4.1 Computational Wear Model Development

In the present study, energy dissipated at the articular interface was considered to be the main driving force causing the mobility of the molecular chains, and contributing to

wear particle generation as molecular bonds within the PE were severed. As discussed in Section 2.2.3, energy may be dissipated between two moving solid bodies in contact through the interactions of asperities. The adhesion between contacting asperities in motion requires either the breaking of the adhesive bonds, or the breaking of cohesive bonds thus resulting in adhesive wear. Additionally, the contact between asperities may result in deformation. In some cases this deformation may only be elastic, however plastic deformation and ultimate fracture of the material may also occur, resulting in abrasive wear (Section 2.2.3). Thus wear may be proportional to a particular fraction of the energy dissipated at the interface. For PE and XPE materials, the formation of deformed layers (Section 2.2.1) through directional strain hardening is also energy dependent and highly influences PE and XPE cohesion and wear. Therefore, a time dependent cross shear – energy dissipation computational wear model (TD-ED) was developed in the present study. The following equations of this section (Equations 10-17) were developed by the author of the present thesis to create the TD-ED wear model. The work (C_w) of a shear force exerted in a single direction over a given time interval for a specific area may be written as:

$$C_w = \mu \cdot P \cdot A \cdot S \tag{10}$$

where μ is the coefficient of friction, P is the contact pressure over the specified area, represented as A, and S is the sliding distance. The trends of POD wear tests [60, 210] have demonstrated a relationship between cross shear (CS) and work which may be best

described by exponential decay. This observed trend may be caused by the mobility characteristics of the molecular chains (Section 2.3.1), as the crystalline lamella realigns itself with the direction of sliding [60, 61, 210]. The CS (CS angle / 90) at the end of a time step (CS_e) may be written as:

$$CS_e = e^{-(C_w+B_w)/M_{mc}} \tag{11}$$

where, $$B_w = -M_{mc} \cdot ln(CS_i) \tag{12}$$

M_{mc} is a measure of the mobility of the molecular chain. B_w represents the theoretical work required to reach the CS at the initiation of the time interval (CS_i). The wear volume (V_{wear}) may then be modeled by the equation:

$$V_{wear} = R_w \cdot \left[\left(1 - e^{-(C_w+B_w)/M_{mc}}\right) - \left(1 - e^{-(B_w)/M_{mc}}\right)\right] \tag{13}$$

where R_w is a measure of the materials resistance to wear and is proportional to the maximum magnitude of wear that can be attained during infinite work done with a shear force in a single direction. The material parameters M_{mc} and R_w, could be determined theoretically or empirically derived from POD data as was performed in the present research to model the properties of GUR1050 non-crosslinked PE. The volumetric wear rate for sixteen POD tests [210, 216, 318] was predicted by the TD-ED wear model using a wide range of material parameters under an exhaustive search method [359]. The

material parameter combination which resulted in the smallest statistical error between the computational and POD wear rate results was selected.

To account for the effects of tractive rolling on wear, a sliding velocity (v) dependent coefficient of friction was added to the TD-ED wear model to generate the TD-ED-TR wear model. The sliding velocity dependent coefficient of friction has been included to replicate the increased coefficient of friction experienced during the transition from static or pure rolling conditions to the sliding condition, as experienced by TKRs (static coefficient of friction at the initiation of sliding) [307]. The coefficient of friction had a minimum value of 0.04 (corresponding to the kinetic coefficient of friction) and a maximum value of 0.24 (corresponding to the static coefficient of friction). These values were selected to be in agreement with POD test results [222, 307] and the rate dependent coefficient of friction (μ) was defined by the following equation.

$$\mu = 0.19 \cdot e^{-2v^2} + 0.04 \quad (14)$$

Currently, a great deal of uncertainty exists towards the effects of contact pressure on wear (Section 2.3.1). The wear of other materials has generally been demonstrated to increase with increasing load [111] and the TD-ED-TR wear model presented above would similarly predict such behaviour. However, the effect of contact pressure on PE or XPE wear rates has been demonstrated to result in a downward parabolic trend under constant loading, as discussed in Section 2.3.1. The results of POD tests therefore suggest that a threshold exists at a contact pressure of approximately 3 MPa, at which point

additional contact pressure results in reduced wear rates (Section 2.3.1, Figure 12). The reason for this trend was previously not understood in the orthopaedic research community, but will be further investigated and explained in the following chapters of the present thesis (Section 3.5-3.7 and 4.5-4.7). However for the present (Section 3.4), a second variant of the TD-ED-TR wear model was developed in the attempt to replicate the complex empirical trends demonstrated by POD tests. The differences between the constant and dynamic loading conditions may be represented by the average energy dissipation rate over a specified time interval. The POD test results of Saikko [222], were utilized to identify an energy dissipation rate threshold and wear rate reduction correlation by the exhaustive search method [359]. The energy dissipation rate factor (*ERF*) was represented as:

$$ERF_i = f\left(\frac{EDR}{EDR_{ref}}\right)^{-1.44} \tag{15}$$

$$ERF = \begin{cases} 1, & ERF_i > 1 \\ ERF_i, & ERF_i \leq 1 \end{cases} \tag{16}$$

where f is a constant and *EDR* is the average rate of work of a standardized area over a standardized time period. EDR_{ref} is a reference rate, corresponding to the initiation of decreased wear rates with increasing energy dissipation rates. The *ERF* was then implemented in the TD-ED and TD-ED-TR wear models through the appending of the term to equation 4:

$$V_{wear} = R_w \cdot \left[\left(1 - e^{-(C_w + B_w)/M_{mc}}\right) - \left(1 - e^{-(B_w)/M_{mc}}\right)\right] \cdot ERF \qquad (17)$$

3.4.2 *In Silico* Experimentation and Verification

Three sets of experiments were conducted to evaluate and compare the accuracy of the TD-ED-TR wear model to several published wear models (Table 5, Figure 28). The previously available wear models which were considered included Archard's wear law (M1) [111], the model of Turell et al. (M2) [60], and the model of Abdelgaied et al. (M3) [261]. Wear was also modeled with a time dependent - contact pressure independent wear model (CPI, M4) which was based on the TD-ED wear model with the contact pressure term removed. This CPI wear model was intended to provide a means for comparison to other time dependant wear models which are contact pressure independent. Finally, the TD-ED wear model including the *ERF* was utilized both without (TD-ED, M5) and with (TD-ED-TR, M6) the sliding velocity dependent coefficient of friction.

For the first set of experiments, FE models of sixteen published POD tests [210, 216, 318] were generated. The volumetric wear rates predicted by each of the wear models were compared with the published POD result.

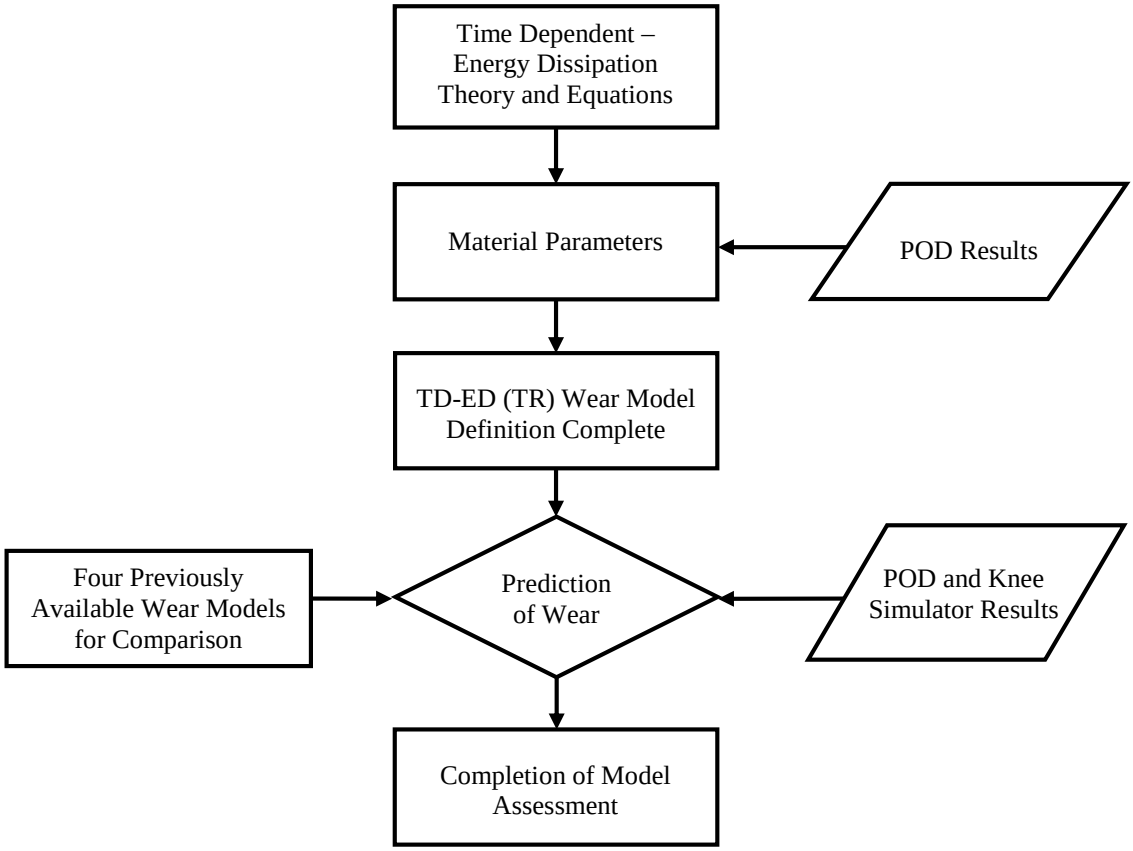

Figure 28: Wear model development and multi-model comparison flow chart.

Table 5: Wear model comparisons.

Model	Model Name	Contact Pressure	Sliding Distances	CS (Time Indep.)	CS (Time Dep.)	Tractive Rolling	Equation	Parameters
M1	Archard's Wear Law	☑	☑				$W_{depth}=k \cdot P \cdot S$	$k=2.0 \cdot 10^{-7}$ mm^3/Nm
M2	Turell et al.	☑	☑	☑			$W_{depth}=k \cdot CS \cdot P \cdot S$	$k=3.3 \cdot 10^{-7}$ mm^3/Nm
M3	Abdelgaied et al.		☑	☑			$W_{depth}=(a+b \cdot CS)^{(-1/c)} \cdot S$	$a=8.5 \cdot 10^{-65}$ $b=9.4 \cdot 10^{-60}$ $c=6.7$
M4	CPI		☑		☑		$V_{wear}=R_w[(1-e((-C_w/P)+B_w)/M_{mc})-(1-e(-B_w/M_{mc}))]$	$M_{mc}=1 \cdot 10^{-4}$ $R_w=3.0 \cdot 10^{-6}$
M5	TD-ED	☑	☑		☑		$V_{wear}=R_w[(1-e(-C_w+B_w)/M_{mc})-(1-e(-B_w/M_{mc}))]\ ERF$	$M_{mc}=1 \cdot 10^{-4}$ $R_w=3.0 \cdot 10^{-6}$
M6	TD-ED-TR	☑	☑		☑	☑	$V_{wear}=R_w[(1-e(-C_w+B_w)/M_{mc})-(1-e(-B_w/M_{mc}))]\ ERF$ [a]	$M_{mc}=1 \cdot 10^{-4}$ $R_w=3.0 \cdot 10^{-6}$

[a] where C_w is calculated with a rate dependent coefficient of friction

Table Abbreviations: CS - Cross Shear; Indep. - Independent; Dep. - Dependent
W_{depth} - Wear Depth; k - Wear Factor; P - Contact Pressure; S - Sliding Distance;
Additional equation symbols as defined above (Equations 10-17)

For the second set of experiments, FE simulations were performed for a TKR, the Anatomic Modular Knee (AMK). The geometric models were generated based on drawings provided by the manufacturer for size 3 components including a cruciate retaining PE tibial insert with a nominal thickness of 10 mm. In-silico wear simulations were conducted under four separate sets of kinematic conditions (Table 6). These kinematic tests enabled the influence of each type of motion on wear to be investigated individually. These same kinematic tests were previously utilized in a knee simulator

wear test by Kawanabe et al. [354] for the cruciate retaining Anatomic Graduated Component (AGC, Biomet Inc. Warsaw, IN) using 50% bovine serum. Although the TKR and lubricant of these knee simulator wear tests varied from that of the in-silico model, the trends demonstrated with respect to the influence of each kinematic condition on wear were expected to be similar. The first test investigated flexion motion only, resulting in pure sliding with minimal CS. The second test introduced internal-external rotation, in addition to the flexion of test 1, resulting in pure sliding with CS. The third test included the anterior displacement of the femoral component relative to the PE insert in addition to the conditions of test 2, which resulted in increased sliding distances relative to test 2. The fourth test replaced the anterior displacement of test 3 with posterior displacement, which resulted in the introduction of rolling/sliding motion (tractive rolling) and decreased sliding distances relative to test 3. To enable the comparison of wear rate trends, the relative wear rate increase (current test wear rate / wear rate of test 1) was calculated for the in-silico and knee simulator wear test results. The difference was calculated as the absolute difference between the predicted result and the knee simulator result divided by the knee simulator result.

Table 6: Input kinematics and relative wear rate increase values of the knee simulator wear tests for the second experiment.

Test	Kinematics	Relative Changes	Relative Wear Rate Increase ± SD
1	Flexion Only	Pure Sliding	1.00 ± 0.17
2	Flexion & IE	Test 1 + Cross-Shear	6.09 ±1.05
3	Flexion, IE & Anterior Displ.	Test 2 + Increased Sliding Distances	8.68 ±1.49
4	Flexion, IE & Posterior Displ.	Test 3 + Rolling/Sliding with Decreased Sliding Distances	10.80 ±1.85

Table Abbreviations: SD -Standard Deviation; IE - Internal External rotation; Displ. - Displacement

Finally, for the third set of experiments, FE simulations were performed with the AMK under ISO 14243-3 displacement controlled knee simulator wear test conditions [250]. The wear rates predicted by the six wear models were then compared to knee simulator wear test results for the same TKR under the same conditions generated by two independent sites [11, 251]. The PE surface damage depths (wear and creep) predicted for the AMK under the stated ISO standard were also compared to clinical PE surface damage depths determined by both radiography [62] and by implant retrieval analysis [360] to relate the predicted values to clinically relevant wear rates. The coefficient of determination (R^2) has commonly been used to evaluate computational wear models [39, 40, 259, 264, 326, 335]. The coefficient of determination compares the predicted or modeled value to the known value and can be calculated according to:

$$R^2 = 1 - (\sum(y_i - f_i)^2)/(\sum(y_i - \overline{y})^2) \quad (18)$$

Where y_i represents a known or experimental value, $\overline{y}$ is the average value of the known or experimental values and f_i represents the predicted or modeled value.

The FE models for each computational experiment were constructed using Abaqus/Explicit following the previously established protocol (Section 3.2.1). Python scripts were created to automate the process of wear calculation, geometric update and FE simulation cycles [259]. The relative predictive capabilities of the newly developed TD-ED and TD-ED-TR models were compared to those of several previously developed computational wear models from the literature. The increased consideration for additional variables known to affect wear, as well as the increased theoretical relevance, of the TD-ED-TR wear model was expected to result in the improved predictive accuracy of the TD-ED-TR wear model over the previously existing computational wear models.

3.5 Investigation of the Influence of Contact Pressure on Polyethylene Wear

The TD-ED-TR wear model developed in the previous section of this thesis (Section 3.4), was expected to result in the improved predictive accuracy of computational wear simulations. However, due to the uncertainty regarding the effects of contact pressure on wear, two variants of the TD-ED-TR wear model were developed. The first variant did not include the energy dissipation rate factor (*ERF*), which was added to the second variant of the model to match the trends demonstrated by POD tests conducted under varying loading. These POD tests have demonstrated trends of initially increasing wear with increasing contact pressure, followed by decreasing wear with increasing contact pressure [210, 216, 222, 318]. The mechanism and reason for this complex wear behaviour has not been previously explained. Previously existing computational wear models have also been unable to accurately predict this wear behaviour [38-40, 60, 61, 259, 261, 334, 336, 337, 348]. However, it remains unknown whether this same trend would occur in knee simulator wear tests, since knee simulator wear test results under varying load while keeping all other conditions constant have not been previously available in the literature. Therefore, further research is necessary to evaluate the effects of contact pressure on wear and identify the mechanisms responsible for any unexplained wear behaviour so that the accuracy of computational wear models can be improved further. Thus, in the present research, knee simulator wear testing was conducted under standard and increased loading to further investigate the influence of contact pressure on PE and XPE wear in TKRs. The TD-ED-TR computational wear model developed in the

previous section was then utilized in comparison to the knee simulator experiment results in order to evaluate the models accuracy under varying TKR contact pressure conditions.

3.5.1 *In Vitro* Knee Simulator Wear Tests

In vitro knee simulator wear testing was conducted to evaluate the effects of increased contact pressure on TKR wear. The PFC-Sigma TKR (PFC-Sigma, DePuy-Synthes, Warsaw, IN) was selected for the analysis to represent a modern TKR design. The PFC-Sigma includes a tibial insert comprised of GUR 1020 XPE sterilized using gamma irradiation with vacuum foil at 2.5-4 MRad to provide a moderately crosslinked XPE insert. This moderate level of crosslinking is typical of modern TKR designs [3]. TKR components of size 3 with a nominal XPE insert thickness of 10 mm were utilized. These particular TKRs had previously been used in a different 10 million cycle (MC) knee simulator wear test [253], under the loading and displacement conditions of the ISO standard 14243-3 [250].

A six station displacement controlled AMTI knee simulator (AMTI, Waltham, MA) was utilized to conduct the knee simulator wear testing. The right bank of the knee simulator was utilized, which included three dynamic wear stations (R1-R3) and two load-soak stations (R4-R5). Each wear station was subjected to the flexion-extension, vertical loading, anterior-posterior motion and internal-external rotation of the ISO standard 14243-3 or with increased vertical loading beyond the ISO standard. The load-soak stations were only subjected to the vertical loads and were used to account for the fluid absorption of the XPE inserts. Therefore, the XPE insert wear could be measured

gravimetrically by subtracting the average change in weight of the load-soak stations from the gravimetric weight loss of each wear station XPE insert.

Each wear station and load-soak station included a dedicated lubricant circulation system. The lubricant circulation system of each station included a peristaltic pump and a 500 ml heated reservoir which maintained a temperature of 37.5^{o}C. The peristaltic pumps circulated lubricant through the wear stations at an approximate rate of 100 ml/min. The lubricant was composed of bovine calf serum diluted with distilled water to a protein concentration of 17 g/l according to ISO 14243-3. Ethylenediaminetetraacetic acid was added (20 mM) to the lubricant to inhibit calcium deposits. Sodium azide was also added (0.2%) to the lubricant to inhibit microbial growth. All inserts were pre-soaked in the lubricant for six weeks prior to commencing the wear test to minimize the change in fluid absorption during wear testing.

A frequency of 1 Hz was used as the gait cycle frequency of all tests, in accordance with the ISO 14243-3 standard [250] and best practices for knee simulator wear testing [3]. Following each 0.5 MC cycle interval, each station was disassembled, the components were cleaned, the lubricant was replaced, and the XPE inserts were weighed. Each XPE insert was weighed using a high precision balance (XP205, Mettler-Toledo, Columbus, OH). Gravimetric measurements were converted to volume using an assumed XPE density of 0.935 mg/mm^3 [3]. Linear regressions were utilized to analyze the steady-state wear rate of the XPE insert of each wear station during each test, using the wear measurements which were recorded every 0.5 MC. The linear regression was not restricted to pass through the origin and the slope of the linear regression was defined to

be the steady-state wear rate (mm^3/MC). 95% confidence intervals were also calculated for the steady-state wear rate of the XPE inserts of each test.

The first test implemented the ISO 14243-3 standard for the loading and displacement conditions. The second test was conducted immediately after the first test and utilized the same components. The second test also implemented the stated ISO standard with the exception of the vertical load being increased 1.7 fold. Knee simulator wear tests are subject to inter-station experimental variability. Each test consisted of at least 1.5 MC or as many cycles as necessary to result in a wear rate 95% confidence interval of less than 20% of the wear rate value. The knee simulator wear rates for both the standard and increased loading tests were calculated based on the mean value of the slopes of linear regressions for each wear station.

3.5.2 *In Silico* Computational Wear Simulations

In-silico computational wear simulations were conducted to analyze which contact pressure – wear trend resulted in greatest agreement with the *in vitro* results, as well as consider the predictive accuracy of *in silico* computational wear simulations under varying TKR contact pressure conditions. FE simulations were conducted to analyze the contact interactions between the femoral component – XPE tibial insert and tibial tray – XPE tibial insert. The simulations were conducted using Abaqus/Explicit according to the previously established protocol (Section 3.2.1). Consistent with the *in vitro* experiments, size 3 PFC-Sigma TKR components were used, with a XPE tibial insert of 10 mm

nominal thickness. Three dimensional computer-aided-design (CAD) models of the components were obtained from the manufacturer.

The contact pressure and sliding displacement vector results of the FE simulations were used to predict XPE wear using the wear model developed in the preceding section of this thesis (Section 3.4). The implemented wear model features time dependent cross shear and energy dissipation wear prediction with consideration for tractive rolling. Three variants of the model were implemented, each of which utilized a different contact pressure – wear trend. The first model (linear, M1) predicts linearly increasing wear with increasing contact pressure according to the energy dissipation theory. The second model (non-linear, M2) includes a non-linear trend in agreement with the contact pressure – wear trends demonstrated by POD tests by using the ERF factor discussed in Section 3.4. The third and final model (independent, M3) predicts wear which is independent of contact pressure magnitude. The wear model parameter M_{mc}, which controls the rate of reorientation of the crystalline lamellae due to cross shear, was specified to be 3.20×10^{-4} [37]. The wear model parameter R_w, which controls wear magnitude, was specified to be 1.12×10^{-6} [37] for the linear (M1) model and was adjusted by iterative linear interpolation for the non-linear (M2) and independent (M3) models during the first test, to result in the same wear magnitude as the linear model and provide an even basis for comparison. All model parameters (M_{mc} and R_w) were maintained consistently throughout the standard and increased loading tests to evaluate whether each wear model variant could accurately predict the increase in wear due to the increase in load.

Throughout the wear process, the contact conditions continuously evolve due to material removal over time. For this reason, wear was predicted using multiple finite

increments to reach the total number of gait cycles of the *in vitro* tests. Each increment included a FE simulation to evaluate the contact conditions, the prediction of wear using the computational wear models and the update of the XPE insert geometry according to the predicted wear and creep. The number of geometric update increments was determined by convergence analyses to limit the geometry update discretization error.

The XPE inserts used in the *in vitro* testing had previously been utilized in a 10 MC knee simulator wear test under the standard loading and displacement conditions of the referenced ISO standard. To account for this within the *in silico* experiments, the previous study was also simulated to provide consistency between the *in silico* and *in vitro* experiments. The predicted wear rates of each computational XPE wear model variant (linear (M1), non-linear (M2) and independent (M3)) were compared to the *in vitro* wear values to evaluate which model resulted in the greatest agreement.

These *in vitro* knee simulator wear test experiments were conducted in order to identify the effects of contact pressure on the XPE wear of TKRs. The similarities and differences between POD and the knee simulator wear tests, regarding the effects of contact pressure on wear were discussed. The potential mechanisms responsible for this behaviour were considered, and the accuracy of computational wear simulations for the prediction of these results was discussed.

3.6 Development of a Colloid Mediated Boundary Lubrication Model

The lubrication of TKRs has previously been demonstrated to greatly influence the PE and XPE wear of TKRs [164, 232]. Furthermore, the lubrication of TKRs may be responsible for the complex wear trends observed under varying contact pressure as discussed in the previous section (Section 3.5). POD tests have demonstrated the trend of initially increasing wear rates, then decreasing wear rates, under increasing contact pressure [210, 216, 222, 318]. Knee simulator wear testing conducted for this thesis (Section 3.5) has demonstrated further complexities to the relationship between contact pressure and wear.

Including consideration for TKR lubrication in computational wear simulations could greatly improve the predictive accuracy of computational wear simulations. Yet, despite the importance of TKR lubrication, none of the previously published TKR computational wear simulations have incorporated a lubrication model, to the author's best knowledge. Since previous research has demonstrated the lubrication of TKRs to occur mainly in the boundary lubrication regime [70], the present research discusses the development of a colloidal protein mediated boundary lubrication (CBL) model to provide consideration for the effects of the lubricant on wear.

Human synovial fluid (as well as calf serum) may be considered a colloidal suspension containing proteins, along with other constituents (Section 2.3.2). The proteins have been shown to adsorb onto the surfaces of TKRs and alter their wear performance [70] (Figure 29). Proteins may adsorb on to the surfaces of TKR

components through physical or chemical interactions (Section 2.2.1). The adsorbed proteins may reduce adhesion between contacting asperities (in comparison to interactions without any adsorbed layers), thereby reducing adhesive wear (Section 2.2.3.1). Through altering the contact interactions of asperities, the adsorbed proteins may also affect abrasive wear (Section 2.2.3.2). However, the strength of the adsorption bond of a protein may be exceeded due to the shear between the contacting asperities, in which case the protein would be removed from the surface (Section 2.2.4.1). Following the removal of a protein from a surface, a new protein may adsorb to take the place of the removed protein due to the continued exposure of the surface to the colloidal suspension (Section 2.2.4.1).

The complexity of the lubrication of TKR components is further increased by the fact that different types of proteins exist within the synovial fluid or calf serum (such as albumin, α-1-globulin, α-2-globulin, β-globulin and γ-globulin; Section 2.3.2). The model was simplified by assuming that albumin, α-1-globulin, and α-2-globulin were sufficiently similar that these proteins could be grouped into one category (group-a) and that the β-globulin and γ-globulin proteins could be grouped into a second category (group-b). The grouping of these categories was selected based on the observed trends from the knee simulator wear tests of Brandt et al. [164]. Proteins may also exist in denatured states, their native states or intermediate states. Protein denaturation can occur through chemical, thermal and mechanical conditions [70, 72, 251, 361]. The articulation of TKR components results in thermal loads, as well as protein shear conditions due to the relative movement of the components. Both of these protein denaturation mechanisms are proportional to the rate of energy dissipation at the interface of the contact interaction

and the amount of time the proteins are exposed to this denaturation energy. The different types of proteins each exhibit different levels of conformational stability and therefore have differing levels of resistance to denaturation [72, 164]. Furthermore, the conditions of the lubricant, such as composition and ph, will also affect the conformational stability of proteins [72, 164]. The following research explains the development of a new computational wear simulation process which incorporates a colloid protein mediated boundary lubrication model.

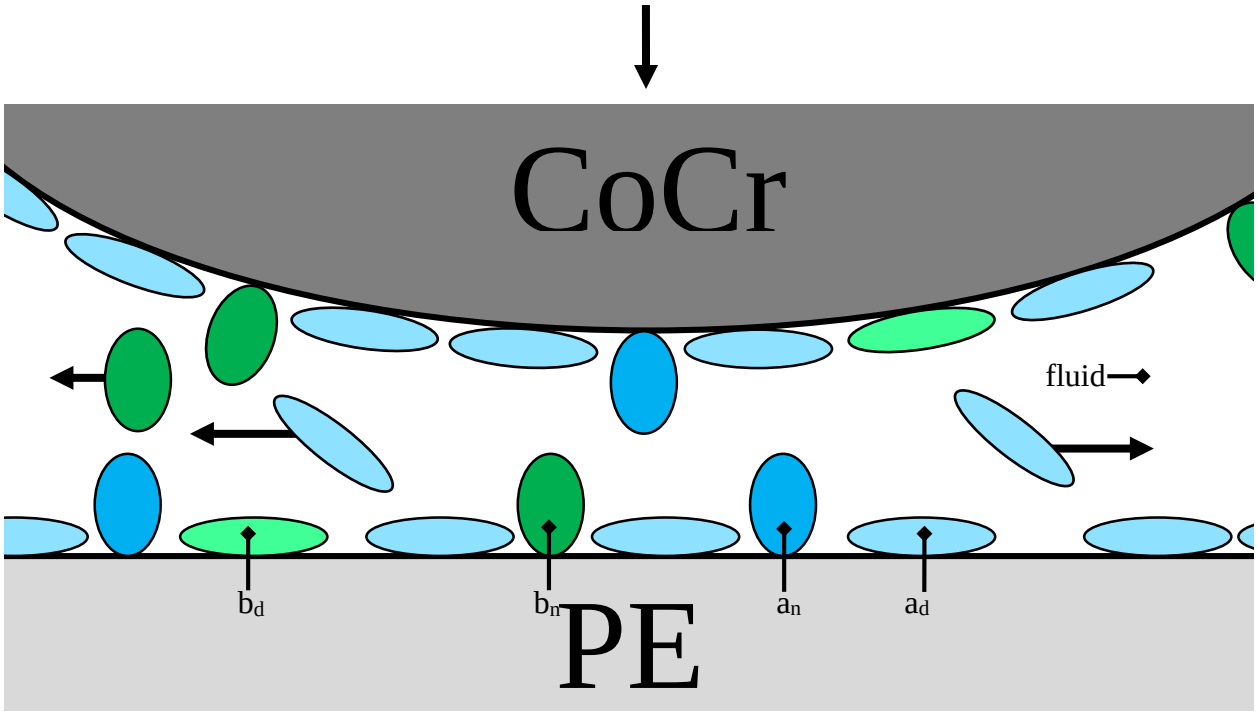

Figure 29: Symbolic representation of colloidal boundary lubrication with albumin or α-globulin proteins in native (a_n) and denatured (a_d) states, as well as β-globulin or γ-globulin proteins in native (b_n) and denatured (b_d) states. As the CoCr alloy and PE components approach each other, suspended proteins flow out of the articulation with the fluid, meanwhile adsorbed proteins will remain on the surfaces and may alter the interactions of asperities.

The majority of computational wear models in the past have utilized a process in which the solid-to-solid contact mechanics are evaluated (such as by FE simulation), followed by the implementation of the contact mechanics simulation results in a computational wear model for the prediction of wear (Figure 30). The geometry must then regularly be updated and the process repeated in wear cycles to simulate the influence of the geometric changes caused by previous wear on the current wear cycle.

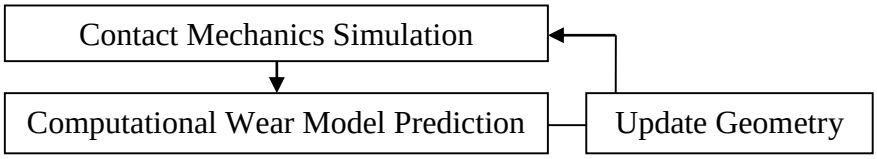

Figure 30: Typical computational wear simulation process.

However in order to provide consideration for the boundary lubrication of TKR components, a new process needed to be developed. The new computational wear simulation process had to enable the prediction of the denaturation of proteins, adsorption of proteins, and the influence of proteins on asperity contact in addition to the traditional components of the typical computational wear simulation process. A new computational wear simulation process was developed, which once again began with the prediction of contact mechanics through FE simulation (Figure 31). Next the results of the contact mechanics simulation are utilized, along with information of the initial lubricant conditions to calculate the fraction of proteins which would have become denatured. The knowledge of the composition of denatured and native proteins is then utilized to predict the adsorption of proteins onto the TKR component surfaces. Finally wear is predicted

using the TD-ED-TR wear model (Section3.4) along with a lubrication model which accounts for the effects of adsorbed proteins on the interactions of asperities and thus wear. To improve the simplicity of terminology, the TD-ED-TR wear model (which does not include the energy dissipation rate factor, *ERF*) will hereafter be referred to as the energy dissipation (ED) model, while the newly developed computational wear model which includes the ED model and accounts for the colloid mediated boundary lubrication, will be referred to as the CBL model. Each step of the new computational wear simulation process is discussed in the following sections (Sections 3.6.1 – 3.6.3). With the exception of Equation 23, all of the equations presented in Section 3.6 have been developed by the author of the present thesis for the development of the CBL model (Equations 19-22, 24-26).

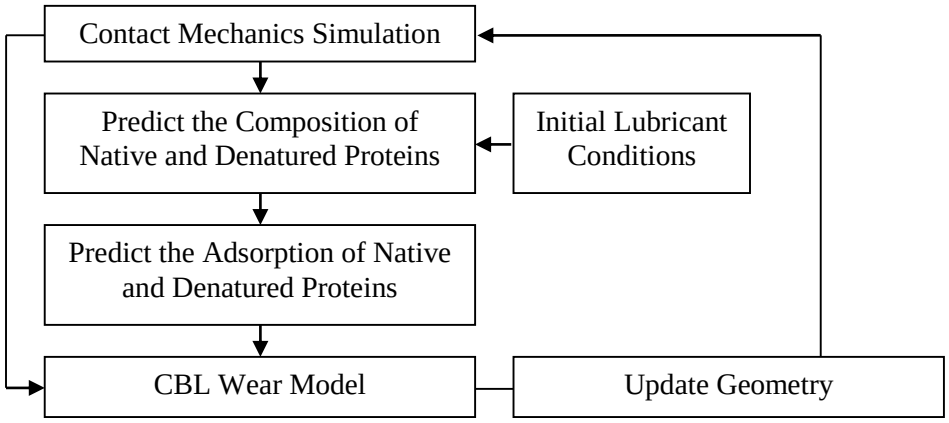

Figure 31: Computational wear simulation process for the CBL computational wear model.

3.6.1 Denaturation of Protein Colloids

The thermal protein denaturation research of Pico et al. [72] and the combined thermal and mechanical denaturation research conducted through knee simulator wear tests of Brandt et al. [164] have both demonstrated denaturation trends which could be well represented by a power law (Figure 32). The thermal induced protein denaturation research of Pico et al. [72] utilized fluorescence spectroscopy measurements of the thermal denaturation of albumin over time at constant temperature loads of 54, 64, 74, and 84^{o}C. The experiments were conducted using a medium sodium phosphate buffer (20 mM, pH 7.4) with a protein concentration of 20 g/l [72]. The knee simulator wear tests of Brandt et al. [164] were conducted under the ISO 14243-3 standard using the AMK TKR design (AMK®, DePuy-Synthes Inc., Warsaw, IN). The fraction of proteins which had become denatured due to the wear testing was measured by electrophoretic profiling, using samples of the lubricant obtained at 0.1 MC intervals.

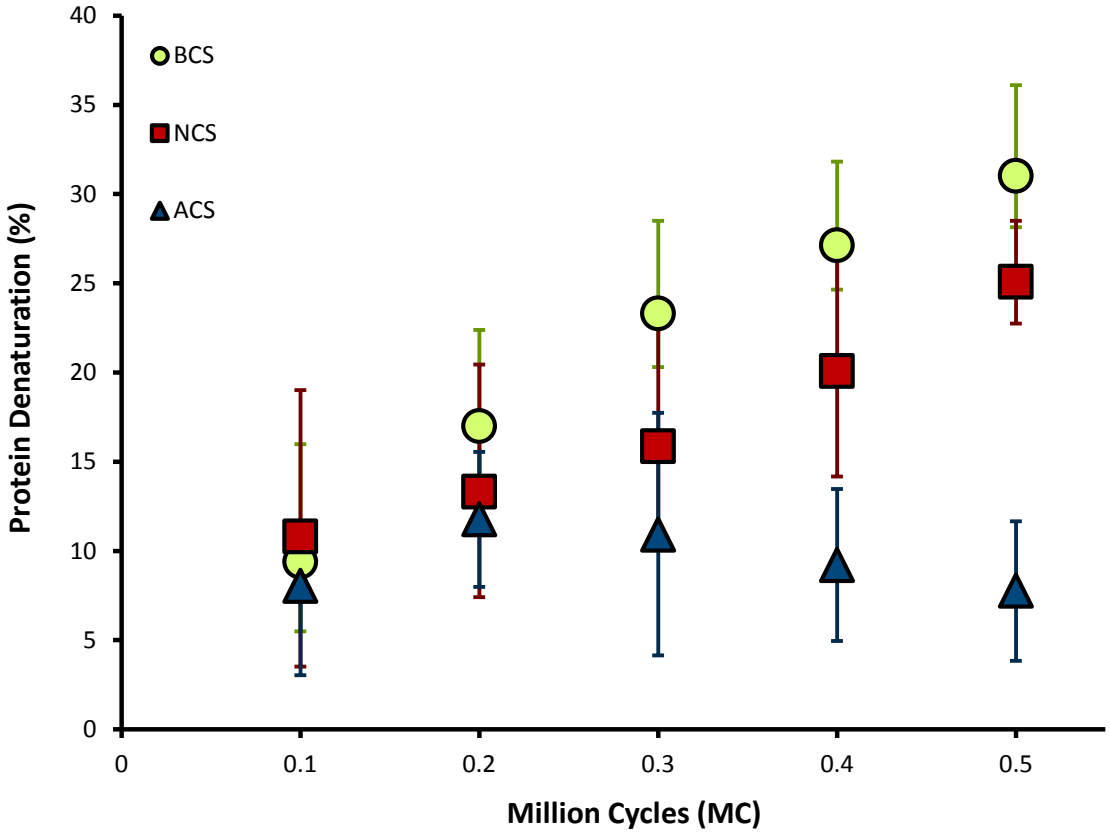

Figure 32: Protein denaturation results from the published knee simulator wear tests of Brandt et al. [164] for bovine calf serum (BCS), newborn calf serum (NCS), and alpha calf serum (ACS) (error bars show standard deviation).

Therefore the denatured fraction was represented by the function:

$$Denatured\ Fraction = D_{Jsm} \cdot (t)^{D_{power}} \tag{19}$$

where the *Denatured Fraction* represents the percent (%) of proteins in the fully denatured state. The variable *t* (minutes) is the length of time in which the lubricant is subjected to the denaturing energy. The variable D_{power} was calculated through least squares regression, utilizing the denaturation results reported in the literature [72, 164] to

identify a single value of D_{power} which would minimize the sum of the squares of errors between the modeled results and the experimental results. The variable D_{Jsm} is proportional to the rate of energy dissipation into the lubricant, as well as the composition of the lubricant and was represented as:

$$D_{Jsm} = J_{SM} \cdot (D_a \cdot F_{aby} - D_b) \tag{20}$$

where J_{SM} is proportional to the energy dissipated at the interface relative to the area of contact and the volume of the lubricant, as discussed in more detail below. Meanwhile, the $(D_a \cdot F_{aby} - D_b)$ portion of the equation is included to account for the relative difference in the amount of energy required for the denaturation of albumin and α-globular proteins relative to β-globulin and γ-globulin proteins [164]. Thus, F_{aby} is the fraction of β-globulin and γ-globulin proteins compared to the total mass of all proteins in the lubricant (%). Lubricants have varying concentrations of these multiple different types of proteins (Section 2.3.2). Each protein type has a different structure and will therefore have different denaturation characteristics. Therefore, in order to calculate the overall fraction of denatured proteins the relative differences in each proteins resistance to denaturation must be considered. For the sake of simplicity the proteins have been grouped into two categories, with albumin and α-globular proteins in the first group (group-a), and β-globulin and γ-globulin proteins in the second group (group-b). This grouping of proteins with most similar denaturation characteristics was specified according to the recommendation of Brandt et al. [164] based on knee simulator wear test

results. The linear function $(D_a \cdot F_{aby} - D_b)$ accounts for the difference in the required energy dissipation rate to result in protein denaturation based on the protein composition. To identify the constants D_a and D_b, computational simulations were conducted for a TKR to replicate the knee simulator wear tests of Brandt et al. [164]. The simulations were conducted according to the previously established TKR simulation protocol (Section 3.2.1). The computational simulations enabled the J_{SM} value of the experiment to be identified and the constants D_a and D_b were then determined using least squares regression to relate the experimental denaturation measurements to the equations above. The J_{SM} parameter is proportional to the rate at which energy is dissipated over an area of contact and is inversely proportional to the volume of the lubricant. As a result, increasing the lubricant volume will require an increased rate of energy dissipation or area to result in the same percentage of proteins to become denatured. The J_{SM} parameter can be calculated according to:

$$J_{SM} = F_s \cdot v \cdot A \cdot \left({}^{1}/_{L_{Vol}}\right) \tag{21}$$

where v represents the relative sliding velocity over the specified time interval (m/s). A represents the area of contact (m^2) and L_{Vol} is the volume of lubricant (m^3). Finally, F_s represents the shear force (N) in the direction of the articulation and can be calculated as:

$$F_s = \mu \cdot F_N = \mu \cdot (P \cdot A) \tag{22}$$

where μ represents the coefficient of friction, F_N represents the normal force (N) and P represents the contact pressure (Pa). The above equations can be used to predict the fraction of proteins which will become denatured due to the conditions of a given contact interaction.

3.6.2 Adsorption of Native and Denatured Protein Colloids

The equations above could be used to evaluate the relative fraction of denatured to native proteins surrounding the TKR components. Next, the adsorption of both native and denatured proteins to the contacting surfaces can be calculated using the previously calculated relative fraction of denatured to native proteins and knowledge of the initial lubricant protein concentration. The Langmuir adsorption model [267] was implemented to predict the adsorption of proteins onto the TKR surfaces. The Langmuir adsorption model can be written as [267]:

$$\Gamma = {\Gamma_{max} c}/{K_L + c} \tag{23}$$

where Γ is the amount of protein adsorbed per unit surface area of the adsorbent (mg/m^2) and Γ_{max} is the maximum adsorption capacity of the adsorbent (mg/m^2). The variable c represents the protein concentration of the lubricant solution (g/l) and K_L is the ratio of desorption and adsorption rate constants. For all native proteins, the Langmuir model parameters were specified according to Serro et al. [73] (Γ_{max}: 7.39 mg/m^2; K_L: 0.948).

Meanwhile, the parameters for the denatured proteins were obtained from the results of Heuberger et al. [70] (Γ_{max}: 5.38 mg/m^2; K_L: 0.75). Unfortunately, the Langmuir adsorption coefficients were determined at temperatures somewhat lower (25^{o}C) [73] than those experienced by TKRs (37^{o}C) [250]. The Langmuir adsorption model also includes many simplifications and does not account for temperature differences or hysteresis. Yet the model has demonstrated strong correlations for the prediction of albumin protein adsorption (R^2=0.997) under a range of protein concentrations (0.05-20 g/l) [73] and is expected to sufficiently approximate the adsorption behaviour of proteins to TKR components.

3.6.3 The Influence of Adsorbed Proteins on PE and XPE Wear

Lastly, the effects of the adsorbed proteins on the boundary lubrication and wear of PE and XPE in TKRs was investigated. First, the relative composition of the proteins adsorbed to the surfaces must be accounted for:

$$C_l = C_a \cdot F_{aby} + C_b \tag{24}$$

where C_l (%) represents the relative strength of adsorption bonds based on the fraction of albumin and α-globulin proteins relative to β-globulin and γ-globulin proteins. C_a and C_b were determined once again through the relationship demonstrated by knee simulator wear test results [164]. This linear equation specifies the relative strength of protein adsorption bonds based on linear interpolation between the strength of adsorption bonds

of group-a proteins (albumin, α-1-globulin, α-2-globulin) and group-b proteins (β-globulin and γ-globulin) based on lubricant composition. The same knee simulator wear tests, performed by Brandt et al. [164], which were used to establish the protein denaturation model (Section 3.6.1) were now utilized to evaluate the constants C_a and C_b. The constants were determined through least squares minimization using the knee simulator wear test results of tests conducted under the ISO 14243-3 conditions [250] with various lubricant compositions.

To analyze the influence of protein adsorption on wear, POD experiments [232] were selected from the literature which varied the lubricant protein concentration while monitoring the relative fraction of denatured proteins and the resulting wear rates during the experiments. The experiments were performed using a circularly translating POD, therefore the relative direction of sliding for the PE pin was continuously changing [232]. The tests were conducted with protein concentrations varying from 2.6-116 g/l [232]. Computational simulations were developed to replicate the conditions of the POD experiments. For each experiment, native and denatured protein adsorption was evaluated using the above equations. Wear rates were predicted using the ED wear model, with a linear relationship between contact pressure and wear according to the energy dissipation approach and without including consideration for the lubricant in the wear prediction. The differences between the POD wear rates and the computationally predicted wear rates without consideration for the lubricant were then correlated with the predicted magnitudes of adsorbed native and denatured proteins for each experiment. Least squares multivariable logarithmic regression was performed using a Python script to identify the constants L_a, L_b and L_c in the equation:

$$L_F = (L_a \cdot \ln(P_{Native}) + L_b \cdot \ln(P_{Denatured}) + L_c) \cdot C_l \qquad (25)$$

where P_{Native} and $P_{Denatured}$ represent the magnitudes of native and denatured proteins adsorbed to the wear surfaces (mg/m^2), respectively. L_F represents the effect of the lubricant on the wear of PE and XPE components in TKRs (%). Equation 24 accounts for the combined contribution of both the native and denatured proteins to the boundary lubrication of TKRs. The relative strength of protein adsorption bonds is accounted for through the C_l parameter. The natural logarithm form used to represent the native and denatured adsorbed proteins was selected based on the trends demonstrated by the POD experiments [232]. L_F can be combined with the previously developed ED wear model (as described in Section 3.4, Equation 13) to form the CBL wear model through multiplying the ED wear prediction value (V_{wear}, mm^3) by L_F:

$$V_{wear} = R_w \cdot \left[\left(1 - e^{-(C_w + B_w)/M_{mc}}\right) - \left(1 - e^{-(B_w)/M_{mc}}\right)\right] \cdot L_F \qquad (26)$$

The resulting CBL wear model provides consideration for the colloidal protein mediated boundary lubrication of TKRs, as well as providing consideration for the time dependent cross shear strain hardening of PE, the energy dissipation at the interface, and the effects of tractive rolling.

3.7 Verification of the CBL Computational Wear Model

The accuracy of the CBL model developed in the previous section (Section 3.6) was evaluated through comparison of the CBL predicted wear rates to a wide range of POD and knee simulator wear test results. In order to develop a model which could be directly implemented for the accurate prediction of wear, a relationship was required to relate the two material parameters of the ED and CBL models to the radiation used in the crosslinking of the XPE material. The results of previous computational simulations using the ED wear model [264, 326] were implemented in a python script to evaluate the relationships between XPE crosslinking radiation and the two material parameters of the ED wear model.

3.7.1 Model Corroboration with Pin-on-Disk Tests

For each POD verification experiment, computational simulations were conducted to replicate the conditions of the POD experiment. Each computational simulation included FE simulations to assess contact mechanics, as well as the CBL wear model to predict lubrication conditions and wear. POD experiments were selected from the literature which had implemented broad ranges of conditions in order to thoroughly establish the accuracy of the CBL wear model. The POD experiments utilized for verification included experiments under widely varying contact pressure conditions (POD 1) [222], as well as varying contact pressure and cross shear conditions for both PE (POD 2) [210, 216, 318]

and XPE (POD 3) [216, 318]. The implemented POD experiments also investigated the effects of cross shear on PE wear through experiments using different aspect ratios of rectangular pin sliding paths (POD 4) [60], as well as through utilizing different sliding distances following pin directional changes for XPE (POD 5) [59]. The input experimental details are summarized in Table 7. All tests utilized polished CoCr alloy disks as the articular counterface. Experiments POD 1, POD4 and POD 5 were included to evaluate the models ability to predict the appropriate wear trend, rather than to also predict correct wear magnitudes as was expected for the other POD experiments. Experiment POD 1 was considered for trend prediction only, since the POD experiment did not include sodium azide, which would alter wear rates and its absence is not accounted for by the CBL model. Meanwhile, for experiments POD 4 and POD 5 the lubricant volume used in the experiment was unknown and have thus been included for consideration of the ability of these models to predict the wear trends only.

Table 7: Summary of POD experiments utilized in the verification of the CBL computational wear simulations.

		Experiments				
		POD 1	**POD 2**	**POD 3**	**POD 4**	**POD 5**
PE Pin Conditions						
	Pin Diameter (mm)	9	5-10	5-8	9	9.5
	Sliding Velocity (mm/s)	32	20-76	20-76	20	64
	PE Crosslink Radiation (MRad)	2.5-4	0	6, 10	0	4, 5
	Contact Pressure (MPa)	0.25-20	1,3,6,10	1, 3	3	4.7
	Cross Shear (%)	1	0-0.25	0-0.25	1	1
Lubrication Conditions						
	Lubricant Volume (ml)	12	40	40	NA*	NA*
	Lubricant Type	ACS	BCS	BCS	BCS	BCS
	Protein Concentration (g/l)	21	15.4	15.4	23	65
	β & γ Fraction (%)	0.16	0.33	0.33	0.33	0.33
	Sodium Azide Concentration (%)	0	0.001	0.001	0.002	0.002
	Lubricant Replacement (hours)	24	92	92	56	50

* Not Specified
ACS and BCS represent Alpha Calf Serum and Bovine Calf Serum, respectively
Units in % range from 0 (minimum) to 1 (maximum)

For each set of POD experiments, computational simulations were conducted which replicated the conditions of each POD experiment. The computational simulations included both FE simulations and Python scripts to automate the FE simulations and wear calculations using the CBL model. The FE models for each experiment were constructed using Abaqus/Explicit following the protocol established in Section 3.2.

3.7.2 Model Corroboration with Knee Simulator Wear Tests

Computational simulations were performed to predict the results of knee simulator wear tests under a wide range of conditions to evaluate the predictive accuracy of the CBL wear model for PE and XPE wear in TKRs (Table 8). Knee simulator wear tests were selected from the literature to evaluate the computational wear simulation methods ability to accurately predict wear under varying kinematics, loading, TKR conformity, XPE crosslink density, design modularity, lubrication volume, lubricant concentration and lubricant composition (Table 9).

For each set of experiments, computational simulations were conducted which replicated the conditions of the knee simulator experiments. The computational simulations included FE simulations performed according to the protocol established in Section 3.2. Python scripts were written to automate the FE simulations and wear calculations using the CBL model. Finally, the validation metric of Oberkampf and Trucano [362] was calculated to quantify the strength of the validation for the use of the CBL computational wear model for the prediction of TKR knee simulator wear test results. The validation metric was calculated according to [362]:

$$VM = 1 - \frac{1}{N}\sum_{n=0}^{N} \tan h \left|\frac{y(t_n) - Y(t_n)}{Y(t_n)}\right| \quad (27)$$

where *VM* is the validation metric, *N* is the total number of samples, *tan h* is the hyperbolic tangent trigonometric function, $y(t_n)$ is the numerically predicted value, and $Y(t_n)$ is the experimentally measured value. The validation metric provides a value

between 1 (perfect agreement) and 0. The validation metric is a highly sensitive measure of agreement between computational and experimental results, and will provide a clear indication of the predictive capability of the newly developed CBL computational wear model for the prediction of knee simulator wear test results [362].

To the best of the author's knowledge, these POD and knee simulator validation experiments represent the most extensive attempt to evaluate any TKR computational wear model. Based on the improved consideration for variables affecting wear, the CBL computational wear model was anticipated to result in greatly improved predictive accuracy over the previously available computational wear models.

Table 8: Summary of knee simulator wear test experiments utilized for the verification of the CBL model.

	TKR Design	Material Crosslinking (MRad)	Kinematics and Kinetics	Lubrication Type (g/l)	Wear Rate (mm^3/MC)	Standard Deviation	Reference
K1	AMK	0	Flexion Only	BCS (35)	1	0.2	[354]
K2	AMK	0	Flexion & IE	BCS (35)	6.1	1.1	[354]
K3	AMK	0	Flexion, IE & (+)AP	BCS (35)	8.7	1.5	[354]
K4	AMK	0	Flexion, IE & (-)AP	BCS (35)	10.8	1.9	[354]
K5	PFC-Sigma	2.5-4	High	NCS (12)	15.9	2.9	[254]
K6	PFC-Sigma	2.5-4	Intermediate	NCS (12)	8.6	3.4	[254]
K7	PFC-Sigma (Flat)	2.5-4	High	NCS (12)	3.4	0.7	[254]
K8	PFC-Sigma (Flat)	2.5-4	Intermediate	NCS (12)	3.1	1.3	[254]
K9	PFC-Sigma	5	High	NCS (12)	13.0	3.9	[16]
K10	PFC-Sigma	2.5-4	Increased Load ISO	BCS (17)	13.6	1.7	[264]
K11	PFC-Sigma	2.5-4	ISO	BCS (17)	9.2	1.3	[264]
K12	PFC-Sigma	2.5-4	ISO	BCS (20) - 250 ml	9.7	1.2	[265]
K13	PFC-Sigma	2.5-4	ISO	BCS (20) - 150 ml	8.8	1.4	[265]
K14	PFC-Sigma	2.5-4	ISO	BCS (20) - 75 ml	5.6	1.2	[265]
K15	PFC-Sigma	2.5-4	ISO	BCS (20) - 45 ml	1.0	0.2	[265]
K16	AMK	0	ISO	BCS (17)	23.6	2.0	[251]
K17	AMK Non-Modular	0	ISO	BCS (17)	19.1	2.0	[251] [11]
K18	AMK	0	ISO	BCS (62)	5.7	2.3	[10]
K19	AMK	0	ISO	NCS (17)	18.2	3.5	[164]
K20	AMK	0	ISO	ACS (17)	14.4	0.9	[164]

Table Abbreviations: ISO - ISO 14243-3; IE - Internal External rotation; AP - Anterior Posterior motion; BCS, NCS and ACS represent: Bovine, Newborn and Alpha Calf Serum, respectively

Table 9: Comparisons of loading and kinematic conditions, design and material variables, and lubrication conditions considered for the verification of the CBL model.

Comparison	**Experiment Numbers**
Kinematics (decoupled)	K1, K2, K3, K4
Kinematics (high/intermediate)	K5, K6, K7, K8
Loading	K10, K11
Conformity	K5, K6, K7, K8
XPE Crosslink Density	K5, K9
Modularity	K16, K17
Lubricant (volume)	K12, K13, K14, K15
Lubricant (concentration)	K16, K18
Lubricant (composition)	K16, K19, K20

.

Chapter 4

Results and Discussion

4.1 Introductory Remarks

Research was conducted for the development of new computational wear simulation models, to evaluate the accuracy of computational wear simulation models and to investigate the effects of TKR design variables and conditions on wear. This chapter includes the presentation and discussion of the results of this research.

4.2 Simulation of Contact Mechanics

The computational wear simulation process requires the accurate simulation of contact mechanics, as the contact mechanics results are required by the computational wear model for the prediction of wear. FE simulations have previously been demonstrated to accurately predict TKR contact mechanics and deformation behaviour [335, 339]. Alternatively, MBD simulations may offer greater computational efficiency and have been widely implemented for the simulation of TKR contact mechanics in the literature [39, 40, 260, 328, 336-338]. However, the accuracy of MBD simulations for the prediction of TKR contact mechanics has not been as extensively verified, in comparison to FE simulations. Therefore, simulations were conducted to develop a PO relationship optimized for the MBD simulation of TKR contact mechanics (Section 3.2). The accuracy of the optimized PO relationship was then assessed through the comparison of the MBD predicted results to the results of previously verified FE simulations. The optimized PO relationship must be demonstrated to be highly correlated (R^2>0.85) with the results of the previously verified FE simulations in order to be accepted as a suitable method for the prediction of TKR contact mechanics in computational wear simulations.

4.2.1 Results

Axis-symmetric simulations were conducted to develop an optimized MBD PO relationship (Figure 33). The comparison between the MBD simulation results and the results of the verified FE simulation enabled a relationship to be determined through least squares minimization curve fitting to determine an optimized PO relationship for the MBD simulations. The fitted natural logarithm curve was determined to be:

$$P = 5 \cdot ln(x) + 37 \tag{28}$$

where P represents contact pressure (MPa) and x represents overclosure (mm). The optimized PO relationship resulted in a coefficient of determination (R^2) of 0.64, indicating relatively poor correlation strength. Additionally, comparing the optimized PO relationship to the data from each test reveals that the optimized PO relationship does not accurately represent all of the tests (Figure 33). The axis-symmetric simulations display the trends of increasing peak contact pressure under increasing load, and decreasing contact pressure under increasing conformity.

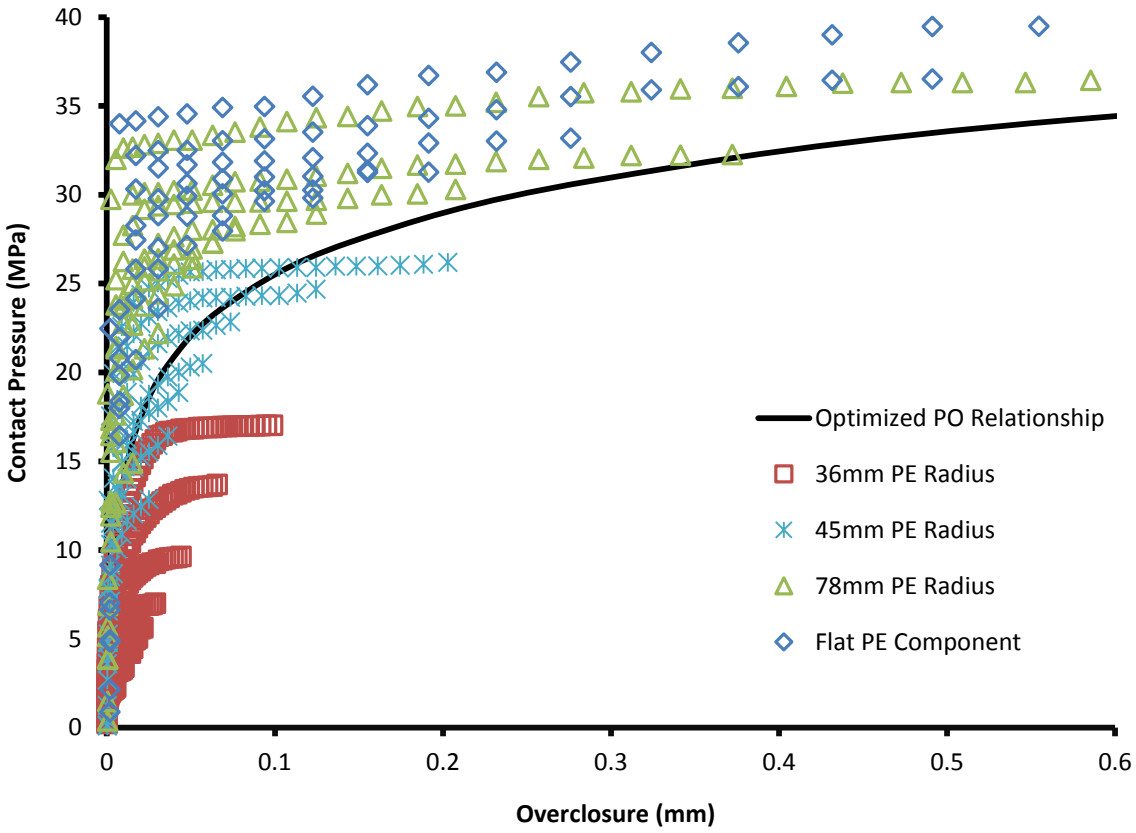

Figure 33: Axis-symmetric simulation results and the optimized PO relationship.

Following the development of the optimized PO relationship, static simulations were conducted to evaluate the accuracy of the MBD simulations in comparison to a previously verified FE simulation procedure (Table 10, Figure 34). The MBD simulation difference (%) was defined as the difference between the MBD and FE simulation results divided by the FE simulation results. Contact area difference ranged from 11.1% under-predicted to 34.4% over-predicted. Contact pressure difference ranged from 24.2% under-predicted to 53.6% over-predicted. The results also demonstrated increasing conformity to result in underpredicted area and overpredicted contact pressure predictions for the MBD simulations relative to the FE simulations (Table 10, Figure 34).

Table 10: Comparison of the contact area (Area) and contact pressure (P) predictions of the FE and MBD static TKR simulations.

Contact Area					
			Load (N)		
			170	**1300**	**2600**
High Conformity	**FE**	**Area (mm²)**	29.3	87.6	131.1
	MBD	**Area (mm²)**	28.6	77.9	120.2
	Difference	**(%)**	-0.024	-0.111	-0.083
Medium Conformity	**FE**	**Area (mm²)**	21.7	56.9	89.2
	MBD	**Area (mm²)**	21.1	60.6	92.5
	Difference	**(%)**	-0.027	0.065	0.037
Low Conformity	**FE**	**Area (mm²)**	8.9	32.6	52.5
	MBD	**Area (mm²)**	11.9	41.4	68.7
	Difference	**(%)**	0.344	0.272	0.309
Contact Pressure					
			Load (N)		
			170	**1300**	**2600**
High Conformity	**FE**	**P (MPa)**	6.3	13.9	18.5
	MBD	**P (MPa)**	9.7	17.2	20.2
	Difference	**(%)**	0.536	0.235	0.093
Medium Conformity	**FE**	**P (MPa)**	9.7	23.3	26.1
	MBD	**P (MPa)**	12.7	20.7	24.1
	Difference	**(%)**	0.309	-0.112	-0.076
Low Conformity	**FE**	**P (MPa)**	23.2	34.3	36.8
	MBD	**P (MPa)**	17.6	26.3	30.2
	Difference	**(%)**	-0.242	-0.235	-0.18

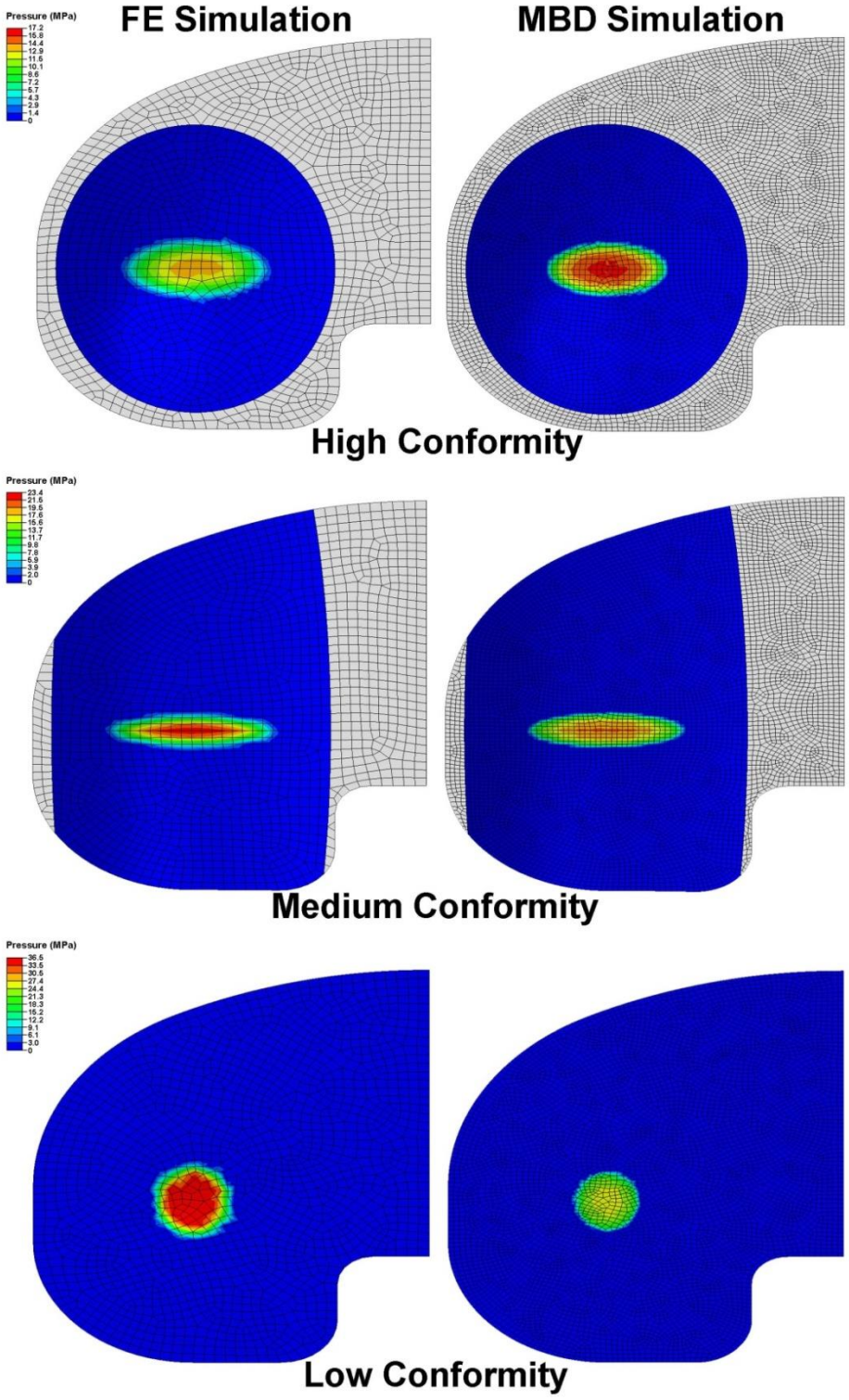

Figure 34: Contact pressure of the PE insert medial condyle predicted by the FE and MBD simulations under varying conformity at a load of 1300 N (the gray colored area is beyond the contact region of the simulations and thus has a contact pressure of 0 MPa).

As a final means of evaluating the accuracy of MBD simulations with the optimized PO relationship, the contact mechanics of a TKR were predicted over the ISO gait cycle. Articular contact area and peak contact pressure were recorded during both the FE and MBD simulations. The MBD simulation required only 4.6% of the computation time required by the FE simulation. The maximum contact area difference over the gait cycle was 35% and the maximum peak contact pressure difference was 41%, for the MBD simulation compared to the FE simulation.

4.2.2 Discussion

The optimization of the MBD PO relationship was conducted using axis-symmetric simulations of varying conformity and load. These axis-symmetric simulations demonstrated a clear and distinct trend for each combination of conformity and loading (Figure 33). Increased load is found to result in the requirement of increased contact pressure from the MBD simulation, even at the same overclosure values relative to decreased loading experiments. Meanwhile, increasing conformity requires decreased contact pressures, even at the same overclosure values relative to less conforming components. From these results it is evident that MBD simulations, unlike FE simulations, are not able to accurately account for the effects of changes to conformity and loading. This deficiency of MBD simulations may be attributed to it's over simplification of the domain as a set of independent springs. The assumption of MBD simulations that each node/spring is unaffected by the deformation of neighbouring nodes/springs provides zero shear stiffness and misrepresents true PE material behaviour.

A natural logarithm curve has been optimized to provide a best-fit through the axis-symmetric simulation data points. However, the agreement of this fitted curve is not of good quality (R^2=0.64) and it is apparent that the fitted curve does not represent any of the axis-symmetric experiments particularly well (Figure 33). If a practical method were available for implementing a different PO relationship in each case based on the load and conformity, then MBD simulations may be able to provide more accurate results. However, it is a requirement of the contact mechanics prediction method that it must be robust and widely applicable to all possible TKR designs and conditions.

Static simulations were performed with TKR components of varying conformity and loading conditions to evaluate the accuracy of the optimized MBD PO relationship. Changes in conformity and load were, once again, demonstrated to have great influence over the contact pressure and contact area predictions (Table 10, Figure 34). Increasing conformity was demonstrated to cause increasing area predictions and decreasing pressure predictions relative to the FE results. The differences were as large as 53.6% and 34.4% for contact pressure and area, respectively. While these differences may be acceptable for kinematic predictive analyses, these differences are unacceptably large for computational wear predictions.

The range of geometric parameters of the static simulations was selected to represent the range of highly to minimally conforming TKR designs. However, it is important to note that these simplified simulations do not represent the full range of conditions which may be experienced by TKRs. Due to the internal-external rotation and anterior-posterior translation between the femoral component and tibial insert, the alignment and relative conformity of the TKR components are constantly changing throughout the gait cycle.

The contact conditions can change greatly with changes to the relative position of the components, such as when the posterior edge of the PE insert is encountered due to the posterior displacement of the femoral component relative to the PE insert. Therefore, for the final simulation scenario, the contact mechanics of a TKR over the ISO gait cycle was predicted. The contact pressure difference (41%) and contact area difference (35%) of the MBD simulation was once again found to be unacceptably high for computational wear simulations, yet may still be within the acceptable limits of kinematic analyses.

Although MBD simulations have often been implemented in the literature for computational wear simulations [39, 40, 260, 328, 337, 338], the evaluation of MBD simulation accuracy for the prediction of contact mechanics across such a broad range of conformity and loading conditions had not been previously considered [328, 345]. Many of these MBD simulations [39, 40, 330, 348] from the literature have implemented the PO relationship developed by Halloran et al. [328]. The optimized PO relationship, developed through the present research, based on the curve fitting of axis-symmetric simulations, resulted in a similar trend (R^2=0.92) compared to the piecewise-linear PO relationship developed by Halloran et al. [328]. The similarity between these two PO relationships, which were developed independently and under different simulated conditions, provides further support that these PO relationships are well optimized based on the conditions of the TKR. Nevertheless, the results of the present research have indicated that the MBD simulation method may be incapable of providing sufficient levels of accuracy to be used in computational wear simulations. Contact pressure and area prediction differences of greater than 15% would have a substantial effect on the predictive accuracy of computational wear simulations. Furthermore, the magnitude of

the differences has been demonstrated to be dependent on conformity and load. This implies that not only would the predicted wear magnitude be inaccurate for MBD computational wear simulations, but the relative ranking of designs may also be inaccurate. The dependence of MBD simulation predictions on geometric conformity and applied load may stem from the fundamental assumption of MBD methods, which specifies that the displacement of each node is independent of the displacement of neighbouring nodes. The independence of nodal displacements does not represent true PE material behaviour and neglects the shear stiffness of the material [339].

If a practical method were available for implementing a different PO relationship during each instant of time and at each location based on the known load and a measurement of local conformity then the accuracy of MBD simulations could be greatly improved. Additionally, an alternative method with the potential of increased accuracy may be to implement relative springs between each neighbouring node so that the shear stiffness of the material may be approximated. However, this relative spring adaptation of MBD methods would no longer qualify as an elastic foundation method, as the deformation of each node would be dependent on the deformation of neighbouring nodes.

Overall, the MBD simulations have demonstrated greatly improved computational efficiency at the expense of decreased agreement relative to FE simulations. The results demonstrated by MBD simulations may be acceptable for kinematic predictive analyses, where the articular surface reaction forces are of key concern and the precise values of contact pressure and area are of less concern. However, for computational wear simulations the predictive capabilities of MBD simulations are insufficient. Furthermore, as MBD simulations cannot predict the contact mechanics of the backside surface, FE

simulation remains the only verified means of accurately predicting the contact mechanics of the PE insert articular and backside surfaces.

4.2.3 Concluding Remarks

Both FE and MBD simulations have previously been used in the literature for the prediction of TKR articular contact mechanics. The accuracy of FE simulations has previously been well verified, yet the accuracy of MBD simulations had not been as thoroughly investigated. Therefore, in the present research, computational simulations were conducted to develop a MBD PO relationship and assess its predictive capabilities relative to a previously verified FE simulation procedure. The MBD simulations resulted in as much as 53% and 35% differences from the FE simulations for the prediction of contact pressure and area, respectively. Prediction differences were demonstrated to be dependent on both load and conformity. MBD simulations with the developed PO relationship may be sufficient for kinematic prediction analyses. Yet, for computational wear simulations the predictive capabilities of these MBD simulations would be insufficient. Therefore, FE simulations are recommended for the prediction of contact mechanics in computational wear simulations, as well as whenever contact pressure and area predictions are of great importance. Thus, FE simulations were hereafter exclusively implemented for the simulation of contact mechanics in the research of this thesis.

4.3 Computational Investigation of the Effects of Insert Thickness on Wear

Tibial insert thickness has previously been demonstrated to affect TKR wear. In the present study, computational simulations were performed for PE and XPE inserts of thicknesses ranging from 5-25mm to investigate the effects of insert thickness on contact pressure, sliding distances and wear for both the articular and backside surfaces. The computational wear simulations utilized FE simulations for the prediction of TKR contact mechanics, as MBD simulations were shown to be insufficiently accurate by the research of the preceding section (Section 4.2). An existing computational wear model from the literature [60] was implemented to enable the effects of insert thickness on wear to be computationally analyzed.

4.3.1 Results

The computational simulations demonstrated the trends of decreasing peak contact pressure and increasing contact area to occur with increasing insert thickness (Figure 35 and Figure 36). For the XPE inserts, the peak contact pressures were higher and the contact areas were lower than those of the PE inserts (Figure 35 and Figure 36). Contact pressures and contact areas were greater medially than laterally for all inserts (Figure 35).

The peak contact pressure of the articular surface decreased nonlinearly with increasing insert thickness (Figure 36). However, this change was shown to be relatively small (≈8%) (Table 11). Articular wear slightly decreased with increasing insert thickness

(Figure 37). The decrease in wear associated with increasing insert thickness was again rather small (≈3%) (Table 11). The results also show that the PE inserts were associated with 2.3-times greater wear on the articular surface than the XPE inserts.

Table 11: Peak contact pressure (P), peak cumulative sliding distances (Slide Dist) and wear (mm^3/million cycles (MC)) for the articular and backside surfaces of tibial inserts of various thicknesses.

Material	Thickness (mm)	Topside		Backside		
		P (MPa)	**Wear (mm^3/MC)**	**P (MPa)**	**Slide Dist (mm)**	**Wear (mm^3/MC)**
PE	5	22.66	15.11	13.80	3.08	0.83
	10	21.96	14.91	13.47	4.86	0.89
	15	21.40	14.75	13.27	6.37	0.93
	20	21.04	14.64	13.13	7.60	0.97
	25	20.88	14.60	13.00	8.55	1.00
XPE	5	23.79	6.60	12.88	2.52	0.31
	10	23.02	6.51	12.76	4.33	0.39
	15	22.46	6.45	12.68	5.88	0.45
	20	22.12	6.40	12.62	7.16	0.51
	25	21.93	6.38	12.58	8.19	0.55
Increased Interference						
PE	5			13.80	2.31	0.62
	10			13.47	3.93	0.67
	15			13.27	5.31	0.70
	20			13.13	6.43	0.73
	25			13.00	7.31	0.75
XPE	5			12.88	2.19	0.27
	10			12.76	3.73	0.34
	15			12.68	5.02	0.40
	20			12.62	6.06	0.45
	25			12.58	6.85	0.49

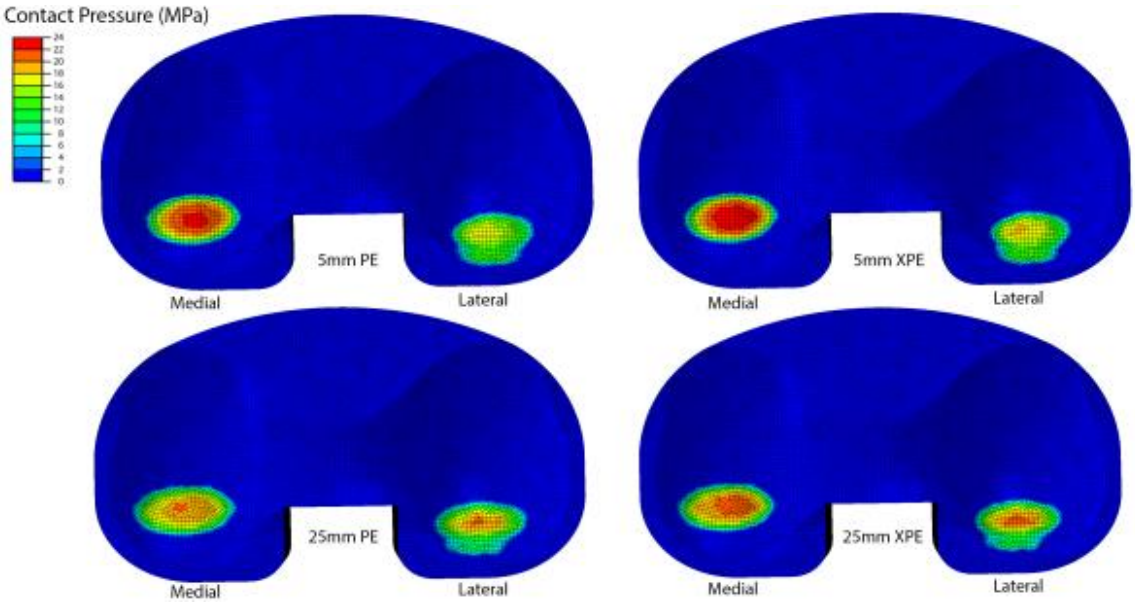

Figure 35: Contact pressure at the articular surface of the PE and XPE inserts during heel-strike (gait cycle: 10%).

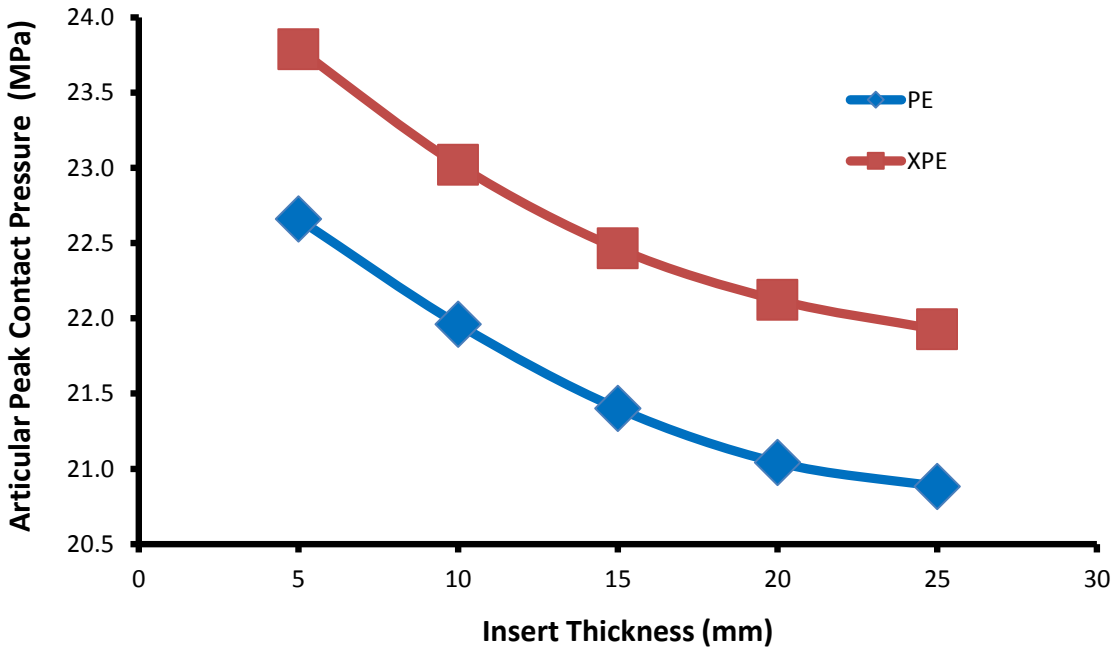

Figure 36: Peak contact pressures at the articular surface for the PE and XPE inserts at heal strike (gait cycle: 10%).

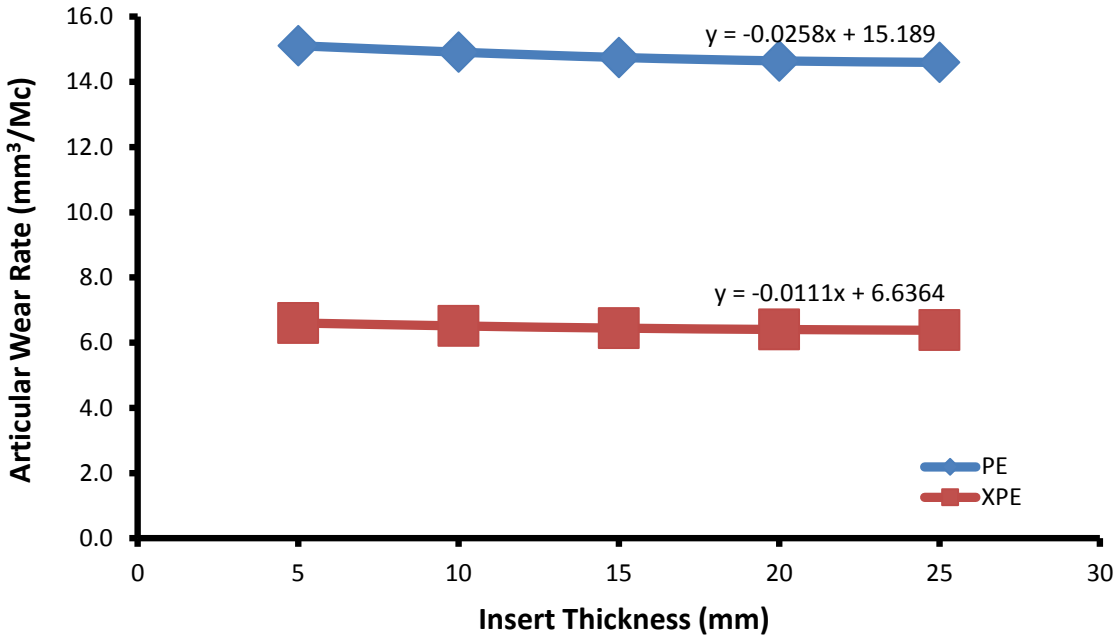

Figure 37: *In silico* predicted articular wear rate for the PE and XPE inserts.

For the backside surface, the peak contact pressure decreased nonlinearly with increasing insert thickness (Figure 38 and Figure 39). As with the articular surface, backside contact pressures and contact areas were greater medially than laterally for all inserts (Figure 38). Peak contact pressures were greater for PE than XPE (Figure 38 and Figure 39). The overall changes in backside contact pressure were small (≈4%) (Table 11).

Backside cumulative sliding distances increased nonlinearly with increasing insert thickness (Figure 40 and Figure 41). Backside cumulative sliding distances of the XPE inserts were less than those of the PE inserts (Figure 40 and Figure 41). The thicker inserts resulted in greater cumulative sliding distances in the posterior region, compared with the locations of higher cumulative sliding distances on the thinner inserts (Figure

40). The overall change in backside cumulative sliding distances was very pronounced (≈101%) for both PE and XPE (Table 11). Backside wear increased with increasing insert thickness (Figure 42). Increasing insert thickness resulted in a large increase in backside wear (≈38%) (Table 11).

Increasing the locking mechanism interference fit appeared to reduce backside sliding distances by 18% and 14% on average for PE and XPE, respectively (Figure 41). The increased interference reduced backside wear by 25% and 11% for PE and XPE, respectively (Figure 42).

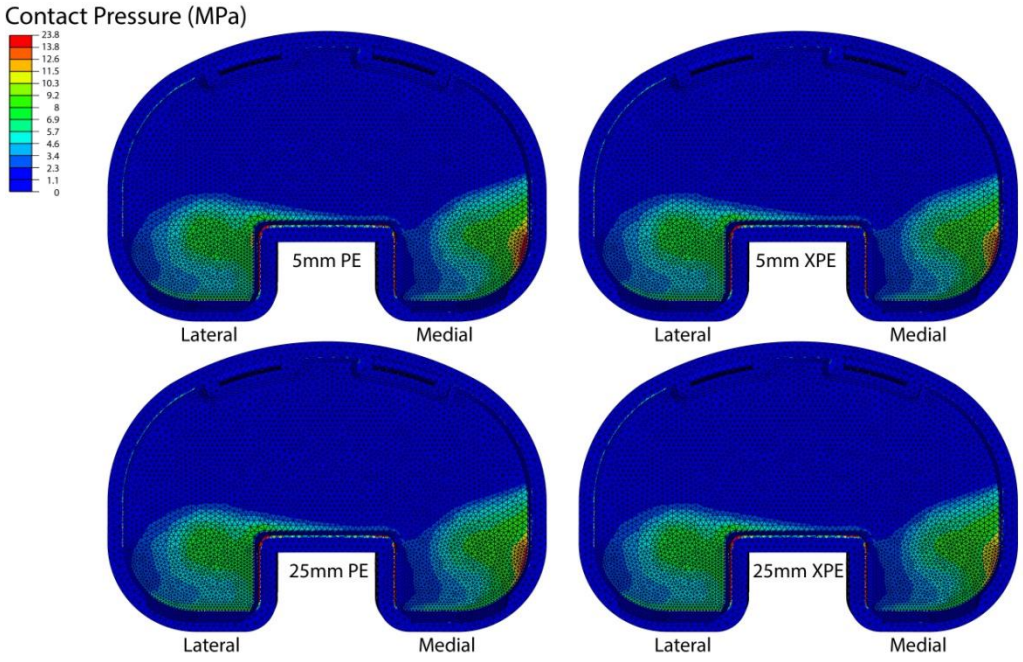

Figure 38: Contact pressure at the backside surface of the PE and XPE inserts during heel-strike (gait cycle =10%).

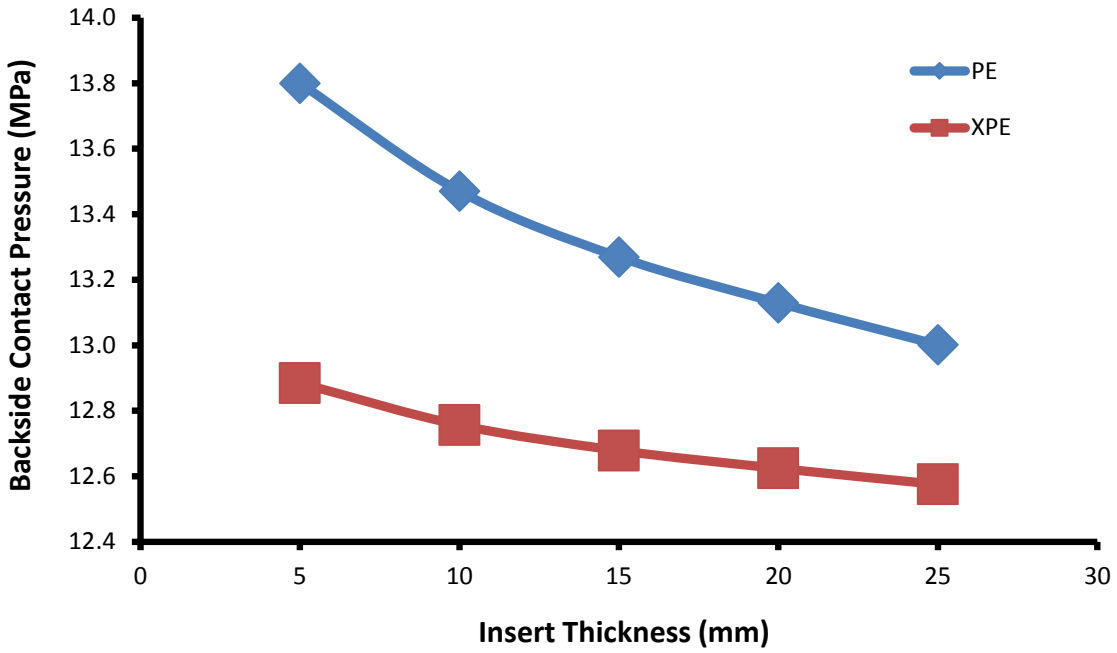

Figure 39: Peak contact pressures at the backside surface for the PE and XPE inserts at heal strike (gait cycle =10%).

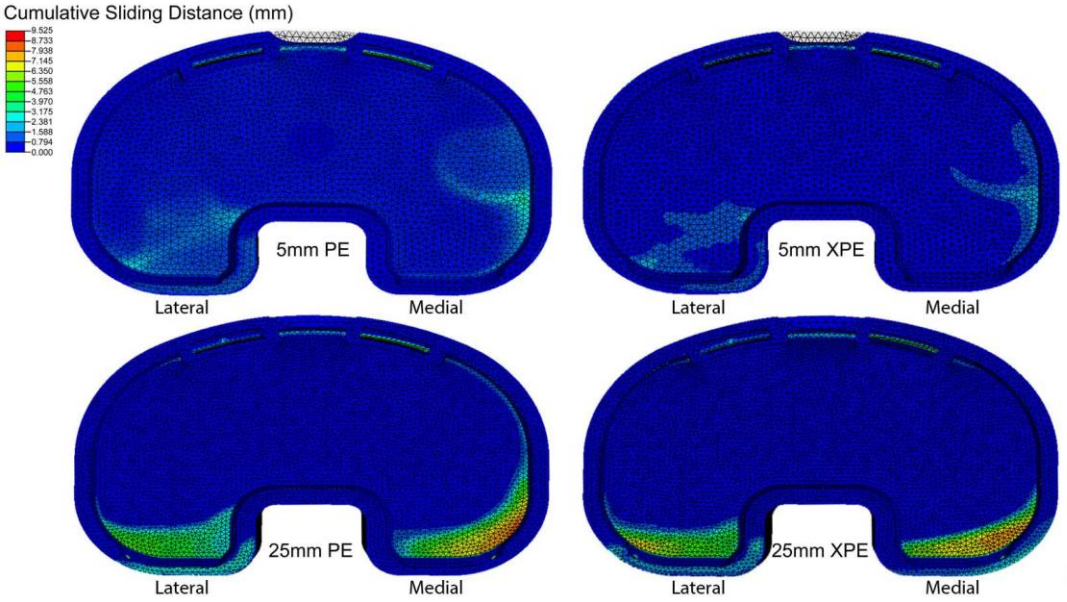

Figure 40: Cumulative sliding distances at the backside surface of the PE and XPE inserts over the gait cycle.

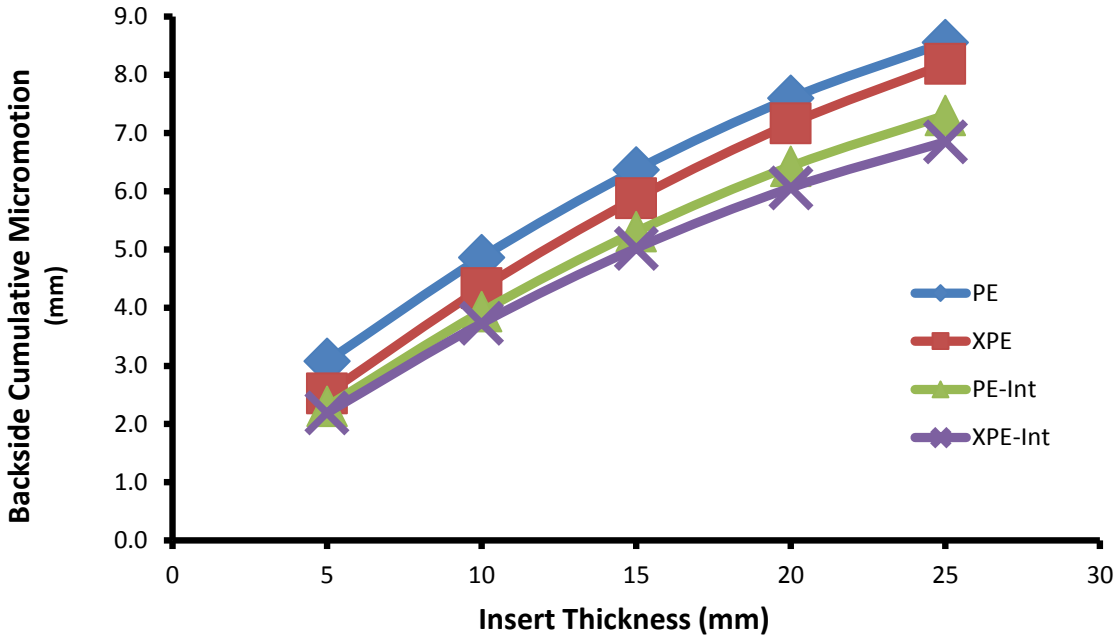

Figure 41: Peak cumulative sliding distances at the backside surface for the PE and XPE inserts of both regular (PE, XPE) and increased interference fit (PE-Int, XPE-Int) over the entire gait cycle.

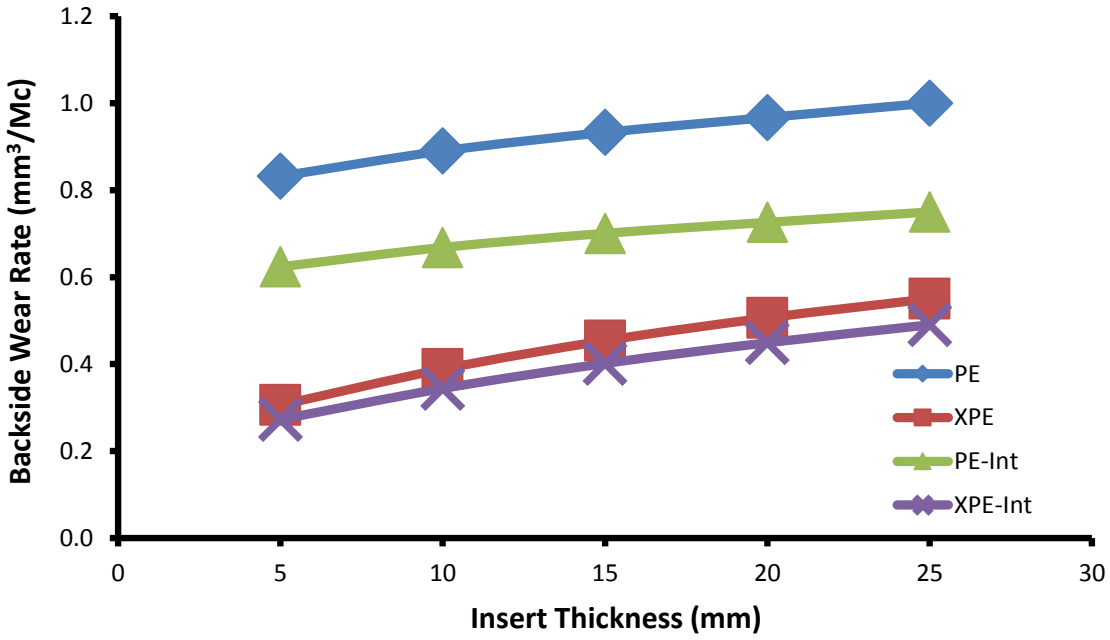

Figure 42: *In silico* predicted backside wear rate for the PE and XPE inserts of both regular and increased interference fit over the gait cycle.

4.3.2 Discussion

Increased insert thickness resulted in increased contact areas and decreased peak contact pressures for the articular surface (Figure 35 and Figure 36). These results are in agreement with the static results of Bartell et al. [256, 257]. Increased insert thickness enables lower peak contact pressures due to the elastic deformation of the additional material, permitting the load to be more evenly distributed over a larger area and thus decreasing peak contact pressure (Figure 35, Figure 36 and Table 11). Although increased insert thickness leads to reduced peak contact pressures, it also results in increased contact area and therefore the reduction in wear was not very pronounced (Figure 37). Contact pressures were greater medially than laterally corresponding to the increased loading of the medial side as per the ISO standard and clinically reported behaviour [17]. The increased contact pressures and stresses associated with thinner inserts would be far more devastating for inserts of reduced mechanical properties [363, 364]. Oxidation has been demonstrated to result in as much as an 85% decrease in ultimate strength [365]. Therefore, the historical failures associated with insufficiently thin inserts for oxidized gamma-air sterilized inserts [363, 364] may not be directly relevant to the outcomes for modern bearing materials. The lower limit of acceptable insert thickness for modern bearing materials may be lower than the historical values. The XPE material demonstrated higher contact pressures and correspondingly smaller contact areas on the articular surface (Figure 35 and Figure 36) due to its increased stiffness which limits elastic deformation [3]. The sliding distances of the articular

surface were not recorded because they remained largely unaffected by the changes in insert thickness.

For the backside surface, increased insert thickness once again led to reduced peak contact pressure due to the elastic deformation of additional material of the thicker inserts (Figure 38 and Figure 39). The contact pressures of the XPE were lower than those for the PE due to the fact that the XPE has a higher modulus of elasticity. Thus, the loads from the less conforming articular surfaces are more evenly distributed before they reach the highly conforming backside surface for the XPE.

Most interestingly, the cumulative sliding distances of the backside surface increased with increasing insert thickness (Figure 40 and Figure 41). It was expected that this trend occurred mainly because for thicker inserts the reaction forces at the articular surface were further away from the locking mechanism, resulting in a greater moment arm (Figure 43). Thus, an articular shear force of 100 N, corresponding to a normal load of 2500 N with a coefficient of friction of 0.04, would result in a moment M_a of 0.5 Nm and 2.5 Nm for the 5 and 25 mm inserts, respectively (Figure 43). Since the locking mechanism dimensions remain constant, the increase in moment (5-times greater for the 25 mm insert than the 5 mm insert) may lead to increased backside micromotion for thicker inserts despite the overall low magnitude of the moments. It was previously suspected by Brandt et al [7] that thicker inserts would result in less peripheral expansion and thereby increase backside sliding distances, and thus surface damage. Interestingly, the present study revealed that increasing insert thickness led to increased peripheral expansion of the inserts, as the additional material enabled additional elastic deformation. This would act to further engage the locking mechanism and reduce backside sliding

distances with increasing insert thickness. However, the magnitude of this peripheral expansion between inserts that varied in thickness was very small (<2%) and thus, it did not confirm the suggestions by Brandt et al. [7].

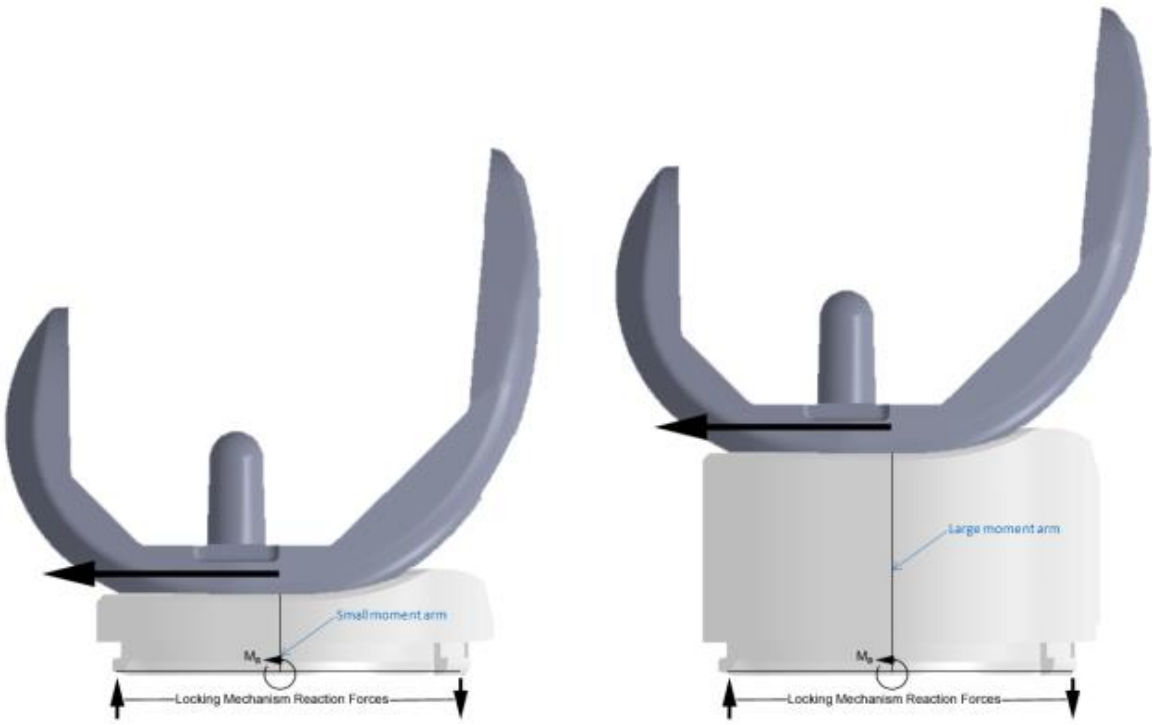

Figure 43: PE inserts of increased thickness have an increased moment arm of the articular surface about the locking mechanism (a 100 N articular shear force would result in 0.5 Nm and 2.5 Nm for the 5 and 25 mm inserts, respectively).

The decreased backside contact pressures associated with increased insert thicknesses were anticipated to reduce backside wear [60]. However, the increased backside sliding distances for thicker inserts would tend to increase backside wear and as a result, backside wear increased with increasing insert thickness (Figure 42). The results of the present study for the backside surface are in agreement with the retrieval results of Brandt

et al. [7], who observed increased backside damage for thicker inserts, assuming a linear relationship between the extent of surface damage and actual wear.

The magnitudes of backside sliding distances and wear have been shown to be highly dependent on the locking mechanism [335]. In the present study, increasing the interference fit of the locking mechanism reduced peak cumulative backside sliding distances for the PE inserts by an average of 18%. Due to the increased stiffness of XPE over PE, the increased interference had a somewhat lesser effect, with XPE peak cumulative backside sliding distances being reduced by 14% on average. The average reduction in backside wear due to the increase in interference fit for PE and XPE were 25% and 11%, respectively. It should be noted that these values differ from the change in sliding distances due to the importance of cross shear and directional strain hardening on wear. The interference fit experiment of the present study demonstrated the importance of the locking mechanism in preventing backside micromotion and thus wear. It also demonstrated how the increased stiffness of XPE, over PE, can result in reduced backside micromotion, demonstrating an additional advantage for XPE over PE. Furthermore, it can be reasonably inferred that with reduced interference fit, backside micromotion and wear can increase significantly [8], since an increase in interference of only 0.254mm resulted in a 18% decrease in micromotion for PE inserts.

The wear rates predicted by the computational simulations of the present study are similar to the values that were observed in knee simulator wear testing. McEwen et al. [16] performed knee simulator wear testing of the PFC-Sigma with 10 mm thick inserts (GUR 1020, 2.5-4 MRad). Unfortunately, these tests were not performed under the ISO standard, yet the conditions were similar and therefore the wear results were expected to

be relevant. The knee simulator wear test values of 16 ± 4 mm^3/million cycles (MC) [16] were found to be very similar in magnitude to the wear rate of 15.8 mm^3/MC determined by the present study. McEwen et al. [16] also performed knee simulator wear testing of moderately crosslinked PE (GUR 1050, 5 MRad) inserts which resulted in a wear rate of 13 ± 3.9 mm^3/MC. The wear rate demonstrated by McEwen et al. [16] for 5 MRad XPE also compares well to the average of the highly crosslinked and non-crosslinked computational results for a 10mm insert of 11.35 mm^3/MC calculated in the present study. Additional knee simulator wear tests were performed under the same kinematics as those of McEwen et al. [16] by Van Citters et al. [358] for GUR 1020, 4 MRad XPE. A linear depth penetration of 21 μm/MC was determined from these knee simulator wear tests [358]. Retrievals of the same TKR were also measured for linear depth penetration and a rate of 47.5 μm/year was obtained [358]. The damage features observed for the retrievals and knee simulator wear tests were considered to be comparable. Van Citters et al. [358] therefore suggested that 2.2 MC of knee simulator wear testing may be equivalent to 1 year of in vivo wear for this particular implant. This relationship may also be applied to the computational simulations, resulting in predicted in vivo average wear rates of 34.8 and 15.2 mm^3/year for the PE and XPE, respectively. Further knee simulator wear testing following the ISO standard 14243-3 utilizing a range of different insert thicknesses, as well as an implant retrieval investigation, would be useful to verify the results of the computational experiments conducted in the present study. Additionally, computational wear simulation methods are continually evolving, with new computational wear models being developed with the objective of increased predictive accuracy. The TD-ED-TR (CBL) developed as part of this thesis research (Sections 3.4,

3.6) was developed following the completion of the present study and was therefore unavailable for application at the time of this research. However, the implementation of a different wear model in the present study may have affected the results.

The availability of a wide range of insert thicknesses is essential to ensure the proper tension within the surrounding soft tissue constraints. The surgeon may also have some control over the approximate insert size required by controlling the amount of tibial bone resected and by using augments, rather than thicker inserts, when the situation permits. Due to recent changes in TKR bearing materials, insert thickness was not expected to have the same effect on wear performance as was demonstrated by PE with high oxidization potential or heat-pressing formed PE. Therefore, computational simulations were conducted in the present study to investigate how insert thickness may affect the contact pressures, sliding distances and wear of TKRs with modern bearing materials in the present study. Overall, increasing insert thicknesses resulted in decreased articular surface wear and increased backside wear. The magnitude of changes to articular wear remained small (≈3%), while the relative changes in backside wear were more pronounced (≈38%). However, since backside wear makes up only 6.5% of total wear on average for this particular design, the overall changes in wear remained small.

Insert thickness may have a greater influence on wear than shown here for inserts with reduced material properties due to oxidation, or for inserts with less effective locking mechanisms then the peripheral locking mechanism of the PFC-Sigma used in the present study. Additionally, if the locking mechanism were to deteriorate through prolonged use, the increased backside sliding distances of thicker inserts may begin to have a greater effect on backside wear. These potential problems could become more

significant in situations of increased tribological demand such as younger, heavier and more active patients.

4.3.3 Concluding Remarks

The effects of insert thickness on the contact pressure, sliding distances and wear of the articular and backside surfaces were investigated using computational simulations. Increasing insert thickness from 5 mm to 25 mm was found to decrease articular peak contact pressure (≈8%) and decrease articular wear (≈3%). Meanwhile for the backside surface, increasing insert thickness from 5 mm to 25 mm was found to decrease peak contact pressure (≈4%), increase peak cumulative sliding distances (≈101%) and increase backside wear (≈38%). This demonstrates that insert thickness can have an even greater relative effect on the sliding distances and wear of the backside surface than the articular surface. The use of XPE over PE was discovered to substantially reduce wear rates (78%). Increasing the interference fit of the tibial locking mechanism by 0.254 mm was found to decrease backside peak cumulative sliding distances (≈16%) and decrease backside wear (≈18%). This observation demonstrates the importance of the locking mechanism design, as even a small increase in interference fit can lead to a substantial change in wear rate. Therefore, it is important that implants are designed to have maximized interference fit within the practical limitations of what can feasibly be assembled in the operating room.

Although insert thickness was demonstrated to affect wear rates, the change in overall wear rate remained small for the range of insert thicknesses considered. These

computational wear simulation results demonstrated that the wear performance of modern bearing materials may be less sensitive to changes in insert thickness compared to historical materials such as heat pressing formed PE and PE with high oxidization potential. However, since decreased insert thickness has been demonstrated to increase stress and articular contact pressures, while increasing insert thickness has been demonstrated to lead to increased backside micromotion and wear, insert thicknesses beyond the range investigated in this study (5 mm to 25 mm) may still present a risk.

4.4 Development of a Time Dependent Cross Shear and Energy Dissipation Wear Model

Previously existing computational wear models have provided consideration for very few of the variables known to affect wear (as discussed in Sections 2.3.1 and 2.4.3.2). These previously existing wear models may still provide useful insight for highly constrained cases, where the effects of a relative change in TKR design or conditions are expected to mainly result in changes to the variables which are considered by the computational wear model. The computational investigation of the effects of insert thickness on wear of the previous section (Section 4.3) was an example of such a case. However, previously existing computational wear models have not demonstrated the necessary correlation strength compared to knee simulator wear tests to enable the full design optimization of TKRs for the reduction of wear. Therefore, the development of a new computational wear model was undertaken (Section 3.4) with the objective of improving the predictive accuracy of computational wear simulations. The present research discusses the results of the development and evaluation of a time dependent cross shear and energy dissipation wear model. The accuracy of the newly developed computational wear model was assessed through comparison to POD and knee simulator wear tests under various kinematic conditions and under the ISO 14243-3 standard.

4.4.1 Computational Results

Six wear models were utilized to predict the volumetric wear rates of POD results (first experiment), knee simulator test results under various kinematic conditions (second experiment) and knee simulator tests under the stated ISO standard (third experiment). For the first experiment, spearman's rank correlation coefficients (ρ) and coefficients of determination (R^2) were calculated for each of the six models compared with the POD volumetric wear rate results (Table 12). The inclusion of the cross shear (*CS*) term (M2-M6 compared to M1) and the implementation of the time dependent - energy dissipation approach (M5 and M6 compared to M1-M4) were both associated with substantial increases in correlation strength (>5%).

Table 12: Spearman's rank correlation coefficients (ρ) and coefficient of determination (R^2) for each of the six wear models compared to the POD test results for the first experiment.

		ρ	**R^2**
M1	Archard's Wear Law	0.25	0.06
M2	Turell et al.	0.43	0.19
M3	Abdelgaied et al.	0.77	0.6
M4	CPI	0.77	0.6
M5	TD-ED	0.84	0.71
M6	TD-ED-TR	0.85	0.72

For the kinematic tests of the second experiment, Archard's wear law (M1) was unable to account for the introduction of CS, resulting in greatly under-predicted wear (Table 13, Figure 44). The CS time dependent wear models (CPI, TD-ED and TD-ED-

TR; M4-M6) resulted in relative wear rate increases within one standard deviation of the knee simulator results for the introduction of CS. The TD-ED and TD-ED-TR (M5 and M6) wear models accurately modeled the relative wear rate increase associated with the first three tests and offered significant improvement over the other models. For the relative wear rate increase between tests 3 and 4, only the TD-ED-TR model (M6) showed any increase in wear (15% increase) corresponding to the introduction of tractive rolling.

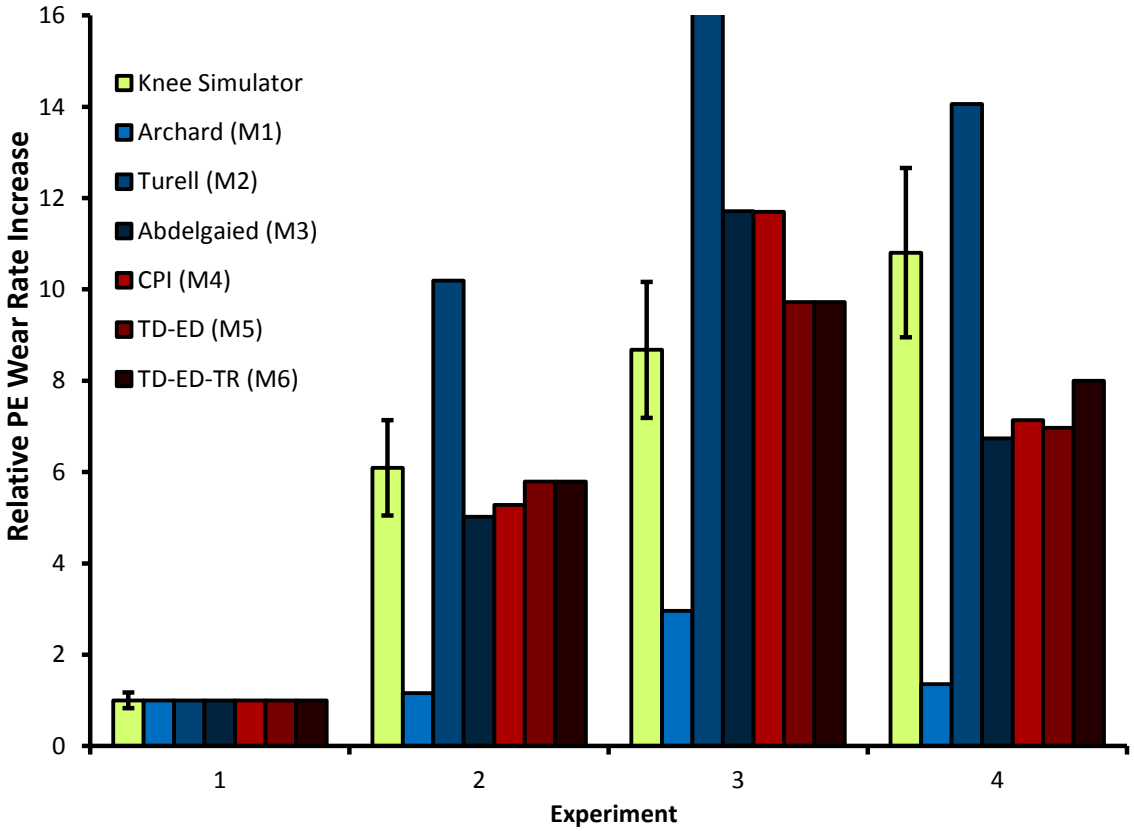

Figure 44: Relative PE wear rate increase for the second experiment: wear under various kinematic conditions.

Table 13: Wear model predicted relative wear rate increase values for the AMK under various kinematic conditions for the second experiment.

Model		Test	Relative Wear Rate Increase	Error
M1	Archard's Wear Law	1	1	NA
		2	1.16	81.0%
		3	2.96	65.9%
		4	1.36	87.5%
M2	Turell et al.	1	1	NA
		2	10.19	67.3%
		3	19.56	125.4%
		4	14.06	30.2%
M3	Abdelgaied et al.	1	1	NA
		2	5.02	17.6%
		3	11.71	35.0%
		4	6.74	37.6%
M4	CPI	1	1	NA
		2	5.28	13.4%
		3	11.7	34.8%
		4	7.14	33.9%
M5	TD-ED	1	1	NA
		2	5.79	5.0%
		3	9.72	12.0%
		4	6.97	35.5%
M6	TD-ED-TR	1	1	NA
		2	5.8	4.8%
		3	9.74	12.3%
		4	8	26.0%

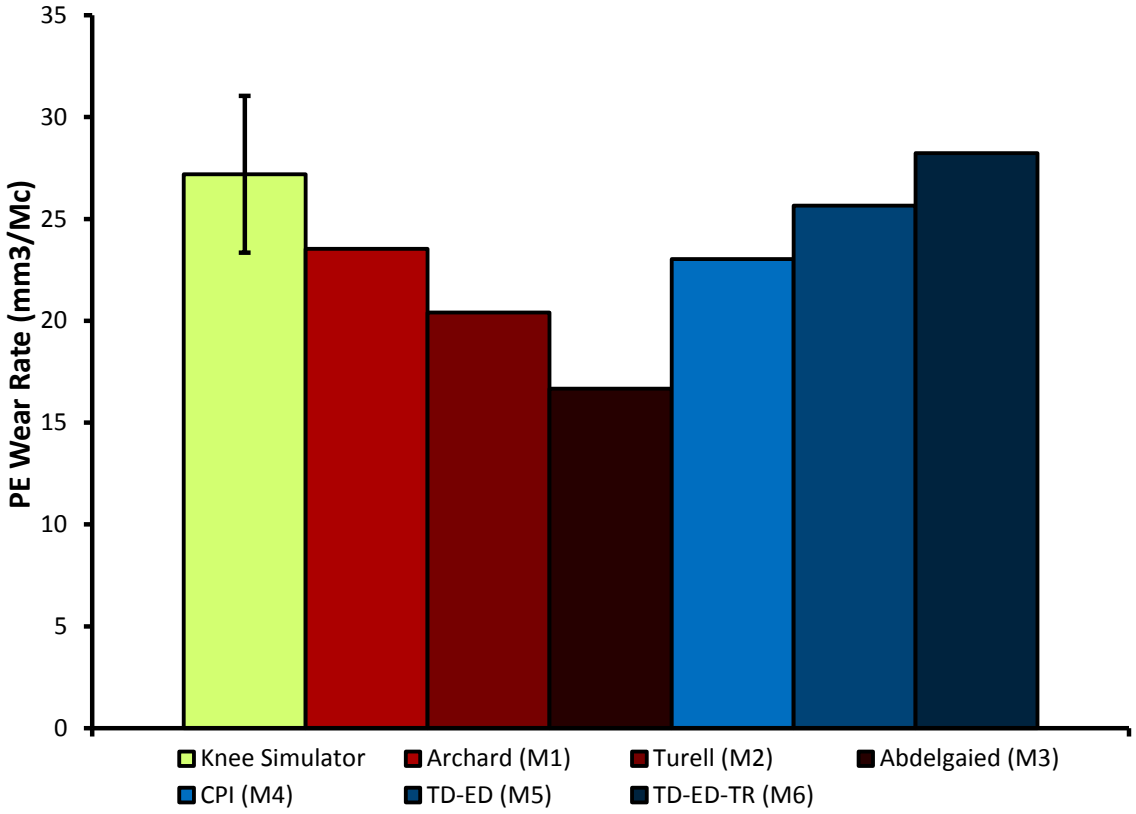

Figure 45: PE wear rate (mm3/MC) for the third experiment: AMK wear under ISO 14243-3.

PE wear was predicted for the AMK following the stated ISO standard for the third experiment (Table 14, Figure 45). The predicted results were compared to knee simulator wear rates for the AMK combined from two independent sources [11, 251] resulting in a combined wear rate of 27.20 ± 3.85 mm^3/ Million cycles (MC). Only Archard's wear law (M1), TD-ED (M5) and TD-ED-TR (M6) predicted wear rates fell within one standard deviation of the knee simulator results. The agreement between the knee simulator mean wear rate and the wear model predicted wear rate was best for the TD-ED-TR wear model (M6) (28.22 mm^3/MC).

Table 14: Wear rate results for the AMK under ISO 14243-3 for the third experiment.

		Wear Rate (mm3/Nm)	**Error**
	Knee Simulator	27.2	
M1	Archard et al.	23.54	13.50%
M2	Turell et al.	20.4	25.00%
M3	Abdelgaied et al.	16.66	38.70%
M4	CPI	23.04	15.30%
M5	TD-ED	25.66	5.70%
M6	TD-ED-TR	28.22	3.80%

4.4.2 Discussion

The six wear models were evaluated against POD and knee simulator wear test results. The TD-ED-TR model (M6) demonstrated the greatest overall correlation strength of all the models. Archard's wear law (M1) is proportional only to sliding distance and contact pressure [258] and therefore resulted in poor agreement with the POD and knee simulator results for the first and second experiments (Table 12 and Table 13). Archard's wear law's (M1) success in the third experiment (Table 14) was mainly due to the selection of a wear factor which was well suited to this specific case. Archard's wear law's (M1) applicability is limited, as it could not account for kinematic changes such as increased CS, as demonstrated by the first and second experiments. The model of Turell et al. (M2) offered an increase in correlation strength over Archard's wear law, for the first and second experiments, due to the inclusion of time independent CS in the

model (Table 12 and Table 13). The time and contact pressure independent wear model of Abdelgaied et al. (M3) offered some improved predictability over the previous models for the trend predicting experiments (first and second experiments), yet under-predicted the wear magnitude for the third experiment (Table 12 – Table 14). The CPI wear model (M4) predicted trends similar to the model of Abdelgaied et al. (M3) for the first and second experiments, yet provided improved predictability for the ISO knee simulator (third) experiment (Table 12 – Table 14).

The TD-ED model (M5) resulted in improved predictability over the previously discussed models (Table 12 – Table 14, Figure 44 and Figure 45). The TD-ED model can accurately replicate the trends of the second experiment (kinematics) for the introduction of CS, and increased sliding distances. However, the TD-ED wear model does not consider the effects of tractive rolling on PE wear [217]. Consequently, the TD-ED wear model predicted a decrease in wear, corresponding to the decrease in sliding distance, between tests 3 and 4 (Table 13, Figure 44). The TD-ED wear model predicted a PE wear rate which fell within one standard deviation of knee simulator values for the prediction of the AMK under the stated ISO standard.

The TD-ED-TR (M6) model offered a slight increase in correlation strength over the TD-ED model (M5) for most experiments, since it included a sliding velocity dependent coefficient of friction (Table 12 – Table 14, Figure 44 and Figure 45). For the fourth test of the second experiment the TD-ED-TR model resulted in a 15% increase in wear, compared to the TD-ED model prediction, in response to the introduction of tractive rolling. However, the increase in wear due to the introduction of tractive rolling was

under predicted, resulting in an under predicted wear rate (Figure 44, Table 13). Therefore, the model requires further development to improve its predictive accuracy regarding the magnitude of increase in wear associated with the introduction of tractive rolling. The TD-ED-TR wear model most accurately matched the knee simulator wear test results for the AMK under the stated ISO standard. Furthermore, the PE surface depth values (0.055 mm/year; based on the assumption of 1 MC/year in vivo) predicted by the TD-ED-TR wear model were within the measured range (minimum-to-maximum) of clinically reported PE surface depths for this particular implant from radiographic (0.046-0.115 mm/year) [62] and retrieval (0.03-1.31 mm/year) [360] wear studies.

Contact pressure exhibits complex trends with regards to wear rates, with a downward parabolic trend under constant loading [210], yet consistently increasing wear under dynamic loading [366]. This behaviour was represented in both the TD-ED and TD-ED-TR models by means of an energy dissipation rate factor (*ERF*). However, the precise mechanism by which this behaviour occurs remains unknown. It is speculated that several mechanisms which may be responsible for this behaviour include thermal effects [209] and the resulting changes to crystalline lamellae behaviour [367], lubrication effects [164], or the effects of material cold flow [222].

The TD-ED (M5) and TD-ED-TR (M6) wear models approximate the effects of contact pressure on PE wear and were therefore able to replicate the complex trends demonstrated by POD tests with regard to contact pressure (Figure 46). With increasing contact pressure, Archard's wear law (M1) and the model of Turell et al. (M2) both predicted linearly increasing wear. The model of Abdelgaied et al. (M3) and the CPI wear

model (M4) both predicted a constant wear rate unaffected by contact pressure. Meanwhile, both the TD-ED and TD-ED-TR wear models (M5 and M6) predicted the complex contact pressure - wear trends demonstrated by POD test results.

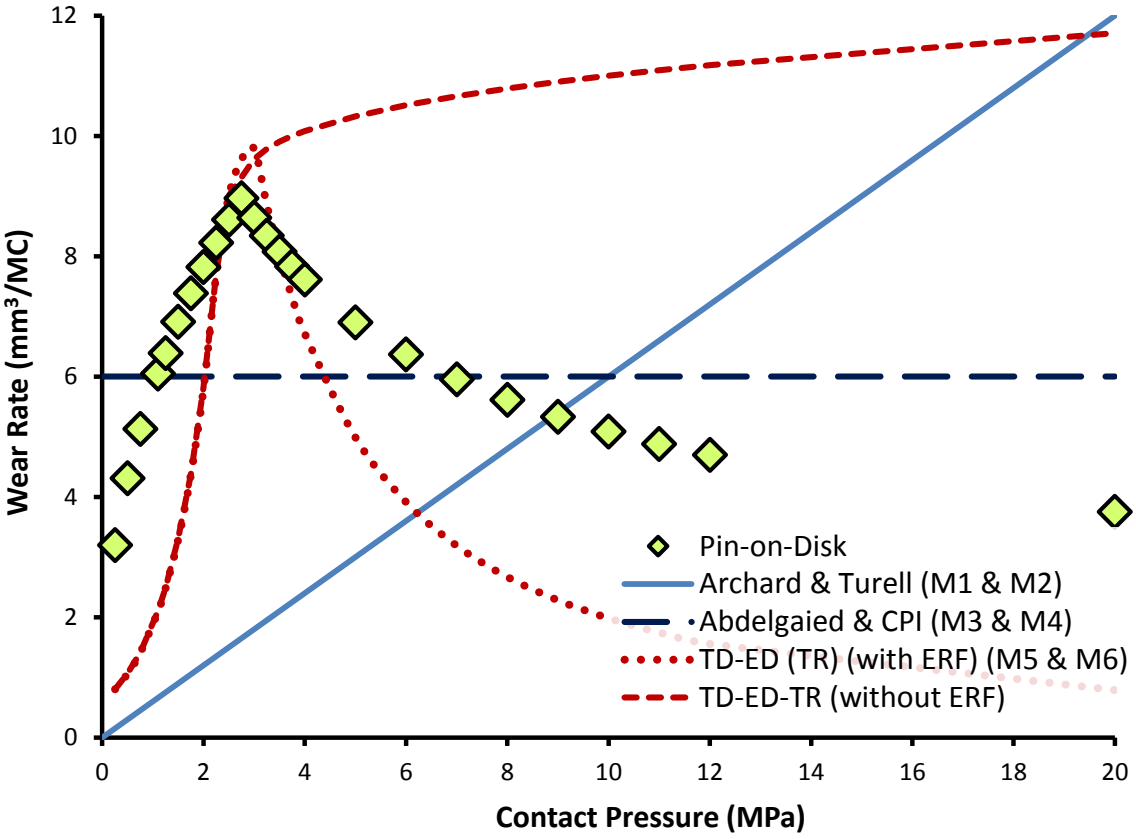

Figure 46: Effect of contact pressure on wear rate as demonstrated by published POD tests [222] and predicted by PE wear models.

Further research must be conducted to identify the precise mechanism responsible for the complex trends related to the effects of contact pressure on PE wear rate. Limitations

of the present study include the approximation of the contact pressure – PE wear behaviour through the energy dissipation rate factor (*ERF*) rather than through the modeling of the precise mechanism responsible for this behaviour. Additionally, the previously discussed differences in experimental conditions between the computational simulation and the knee simulator for the second experiment may have introduced error into the results. Further work, in the following sections of this thesis, aims to address these limitations and continue the development of computational PE wear modeling.

4.4.3 Concluding Remarks

The TD-ED-TR wear model, which incorporated consideration of the time dependent molecular behaviour of PE, aspects of tractive rolling and contact pressure, resulted in an increase in correlation strength over several previously developed wear models compared to POD and knee simulator wear test results. The results of this study warrant the further investigation of the time dependent – energy dissipation approach to the computational wear modeling of TKRs. Further research into the effects of contact pressure on wear and the incorporation of these findings into the TD-ED-TR wear model may further improve the predictive accuracy of computational wear simulations.

4.5 Investigation of the Influence of Contact Pressure on Polyethylene Wear

The TD-ED-TR wear model developed and evaluated in the preceding section (Section 4.4) was demonstrated to provide greatly improved correlation strength for the prediction of TKR wear over several previously existing wear models. However, the results also indicated the need for further research into the effects of contact pressure on wear (Section 4.4). Contact pressure has previously been demonstrated to have a complex effect on wear in POD tests, yet it was previously not known whether the same trends would occur for TKRs. Therefore, *in vitro* knee simulator wear tests and corresponding *in silico* computational wear simulations were performed to further investigate the effects of contact pressure on wear, as well as to evaluate the ability of computational wear models to predict the influence of contact pressure on wear.

4.5.1 *In Vitro* Knee Simulator Wear Test Results

The first knee simulator wear test was conducted under standard loading, over 2 MC and provided a wear rate of 3.37 ± 0.60 mm^3/MC (mean ± 95% confidence interval). The second knee simulator wear test was conducted under increased loading, over 1.5 MC and resulted in a wear rate of 15.12 ± 3.17 mm^3/MC. Therefore, the 1.7 fold increase in load resulted in a 4.49 fold increase in wear rate (Figure 47, Table 15 and Table 16). The surface damage features of the XPE tibial inserts were similar for both the standard loading and increased loading tests and appeared as smooth polished regions. The

increased loading experiment demonstrated a slightly larger surface damage area than the standard loading experiment. Protein precipitation was observed in the lubricant reservoir after each 0.5 MC test interval for all tests.

4.5.2 *In Silico* Computational Wear Simulation Results

During the 2 MC of standard loading the *in silico* computational wear simulations predicted a wear rate of 4.25 mm^3/MC. The computational model parameter R_w of the non-linear (M2) and independent (M3) model variants were adjusted by iterative linear interpolation to match their predicted wear rates with the wear rate of the linear (M1) model variant with an R_w of 1.12×10^{-6}. The computational model parameters R_w for the non-linear (M2) and independent (M3) model variants were found to be 4.44×10^{-6} and 7.23×10^{-7}, respectively. During the 1.5 MC of increased loading the linear (M1), non-linear (M2) and independent (M3) models predicted average wear rates of 6.01, 5.32, and 4.99 mm^3/MC, respectively (Figure 47, Table 16). Wear rate fold increases of 1.41, 1.25, and 1.17 were predicted by the linear (M1), non-linear (M2) and independent models (M3), respectively. The increase in load was found to typically result in an approximate 1.3 fold increase in contact area (Figure 48 - Figure 51). Meanwhile, the contact pressure was shown to typically increase by approximately 1.4 fold due to the increased loading (Figure 48 - Figure 51). The worn areas of XPE inserts were similar between the *in silico* computational wear simulations and the *in vitro* knee simulator wear tests.

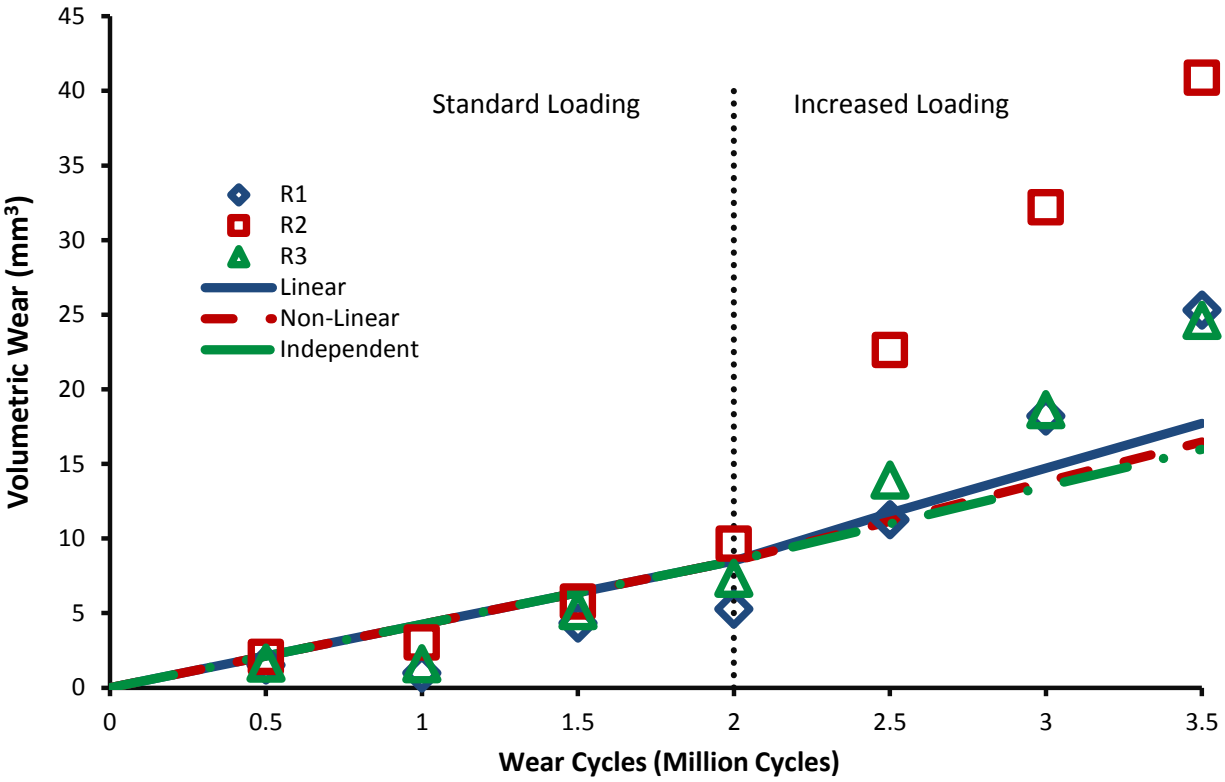

Figure 47: *In vitro* knee simulator wear rates (R1-R3) and *in silico* computational wear predictions of the linear (M1), non-linear (M2) and independent (M3) contact pressure computational wear model variants, under standard (0-2 MC) and increased loading (2-3.5 MC).

Table 15: *In vitro* knee simulator cumulative wear measurements for stations R1, R2 and R3.

Wear Measurement Intervals (MC)	Cumulative Wear (mm^3)		
	R1	R2	R3
0.0	0.00	0.00	0.00
0.5	1.52	2.06	1.66
1.0	1.00	3.03	1.62
1.5	4.32	5.78	5.17
2.0	5.28	9.64	7.34
2.5	11.27	22.64	13.92
3.0	18.21	32.19	18.64
3.5	25.30	40.89	24.63

Table 16: *In vitro* knee simulator mean wear rates and *in silico* computational wear simulation results under standard and increased loading.

	Computational Model Parameter R_w	**Wear Rate (mm^3/MC)**		**Fold Increase in Wear**
		Standard Load	**Increased Load**	
Knee Simulator	NA	3.37	15.13	4.49
Linear (M1)	1.12E-06	4.25	6.01	1.41
Non-Linear (M2)	4.44E-06	4.25	5.31	1.25
Independent (M3)	7.23E-07	4.25	4.98	1.17

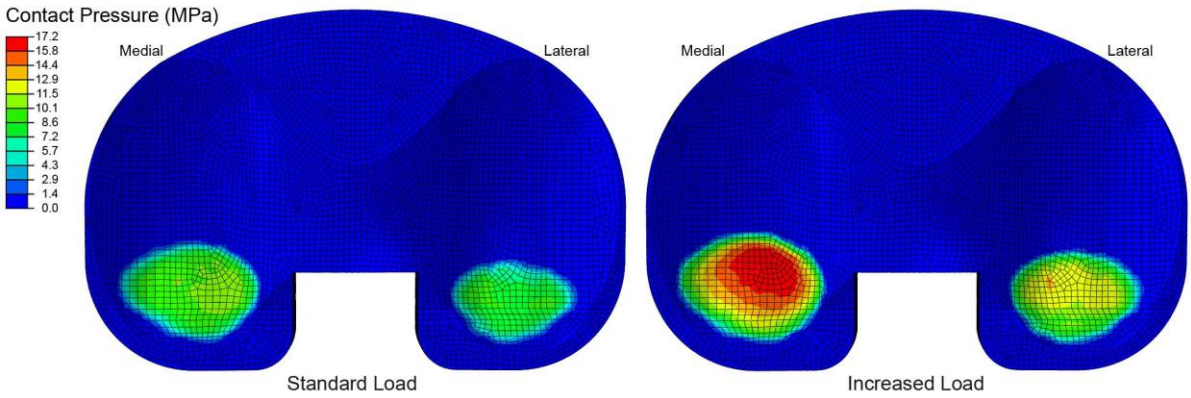

Figure 48: Contact pressure at the XPE insert articular surface predicted by the finite element simulations at the first wear increment during peak loading (t=13%) for the standard and increased loading conditions.

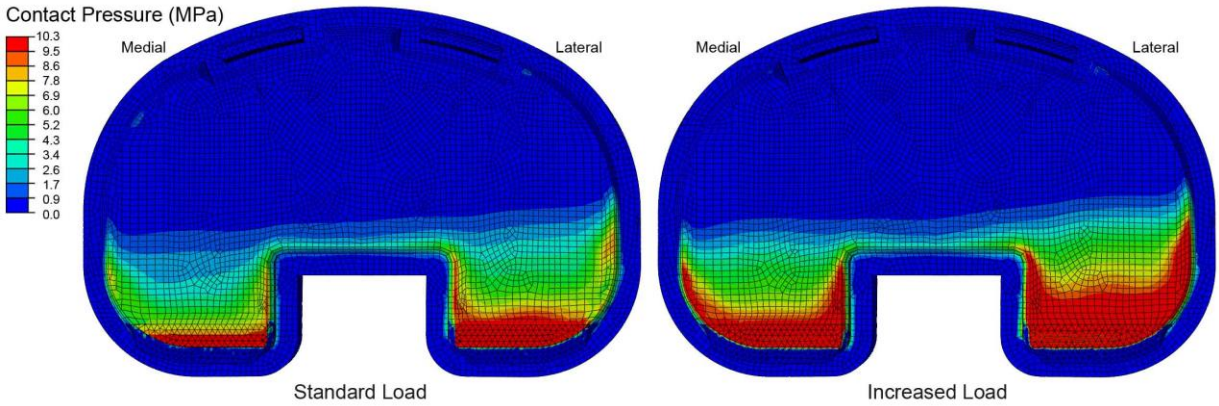

Figure 49: Contact pressure at the XPE insert backside surface predicted by the finite element simulations at the first wear increment during peak loading (t=13%) for the standard and increased loading conditions.

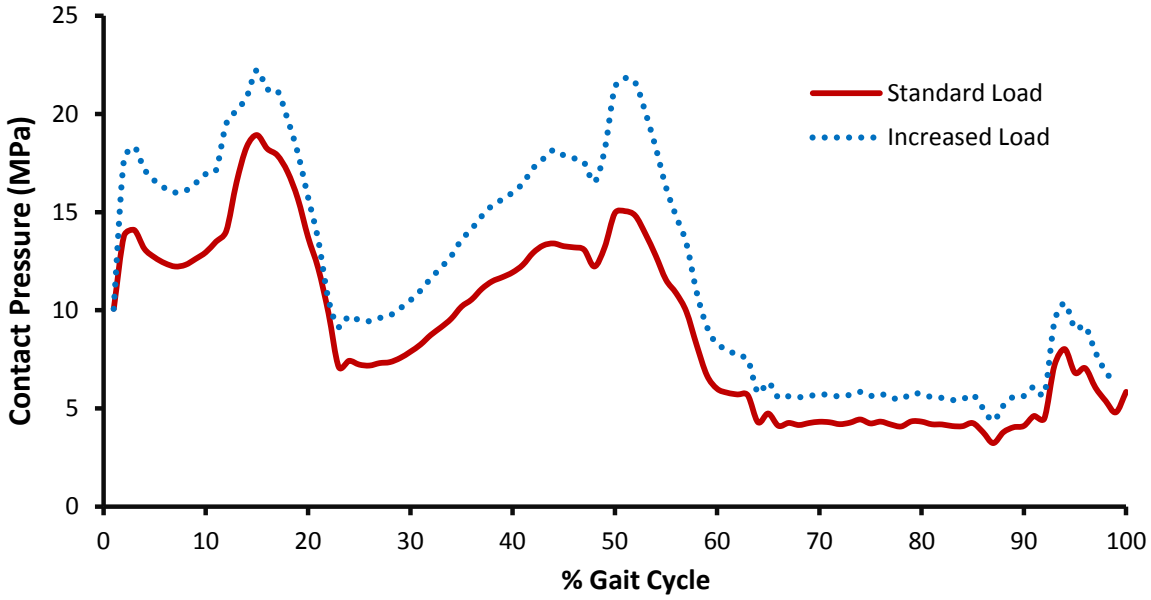

Figure 50: Peak contact pressure at the XPE insert articular surface predicted by the finite element simulations at the first wear increment over the full gait cycle for the standard and increased loading conditions.

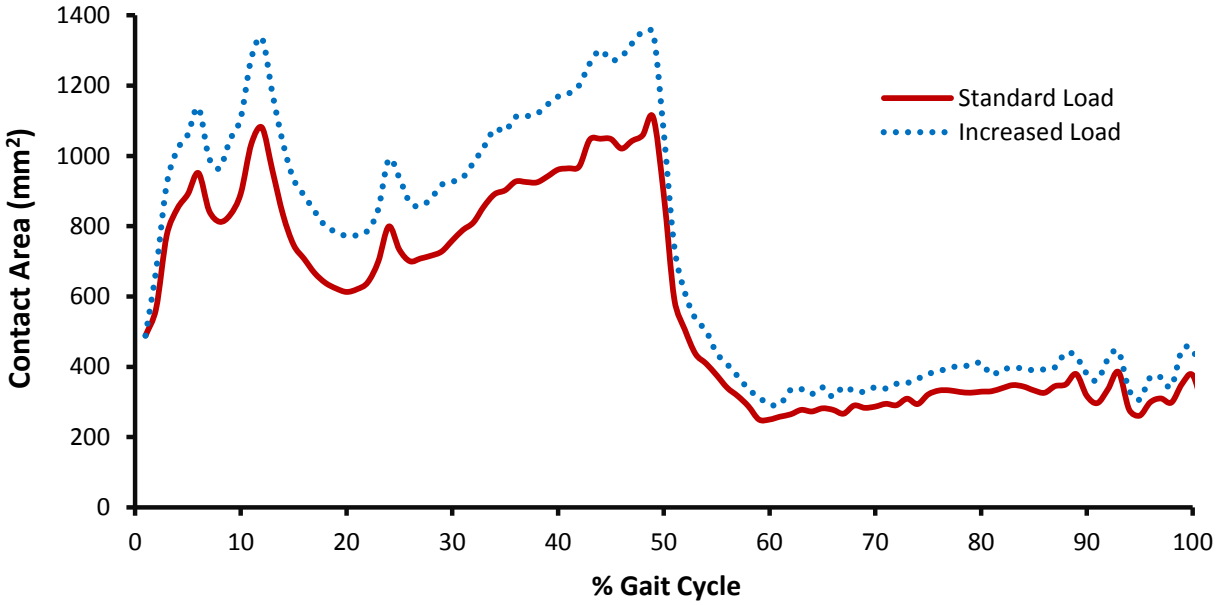

Figure 51: Contact area at the XPE insert articular surface predicted by the finite element simulations at the first wear increment over the full gait cycle for the standard and increased loading conditions.

4.5.3 Discussion

In vitro knee simulator wear tests and *in silico* computational wear simulations were conducted under standardized and increased loading to investigate the effects of contact pressure on XPE wear and evaluate various computational contact pressure models. The *in vitro* knee simulator wear tests under standard loading (3.37 ± 0.60 mm^3/MC) produced similar wear rates to the 3 mm^3/MC wear rate produced under similar kinematics reported by Brockett et al. [368]. The knee simulator wear tests conducted with a 1.7 fold increase in vertical load resulted in a 4.49 fold increase in wear. This increase in knee simulator wear rate was greater than anticipated, based on the results of POD tests which generally demonstrate the trend of decreasing wear with increasing

contact pressure [210, 216, 222, 254, 318]. The FE simulations demonstrated the increased load to result in an approximate 1.3 fold increase in contact area. Based on the 4.49 fold increase in wear of the knee simulator wear tests and the limited increase in contact area predicted by the FE simulations, the results suggest that TKR XPE wear does increase with increasing contact pressure.

In silico computational wear simulations were performed to evaluate the accuracy of the linear (M1), non-linear (M2) and independent (M3) contact pressure wear model variants. All three wear model variants predicted increased articular wear and increased backside wear for the XPE tibial inserts under increased loading. The increased load resulted in increased articular contact pressure, contact area (Figure 48, Figure 50 and Figure 51) and articular wear (Figure 47, Table 16). However, the increase in articular wear was not only dependent on the change in contact area for the independent (M3) model, or the change in contact pressure and contact area for the linear (M1) and non-linear (M2) models. The time dependent cross shear of the material, energy dissipation, and tractive rolling were also accounted for by the computational wear model [37]. The increased loading resulted in increased backside contact pressure and sliding distances (Figure 49). The increased loading at the articular surface led to greater reaction forces at the femoral – XPE tibial insert interface, which resulted in increased backside sliding distances. The increase in backside contact pressure and sliding distances led to increased backside wear. Therefore, increased loading may also be a variable effecting backside wear and locking mechanism degradation [7]. The predicted articular peak contact pressure and contact area trends (Figure 50 and Figure 51) were similar to the trends previously reported for other TKR designs [64]. Of the computational wear model

variants implemented in this study, the non-linear (M2) model has previously been identified to predict the results of POD tests with improved correlation strength over the linear (M1) and independent (M3) computational wear model variants [37]. Yet for the knee simulator wear tests, the linear (M1) model demonstrated improved predictive accuracy over the non-linear (M2) and independent (M3) computational wear model variants (Figure 47). All three of the contact pressure models greatly under-predicted the wear rate increase demonstrated by the knee simulator wear tests (Figure 47). The improved agreement of the linear (M1) contact pressure wear model variant with the knee simulator wear tests, over the other wear model variants, suggests that wear increases with increasing contact pressure in TKRs.

During the knee simulator wear testing, station R2 provided increased wear rates compared to stations R1 and R3 due to inter-station experimental variability. Experimental variability was also observed within each station (Figure 47). However, the error due to experimental variability was limited by specifying the requirement of obtaining a 95% confidence interval of no greater than 20% of the mean wear rate. The TKR components used in the knee simulator wear tests of the current study had also previously been utilized for 10 MC as part of another study [253]. The loading and displacement conditions of ISO 14243-3 had been implemented in this previous study, in agreement with the standard loading and displacement conditions applied for the first 2 MC of the present study. The surface roughness' of the femoral condyles were measured, prior to and after completion of this earlier study, and were found not to have changed substantially [253]. This earlier study was also simulated in the *in silico* computational

wear simulations in the attempt to provide the same starting point for each test, however, such an approach may have introduced additional error.

Based on both the *in vitro* and *in silico* results of this study, it appears that TKR XPE wear may generally increase with increasing contact pressure. These results reveal a discrepancy between knee simulator wear testing, which demonstrated increasing wear with increasing contact pressure, and POD testing, which generally demonstrates decreasing wear with increasing contact pressure within the same contact pressure range. This discrepancy may be due to the differences in lubrication conditions between knee simulators and POD testers. POD tests exhibit flat-on-flat contact under pure sliding while knee simulators exhibit curve-on-curve contact under rolling-sliding. These differences in contact conditions may affect the TKR lubrication. The lubricant properties may change over the course of the tests to different extents through mechanisms such as protein degradation and bacterial growth, based on the different conditions applied and whether or not the lubricant was circulated [232, 251, 361]. Accounting for the differences in lubrication between TKR and POD tests may explain why contact pressure effects wear differently between these two testing methods. The increase in wear demonstrated by the knee simulator under increased loading was greater than that predicted by the computational wear simulation with the linear increasing wear under increasing contact pressure trend (M1). The simulation of TKR lubrication may also account for this discrepancy, as the different conditions between these tests may result in different boundary lubrication conditions. The simulation of lubrication in computational wear simulations may improve the predictive accuracy of computational wear simulations and enable the prediction of both POD and knee simulator wear test results. Further

research must be conducted to investigate this hypothesis and improve our understanding of the effects of contact pressure on wear.

4.5.4 Concluding Remarks

In conclusion, the *in vitro* knee simulator wear tests and *in silico* computational wear simulations demonstrated wear to increase with increasing contact pressure. The computational wear model with the trend of linearly increasing wear with increasing contact pressure, according to the energy dissipation theory, resulted in the greatest agreement with the knee simulator wear test results. However, the linearly increasing wear with increasing contact pressure computational wear model still under-predicted the increase in wear demonstrated by the knee simulator. The non-linearly increasing then decreasing and contact pressure independent wear models greatly under-predicted the increase in wear due to increased load. These results suggest that the trends of POD tests may not be directly applicable to TKRs with regard to contact pressure. Clinically, these results suggest that heavier patients may be at risk of increased wear in comparison to lighter patients with identical kinematics and activity. With regard to TKR conformity and the design of TKRs, a balance must be found between appropriate contact pressure levels, contact area and resultant kinematics. Further research should be conducted to clarify the reasons for the dissimilar trends of POD tests and knee simulator wear tests concerning the effects of contact pressure on wear and to further advance the predictive accuracy of computational wear simulations.

4.6 Development of a Colloid Mediated Boundary Lubrication Model

None of the previous computational wear simulations for TKRs have included a lubrication model to account for the effects of the lubricant on wear, to the best of the author's knowledge. Yet the lubrication of TKRs is known to have a great effect on TKR wear (Section 2.3.2) and may also explain the previously misunderstood trends regarding the effects of contact pressure on wear (Section 4.5). Therefore, in the research of the present section, a colloid protein mediated boundary lubrication model was developed to enable the influence of the lubricant on wear to be considered. The development of the model included the development of relationships for the denaturation, adsorption and boundary lubrication of proteins. The development of a lubrication model was anticipated to explain the complex trends demonstrated by published POD and knee simulator wear tests under varying levels of contact pressure (Section 4.5) and improve the accuracy of computational wear simulations.

4.6.1 Results

The development of the CBL model required the evaluation of several variables to complete the models for the prediction of protein denaturation, adsorption and the effects of the boundary lubrication on wear. First, the variable D_{power}, was identified through conducting least squares regression, utilizing denaturation results obtained from the literature [72, 164]. The variable D_{power} was identified to have a value of 0.5. The

specified value of 0.5 for D_{power} provided a coefficient of determination of 0.90 compared to the experimental values used for its evaluation. As a result of specifying D_{power} as 0.5, the *Denatured Fraction* equation can now be written as:

$$Denatured\ Fraction = D_{Jsm} \cdot (t)^{0.5} \tag{29}$$

By utilizing published knee simulator wear test results which included protein denaturation measurements [164], and conducting computational TKR wear simulations to match the conditions of the knee simulator wear tests, the constants D_a and D_b were identified as 0.0541 and 0.00465, respectively. These specified values provided a coefficient of determination of 0.75 for the modeled result compared to the experimental values used for the evaluation of the constants (Figure 52). Therefore, the D_{Jsm} equation can be written as:

$$D_{Jsm} = J_{SM} \cdot (0.0541 \cdot F_{aby} - 0.00465) \tag{30}$$

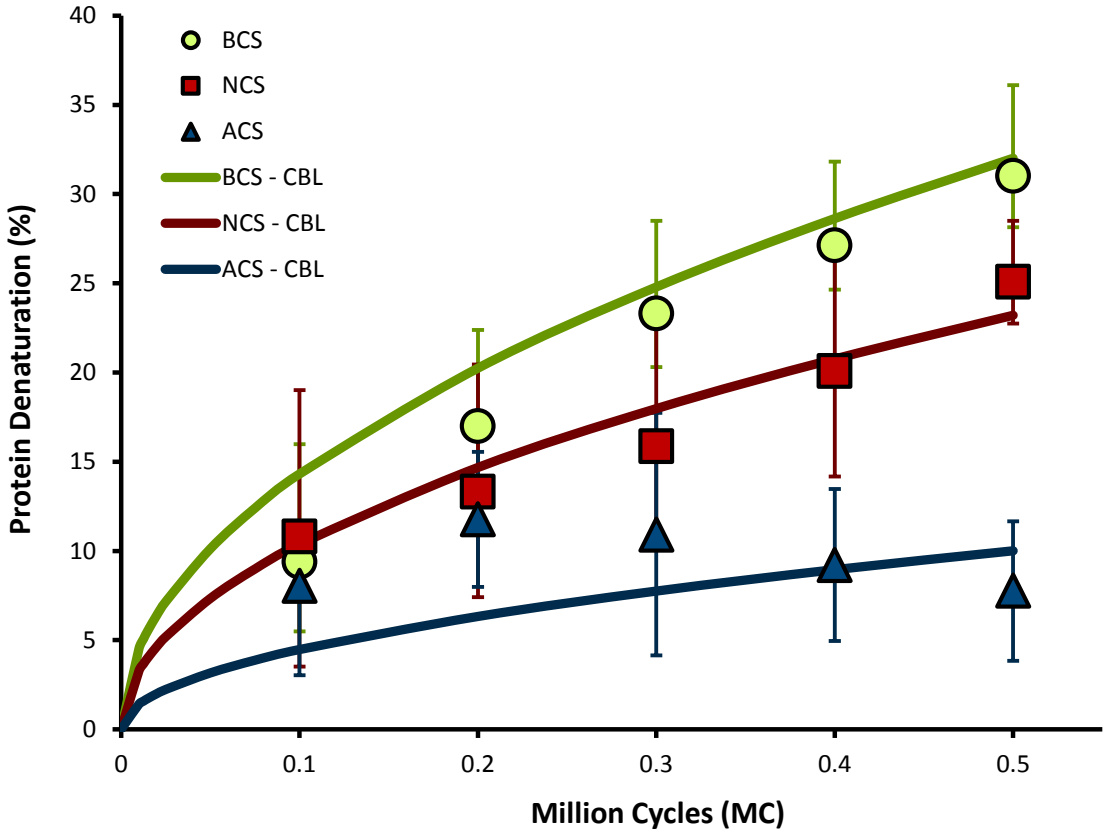

Figure 52: Protein denaturation predictions by the CBL model for bovine calf serum (BCS), newborn calf serum (NCS), and alpha calf serum (ACS) compared to published knee simulator wear test results [165].

Similarly, the constants C_a and C_b were determined using knee simulator wear tests results and were determined to be 3.0 and 0.2, respectively. Therefore, the equation for C_l could be written as:

$$C_l = 3.0 \cdot F_{aby} + 0.2 \tag{31}$$

Lastly, the relationship between adsorbed native and adsorbed denatured proteins with wear was analyzed by considering the difference between computational wear predictions

which did not include consideration for the lubricant compared to POD experiments. The constants L_a, L_b and L_c were established to be 0.288, 0.281 and 0.308, respectively. Thus, the lubrication factor L_F equation can be written as:

$$L_F = [0.288 \cdot \ln(P_{Native}) + 0.281 \cdot \ln(P_{Denatured}) + 0.308] \cdot C_l \quad (32)$$

Comparing the CBL model predicted results to the wear rates demonstrated by the POD experiment used to evaluate the constants L_a, L_b and L_c resulted in a coefficient of determination (R^2) of 0.75 (Figure 53).

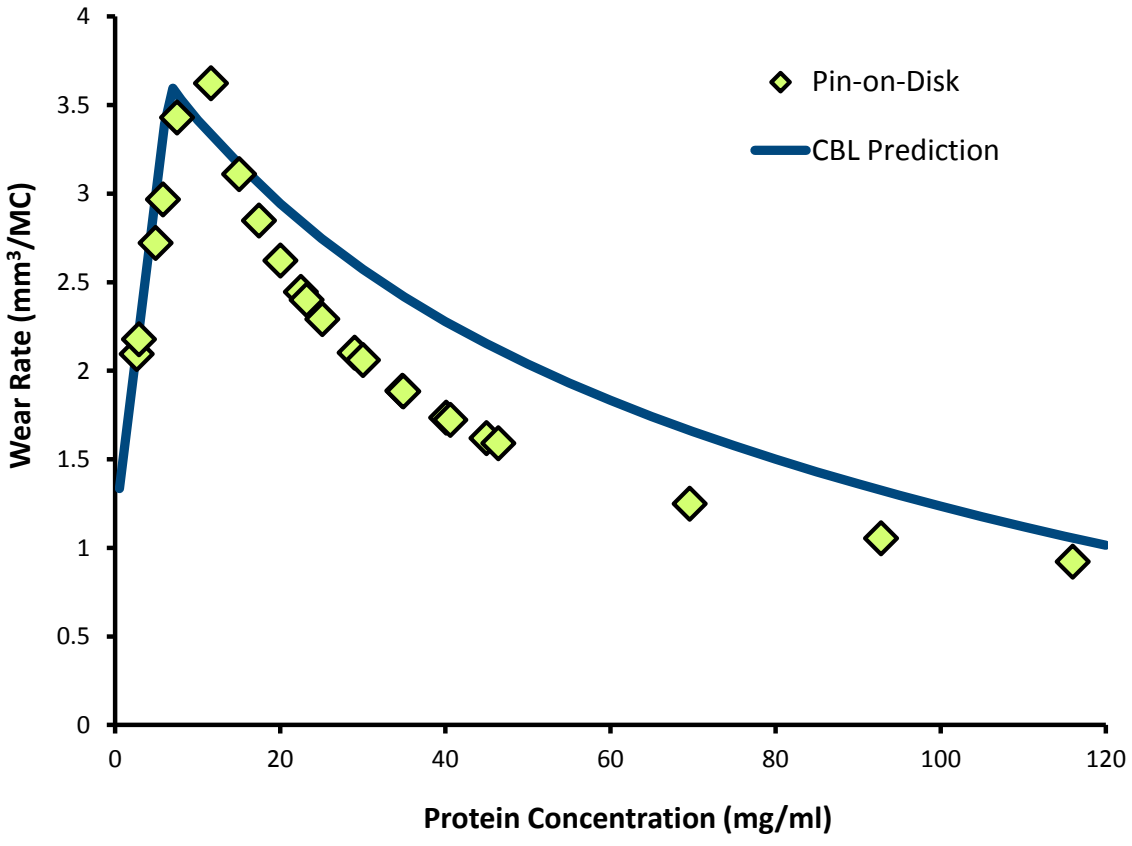

Figure 53: CBL wear rate predictions compared to POD experiments [232] with varying protein concentrations.

4.6.2 Discussion

The CBL model has been developed to predict the denaturation, adsorption and boundary lubrication of proteins from calf serum or human synovial fluid. The CBL model first predicts the denaturation of proteins, as denatured proteins have been demonstrated to result in greatly different boundary lubrication behaviour compared to native proteins [61, 70, 164, 232, 265]. Since β-globulin and γ-globulin proteins have been shown to denature more readily than albumin and α-globulin proteins [164], the relative fraction between these two protein groups is accounted for in the initial denaturation equations. Apart from the composition of the lubricant, the denatured fraction is calculated based on the energy dissipated, the apparent contact area, the time in which the proteins are exposed to the denaturing energy, and the denaturing enthalpy of the proteins. The denatured fraction is also suggested to be inversely proportional to lubricant volume. For simplicity, the relative composition (such as albumin, α-1-globulin, α-2-globulin, β-globulin and γ-globulin) of proteins adsorbed to the surface was assumed to be proportional to the composition of proteins in the lubricant. The competitive adsorption of proteins in their native and denatured states were calculated according to the well established Langmuir model [267]. Finally, the effects of the adsorbed proteins on wear can be calculated based on the fraction of native and denatured proteins adsorbed, as well as the relative composition of those proteins, and their relative strength of adsorption bonding.

The CBL model represents the first TKR computational wear model which provides consideration for the boundary lubrication of TKRs. The CBL model provides

consideration for some of the lubrication variables which have been shown to most greatly affect wear. However, the CBL model also involves many simplifications, since the CBL model development was limited by the available information regarding the denaturation, adsorption and boundary lubrication of proteins. Through conducting further experimentation in the future, it would be possible to further develop the CBL model, reduce the simplifications of the model and further improve its predictive accuracy.

One of the simplifications of the CBL model involved the grouping of protein types into two categories or groups. Group-a proteins included albumin, α-1-globulin, α-2-globulin, while group-b proteins included β-globulin and γ-globulin. The sorting of protein types into these two groups was specified according to the suggestion of Brandt et al. [164] based on findings from knee simulator wear testing. By assuming all protein types within each of these two groups would behave similarly, it was possible to develop correlations for each using the limited data available in the literature. Although the behaviour of albumin has been well researched [32, 33, 69-73, 234, 236, 238], there is comparatively little data available for the other protein types. Therefore, grouping the proteins enabled the analysis to be conducted based on the limited information available. The accuracy of the CBL model could be improved further by conducting experiments to study the denaturation, adsorption and boundary lubrication of each protein type independently, as well as the interactions between different types of proteins. Investigation into the influence of the lubricant composition beyond the proteins would also be of great benefit. Currently, the CBL model only considers the proteins and cannot account for other changes to the lubricant composition, including changes such as

altering the concentration of hyaluronic acid, lipids, sodium azide, ethylenediaminetetraacetic acid, or the use of PBS rather than distilled water (Section 2.3.2).

The CBL model specifies protein denaturation to be proportional to the rate of energy dissipation at the interface. However, the predictive accuracy of the CBL model could be improved by addressing each mode (thermal and shear) of denaturation individually, as well as for each protein type. Such an approach would require experiments to be performed for each denaturation mode and protein type; as such experiments could not be identified in the existing literature. Such an approach would enable the shear conditions to be obtained from the FE simulation results to predict shear denaturation, and the full thermal simulation of TKRs with the surrounding experimental apparatus and environment would enable the thermal denaturation to be predicted. The accuracy of the thermal simulation could be verified through performing the experimental investigation of the localized temperature increases in TKRs, in a similar manner to what has been conducted for total hip replacements [369]. Molecular dynamics simulations may also help to explore the theoretical aspects of protein denaturation [33, 71, 240]. These further improvements to the CBL model would reduce the simplifications of the current CBL model and likely improve the models predictive accuracy. However, these improvements would require further experiments to be performed, as the results of these necessary experiments are not currently reported in the literature.

The protein adsorption model could, once again, be improved through independently addressing each protein type and the lubricant composition, rather than by only addressing two protein groups. The protein boundary lubrication wear model could also

be improved through further experimentation to reduce the simplifications which were required by the current CBL model. However, due to the limited availability of information demonstrating the precise effects of each protein type on asperity interactions, simplifications were required in order to form the CBL model from the existing data. More directly addressing the asperity contacts may also enable additional variables such as roughness to be considered in the CBL model. Both physical experiments and molecular dynamics simulations could contribute to increasing the predictive accuracy of the CBL model in the future by reducing the simplifications of this model.

4.6.3 Concluding Remarks

The proposed CBL model is based upon simplified protein denaturation, adsorption and boundary lubrication theory, with constants which have been derived from physical tests that were available in the literature. To verify the complete CBL wear model, the model must be corroborated with a broad range of experiments to evaluate the models predictive capabilities.

4.7 Verification of the CBL Computational Wear Model

The accuracy of the CBL model was verified by comparing the wear predictions of the model to a broad range of wear tests including POD and knee simulator wear tests. Computational simulations were performed to replicate the experimental conditions of each experiment for the direct comparison of results.

4.7.1 Results

First, the material parameter M_{mc} was represented using a symmetric sigmoid function to relate crosslinking radiation to the material parameters of the CBL model. The sigmoid approach was selected based on the wear results of hip wear simulator experiments conducted under a broad range of crosslink densities [61]. The material parameter R_w was also initially modeled using the symmetric sigmoid function. However, a simple exponential function was discovered to provide equivalent results to the sigmoid function for the material parameter R_w, and an exponential function was therefore selected for the sake of simplicity. The constants of the functions were determined based on previous ED wear simulation results (Sections 4.4 - 4.5), and the functions were specified as:

$$M_{mc} = 0.018 + 0.037/\left(1+(M_{Rad}/3.12)^{14.8}\right) \quad (33)$$

$$R_w = (1.25 \cdot 10^{-6}) + [(2.75 \cdot 10^{-6}) \cdot (e^{-MRad})] \quad (34)$$

Following the establishment of the relationships between the CBL material parameters, wear could be predicted for any POD or TKR test utilizing CoCr alloy and PE or XPE lubricated using any calf serum or synovial fluid.

4.7.1.1. Model Corroboration with Pin-on-Disk Wear Tests

Computational wear simulations using the CBL model were performed to predict the results of five sets of POD tests (POD 1 – POD 5). The CBL wear simulations predicted the POD test results with an overall coefficient of determination (R^2) of 0.85 (Table 17) (Figure 54 - Figure 61).

Table 17: Correlations of the CBL computational wear simulation for POD experiments.

	Experiments				
	POD 1	**POD 2**	**POD 3**	**POD 4**	**POD 5**
PE Pin Conditions					
Pin Diameter (mm)	9	5-10	5-8	9	9.5
Sliding Velocity (mm/s)	32	20-76	20-76	20	64
PE Crosslink Radiation (MRad)	2.5-4	0	6, 10	0	4, 5
Contact Pressure (MPa)	0.25-20	1,3,6,10	1, 3	3	4.7
Cross Shear (%)	1	0-0.25	0-0.25	1	1
Lubrication Conditions					
Lubricant Volume (ml)	12	40	40	NA*	NA*
Lubricant Type	ACS	BCS	BCS	BCS	BCS
Protein Concentration (g/l)	21	15.4	15.4	23	65
β & γ Fraction (%)	0.16	0.33	0.33	0.33	0.33
Sodium Azide Concentration (%)	0	0.001	0.001	0.002	0.002
Lubricant Replacement (hours)	24	92	92	56	50
CBL Results					
Coefficient of Determination (R^2)	**0.75**	**0.92**	**0.83**	**0.84**	**0.97**
Average Coefficient of Determination (R^2)	**0.85**				

* Not Specified
ACS and BCS represent Alpha Calf Serum and Bovine Calf Serum, respectively
Units in % range from 0 (minimum) to 1 (maximum)

The first set of POD tests (POD 1) investigated the effects of contact pressure on wear [222]. The POD tests demonstrate the controversial trend of initially increasing and then decreasing wear under increasing contact pressure. The ED model predicts the trend of initially increasing wear, followed by a plateau for high contact pressures (Figure 54). Meanwhile, the CBL model accurately predicts both the ascending and descending wear behaviour under increasing contact pressure through accounting for the increasing denaturation of proteins at higher contact pressures (R^2=0.75).

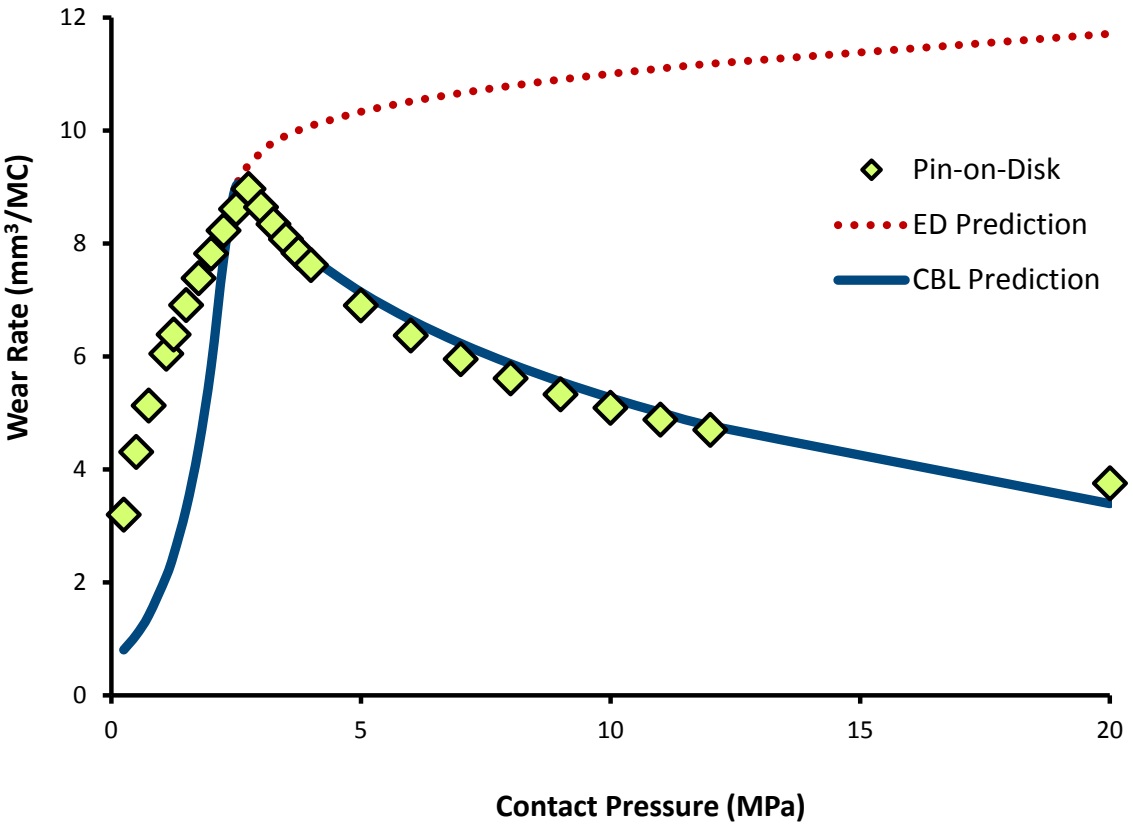

Figure 54: XPE wear predictions compared to POD results under varying contact pressure conditions (POD 1).

The second set of POD tests [210, 216, 318] (POD 2) considered the effects of varying cross shear, sliding distance and contact pressure on PE wear. The ED wear model provided accurate wear predictions for the tests in which the energy dissipation was low (Figure 55), but provided decreasing levels of accuracy as the energy dissipation was increased through increased contact pressures (Figure 56 and Figure 57). Meanwhile the CBL model more accurately predicted wear across the broad range of contact pressure values through accounting for the increasing denaturation of proteins for high contact pressures (Figure 55 – Figure 57). The CBL model provided a coefficient of determination of R^2=0.92.

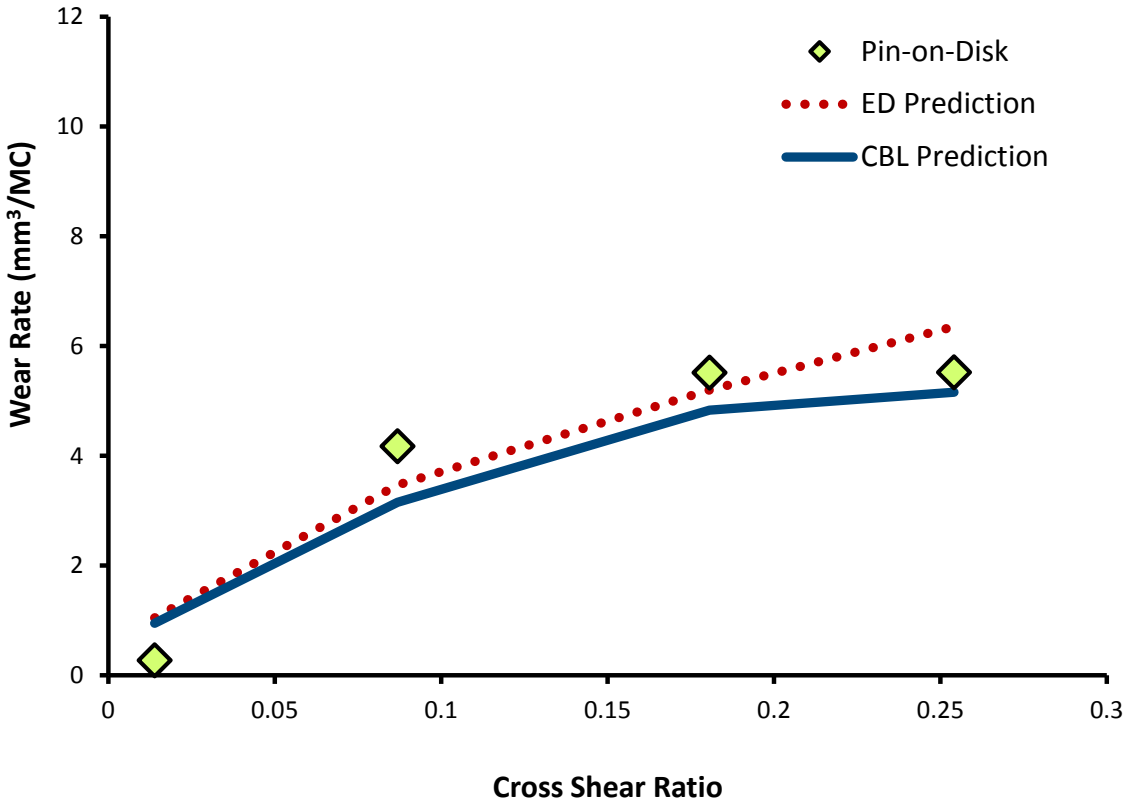

Figure 55: PE wear predictions compared to POD results under varying cross shear conditions at 1 MPa of contact pressure (POD 2).

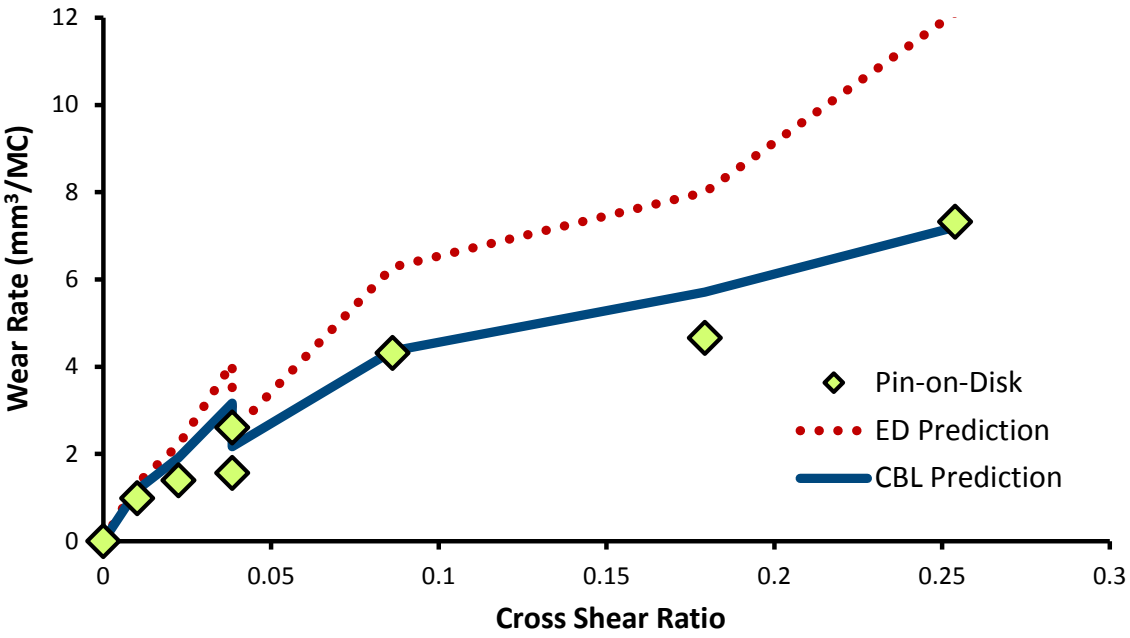

Figure 56: PE wear predictions compared to POD results under varying cross shear conditions at 3 MPa of contact pressure (POD 2).

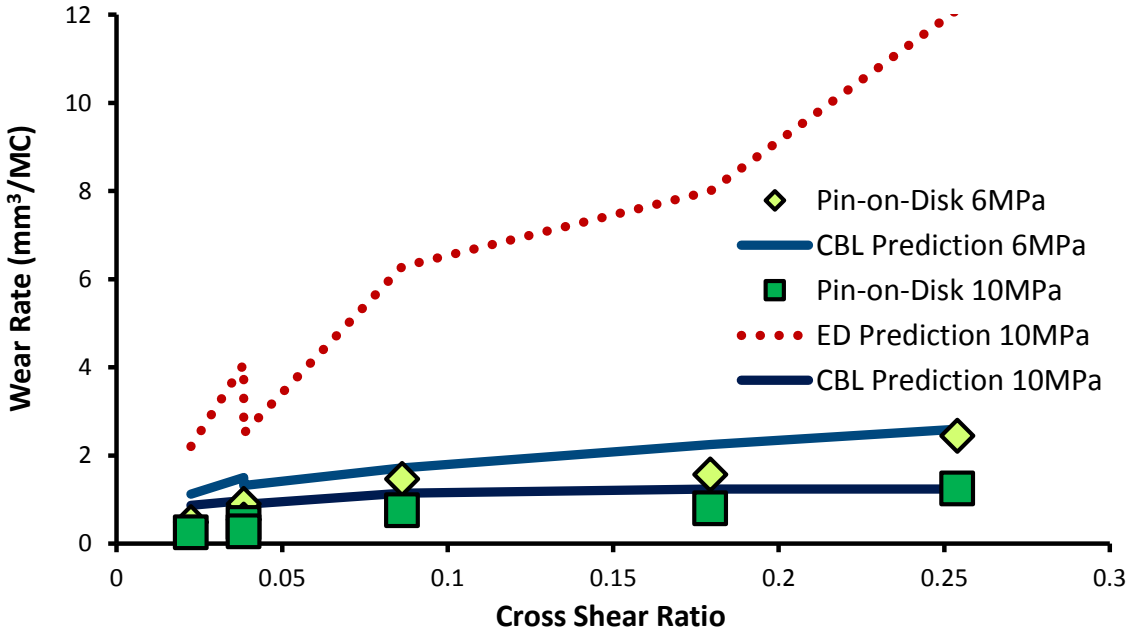

Figure 57: PE wear predictions compared to POD results under varying cross shear conditions at 6 MPa and 8 MPa of contact pressure (POD 2).

The third set of POD tests [216, 318] (POD 3) used some of the same experimental conditions as the second set of POD tests, but utilized XPE instead of the PE used in the second set of POD tests. The altered crosslink density of the material caused a decrease in wear rates relative to the second set of POD tests (Figure 58 and Figure 59). The CBL model once again demonstrated a strong correlation for the prediction of POD wear rates (R^2=0.83).

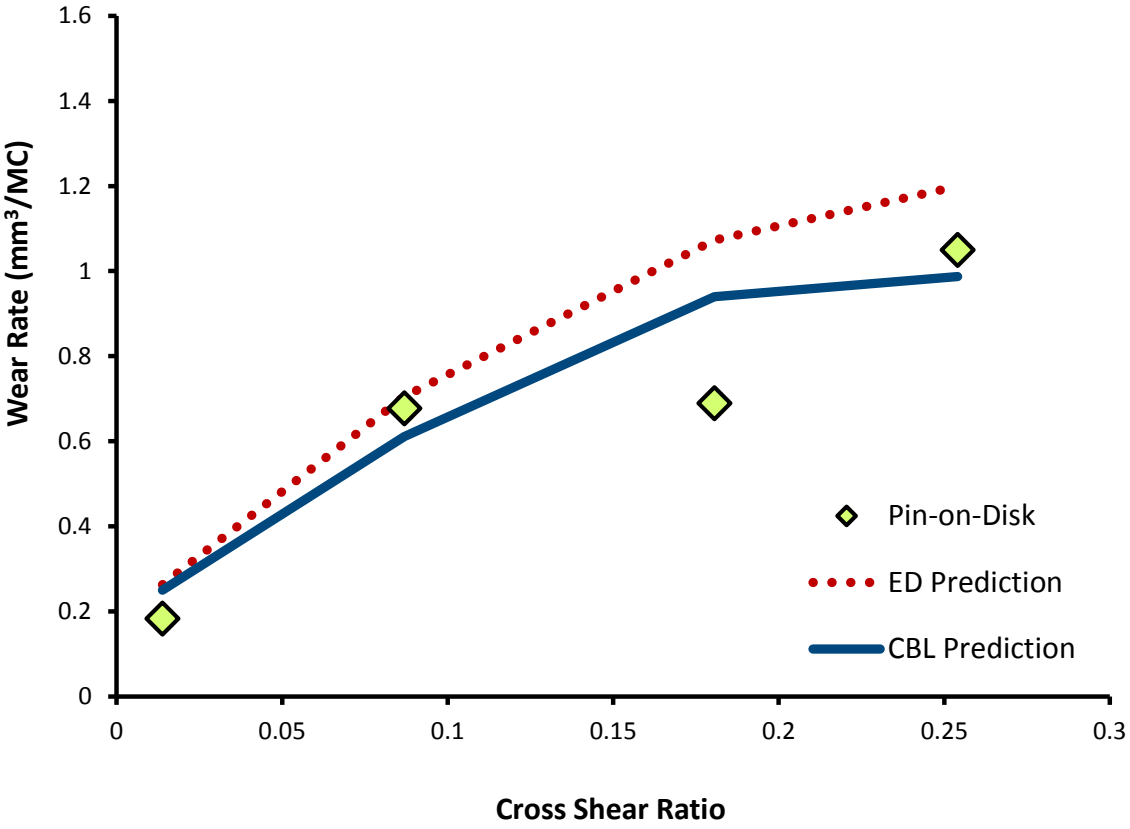

Figure 58: XPE wear predictions compared to POD results under varying cross shear conditions at 1 MPa of contact pressure (POD 3).

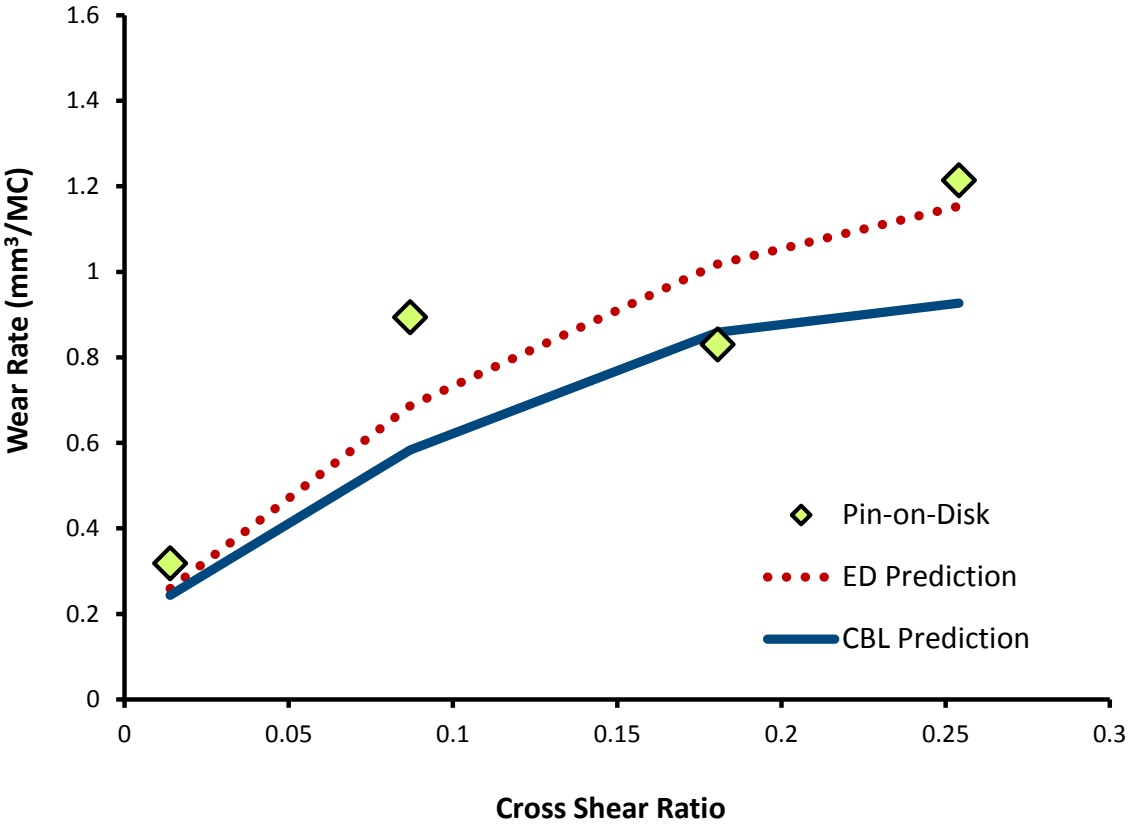

Figure 59: XPE wear predictions compared to POD results under varying cross shear conditions at 3 MPa of contact pressure (POD 3).

The fourth set of POD tests [60] (POD 4), utilized rectangular slide paths for PE pins with varying aspect ratios of the rectangular sliding path. The CBL model not only accurately predicted the general trend of increasing wear with increasing aspect ratio, but also predicted the nonlinear behaviour of this trend (Figure 60), providing a coefficient of determination of R^2=0.84.

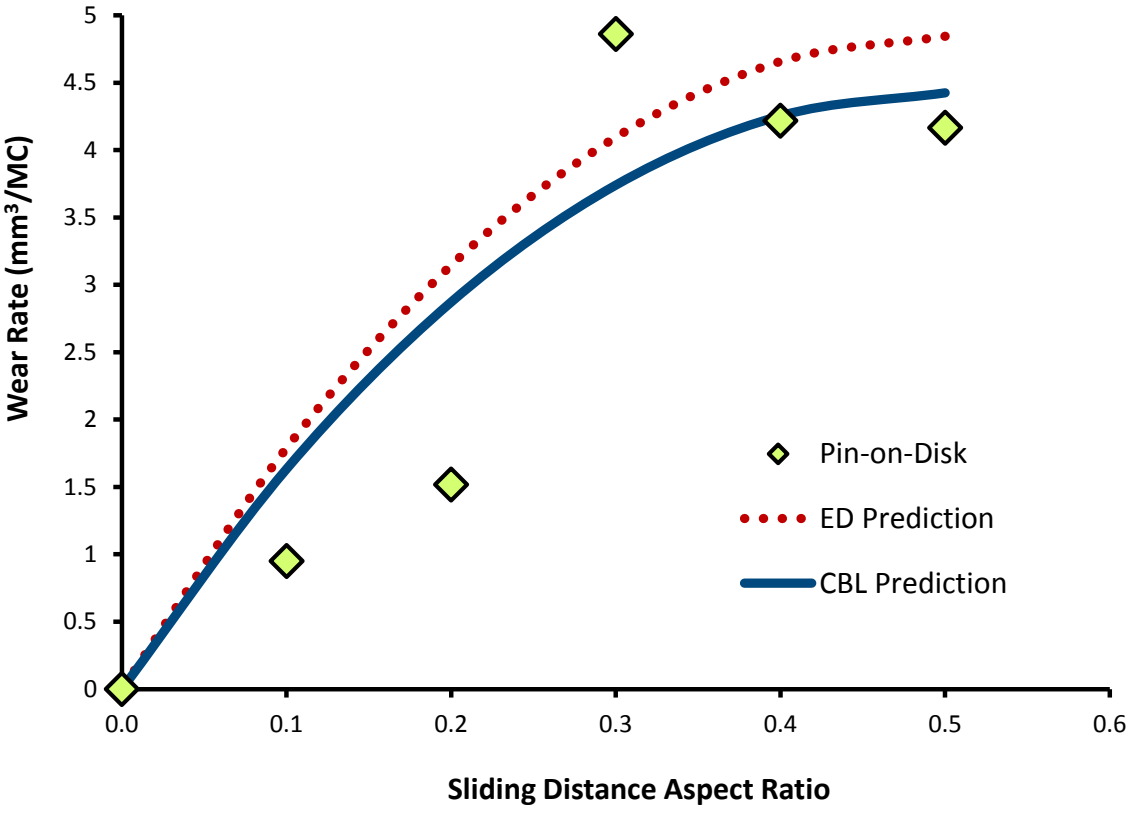

Figure 60: PE wear predictions compared to POD results under varying sliding distance aspect ratios for POD tests with rectangular slide patterns (POD 4).

The final set of POD tests [59] (POD 5), utilized square slide paths for XPE pins with varying slide lengths. These tests demonstrated the importance of a time dependent cross shear wear model. The ED model accurately predicts the trends of these tests (Figure 61). The CBL model accounted for protein denaturation in addition to the time dependent cross shear directional strain hardening of the material, providing a coefficient of determination of R^2=0.97.

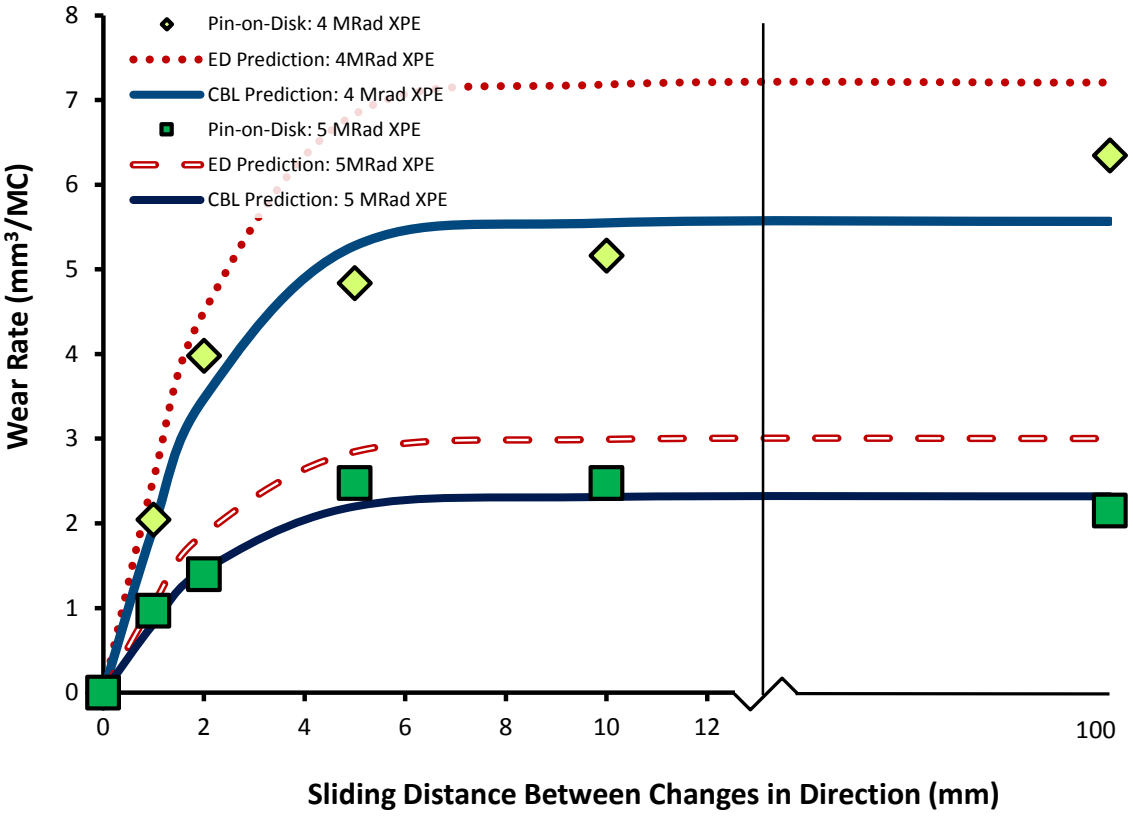

Figure 61: XPE wear predictions compared to POD results with varying slide distances between each 90° direction change (POD 5).

4.7.1.2. Model Corroboration with Knee Simulator Tests

The wear rates of 20 knee simulator wear test experiments were predicted using the ED and CBL wear models. The results of the experiments were compared to analyze the wear models abilities to accurately predict wear under varying kinematics (Figure 62 - Figure 63), loading (Figure 64), TKR conformity (Figure 65), XPE crosslinking radiation (Figure 66), tibial modularity (Figure 67), lubrication volume (Figure 68), lubricant concentration (Figure 69) and finally lubricant composition (Figure 70).

The first knee simulator wear test comparison involved the comparison of TKR wear rates under various kinematic motions to analyze the effects of these kinematics on wear [354]. The tests included flexion only; flexion and internal-external rotation; flexion, internal-external rotation and positive anterior-posterior displacement; and finally flexion, internal-external rotation and negative anterior-posterior displacement. Since the majority of the relative sliding was due to the flexion of the TKR, the protein denaturation of each of the four tests remained similar, resulting in similar predictions between the ED and CBL models (Figure 62). Both the ED and CBL models predicted results which fell within the standard deviation of the knee simulator wear test results.

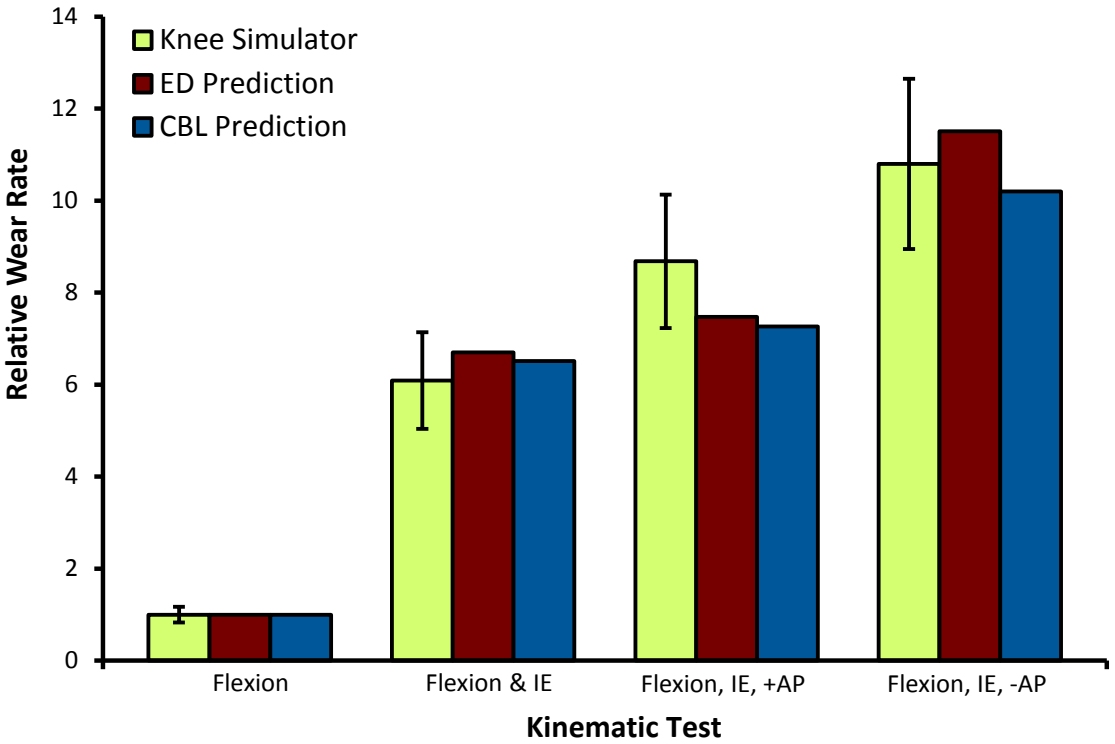

Figure 62: TKR wear prediction under varying kinematic conditions (decoupled kinematics) (+ or - AP represents positive or negative Anterior-Posterior displacement direction).

The second kinematic comparison investigated the effects both high and intermediate kinematics (reduced anterior-posterior displacement) on the wear of two different TKR designs [254]. Similar trends were predicted by the ED and CBL wear models and the predictions of the CBL model fell within the standard deviation of the knee simulator wear tests (Figure 63).

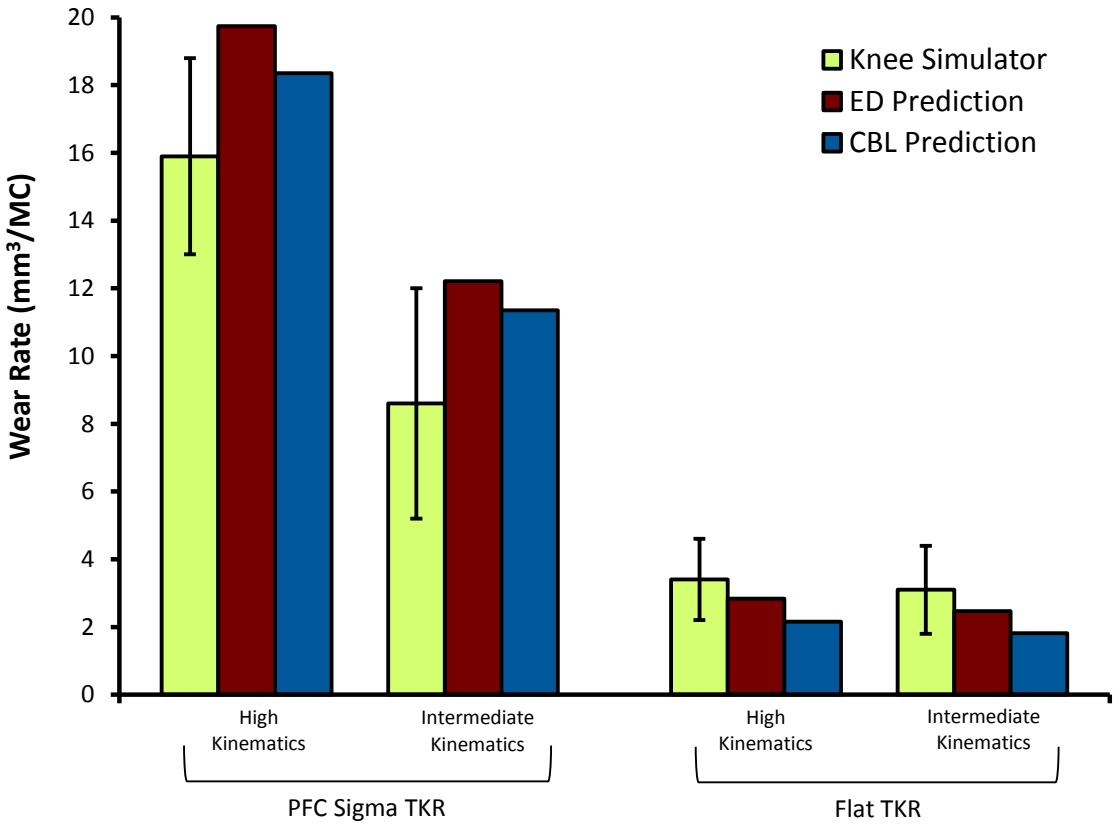

Figure 63: TKR wear prediction under varying kinematic conditions (high and intermediate).

The influence of load on TKR wear was also investigated through the analysis of wear under the ISO standard 14243-3 and for an increased loading case which included a 1.7 fold increase in load [264]. The knee simulator wear rates were calculated using linear regression over the last 3 wear intervals (0.5MC) for each loading condition. The comparison between ED and CBL models reveals the increased denaturation of proteins to have occurred for the increased loading case (Figure 64). The CBL model resulted in predicted wear rates which fell within the standard deviation of the knee simulator wear test results.

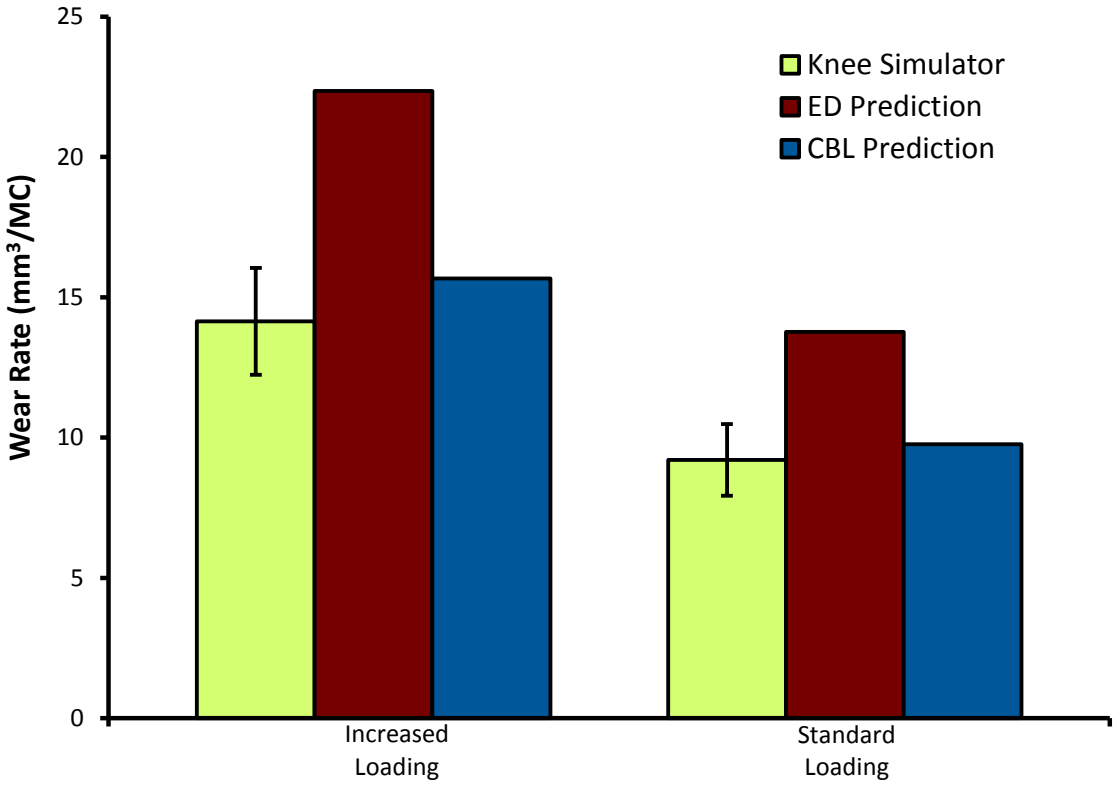

Figure 64: TKR wear prediction under standard and increased loading conditions.

The influence of TKR articular conformity on wear was analyzed by comparing the wear rates of the PFC-Sigma TKR and a flat version of the PFC-Sigma in which the articular surface of the XPE tibial insert had been machined flat [254]. The changes in conformity resulted in alterations to the contact pressure and contact area. As a consequence of the altered contact areas and location of contact on the XPE insert, cross shear and sliding distances were also altered. These changes led to greatly reduced wear rates, predicted by both the ED and CBL models (Figure 65). The CBL model predicted wear rates fell within the standard deviation of the knee simulator wear tests.

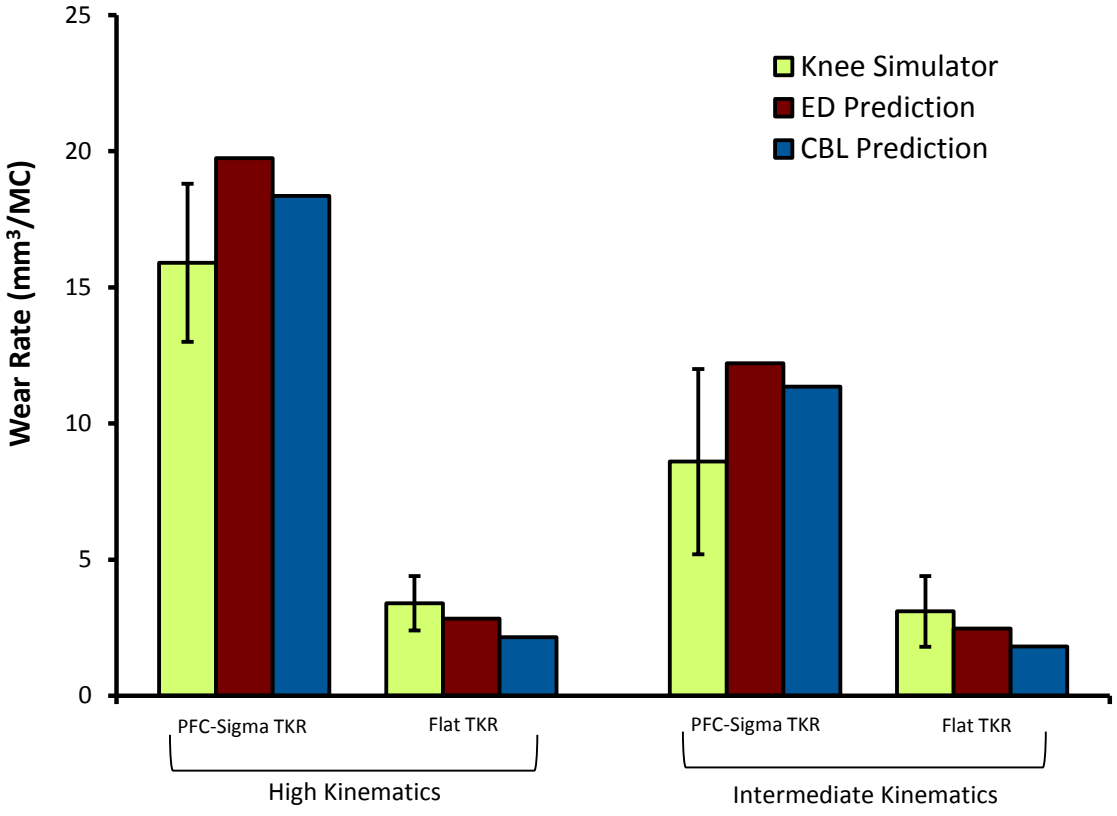

Figure 65: TKR wear prediction under varying levels of conformity.

The influence of increased crosslink density was investigated through comparing the wear rates of two TKRs under the same conditions but with XPE inserts of different crosslink densities (PFC-Sigma: 2.5-4 MRad and modified-PFC-Sigma: 5 MRad) [16, 254]. The difference between the ED and CBL models was the same for both TKRs, and the CBL model once again predicted results which fell within the standard deviation of the knee simulator wear test results (Figure 66).

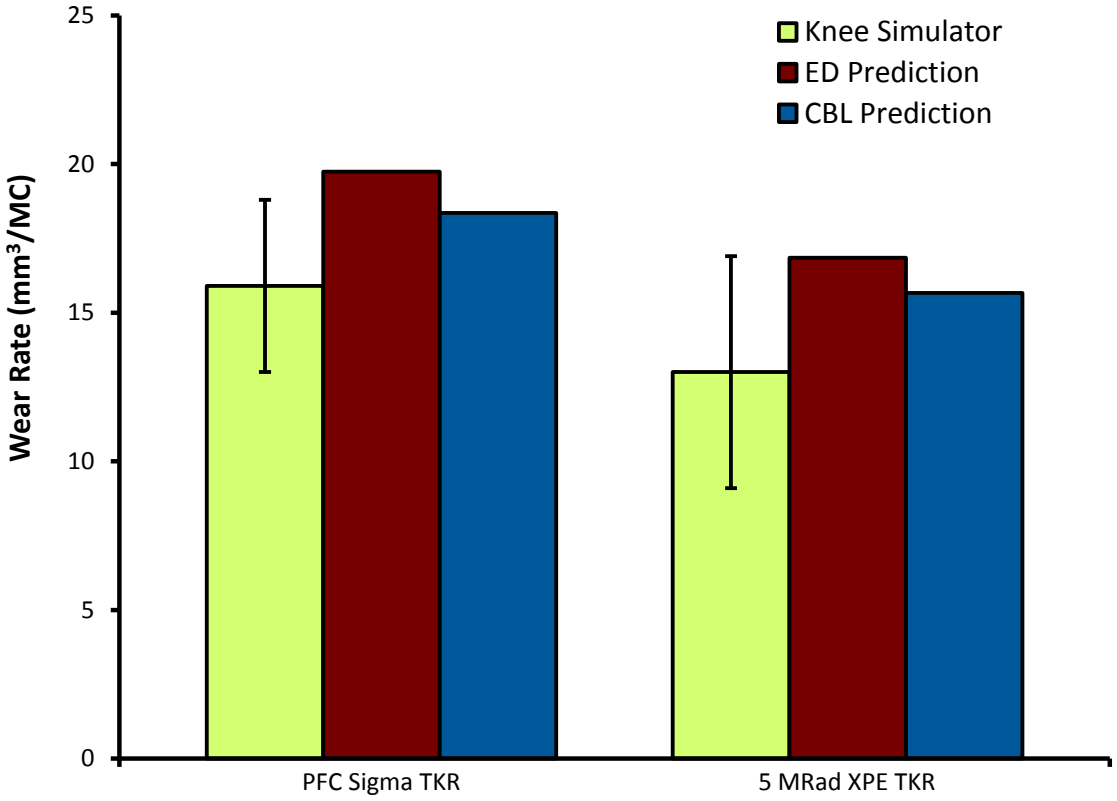

Figure 66: TKR wear prediction for XPE subjected to different levels of crosslinking radiation.

The effect of including a modular tibial interface was analyzed through the comparison of TKRs of the same design [11] but which either included or did not include a modular interface. The difference between the ED and CBL model predicted wear rates was very similar between the two designs, as the backside interface made a much smaller contribution to protein denaturation in comparison to the articular surface. The CBL predicted wear rates fell within the standard deviation of the knee simulator wear rates, indicating the accurate prediction of backside wear magnitudes (Figure 67).

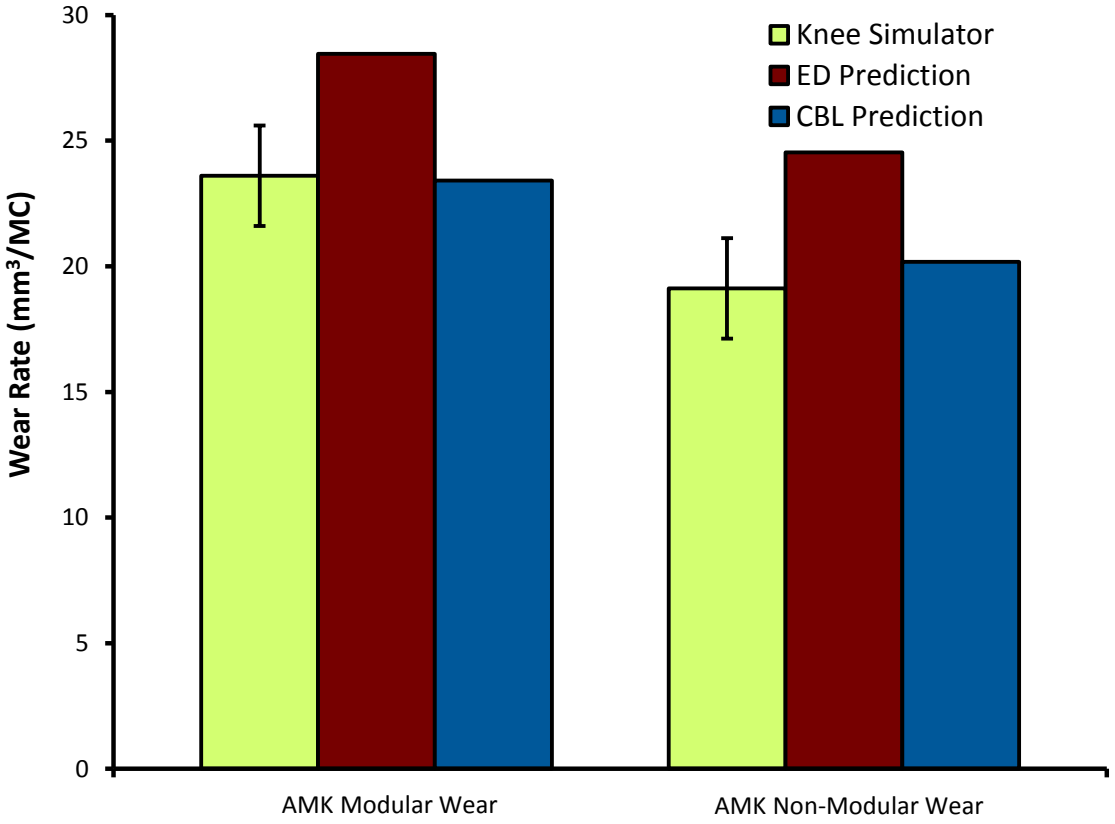

Figure 67: TKR wear prediction of modular and non-modular designs.

The influence of lubricant volume and its effects on protein denaturation and XPE wear was considered through varying the volume of the lubricant surrounding the TKR components [265]. The ED model predicted consistent wear rates regardless of lubricant volume (Figure 68). Meanwhile, the CBL model predicted the trend of decreasing wear with decreasing lubricant volume due to increasing fractions of the proteins becoming denatured. The CBL model predicted wear rates which fell within the standard deviation of the knee simulator wear test results apart from the wear rate at 75 ml. The CBL model provided a strong correlation for the prediction of the knee simulator wear rates, with a coefficient of determination of R^2=0.84.

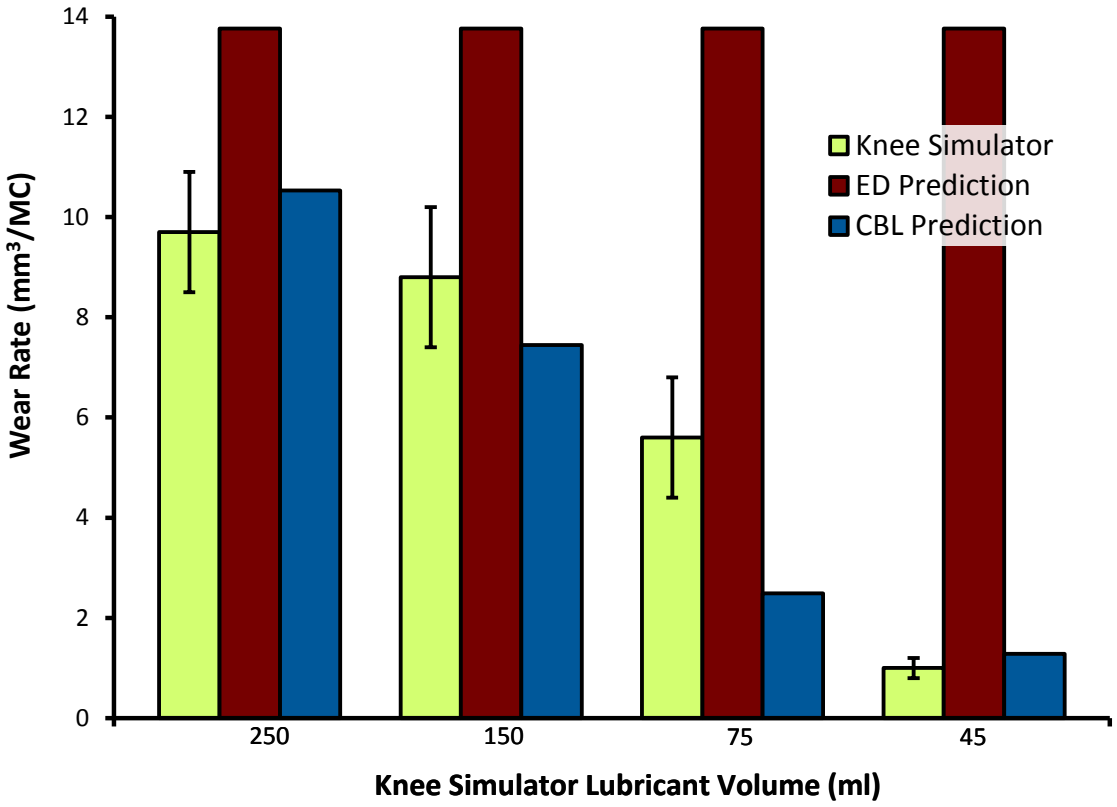

Figure 68: TKR wear prediction under varying lubricant volumes.

The influence of the lubricant on wear was further investigated through the comparison of wear rates for the same TKR design (AMK) under the ISO standard 14243-3 with a bovine calf serum protein concentration of 17 g/l, compared with a bovine calf serum protein concentration of 62 g/l and reduced anterior-posterior translation. The ED model predicted a relative decrease in wear associated with the decrease in anterior posterior displacement (Figure 69). The CBL model predicted a decrease in wear rate associated with the increase in protein concentration as well as altered kinematics, and predicted wear rates which fell within the standard deviation of the knee simulator wear test results.

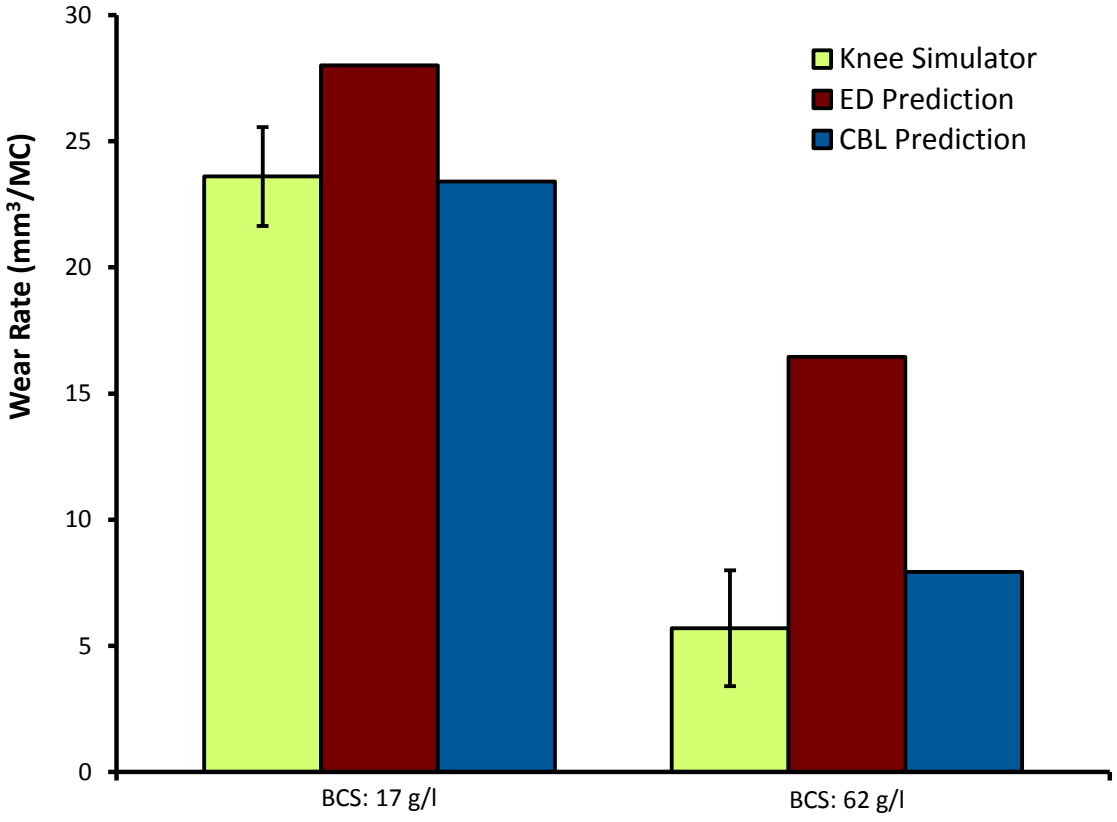

Figure 69: TKR wear prediction using bovine calf serum diluted to different protein concentrations.

The final comparison investigated the effects of different calf serum types (alpha, newborn and bovine) on TKR wear [164]. The ED model predicted the same wear rate for all tests, since the ED model does not provide consideration for the lubrication of TKRs (Figure 70). The CBL model accurately predicted wear rates within the standard deviation of the knee simulator wear test results.

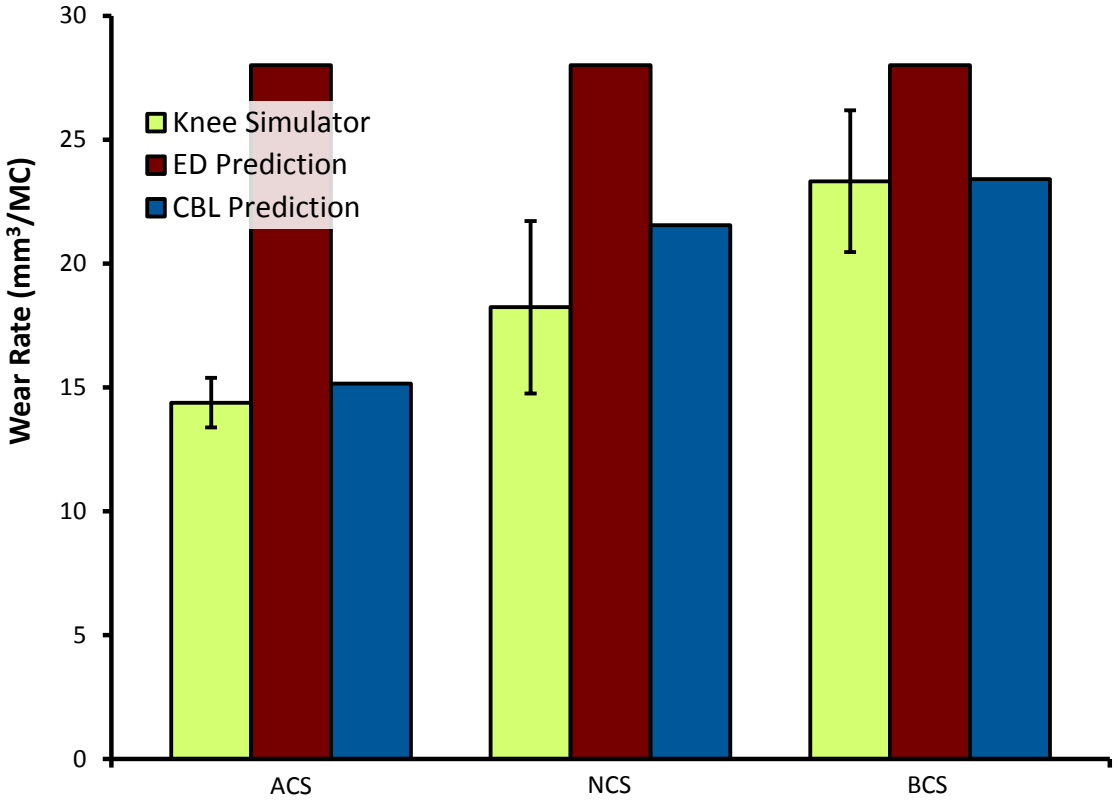

Figure 70: TKR wear prediction using three different lubricants; alpha calf serum (ACS), newborn calf serum (NCS) and bovine calf serum (BCS).

4.7.2 Discussion

4.7.2.1. Model Corroboration with Pin-on-Disk Wear Tests

The first POD experiment (POD 1, Figure 54) demonstrated the capability of the CBL wear model to predict the trend of initially increasing, then decreasing wear under increasing contact pressure. Previously available computational wear models have either predicted continually increasing wear with increasing contact pressure or have been developed to be contact pressure independent and would have predicted a consistent wear rate for all contact pressure values. Furthermore, any time independent cross shear wear model would also have been unable to predict the results of a POD test such as POD 1, since this experiment requires the continuous reorientation of the crystalline lamellae to be predicted in order to match the experimental conditions of the POD. Not only have previously available computational wear models been unable to predict the trends demonstrated by POD tests under varying contact pressure conditions, but an explanation for this observed trend has previously not been available. However, through the protein denaturation, boundary lubrication and energy dissipation research of this thesis, this trend can finally be explained and predicted. Through accounting for the time dependent directional strain hardening of the material (according to the ED wear model), an initially increasing wear rate was predicted by the ED wear model for low contact pressures. Once contact pressures of approximately 3 MPa are reached, the increase in wear rate under increasing contact pressure becomes much less appreciable according to the ED wear model. This is because the increased energy dissipation, corresponding to the increased

contact pressure, causes the more rapid alignment of the crystalline lamellae molecular orientation. Therefore, the cross shear angles become less severe and there is not a great increase in wear under increasing contact pressure in the high contact pressure range. The trend predicted by the ED wear model is consistent with what could be expected if the POD experiment utilized a continuous changeover of the lubricant in order to limit the potential for denatured proteins to remain in the system. However, to fully predict the trend of this POD experiment, the denaturation of proteins must also be predicted. The CBL wear model predicted the increasing denaturation of proteins under increasing contact pressure as a result of the additional dissipation of protein denaturing energy. Therefore, the CBL wear model was able to successfully predict the decreasing wear with increasing contact pressure trends for contact pressures above 3 MPa as a result of the improved wear protection offered by denatured proteins relative to native proteins. The computational simulations provided a coefficient of determination of 0.75 compared to the POD experiments and provided greatly improved predictive accuracy over the continually increasing wear with increasing contact pressure, or contact pressure independent predictions which would be provided by previously existing computational wear models.

The ability of the CBL wear model to predict the trend of initially increasing, then decreasing, wear under increasing contact pressure is very significant. The author is not aware of any previously existing TKR computational wear model which can predict this trend. Not only have previously available computational wear models been unable to predict this complex behaviour, but the mechanism for this behaviour was also previously unknown [210, 216, 222, 254, 318]. This complex trend has previously been used to

advocate that PE and XPE wear is contact pressure independent [39, 254, 261], due to the lack of available explanation for the mechanism which might cause this complex trend. However, through accounting for the energy dissipation, time dependent cross shear, protein denaturation and boundary lubrication, the CBL model provides an explanation for this trend. Understanding this trend is very important not only for the prediction of TKR wear, but also for making fundamental TKR design decisions. This trend has also previously been referred to as a reason to design non-conforming designs with high contact pressure and low contact area, as an approach to reduce wear [254]. Although reducing contact area would tend to reduce wear, increasing contact pressure alone would not have the effect of reducing wear if denatured proteins did not remain in the articulation. In a human knee synovial fluid is continually being regenerated and therefore this same trend may not occur.

The second experiment (POD 2, Figure 55 - Figure 57) investigated PE wear under various contact pressures, cross shear ratios and sliding distances using a linearly reciprocating and continuously rotating PE pin [318]. The wear rates predicted by the ED wear model were generally similar in trend but inaccurate in terms of wear magnitude since the ED wear model did not account for changes in boundary lubrication associated with increasing protein denaturation. The greatest amount of protein denaturation not only occurred for tests completed at higher contact pressures, but also for tests with greater sliding distances and cross shear ratios, since these tests also generally had increased sliding velocities. Overall, the CBL model accurately predicted the trends of decreasing wear for tests of high contact pressure and high energy dissipation rates. The tests performed at 3, 6 and 10 MPa contact pressures included multiple tests at cross

shear values of 0.038, with the second of these values having decreased sliding distances. Both the ED and CBL wear models were able to accurately predict the decrease in wear associated with decreased sliding distances for these tests. Overall for the second experiment (POD 2), the computational simulations well matched the trends of the POD experiments and provided a coefficient of determination of 0.92.

The third experiment (POD 3, Figure 58 and Figure 59) investigated the wear of highly crosslinked XPE under various contact pressures, cross shear ratios and sliding distances using the same linearly reciprocating POD apparatus as in the second experiment. Due to the lower contact pressures and sliding velocities, the denaturation of proteins played a smaller role in the results of this experiment, compared to the previous experiment. Once again the CBL wear model provided good agreement with the POD experiment, providing a coefficient of determination of 0.83.

The forth experiment (POD 4, Figure 60) investigated the influence of sliding distance aspect ratio during rectangular path POD experiments. Unlike the fifth experiment (POD 5), this experiment used non-square rectangular sliding paths, in which the aspect ratio (rectangle length / width) was varied. As a result, this experiment also included some sliding lengths in which the crystalline lamellae had become fully aligned, as well as section slide lengths in which it had not become fully aligned. The CBL wear model provided good agreement with the POD experiment results once again, providing a coefficient of determination of 0.84.

The fifth and final experiment (POD 5, Figure 61) investigated the wear of XPE using a POD apparatus with square sliding paths and varying slide distances between each change in direction. This experimental approach was very useful for verifying the ED

wear models prediction of the reorientation of the crystalline lamellae. For small sliding distances, less than 5mm in this experiment, the crystalline lamellae did not become fully aligned with the direction of sliding before the change in direction was encountered. This resulted in the trend of increasing wear with increasing sliding distances for sliding distances of less than approximately 5mm. Since the crystalline lamellae became fully aligned with the direction of sliding after approximately 5mm, additional sliding did not generally result in an appreciable increase in wear. The importance of implementing a computational wear model which includes time dependent cross shear is clearly demonstrated by this experiment, since a time independent cross shear wear model would predict continually increasing wear with increasing sliding distances. The CBL wear model provided outstanding agreement with the POD experiment results, providing a coefficient of determination of 0.97.

Overall, the CBL wear model demonstrated excellent predictability (R^2=0.85) across the wide range of POD experiments utilized in this research. The POD tests varied material properties (crosslink density and GUR resin type), lubricants (alpha calf serum and bovine calf serum under a range of protein concentrations), loading (1-20 MPa) and kinematics (continuous and discrete cross shear across the full range of cross shear values).

4.7.2.2. Model Corroboration with Knee Simulator Wear Tests

Following the completion of the POD experiments, the wear rates of 20 knee simulator wear test experiments were predicted using the ED and CBL wear models. The

results of the experiments were compared to analyze the wear models abilities to accurately predict wear under varying kinematics, loading, TKR conformity, XPE crosslink density, design modularity, lubrication volume, lubricant concentration and lubricant composition (Table 9).

The first kinematic comparison (Figure 62) reproduced the tests of Kawanabe et al. [354]. The first test investigated flexion motion only, resulting in pure sliding with minimal CS. The second test introduced internal-external rotation, in addition to the flexion of test 1, resulting in sliding with cross shear. The third test included the anterior displacement of the femoral component relative to the PE insert in addition to the conditions of test 2, which resulted in increased sliding distances relative to test 2. The fourth test replaced the anterior displacement of test 3 with posterior displacement, which resulted in the introduction of rolling/sliding motion (tractive rolling) and decreased sliding distances relative to test 3. Since the computational simulations utilized a different TKR design (AMK) than the TKR design which was implemented in the published knee simulator wear test results (AGC, Biomet Inc. Warsaw, IN), the relative wear rate increases relative to the first test were compared. The CBL model was able to predict the results to within the standard deviation of the knee simulator wear tests for each test, demonstrating the models ability to accurately predict the influence of each kinematic motion on wear.

The second kinematic comparison involved the comparison of high kinematics to intermediate kinematics, which included reduced anterior-posterior displacement (Figure 63). Once again the CBL model was able to accurately predict the effect of anterior-

posterior displacement on wear for both the PFC-Sigma TKR and a modified version of the PFC-Sigma which included a flat tibial insert.

The loading comparison (Figure 64) involved the prediction of wear for the PFC-Sigma TKR under the standard (ISO 14243-3) loading and under increased loading conditions in which the load was increased 1.7 fold beyond the standard loading conditions. The CBL wear model was able to accurately predict the increase in wear associated with the increase in loading. The ED wear model prediction would have over-predicted the increase in wear due to the increased load, however, the CBL model also accounted for the increased protein denaturation due to the increased energy dissipation resulting from the 1.7 fold increased load, leading to an accurate prediction for the CBL wear model.

The conformity comparison (Figure 65) involved the prediction of wear for the PFC-Sigma TKR and the wear of a modified version of the PFC-Sigma which had the articular surface of the tibial insert machined to provide a flat surface. As a result of the reduced conformity, contact areas generally decreased and contact pressures generally increased. Due to the greatly changed conformity, the regions of contact throughout the gait cycle also changed, leading to greatly changed wear rates which the CBL wear model was able to accurately predict under both high and intermediate kinematics.

It is very important to note that the CBL model was able to predict both the increase in wear associated with the increased load of the loading comparison, as well as the decreased wear through decreased conformity of the conformity comparison. Decreasing conformity and increasing load each led to increasing contact pressure, yet in each set of experiments the wear rate has an opposite response. In these cases it is not enough to

consider contact pressure alone, but the effects of the changes in conformity and load on the regions of contact are of key importance. With an increase in load, the general regions of contact remain very similar, but the contact area increases slightly. However, the decrease in conformity leads to greatly reduced contact areas as well as major changes to the regions in contact. The reduced conformity generally resulted in each area of the tibial insert being contacted during a smaller time period of the gait cycle. As a result, the crystalline lamella at each location on the tibial insert experienced greatly reduced cross shear over the gait cycle in comparison to the highly conforming TKR design. The time dependent representation of cross shear in the CBL model accounted for these differences in cross shear and as a result the CBL wear model was able to accurately predict the results of both the loading and conformity comparisons.

Wear was predicted for a TKR (PFC-Sigma) using XPE tibial inserts which had been subjected to different levels of crosslinking radiation (Figure 66). The CBL wear model accurately predicted the knee simulator wear test results to within one standard deviation. The CBL wear model also provided accurate wear predictions for the TKRs with non-crosslinked PE tibial inserts (Figure 67). This demonstrates the ED and CBL wear models abilities to accurately predict wear under a very broad range of crosslink densities.

The decision of tibial modularity is another important design consideration, along with the previously discussed decisions of conformity and the level of material crosslinking. Although including a modular interface between the tibial insert and the tibial tray can enable the easy revision of the insert at a later time, it also creates another interface to which wear occurs. Despite the complexity of predicting wear for the backside surface, the CBL wear model was able to accurately predict the wear of both

surfaces, leading to results within the standard deviation of the knee simulator wear test results (Figure 67).

The final three experimental comparisons all evaluated the ability of the CBL model to accurately predict wear despite changing lubrication conditions. Knee simulator wear tests [265] and hip simulator wear tests [61] have both demonstrated the trends of decreasing wear with decreasing lubricant volume. The CBL model accurately predicted the trend of the increasing proportion of proteins which became denatured as lubricant volume decreased, which resulted in reduced wear rates for smaller lubricant values (Figure 68). The predicted magnitudes fell within the standard deviation of the knee simulator wear test results for all of the tests, apart from the test at 75ml which was underpredicted. However, since these tests involved only three wear stations [265], it is possible that a greater sample size would lead to improved agreement.

A comparison was performed to predict the wear of the AMK under the ISO standard compared to under reduced anterior-posterior translation and greatly increased protein concentration (Figure 69). The ED wear model predicted a decrease in wear associated with the decrease in anterior-posterior translation, but this decrease fell far short of the decrease shown by the knee simulator wear tests. The CBL wear model was able to accurately predict the decrease in wear associated with increased protein concentration and predicted results which once again fell within the standard deviation of the knee simulator wear tests.

Finally, the wear rates of the AMK under the ISO standard for alpha calf, newborn calf and bovine calf sera were compared (Figure 70). The CBL model accurately

predicted the increasing wear rate that resulted from the decreasing relative fraction of albumin and α-globulin proteins to the total protein composition.

The validation metric, proposed by Oberkampf and Trucano [362], was calculated for the prediction of the broad range of 20 knee simulator wear test results using the CBL model. The CBL model demonstrated a validation metric of *VM*=0.85 for the prediction of knee simulator wear test results. This high validation metric demonstrates the strong agreement between the CBL computational wear model and the experimental knee simulator wear test results. This validation metric of Oberkampf and Trucano [362] provides an extremely sensitive measure of the agreement in both magnitude and trend, as well as ensures that positive and negative errors cannot cancel each other out. This strong validation metric confirms that the CBL computational wear model can be implemented for the prediction of knee simulator wear test results and is sufficiently accurate to be utilized for the wear optimization of TKRs.

4.7.2.3. Model Performance and Simplifications

The accuracy of the CBL model was evaluated through the prediction of five sets of POD experiments and 20 different knee simulator wear tests. The experiments included a large variety of PE or XPE material crosslink densities, contact conformity, kinematics, loading, and lubrication conditions. The CBL model resulted in a coefficient of determination of 0.85 compared to the broad range of POD results and predicted wear rates which fell within the standard deviation of the knee simulator wear test values (with one slight exception; R^2=0.96). The CBL model demonstrated a validation metric of 0.85

for the prediction of TKR knee simulator wear test results, indicating the great strength of the CBL model for the prediction of knee simulator wear test results.

However, the CBL model does include several simplifications and its predictive accuracy could be further improved through reducing the simplifications of the model (as discussed in Section 4.6.2). Through conducting molecular dynamics simulations and conducting experiments for each protein type, the interactions of each protein with the surfaces as well as other proteins could be further explored. Currently, the CBL model groups proteins into two categories (albumin and α-globulin or β-globulin and γ-globulin) for the prediction of denaturation and to predict the effects of the protein on the boundary lubrication of the surfaces. Furthermore, although the competitive adsorption of native and denatured proteins are considered for the adsorption of proteins onto the surfaces, the relative composition of protein types adsorbed are assumed to be the same as the bulk lubricant and all protein types are assumed to have the same Langmuir constants as albumin. This simplification was implemented due to a lack of experimental data availability to determine the Langmuir constants for other protein types. However, the accuracy of the model may be improved through providing greater consideration for the differences between proteins. Some of the constants of the CBL model were determined using a limited range of experimental data and it may therefore also be possible to further improve the predictive accuracy of the model through the refinement of the constants utilized in the CBL model.

4.7.2.4. Clinical Relevance of the CBL Model

The CBL computational wear model developed and verified in this thesis has demonstrated a high level of agreement compared to the *in vitro* wear testing methods of POD (R^2=0.85) and knee simulator wear tests (R^2=0.96; *VM*=0.85). Both of these *in vitro* wear testing methods enable the conditions of the test to be carefully controlled, thereby providing an excellent means of verifying the computational wear model [3, 38-40]. Since knee simulator wear tests are also the current standard for evaluating TKR designs [3, 250], this also makes knee simulator wear tests an excellent method by which to verify the accuracy of computational wear models. However, the simplifications of knee simulator wear tests, relative to *in vivo* wear, may limit the clinical relevance of knee simulator wear tests. Since the intended application of the CBL wear model would be as a design tool for TKRs, it is important to consider the differences between *in vivo* conditions and the conditions of the knee simulator wear tests against which the model has been verified. Additionally, the abilities of the CBL model to predict the clinical wear performance of TKRs *in vivo*, rather than in a knee simulator wear test, must be discussed. Unfortunately, the direct verification of the model by comparison to *in vivo* wear results is not possible due to the limitations of assessing *in vivo* wear and accounting for patient variability (as discussed in Section 2.4.1).

Although knee simulator wear testing has been developed to simulate *in vivo* conditions in the laboratory setting, the simplifications of knee simulator wear testing may somewhat limit its clinical relevance. Knee simulator wear tests have been developed to utilize calf serum to represent synovial fluid [250], as obtaining synovial

fluid in the necessary quantities for knee simulator wear testing would be impractical. Calf serum is derived from blood (bovine calf, newborn calf, or alpha calf). As a result, the composition of calf serum is not identical to that of the human knee [164] (as discussed in Section 2.3.2). Although the protein concentration is typically controlled through dilution for knee simulator wear tests, the protein composition of the calf sera typically used in knee simulator wear tests is not identical to that of the human knee [164]. Furthermore, lubricin is typically absent from knee simulator wear tests because it is not found in calf sera, however lubricin does exist in human synovial fluid [241, 242]. Currently, the CBL model groups proteins into two groups (albumin and α-globulin, or β-globulin and γ-globulin). This protein grouping simplification may affect the accuracy of the CBL model for both the prediction of knee simulator wear tests and *in vivo* wear. Yet despite this simplification, a high level of accuracy (*VM*=0.85) has been demonstrated between the CBL model predictions and knee simulator wear test results. The CBL model enables any relative fraction between the two protein groups to be specified and can be made to match *in vivo* conditions, rather than being limited to the compositions of the available calf sera typically used in knee simulator wear tests. In the future, the model could also be further developed to provide consideration for each protein type individually (including lubricin), which may still further increase the clinical relevance of the CBL model.

Knee simulator wear tests typically utilize increased lubricant volumes, as well as include the replacement of the lubricant at regular intervals (Section 3.5.1), as an attempt to approximate the effects of the continual renewal of proteins which occurs *in vivo* [265]. This approximation of protein renewal may also limit the clinical relevance of

knee simulator wear tests [265]. Conversely, the continual renewal of proteins can be conveniently specified for the CBL model (Section 3.6) to directly replicate the conditions of the human body.

The ionic strength of the calf serum used in knee simulator wear tests is not typically controlled to match that of human synovial fluid [250]. However, lubricant ionic strength may have an effect on protein stability and adsorption [34, 72]. Further research should be conducted to quantify the effects of lubricant ionic strength on protein stability and adsorption. Consideration for the effects of ionic strength on protein stability, protein adsorption and wear could be added to the CBL model in the future, but is not currently included in the CBL model.

Human synovial fluid includes hyaluronic acid, however, the calf sera used in knee simulator wear tests have not typically included hyaluronic acid [34, 250]. Very few knee simulator wear tests have been reported in the literature which have utilized a lubricant which included hyaluronic acid [213, 252]. As discussed in Section 2.3.2, hyaluronic acid may interact with proteins to alter their tribological behaviour [34, 73, 213, 246-249, 370]. As with knee simulator wear tests, which are typically performed without hyaluronic acid [34, 250], the CBL model does not currently include consideration for the influence of hyaluronic acid on the behaviour of the proteins. However, consideration for the influence of hyaluronic acid could be added to this computational wear model in the future.

The lubricant of knee simulator wear tests typically also includes sodium azide or antibiotics, to inhibit microbial growth [34, 250, 252]. Microbial growth has been found to influence wear rates and reduce clinical relevance [252]. However, the addition of

sodium azide or antibiotics may also have an effect on TKR lubrication and wear [252]. The CBL wear model currently assumes the presence of sodium azide in the lubricant in order to match the typical conditions of most knee simulator wear tests. Yet further developing the model to provide consideration for the presence or absence of sodium azide or antibiotics may further improve the clinical relevance of the CBL model.

The loading and kinematics of knee simulator wear tests may also differ from those experienced *in vivo*. Firstly, the simple walking cycle of the ISO 14243 standards is not the only activity performed by the knee [250]. Activities such as turning corners while walking, stair climbing, chair rising/descending, running and many other activities, may also be a part of daily life for TKR patients [371]. Additionally, conditions such as stationary periods and the momentary separation of contacting components may affect TKR wear. Not only are the activities utilized by knee simulator wear tests highly simplified, but the removal of patient variability to create standardized conditions may have caused many of the possible worst case scenarios to be excluded from consideration. The surgical alignment of TKR components can vary greatly between patients and can affect kinematics and wear rates [372]. Furthermore, patient anatomy is highly variable and can also affect kinematics and wear rates [373-376]. Since knee simulator wear tests may not be able to accommodate this variability in a cost and time efficient manner, it may limit the clinical relevance of such tests [3, 38]. However, the improved cost and time efficiency of computational wear simulations, relative to knee simulator wear tests, may enable a greater range of variability and conditions to be considered [38]. Computational simulations can be used to simultaneously predict kinematics and wear in a cost and time effective manner, thereby allowing probabilistic studies to be conducted

across a wider range of clinical conditions than would be practical using knee simulator wear tests alone.

Due to hardware limitations, knee simulators may have difficulty simulating the wear of posterior stabilized TKRs (Section 2.4.2.2). Additionally, displacement controlled knee simulators have difficulty simulating the wear of high conforming designs, while force controlled knee simulators have difficulty simulating the wear of low conforming designs (Section 2.4.2.2). Meanwhile, the CBL wear model could predict wear for any TKR design, enabling the model to be used for exploration of TKR designs prior to any costly and time consuming knee simulator wear testing.

Overall, the CBL model presented in the present thesis has demonstrated excellent predictive capabilities in comparison to knee simulator wear tests (R^2=0.96; *VM*=0.85), which are the current standard for TKR wear analyses prior to FDA or Health Canada approval and large scale implementation. Despite the excellent current success of the CBL model, further development still has the potential to further increase the clinical relevance of the CBL model. The CBL model is not affected by some of the practical limitations of knee simulator wear tests, which limit the clinical relevance of knee simulator wear tests. The efficiency, clinical relevance and predictive accuracy of the CBL model may enable the model to be utilized to explore a wider range of design variables and clinical conditions in comparison to knee simulator wear testing alone. As a result, the CBL model may have the potential to improve the design of TKRs prior to conducting expensive and time consuming knee simulator wear tests, thereby potentially improving TKR designs while also reducing development costs. Additionally, although the focus of this thesis has been on TKRs, the computational wear model could also be

applied and further developed for total hip replacements, total shoulder replacements and total disk replacements.

4.7.3 Concluding Remarks

The CBL model demonstrated excellent predictability compared to the POD and knee simulator wear test results. To the author's best knowledge, this is the first TKR computational wear model to provide consideration for the lubricant. Although this model could still benefit from further development, the CBL model has demonstrated the high level of accuracy necessary for utilization in the TKR design process.

Chapter 5

Conclusions

5.1 Conclusions

TKRs are essential to alleviating pain and restoring mobility to patients suffering from disorders and diseases such as arthritis. However, the long-term success of TKRs can be limited by the wear of the PE or XPE tibial insert. The cost and time requirements of current TKR design and testing methods may limit the range of design variables which can be considered, preventing the optimization of TKRs for the reduction of wear. Therefore, the development of an accurate and efficient computational wear simulation method may enable a greater range of TKR design variables to be considered and may enable the optimization of TKRs for the reduction of wear.

The computational wear simulation process requires the prediction of contact pressure and sliding displacement vectors at each wear surface, which includes both the articular and backside surfaces of modular cruciate retaining PE and XPE tibial inserts. FE simulation with the J_2-plasticity constitutive model has previously been demonstrated to

provide accurate results for both the articular and backside surfaces. However, a more computationally efficient method would still be of great benefit. For this reason, MBD simulations have been considered for the articular surface in the present thesis. Simulations were conducted to develop an optimized PO relationship for MBD contact mechanics simulations. The optimized PO relationship was then evaluated through static and dynamic TKR simulations. The results demonstrated the MBD simulation method to be unable to provide the desired level of correlation strength for the prediction of contact pressure and contact area. Therefore, the implementation of deformable FE simulations using the J_2-plasticity model was recommended for the prediction of contact mechanics in all future research.

Secondly, a previously existing computational wear model was implemented to predict the influence of insert thickness on PE and XPE wear. Increasing insert thickness was found to decrease articular wear and increase backside wear. Although insert thickness was demonstrated to affect wear rates, the change in overall wear rate remained small for the range of insert thicknesses considered. These computational wear simulation results suggest that the wear performance of modern bearing materials may be less sensitive to changes in insert thickness compared to historical materials such as heat pressing formed PE and PE (or XPE) with high oxidization potential. However, insert thicknesses beyond the range investigated in this study (5mm to 25mm) may still present a risk, as decreased insert thickness has been demonstrated to increase stress and contact pressures, while increasing insert thickness has been demonstrated to increase backside micromotion and wear.

Due to the limited accuracy of computational wear models in the literature, the development of a new computational wear model was undertaken. The objectives were to develop a computational wear model capable of improved predictive accuracy with improved agreement to basic polymer wear theory. The TD-ED-TR wear model was developed, which incorporated consideration for the time dependent molecular behaviour of polyethylene, aspects of tractive rolling and contact pressure. The TD-ED-TR wear model was demonstrated to result in an increase in accuracy over several previously developed wear models compared to POD and knee simulator wear test results. Therefore, the development of this new computational wear model has made a substantial contribution towards the improvement of the predictive accuracy of computational wear models.

The effect of contact pressure on the wear of TKRs remained a subject of great controversy in the literature prior to the research of this thesis. Many of the most recently developed computational wear models have been developed as contact pressure independent due to the complex trends demonstrated by POD tests. To evaluate the true influence of this controversial parameter directly on a TKR, knee simulator wear tests were conducted along with corresponding computational simulations. The knee simulator wear test demonstrated the 1.7 fold increase in load to result in a 4.37 fold increase in wear. This increase in wear was greater than the increase predicted by any of the considered computational wear models. The contribution of this research is very substantial, as it provides direct evidence that PE and XPE wear can increase with increasing load in a TKR, which is crucial information that was previously unknown. This research also indicated that a mechanism which has not been accounted for may be

causing entirely different behaviours under increasing load for POD tests compared to knee simulator wear tests. The author of this thesis developed the hypothesis that the lubrication may be responsible for these previously unexplained trends of contact pressure's effect on wear. Therefore, a lubrication model was developed in the present thesis in order to evaluate this hypothesis.

Previous computational wear simulation methods in the literature have omitted the simulation of the lubricant. However, the omission of the lubricant in the simulation methods may be one of the greatest sources of error in current TKR computational wear simulations. Therefore, a colloidal protein mediated boundary lubrication model was developed to predict the protein denaturation, protein adsorption and boundary lubrication of TKRs. The model enabled the prediction and explanation of previously unexplained POD and knee simulator wear test trends results with regard to contact pressure. The model also was able to predict the wear results of 75 POD tests (R^2=0.85) as well as predict the results of 20 knee simulator wear tests (R^2=0.96; *VM*=0.85) to within the standard deviation of the knee simulator wear tests (with the slight exception of one sublevel experiment). The development of this new time dependent cross shear, energy dissipation and colloid mediated boundary lubrication model represents a great contribution to both computational wear simulation methods as well as TKR research. The CBL wear model developed within the research of this thesis has been demonstrated to have the greatest agreement compared to POD and knee simulator wear testing results in comparison to the other computational wear models available in the literature (Table 18).

Table 18: Comparison of the predictive correlations for various computational wear models.

Wear Model	Wear Formulation	Reported TKR Correlation (R^2)	Reference
Archard	$W = k \cdot P \cdot S$	0.12	[40, 111]
Turell	$W = k \cdot P \cdot S \cdot CS$	0.60	[40, 60]
Strickland	$W = k \cdot f(S) \cdot f(CS)$	0.65	[39]
O'Brien	Sections 3.5 -3.6	0.96	Present Thesis

Table Abbreviations: TKR -Total Knee Replacement; *W*-Wear Volume; *k*-Wear Factor; *P*-Contact Pressure; *S*-Sliding Distance; *CS*-Cross Shear; *f()*-Function of

Despite the great success of the CBL model, further work could still be undertaken to provide consideration for additional variables affecting wear and reduce the number of simplifications of the CBL model. The CBL model grouped proteins into two main categories (albumin, α-1-globulin and α-2-globulin in one group, with β-globulin and γ-globulin in the second group). By conducting further experimentation and molecular dynamics simulations, the CBL model could be developed to address each protein type individually for denaturation, adsorption and boundary lubrication. Additionally, addressing asperity adhesion and asperity deformations independently, rather than through predicting their combined contribution to wear, would reduce the simplifications of the CBL model and may also enable the consideration of additional variables such as surface roughness. Lastly, accounting for the changes in lubricant composition beyond the protein composition, such as changes to hyaluronic acid concentration, ionic strength and antimicrobial inhibitors would also reduce the simplifications of the CBL model. However despite the simplifications of the CBL model, the model has demonstrated a strong correlation for the prediction of TKR wear (R^2=0.96; *VM*=0.85) across a broad range of experimental conditions. Therefore, the CBL model may enable the wear

optimization of TKRs for the reduction of wear. Future work which implements this computational wear model for the optimization of TKRs would be of great benefit. The CBL model could also be easily combined with other computational processes for the multiobjective optimization of TKRs, such as the simultaneous optimization of kinematics and wear performance. Future work implementing the CBL wear model has the potential to greatly improve the long term wear performance of TKRs for the reduction of wear. The improvement in TKR wear performance may lead to the reduction in risk of wear particle induced osteolysis and improve the long term performance of TKRs, thereby reducing health care costs and improving patient care.

The accuracy of the CBL model was evaluated through the prediction of five sets of POD experiments and 20 different knee simulator wear tests. The experiments included a large variety of PE or XPE material crosslink densities, contact conformity, kinematics, loading, and lubrication conditions. The CBL model resulted in a coefficient of determination (R^2) of 0.85 compared to the broad range of POD results and predicted wear rates which fell within the standard deviation of the knee simulator wear test values (R^2=0.96; *VM*=0.85). The computational wear simulation models developed in this thesis have demonstrated sufficient accuracy to enable the optimization of TKRs for the reduction of wear, which may improve the long term success of these necessary clinical devices.

Bibliography

6.1 Bibliography

[1] S. Kurtz, K. Ong, E. Lau, F. Mowat, and M. Halpern, "Projections of Primary and Revision Hip and Knee Arthroplasty in the United States from 2005 to 2030," *Journal of Bone and Joint Surgery (Am)*, vol. 89, pp. 780-785, April 1, 2007 2007.

[2] Canadian Joint Replacement Registry, "Hip and Knee Replacements in Canada," 2006.

[3] S. Kurtz, *UHMWPE Biomaterials Handbook: Ultra High Molecular Weight Polyethylene in Total Joint Replacement and Medical Devices*: Elsevier/Academic Press, 2009.

[4] J.-M. Brandt, L. Guenther, S. O'Brien, A. Vecherya, T. Turgeon, and E. Bohm, "Surface Characterization and Clinical Performance of Femoral Knee Components Made From Cobalt-Chromium Alloy and Oxidized Zirconium,"

Bone & Joint Journal Orthopaedic Proceedings Supplement, vol. 95, pp. 137-137, 2013.

[5] R. Gandhi, D. Tsvetkov, J. Davey, and N. Mahomed, "Survival and clinical function of cemented and uncemented prostheses in total knee replacement A META-ANALYSIS," *Journal of Bone & Joint Surgery, British Volume,* vol. 91, pp. 889-895, 2009.

[6] Canadian Joint Replacement Registry, "Hip and Knee Replacements in Canada," 2015.

[7] J. M. Brandt, S. J. MacDonald, R. B. Bourne, and J. B. Medley, "Retrieval analysis of modular total knee replacements: factors reducing backside surface damage," *The Knee,* vol. 19, pp. 306-315, 2011.

[8] G. A. Engh, S. Lounici, A. R. Rao, and M. B. Collier, "In Vivo Deterioration of Tibial Baseplate Locking Mechanisms in Contemporary Modular Total Knee Components," *Journal of Bone and Joint Surgery (Am),* vol. 83, pp. 1660-1665, November 1, 2001 2001.

[9] E. M. Keating, J. B. Meding, P. M. Faris, and M. A. Ritter, "Long-term followup of nonmodular total knee replacements," *Clinical Orthopaedics and Related Research,* vol. 404, pp. 34-39, 2002.

[10] D. McNulty, S. Swope, and M. Disilvestro, "Influence of Tray Surface Finish on Modular Tibial Tray Micromotion and Wear," in *51st Annual Meeting of the Orthopaedic Research Society*, Washington DC, USA, 2005.

[11] D. McNulty and S. W. Swope, "Wear of nonmodular and modular total knee tibial components," in *Proceedings of the 31st Annual Meeting of the Society for Biomaterials*, Memphis, TN, USA, 2005.

[12] A. E. Pour, J. Parvizi, N. Slenker, J. J. Purtill, and P. F. Sharkey, "Rotating hinged total knee replacement: use with caution," *J Bone Joint Surg Am*, vol. 89, pp. 1735-1741, 2007.

[13] P. Aglietti, A. Baldini, R. Buzzi, D. Lup, and L. De Luca, "Comparison of mobile-bearing and fixed-bearing total knee arthroplasty: a prospective randomized study," *The Journal of Arthroplasty*, vol. 20, pp. 145-153, 2005.

[14] S. Bhan, R. Malhotra, E. K. Kiran, S. Shukla, and M. Bijjawara, "A comparison of fixed-bearing and mobile-bearing total knee arthroplasty at a minimum follow-up of 4.5 years," *J Bone Joint Surg Am*, vol. 87, pp. 2290-2296, 2005.

[15] T. Grupp, C. Kaddick, J. Schwiesau, A. Maas, and S. Stulberg, "Fixed and mobile bearing total knee arthroplasty–influence on wear generation, corresponding wear areas, knee kinematics and particle composition," *Clinical Biomechanics*, vol. 24, pp. 210-217, 2009.

[16] H. McEwen, P. Barnett, C. Bell, R. Farrar, D. Auger, M. Stone, and J. Fisher, "The influence of design, materials and kinematics on the in vitro wear of total knee replacements," *Journal of biomechanics,* vol. 38, pp. 357-365, 2005.

[17] S. Yoshiya, N. Matsui, R. D. Komistek, D. A. Dennis, M. Mahfouz, and M. Kurosaka, "In vivo kinematic comparison of posterior cruciate-retaining and posterior stabilized total knee arthroplasties under passive and weight-bearing conditions," *The Journal of Arthroplasty,* vol. 20, pp. 777-783, 2005.

[18] M. P. Abdel, M. E. Morrey, M. R. Jensen, and B. F. Morrey, "Increased long-term survival of posterior cruciate-retaining versus posterior cruciate-stabilizing total knee replacements," *J Bone Joint Surg Am,* vol. 93, pp. 2072-2078, 2011.

[19] M. Skolnick, R. Bryan, and L. Peterson, "Unicompartmental polycentric knee arthroplasty: description and preliminary results.," *Clinical Orthopedics and Related Research,* pp. 208-14, 1975.

[20] W. Jones, R. Bryan, L. Peterson, and D. Ilstrup, "Unicompartmental knee arthroplasty using polycentric and geometric hemicomponents," *Journal of Bone and Joint Surgery (Am),* vol. 63, pp. 946-54, 1973.

[21] T. Akisue, M. Yamaguchi, T. W. Bauer, S. Takikawa, J. P. Schils, S. Yoshiya, and M. Kurosaka, ""Backside" polyethylene deformation in total knee arthroplasty," *The Journal of Arthroplasty,* vol. 18, pp. 784-791, 2003.

[22] M. G. Azzam, M. E. Roy, and L. A. Whiteside, "Second-Generation Locking Mechanisms and Ethylene Oxide Sterilization Reduce Tibial Insert Backside Damage in Total Knee Arthroplasty," *The Journal of Arthroplasty,* vol. 26, pp. 523-530, 2011.

[23] M. A. Conditt, S. K. Ismaily, J. W. Alexander, and P. C. Noble, "Backside Wear of Modular Ultra-High Molecular Weight Polyethylene Tibial Inserts," *Journal of Bone and Joint Surgery (Am),* vol. 86, pp. 1031-1037, May 1, 2004 2004.

[24] G. A. Engh, L. M. Koralewicz, and T. R. Pereles, "Clinical Results of Modular Polyethylene Insert Exchange with Retention of Total Knee Arthroplasty Components," *Journal of Bone and Joint Surgery (Am),* vol. 82, pp. 516-, April 1, 2000 2000.

[25] R. C. Wasielewski, N. Parks, I. Williams, H. Surprenant, J. P. Collier, and G. Engh, "Tibial Insert Undersurface as a Contributing Source of Polyethylene Wear Debris," *Clinical Orthopaedics and Related Research,* vol. 345, pp. 53-59, 1997.

[26] S. Puloski, R. McCalden, S. MacDonald, C. Rorabeck, and R. Bourne, "Tibial post wear in posterior stabilized total knee arthroplasty. An unrecognized source of polyethylene debris.," *Journal of Bone and Joint Surgery (Am),* vol. 83, pp. 390-397, 2001.

[27] M. Jasty, W. Floyd, A. Schiller, S. Goldring, and W. Harris, "Localized osteolysis in stable, non-septic total hip replacement," *Journal of Bone and Joint Surgery (Am)*, vol. 68, pp. 912-919, July 1, 1986 1986.

[28] M. E. Berend, M. A. Ritter, J. B. Meding, P. M. Faris, E. M. Keating, R. Redelman, G. W. Faris, and K. E. Davis, "The Chetranjan Ranawat Award: Tibial Component Failure Mechanisms in Total Knee Arthroplasty," *Clinical Orthopaedics and Related Research*, vol. 428, pp. 26-34 10.1097/01.blo.0000148578.22729.0e, 2004.

[29] M. B. Collier, J. C. A. Engh, J. P. McAuley, S. D. Ginn, and G. A. Engh, "Osteolysis after Total Knee Arthroplasty: Influence of Tibial Baseplate Surface Finish and Sterilization of Polyethylene Insert," *Journal of Bone and Joint Surgery (Am)*, vol. 87, pp. 2702-2708, 2005.

[30] S. K. Gupta, A. Chu, A. S. Ranawat, J. Slamin, and C. S. Ranawat, "Review Article: Osteolysis After Total Knee Arthroplasty," *The Journal of Arthroplasty*, vol. 22, pp. 787-799, 2007.

[31] M. R. O'Rourke, J. J. Callaghan, D. D. Goetz, P. M. Sullivan, and R. C. Johnston, "Osteolysis Associated with a Cemented Modular Posterior-Cruciate-Substituting Total Knee Design : Five to Eight-Year Follow-up," *Journal of Bone and Joint Surgery (Am)*, vol. 84, pp. 1362-1371, August 1, 2002 2002.

[32] A. Serro, M. Gispert, M. Martins, P. Brogueira, R. Colaco, and B. Saramago, "Adsorption of albumin on prosthetic materials: implication for tribological behavior," *Journal of Biomedical Materials Research Part A,* vol. 78, pp. 581-589, 2006.

[33] H.-W. Fang, M.-L. Shih, J.-H. Zhao, H.-T. Huang, H.-Y. Lin, H.-L. Liu, C.-H. Chang, C.-B. Yang, and H.-C. Liu, "Association of polyethylene friction and thermal unfolding of interfacial albumin molecules," *Applied surface science,* vol. 253, pp. 6896-6904, 2007.

[34] J. M. Brandt, L. Brière, J. Marr, S. MacDonald, R. Bourne, and J. Medley, "Biochemical comparisons of osteoarthritic human synovial fluid with calf sera used in knee simulator wear testing," *Journal of Biomedical Materials Research Part A,* vol. 94, pp. 961-971, 2010.

[35] T. P. Schmalzried, M. Jasty, A. Rosenberg, and W. H. Harris, "Polyethylene wear debris and tissue reactions in knee as compared to hip replacement prostheses," *Journal of Applied Biomaterials,* vol. 5, pp. 185-190, 1994.

[36] M. Horikoshi, W. Macaulay, R. E. Booth, L. S. Crossett, and H. E. Rubash, "Comparison of Interface Membranes Obtained From Failed Cemented and Cementless Hip and Knee Prostheses," *Clinical Orthopaedics and Related Research,* vol. 309, pp. 69-87, 1994.

[37] P. F. Sharkey, P. M. Lichstein, C. Shen, A. T. Tokarski, and J. Parvizi, "Why are total knee arthroplasties failing today—has anything changed after 10 years?," *The Journal of Arthroplasty*, vol. 29, pp. 1774-1778, 2014.

[38] L. A. Knight, S. Pal, J. C. Coleman, F. Bronson, H. Haider, D. L. Levine, M. Taylor, and P. J. Rullkoetter, "Comparison of long-term numerical and experimental total knee replacement wear during simulated gait loading," *Journal of biomechanics,* vol. 40, pp. 1550-1558, 2007.

[39] M. A. Strickland, M. R. Dressler, and M. Taylor, "Predicting implant UHMWPE wear in-silico: A robust, adaptable computational–numerical framework for future theoretical models," *Wear,* vol. 274–275, pp. 100-108, 2012.

[40] M. A. Strickland and M. Taylor, "In-silico wear prediction for knee replacements—methodology and corroboration," *Journal of biomechanics*, vol. 42, pp. 1469-1474, 2009.

[41] H. P. Jost, "Tribology—origin and future," *Wear*, vol. 136, pp. 1-17, 1990.

[42] P. Jost, "Lubrication (tribology)," *London: Her Majesty's Stationary Office,* 1966.

[43] D. Dowson, "History of Tribology. 2nd," *London: Professional Engineering,* vol. 577, 1998.

[44] C. Davidson, "Bearings since the stone age," *Engineering,* vol. 183, pp. 2-5, 1957.

[45] G. Amontons, "“De la resistance caus’ ee dans les machines,”" *Mémoires de l’Académie Royale A,* pp. 251-282, 1699.

[46] C. Coulomb, "Théorie des machines simples en ayant égard au frottement de leurs parties et à la roideur de leurs cordages," *Bachelier, Librairie, quai des Augustins, Paris,* 1785.

[47] B. Tower, "First report on friction experiments," *Proceedings of the Institution of Mechanical Engineers,* vol. 35, pp. 29-35, 1884.

[48] O. Reynolds, "On the Theory of Lubrication and Its Application to Mr. Beauchamp Tower's Experiments, Including an Experimental Determination of the Viscosity of Olive Oil," *Proceedings of the Royal Society of London,* vol. 40, pp. 191-203, 1886.

[49] H. Gatos, "Structure of surfaces and their interactions," 1968.

[50] A. Haltner, "The physics and chemistry of surfaces: surface energy, wetting and adsorption," *Boundary Lubrication,* pp. 39-60, 1969.

[51] D. H. Buckley, "Surface effects in adhesion, friction, wear, and lubrication," 1981.

[52] B. Bhushan, *Introduction to tribology*: John Wiley & Sons, 2013.

[53] L. Samuels, "Damaged Surface Layers: Metals," *The Surface Chemistry of Metals and Semiconductors,* pp. 82-103, 1960.

[54] B. Bhushan, "Tribology and mechanics of magnetic storage devices," *Spring-Verlag Inc,* 1996.

[55] M. Shaw and A. Vyas, "The mechanism of chip formation with hard turning steel," *CIRP Annals-Manufacturing Technology,* vol. 47, pp. 77-82, 1998.

[56] N. Cook and B. Bhushan, "Sliding surface interface temperatures," *Journal of Lubrication Technology,* vol. 95, pp. 59-64, 1973.

[57] O. Kubaschewski and B. E. Hopkins, *Oxidation of metals and alloys*: Butterworths, 1967.

[58] B. M. W. Trapnell and D. O. Hayward, *Chemisorption*: Butterworths, 1964.

[59] M. R. Dressler, M. A. Strickland, M. Taylor, T. D. Render, and C. N. Ernsberger, "Predicting wear of UHMWPE: Decreasing wear rate following a change in direction," *Wear,* vol. 271, pp. 2879-2883, 2011.

[60] M. Turell, A. Wang, and A. Bellare, "Quantification of the effect of cross-path motion on the wear rate of ultra-high molecular weight polyethylene," *Wear,* vol. 255, pp. 1034-1039, 2003.

[61] A. Wang, "A unified theory of wear for ultra-high molecular weight polyethylene in multi-directional sliding," *Wear,* vol. 248, pp. 38-47, 2001.

[62] M. B. Collier, C. A. Engh, K. M. Hatten, S. D. Ginn, T. M. Sheils, and G. A. Engh, "Radiographic Assessment of the Thickness Lost from Polyethylene Tibial

Inserts That Had Been Sterilized Differently," *Journal of Bone and Joint Surgery (Am)*, vol. 90, pp. 1543-1552, July 1, 2008 2008.

[63] B. H. Currier, J. H. Currier, J. P. Collier, M. B. Mayor, and R. D. Scott, "Shelf Life and In Vivo Duration; Impacts on Performance of Tibial Bearings," *Clinical Orthopaedics and Related Research*, vol. 342, pp. 111-122, 1997.

[64] J. P. Halloran, S. K. Easley, A. J. Petrella, and P. J. Rullkoetter, "Comparison of deformable and elastic foundation finite element simulations for predicting knee replacement mechanics," *Journal of biomechanical engineering*, vol. 127, pp. 813-818, 2005..

[65] J. P. Collier, V. A. Surprenant, R. E. Jensen, M. B. Mayor, and H. P. Surprenant, "Corrosion between the components of modular femoral hip prostheses," *Journal of Bone & Joint Surgery, British Volume*, vol. 74, pp. 511-517, 1992.

[66] J. P. Collire, V. A. Surprenant, R. E. Jensen, and M. B. Mayor, "Corrosion at the interface of cobalt-alloy heads on titanium-alloy stems," *Clinical Orthopaedics and Related Research*, vol. 271, p. 305, 1991.

[67] T. M. Grupp, T. Weik, W. Bloemer, and H.-P. Knaebel, "Modular titanium alloy neck adapter failures in hip replacement-failure mode analysis and influence of implant material," *BMC Musculoskeletal Disorders*, vol. 11, p. 1, 2010.

[68] R. Dyrkacz, J. Brandt, J. Morrison, S. O'Brien, O. Ojo, T. Turgeon, and U. Wyss, "Finite element analysis of the head–neck taper interface of modular hip prostheses," *Tribology International*, vol. 91, pp. 206-213, 2015.

[69] B. Feng, J. Weng, B. Yang, J. Chen, J. Zhao, L. He, S. Qi, and X. Zhang, "Surface characterization of titanium and adsorption of bovine serum albumin," *Materials Characterization*, vol. 49, pp. 129-137, 2002.

[70] M. P. Heuberger, M. R. Widmer, E. Zobeley, R. Glockshuber, and N. D. Spencer, "Protein-mediated boundary lubrication in arthroplasty," *Biomaterials*, vol. 26, pp. 1165-1173, 2005.

[71] H.-W. Fang, M.-C. Hsieh, H.-T. Huang, C.-Y. Tsai, and M.-H. Chang, "Conformational and adsorptive characteristics of albumin affect interfacial protein boundary lubrication: from experimental to molecular dynamics simulation approaches," *Colloids and Surfaces B: Biointerfaces*, vol. 68, pp. 171-177, 2009.

[72] G. A. Picó, "Thermodynamic features of the thermal unfolding of human serum albumin," *International Journal of Biological Macromolecules*, vol. 20, pp. 63-73, 1997.

[73] A. Serro, K. Degiampietro, R. Colaço, and B. Saramago, "Adsorption of albumin and sodium hyaluronate on UHMWPE: a QCM-D and AFM study," *Colloids and Surfaces B: Biointerfaces*, vol. 78, pp. 1-7, 2010.

[74] I. O. f. S. ISO, "Geometrical Product Specifications (GPS) -- Surface texture," ed. Geneva, Switzerland: International Organization for Standardization.

[75] ASME, "B46.1-2009 Surface Texture (Surface Roughness, Waviness, and Lay)," ed. New York, NY: American National Standard, 2009.

[76] B. Bhushan, "Contact mechanics of rough surfaces in tribology: single asperity contact," *Applied mechanics reviews,* vol. 49, pp. 275-298, 1996.

[77] B. Bhushan, "Contact mechanics of rough surfaces in tribology: multiple asperity contact," *Tribology letters,* vol. 4, pp. 1-35, 1998.

[78] M. Sikorski, "Correlation of the coefficient of adhesion with various physical and mechanical properties of metals," *Journal of Fluids Engineering,* vol. 85, pp. 279-285, 1963.

[79] F. Bowden and G. W. Rowe, "The adhesion of clean metals," in *Proceedings of the Royal Society of London A: Mathematical, Physical and Engineering Sciences,* 1956, pp. 429-442.

[80] W. D. Callister and D. G. Rethwisch, *Materials science and engineering: an introduction* vol. 7: Wiley New York, 2007.

[81] M. Hein and S. Arena, *Foundations of college chemistry*: John Wiley & Sons, 2010.

[82] A. Johnsen and K. Rahbek, "A physical phenomenon and its applications to telegraphy, telephony, etc," *Electrical Engineers, Journal of the Institution of,* vol. 61, pp. 713-725, 1923.

[83] S. M. Skinner, R. L. Savage, and J. E. Rutzler Jr, "Electrical phenomena in adhesion. I. Electron atmospheres in dielectrics," *Journal of Applied Physics,* vol. 24, pp. 438-450, 1953.

[84] D. Davies, "Surface charge and the contact of elastic solids," *Journal of Physics D: Applied Physics,* vol. 6, p. 1017, 1973.

[85] A. Wåhlin and G. Bäckström, "Sliding electrification of Teflon by metals," *Journal of Applied Physics,* vol. 45, pp. 2058-2064, 1974.

[86] B. Derjaguin, N. Krotova, and V. Smilga, ""“Adhesion of Solids”, Vol. 4," 1978.

[87] D. Keller, "Adhesion between solid metals," *Wear,* vol. 6, pp. 353-365, 1963.

[88] B. Bhushan, "Adhesion and stiction: mechanisms, measurement techniques, and methods for reduction," *Journal of Vacuum Science & Technology B,* vol. 21, pp. 2262-2296, 2003.

[89] B. V. Derjaguin, V. M. Muller, and Y. P. Toporov, "Effect of contact deformations on the adhesion of particles," *Journal of Colloid and interface science,* vol. 53, pp. 314-326, 1975.

[90] J. N. Israelachvili, "Intermolecular and Surface Forces: With Applications to Colloidal and Biological Systems (Colloid Science)," ed: Academic press London, 1992.

[91] A. A. Maradudin and P. Mazur, "Effects of surface roughness on the van der Waals force between macroscopic bodies," *Physical Review B*, vol. 22, p. 1677, 1980.

[92] J. Whitehead, "Surface deformation and friction of metals at light loads," in *Proceedings of the Royal Society of London A: Mathematical, Physical and Engineering Sciences*, 1950, pp. 109-124.

[93] B. Bhushan and A. V. Kulkarni, "Effect of normal load on microscale friction measurements," *Thin Solid Films*, vol. 278, pp. 49-56, 1996.

[94] P. Blau, "ASM Handbook: Friction, Lubrication, and Wear Technology. vol. 18," *USA: ASM International Handbook Committee*, 1992.

[95] E. Rabinowicz, "Material properties that influence surface interaction. Friction and wear of materials," ed: New York, Wiley, cop, 1995.

[96] F. Bowden and D. Tabor, "The Friction and Lubrication of Solids, Part II, Clarendon," ed: Oxford, 1964.

[97] B. Bhushan and W. Jahsman, "Measurement of dynamic material behavior under nearly uniaxial strain conditions," *International Journal of Solids and Structures*, vol. 14, pp. 739-753, 1978.

[98] B. Bhushan and W. Jahsman, "Propagation of weak waves in elastic-plastic and elastic-viscoplastic solids with interfaces," *International Journal of Solids and Structures*, vol. 14, pp. 39-51, 1978.

[99] F. Bowden and D. Tabor, "Friction and Lubrication of Solids, vol. I. Clarendon," ed: Oxford, 1950.

[100] F. P. Bowden and D. Tabor, *Friction: an introduction to tribology*: RE Krieger Publishing Company, 1973.

[101] D. Rigney and J. Hirth, "Plastic deformation and sliding friction of metals," *Wear*, vol. 53, pp. 345-370, 1979.

[102] K. Tanaka, "Friction and deformation of polymers," *Journal of the Physical Society of Japan*, vol. 16, pp. 2003-2016, 1961.

[103] K. Ludema and D. Tabor, "The friction and visco-elastic properties of polymeric solids," *Wear*, vol. 9, pp. 329-348, 1966.

[104] D. F. Moore, *The friction and lubrication of elastomers* vol. 9: Pergamon, 1972.

[105] J. Griffioen, "Infrared Surface Temperature Measurements in a Sliding Ceramic--Ceramic Contact," *Mechanisms and Surface Distress. Global Studies of Mechanisms and Local Analyses of Surface Distress Phenomona, Institut National des Sciences Appliquees*, pp. 238-245, 1985.

[106] B. Bhushan, "Temperature and friction of sliding surfaces," Massachusetts Institute of Technology, 1971.

[107] B. Bhushan, *Principles and applications of tribology*: John Wiley & Sons, 2013.

[108] Z. Lu and H. McKellop, "Frictional heating of bearing materials tested in a hip joint wear simulator," *Proceedings of the Institution of Mechanical Engineers, Part H: Journal of Engineering in Medicine,* vol. 211, pp. 101-108, 1997.

[109] S. Jones, I. Pinder, C. Moran, and A. Malcolm, "Polyethylene wear in uncemented knee replacements," *Journal of Bone & Joint Surgery, British Volume,* vol. 74, pp. 18-22, 1992.

[110] J.-M. Brandt, "Wear and Boundary Lubrication in Modular Total Knee Replacements," Doctor of Philosophy in Mechanical Engineering, Mechanical Engineering, University of Waterloo, Waterloo, 2008.

[111] J. F. Archard and W. Hirst, "The wear of metals under unlubricated conditions," *Proceedings of the Royal Society A,* vol. 236, pp. 397–410, 1956.

[112] B. Bhushan, R. E. Davis, and H. R. Kolar, "Metallurgical re-examination of wear modes II: Adhesive and abrasive," *Thin Solid Films,* vol. 123, pp. 113-126, 1985.

[113] S. T. O'Brien, C. D. Burnell, D. R. Hedden, and J.-M. Brandt, "Abrasive Wear and Metallosis Associated With Cross-Linked Polyethylene in Total Hip Arthroplasty," *The Journal of Arthroplasty*, 2010.

[114] N. P. Suh, "Tribophysics," *Pretice-Hall, Englewood Cliffs, New Jersey 07632, USA, 1986.*, 1986.

[115] M. Khruschov, "Resistance of metals to wear by abrasion as related to hardness," in *Proc. Conf. on Lubrication and Wear*, 1957, pp. 655-659.

[116] M. Khruschov, "Principles of abrasive wear," *Wear,* vol. 28, pp. 69-88, 1974.

[117] J. Goddard and H. Wilman, "A theory of friction and wear during the abrasion of metals," *Wear,* vol. 5, pp. 114-135, 1962.

[118] T. Mulhearn and L. Samuels, "The abrasion of metals: a model of the process," *Wear,* vol. 5, pp. 478-498, 1962.

[119] A. Misra and I. Finnie, "Some observations on two-body abrasive wear," *Wear,* vol. 68, pp. 41-56, 1981.

[120] F. Aleinikov, "THE INFLUENCE OF ABRASIVE POWDER MICROHARDNESS ON THE VALUES OF COEFFICIENTS OF VOLUME REMOVAL, DETERMINED BY THE LAPPING METHOD," *Soviet Physics-Technical Physics,* vol. 2, pp. 505-511, 1957.

[121] R. Richardson, "The wear of metals by relatively soft abrasives," *Wear,* vol. 11, pp. 245-275, 1968.

[122] E. Rabinowicz, "Abrasive wear resistance as a materials test," *Lubr. Eng.*, vol. 33, pp. 378-381, 1977.

[123] E. Rabinowicz, "The wear of hard surfaces by soft abrasives," *Wear of Materials 1983*, pp. 12-18, 1983.

[124] W. Weibull, "Wide applicability," *Journal of applied mechanics,* vol. 103, p. 33, 1951.

[125] I. O. f. S. ISO, "ISO/TS 16281:2008 - Rolling bearings -- Methods for calculating the modified reference rating life for universally loaded bearings," ed. Geneva, Switzerland: International Organization for Standardization.

[126] E. Bamberger, *Life Adjustment Factors for Ball and Roller Bearings: An Engineering Design Guide*: American Society of Mechanical Engineers, 1971.

[127] T. Harris, "Rolling bearing analysis, 1991," ed: John Wiley and Sons, Inc., New York, NY.

[128] E. V. Zaretsky, "STLE life factors for rolling bearings," *STLE SPECIAL PUBLICATION SP*, 1992.

[129] E. Ioannides and T. Harris, "A new fatigue life model for rolling bearings," *Journal of Tribology,* vol. 107, pp. 367-377, 1985.

[130] L. G. Johnson, *The statistical treatment of fatigue experiments* vol. 10: Elsevier Amsterdam, 1964.

[131] W. Nelson, "Applied Life Data Analysis, New York: JohnWiley," *NelsonApplied Life Data Analysis1982*, 1982.

[132] B. R. Lawn, "Indentation of ceramics with spheres: a century after Hertz," *Journal of the American Ceramic Society,* vol. 81, pp. 1977-1994, 1998.

[133] A. Patnaik, A. Satapathy, N. Chand, N. Barkoula, and S. Biswas, "Solid particle erosion wear characteristics of fiber and particulate filled polymer composites: A review," *Wear,* vol. 268, pp. 249-263, 2010.

[134] R. Malka, S. Nešić, and D. A. Gulino, "Erosion–corrosion and synergistic effects in disturbed liquid-particle flow," *Wear,* vol. 262, pp. 791-799, 2007.

[135] R. Singh, S. Tiwari, and S. K. Mishra, "Cavitation erosion in hydraulic turbine components and mitigation by coatings: Current status and future needs," *Journal of materials engineering and performance,* vol. 21, pp. 1539-1551, 2012.

[136] L. Ives and A. Ruff, "Electron microscopy study of erosion damage in copper," in *Erosion: Prevention and Useful Applications*, ed: ASTM International, 1979.

[137] P. A. Engel, *Impact wear of materials* vol. 2: Elsevier, 1978.

[138] G. Manivasagam, D. Dhinasekaran, and A. Rajamanickam, "Biomedical implants: Corrosion and its prevention-a review," *Recent Patents on Corrosion Science,* vol. 2, pp. 40-54, 2010.

[139] R. J. Wood, "Tribo-corrosion of coatings: a review," *Journal of Physics D: Applied Physics,* vol. 40, p. 5502, 2007.

[140] R. Holm, *Electric contacts: theory and application*: Springer Science & Business Media, 2013.

[141] R. Waterhouse, "Fretting fatigue," *International materials reviews,* vol. 37, pp. 77-98, 1992.

[142] S. M. Kurtz, C. M. Rimnac, W. J. Hozack, J. Turner, M. Marcolongo, V. M. Goldberg, M. J. Kraay, and A. A. Edidin, "In vivo degradation of polyethylene liners after gamma sterilization in air," *The Journal of Bone & Joint Surgery,* vol. 87, pp. 815-823, 2005.

[143] R. Stribeck, "Characteristics of plain and roller bearings," *Zeit. VDI,* vol. 46, 1902.

[144] A. Sommerfeld, "Zur hydrodynamischen theorie der schmiermittelreibung," *Z. Math. Phys,* vol. 50, pp. 97-155, 1904.

[145] O. Pinkus and B. Sternlicht, *Theory of hydrodynamic lubrication*: McGraw-Hill, 1961.

[146] A. Cameron, "Basic Lubrication Theory. 2nd edit," ed: New York, London, Sydney, Toronto: Halsted Press, J. Wiley & Sons, 1976.

[147] W. A. Gross, L. Matsch, V. Castelli, A. Eshel, J. Vohr, and M. Wildmann, "Fluid film lubrication," John Wiley and Sons, Inc., New York, NY1980.

[148] E. R. Booser, "CRC handbook of lubrication. Theory and practice of tribology: volume II: theory and design," 1984.

[149] M. Neale and D. Fuller, "Theory and practice of lubrication for engineers," ed: Elsevier, 1984.

[150] J. Frene, D. Nicolas, B. Degueurce, D. Berthe, and M. Godet, *Hydrodynamic lubrication: bearings and thrust bearings* vol. 33: Elsevier, 1997.

[151] M. Robbins, M. Müser, and B. Bhushan, "Modern Tribology Handbook," ed: CRC Press Boca Raton, FL, 2001.

[152] M. Khonsari and E. Booser, "Applied Tribology Bearing-Design and Lubrication John Wiley & Sons," *Inc New York, NY*, 2001.

[153] B. J. Hamrock, S. R. Schmid, and B. O. Jacobson, *Fundamentals of fluid film lubrication*: CRC press, 2004.

[154] A. Z. Szeri, *Fluid film lubrication: theory and design*: Cambridge University Press, 2005.

[155] R. W. Bruce, *Handbook of Lubrication and Tribology, Volume II: Theory and Design* vol. 2: CRC press, 2012.

[156] F. F. Ling, E. E. Klaus, and R. Fein, "BOUNDARY LUBRICATION. AN APPRAISAL OF WORLD LITERATURE," 1969.

[157] P. M. Ku, "Interdisciplinary approach to liquid lubricant technology," 1973.

[158] A. Beerbower, "Boundary lubrication," DTIC Document1972.

[159] B. Bhushan, *Modern tribology handbook. 2. Materials, coatings, and industrial applications*: CRC Press, 2001.

[160] J. Georges, "Colloidal behaviour of films in boundary lubrication," *Microscopic aspects of Adhesion and Lubrication*, pp. 729-761, 1981.

[161] J.-M. Georges and D. Mazuyer, "Pressure effects on the shearing of a colloidal thin film," *Journal of Physics: Condensed Matter*, vol. 3, p. 9545, 1991.

[162] J.-M. Georges, D. Mazuyer, J.-L. Loubet, and A. Tonck, "Friction with colloidal lubrication," in *Fundamentals of Friction: Macroscopic and Microscopic Processes*, ed: Springer, 1992, pp. 263-286.

[163] J.-M. Georges, D. Mazuyer, A. Tonck, and J.-L. Loubet, "Lubrication with a thin colloidal layer," *Journal of Physics: Condensed Matter*, vol. 2, p. SA399, 1990.

[164] J.-M. Brandt, K. Charron, L. Zhao, S. J. MacDonald, and J. B. Medley, "Calf serum constituent fractions influence polyethylene wear and microbial growth in knee simulator testing," *Proceedings of the Institution of Mechanical Engineers, Part H: Journal of Engineering in Medicine*, vol. 226, pp. 427-440, 2012.

[165] T. Graham, "XXXV.—On the properties of silicic acid and other analogous colloidal substances," *Journal of the Chemical Society*, vol. 17, pp. 318-327, 1864.

[166] S. Granick, S. K. Kumar, E. J. Amis, M. Antonietti, A. C. Balazs, A. K. Chakraborty, G. S. Grest, C. Hawker, P. Janmey, and E. J. Kramer, "Macromolecules at surfaces: Research challenges and opportunities from tribology to biology," *Journal of Polymer Science Part B: Polymer Physics,* vol. 41, pp. 2755-2793, 2003.

[167] J. Georges, S. Millot, J. Loubet, and A. Tonck, "Drainage of thin liquid films between relatively smooth surfaces," *The Journal of chemical physics,* vol. 98, pp. 7345-7360, 1993.

[168] E. Pelletier, J. Montfort, J. Loubet, A. Tonck, and J. Georges, "Dynamics of compressed polymer layers adsorbed on solid surfaces," *Macromolecules,* vol. 28, pp. 1990-1998, 1995.

[169] H.-W. Hu and S. Granick, "Viscoelastic dynamics of confined polymer melts," in *Annual Meeting, Los Angeles*, 1991.

[170] G. Marin, E. Menezes, V. Raju, and W. Graessley, "Propriétés viscoélastiques linéaires de solutions de polybutadiène en régime semi-dilué et concentré," *Rheologica Acta,* vol. 19, pp. 462-476, 1980.

[171] P. Bajpai, A. Kahraman, and N. Anderson, "A surface wear prediction methodology for parallel-axis gear pairs," *Journal of Tribology,* vol. 126, pp. 597-605, 2004.

[172] A. Flodin and S. Andersson, "A simplified model for wear prediction in helical gears," *Wear,* vol. 249, pp. 285-292, 2001.

[173] I. McColl, J. Ding, and S. Leen, "Finite element simulation and experimental validation of fretting wear," *Wear,* vol. 256, pp. 1114-1127, 2004.

[174] C. Yuksel and A. Kahraman, "Dynamic tooth loads of planetary gear sets having tooth profile wear," *Mechanism and Machine Theory,* vol. 39, pp. 695-715, 2004.

[175] M. W. C. B. D. EDWARDS and S. AMlN, "Dynamic modeling and wear-based remaining useful life prediction of high power clutch systems," 2004.

[176] S. Mukras, N. H. Kim, W. G. Sawyer, D. B. Jackson, and L. W. Bergquist, "Numerical integration schemes and parallel computation for wear prediction using finite element method," *Wear,* vol. 266, pp. 822-831, 2009.

[177] R.-S. Lee and J.-L. Jou, "Application of numerical simulation for wear analysis of warm forging die," *Journal of Materials Processing Technology,* vol. 140, pp. 43-48, 2003.

[178] J. Kang, I. Park, J. Jae, and S. Kang, "A study on a die wear model considering thermal softening:(I) Construction of the wear model," *Journal of Materials Processing Technology,* vol. 96, pp. 53-58, 1999.

[179] P. Põdra and S. Andersson, "Wear simulation with the Winkler surface model," *Wear,* vol. 207, pp. 79-85, 1997.

[180] A. Flodin and S. Andersson, "Simulation of mild wear in spur gears," *Wear,* vol. 207, pp. 16-23, 1997.

[181] R. Holm, "Electrical Contacts, Stockholm, H," ed: Gerbers, 1946.

[182] K.-H. Zum Gahr, *Microstructure and wear of materials* vol. 10: Elsevier, 1987.

[183] H. Meng and K. Ludema, "Wear models and predictive equations: their form and content," *Wear,* vol. 181, pp. 443-457, 1995.

[184] F. Barwell, "Wear of metals," *Wear,* vol. 1, pp. 317-332, 1958.

[185] S. Rhee, "Wear equation for polymers sliding against metal surfaces," *Wear,* vol. 16, pp. 431-445, 1970.

[186] J. McGrew, "Design for Wear of Sliding Bearings," *ASTM Standardization News,* vol. 2, pp. 9-28, 1974.

[187] G. Massouros, "Model of wear in a plain bearing under boundary lubrication," *Tribology International,* vol. 15, pp. 193-197, 1982.

[188] R. Bayer, "Prediction of wear in a sliding system," *Wear,* vol. 11, pp. 319-332, 1968.

[189] A. Atkins and M. Omar, "The load dependence of fatigue wear in polymers," in *Proc. Int. Conf. on Wear of Materials, American Society of Mechanical Engineers,* 1985, pp. 405-409.

[190] J. Halling, "A contribution to the theory of mechanical wear," *Wear,* vol. 34, pp. 239-249, 1975.

[191] I. Kraghelskii and A. Loginov, "Prediction of wear rate by theoretical experimental method," *Wear of Materials 1983,* pp. 394-401, 1983.

[192] H. Da-Yue, G. Ting-Hong, L. Hang-Chau, and Q. Rui-Zhong, "A wear equation for epoxy bonded MoS2 solid lubricant coating," Guangzhou Machine Tool Research Inst., Guangzhou, People's Republic of China1981.

[193] K. Kato, "Tribology of ceramics," *Wear,* vol. 136, pp. 117-133, 1990.

[194] Z. Rymuza, "Wear in polymer micro-pairs," in *Proceedings of 3rd international conference on wear of materials*, 1981.

[195] G. Fleischer, "Energetische methode der bestimmung des verschleißes," *Schmierungstechnik,* vol. 4, pp. 269-274, 1973.

[196] H. Krause and G. Poll, "Wear of wheel-rail surfaces," *Wear,* vol. 113, pp. 103-122, 1986.

[197] R. Matveevsky, "The critical temperature of oil with point and line contact machines," *Journal of Basic Engineering,* vol. 87, pp. 754-759, 1965.

[198] A. Plint, "Machines and Methodologies for Wear Testing Extreme Pressure and Anti-Wear Properties of Lubricants," in *Proceedings of the XI National Congress on Industrial Tribology, Delhi*, 1995, pp. 375-386.

[199] H. Mohrbacher, B. Blanpain, J.-P. Celis, J. Roos, L. Stals, and M. Van Stappen, "Oxidational wear of TiN coatings on tool steel and nitrided tool steel in unlubricated fretting," *Wear,* vol. 188, pp. 130-137, 1995.

[200] M. Huq and J.-P. Celis, "Reproducibility of friction and wear results in ball-on-disc unidirectional sliding tests of TiN-alumina pairings," *Wear,* vol. 212, pp. 151-159, 1997.

[201] M. Huq and J.-P. Celis, "Expressing wear rate in sliding contacts based on dissipated energy," *Wear,* vol. 252, pp. 375-383, 2002.

[202] U. Olofsson, "Cyclic micro-slip under unlubricated conditions," *Tribology International,* vol. 28, pp. 207-217, 1995.

[203] D. Dowson and G. R. Higginson, *Elasto-hydrodynamic lubrication: international series on materials science and technology* vol. 23: Elsevier, 2014.

[204] P. Lugt and G. E. Morales-Espejel, "A review of elasto-hydrodynamic lubrication theory," *Tribology Transactions,* vol. 54, pp. 470-496, 2011.

[205] H. Washizu, S. Sanda, S.-a. Hyodo, T. Ohmori, N. Nishino, and A. Suzuki, "Molecular dynamics simulations of elasto-hydrodynamic lubrication and boundary lubrication for automotive tribology," in *Journal of Physics: Conference Series*, 2007, p. 012009.

[206] C. M. Mate, "Tribology on the small scale," *Oxford University Press, Oxford,* 2008.

[207] S. M. Hsu and R. Gates, "Boundary lubricating films: formation and lubrication mechanism," *Tribology International,* vol. 38, pp. 305-312, 2005.

[208] M. Ruths and J. N. Israelachvili, "Surface forces and nanorheology of molecularly thin films," in *Nanotribology and nanomechanics*, ed: Springer, 2008, pp. 417-515.

[209] A. Peacock, *Handbook of Polyethylene: Structures: Properties, and Applications*: Taylor & Francis, 2000.

[210] L. Kang, A. L. Galvin, J. Fisher, and Z. Jin, "Enhanced computational prediction of polyethylene wear in hip joints by incorporating cross-shear and contact pressure in additional to load and sliding distance: Effect of head diameter," *Journal of biomechanics,* vol. 42, pp. 912-918, 2009 2009.

[211] S. S. Brown and I. C. Clarke, "A review of lubrication conditions for wear simulation in artificial hip replacements," *Tribology transactions,* vol. 49, pp. 72-78, 2006.

[212] D. Mazzucco, R. Scott, and M. Spector, "Composition of joint fluid in patients undergoing total knee replacement and revision arthroplasty: correlation with flow properties," *Biomaterials,* vol. 25, pp. 4433-4445, 2004.

[213] J. DesJardins, A. Aurora, S. Tanner, T. Pace, K. Acampora, and M. LaBerge, "Increased total knee arthroplasty ultra-high molecular weight polyethylene wear using a clinically relevant hyaluronic acid simulator lubricant," *Proceedings of the*

Institution of Mechanical Engineers, Part H: Journal of Engineering in Medicine, vol. 220, pp. 609-623, 2006.

[214] J. Yao, M. Laurent, T. Johnson, C. Blanchard, and R. Crowninshield, "The influences of lubricant and material on polymer/CoCr sliding friction," *Wear,* vol. 255, pp. 780-784, 2003.

[215] T. Peters Jr, *All about albumin: biochemistry, genetics, and medical applications*: Academic press, 1995.

[216] L. Kang, A. L. Galvin, T. D. Brown, Z. Jin, and J. Fisher, "Quantification of the effect of cross-shear on the wear of conventional and highly cross-linked UHMWPE," *Journal of biomechanics,* vol. 41, pp. 340-346, 2008 2008.

[217] M. A. Wimmer and T. P. Andriacchi, "Tractive forces during rolling motion of the knee: Implications for wear in total knee replacement," *Journal of biomechanics,* vol. 30, pp. 131-137, 1997.

[218] T. Schwenke, L. L. Borgstede, E. Schneider, T. P. Andriacchi, and M. A. Wimmer, "The influence of slip velocity on wear of total knee arthroplasty," *Wear,* vol. 259, pp. 926-932, 2005.

[219] M. Spector, M. D. Ries, R. B. Bourne, W. S. Sauer, M. Long, and G. Hunter, "Wear performance of ultra-high molecular weight polyethylene on oxidized zirconium total knee femoral components," *Journal of Bone and Joint Surgery (Am),* vol. 83A, 2001.

[220] V. Saikko, O. Calonius, and J. Keränen, "Effect of counterface roughness on the wear of conventional and crosslinked ultrahigh molecular weight polyethylene studied with a multi-directional motion pin-on-disk device," *Journal of Biomedical Materials Research,* vol. 57, pp. 506-512, 2001.

[221] D. J. Kilgus, J. R. Moreland, G. A. Finerman, T. T. Funahashi, and J. S. Tipton, "Catastrophic wear of tibial polyethylene inserts," *Clinical Orthopaedics and Related Research,* vol. 273, pp. 223-231, 1991.

[222] V. Saikko, "Effect of contact pressure on wear and friction of ultra-high molecular weight polyethylene in multidirectional sliding," *Proceedings of the Institution of Mechanical Engineers, Part H: Journal of Engineering in Medicine,* vol. 220, pp. 723-731, 2006.

[223] A. Amin, R. Clayton, J. Patton, M. Gaston, R. Cook, and I. Brenkel, "Total knee replacement in morbidly obese patients results of a prospective, matched study," *Journal of Bone & Joint Surgery, British Volume,* vol. 88, pp. 1321-1326, 2006.

[224] J. R. Foran, M. A. Mont, G. Etienne, L. C. Jones, and D. S. Hungerford, "The outcome of total knee arthroplasty in obese patients," *The Journal of Bone & Joint Surgery,* vol. 86, pp. 1609-1615, 2004.

[225] F. M. Griffin, G. R. Scuderi, J. N. Insall, and W. Colizza, "Total knee arthroplasty in patients who were obese with 10 years followup," *Clinical orthopaedics and related research,* vol. 356, pp. 28-23, 1998.

[226] M. A. Mont, S. K. Mathur, K. A. Krackow, J. W. Loewy, and D. S. Hungerford, "Cementless total knee arthroplasty in obese patients: a comparison with a matched control group," *The Journal of arthroplasty,* vol. 11, pp. 153-156, 1996.

[227] D. Spicer, D. Pomeroy, W. Badenhausen, J. L. Schaper, J. Curry, K. Suthers, and M. Smith, "Body mass index as a predictor of outcome in total knee replacement," *International orthopaedics,* vol. 25, pp. 246-249, 2001.

[228] S. Stern and J. Insall, "Total knee arthroplasty in obese patients," *The Journal of Bone & Joint Surgery,* vol. 72, pp. 1400-1404, 1990.

[229] C. D. McClung, C. A. Zahiri, J. K. Higa, H. C. Amstutz, and T. P. Schmalzried, "Relationship between body mass index and activity in hip or knee arthroplasty patients," *Journal of Orthopaedic Research,* vol. 18, pp. 35-39, 2000.

[230] M. Gispert, A. Serro, R. Colaco, and B. Saramago, "Friction and wear mechanisms in hip prosthesis: Comparison of joint materials behaviour in several lubricants," *Wear,* vol. 260, pp. 149-158, 2006.

[231] B. Hills, "Boundary lubrication in vivo," *Proceedings of the Institution of Mechanical Engineers, Part H: Journal of Engineering in Medicine,* vol. 214, pp. 83-94, 2000.

[232] V. Saikko, "Effect of lubricant protein concentration on the wear of ultra-high molecular weight polyethylene sliding against a CoCr counterface," *Journal of Tribology,* vol. 125, pp. 638-642, 2003.

[233] L. E. Guenther, B. W. Pyle, T. R. Turgeon, E. R. Bohm, U. P. Wyss, T. A. Schmidt, and J.-M. Brandt, "Biochemical analyses of human osteoarthritic and periprosthetic synovial fluid," *Proceedings of the Institution of Mechanical Engineers, Part H: Journal of Engineering in Medicine*, p. 0954411913517880, 2014.

[234] D. C. Carter and J. X. Ho, "Structure of serum albumin," *Advances in Protein Chemistry*, vol. 45, pp. 153-203, 1994.

[235] C. Lapresle, M. Kaminski, and C. E. Tanner, "Immunochemical study of the enzymatic degradation of human serum albumin: an analysis of the antigenic structure of a protein molecule," *The Journal of Immunology*, vol. 82, pp. 94-102, 1959.

[236] B. Farruggia and G. A. Picó, "Thermodynamic features of the chemical and thermal denaturations of human serum albumin," *International Journal of Biological Macromolecules*, vol. 26, pp. 317-323, 1999.

[237] K. M. Oates, W. E. Krause, R. L. Jones, and R. H. Colby, "Rheopexy of synovial fluid and protein aggregation," *Journal of the royal society interface*, vol. 3, pp. 167-174, 2006.

[238] C.-B. Yang, H.-W. Fang, H.-L. Liu, C.-H. Chang, M.-C. Hsieh, W.-M. Lee, and H.-T. Huang, "Frictional characteristics of the tribological unfolding albumin for

polyethylene and cartilage," *Chemical physics letters,* vol. 431, pp. 380-384, 2006.

[239] C. Myant, R. Underwood, J. Fan, and P. Cann, "Lubrication of metal-on-metal hip joints: the effect of protein content and load on film formation and wear," *Journal of the mechanical behavior of biomedical materials,* vol. 6, pp. 30-40, 2012.

[240] H.-W. Fang, Y.-C. Su, H.-T. Huang, W.-B. Tsai, and H.-L. Liu, "Investigation of the friction induced conformational change of protein and wear of UHMWPE by a wear process with microfabricated surfaces," *Materials Science and Engineering: C,* vol. 29, pp. 1118-1123, 2009.

[241] L. Morawietz, T. Gehrke, L. Frommelt, P. Gratze, A. Bosio, J. Möller, B. Gerstmayer, and V. Krenn, "Differential gene expression in the periprosthetic membrane: lubricin as a new possible pathogenetic factor in prosthesis loosening," *Virchows Archiv,* vol. 443, pp. 57-66, 2003.

[242] G. D. Jay, "Lubricin and surfacing of articular joints," *Current Opinion in Orthopaedics,* vol. 15, pp. 355-359, 2004.

[243] K. R. Grymonpré, B. A. Staggemeier, P. L. Dubin, and K. W. Mattison, "Identification by integrated computer modeling and light scattering studies of an electrostatic serum albumin-hyaluronic acid binding site," *Biomacromolecules,* vol. 2, pp. 422-429, 2001.

[244] F. C. Linn, "Lubrication of animal joints," *Journal of biomechanics,* vol. 1, pp. 193-205, 1968.

[245] F. C. Linn, "Lubrication of animal joints: II the mechanism," *Journal of biomechanics,* vol. 1, pp. 193-205, 1968.

[246] K. Mabuchi, Y. Tsukamoto, T. Obara, and T. Yamaguchi, "The effect of additive hyaluronic acid on animal joints with experimentally reduced lubricating ability," *Journal of Biomedical Materials Research,* vol. 28, pp. 865-870, 1994.

[247] A. Ogston and J. Stanier, "On the state of hyaluronic acid in synovial fluid," *Biochemical Journal,* vol. 46, p. 364, 1950.

[248] A. Ogston and J. Stanier, "Further observations on the preparation and composition of the hyaluronic acid complex of ox synovial fluid," *Biochemical Journal,* vol. 52, p. 149, 1952.

[249] S. Xu, J. Yamanaka, S. SATo, I. MIYAMA, and M. YoNEsE, "Characteristics of complexes composed of sodium hyaluronate and bovine serum albumin," *Chemical and pharmaceutical bulletin,* vol. 48, pp. 779-783, 2000.

[250] International Organization for Standardization, "Implants for surgery -- Wear of total knee-joint prostheses," in *Part 3: Loading and displacement parameters for wear-testing machines with displacement control and corresponding environmental conditions for test* vol. 14243-3:2004, ed, 2009.

[251] J.-M. Brandt, K. D. J. Charron, L. Zhao, S. J. MacDonald, and J. B. Medley, "Commissioning of a displacement-controlled knee wear simulator and exploration of some issues related to the lubricant," *Proceedings of the Institution of Mechanical Engineers, Part H: Journal of Engineering in Medicine,* June 24, 2011 2011.

[252] J.-M. Brandt, K. Mahmoud, S. Koval, S. MacDonald, and J. Medley, "Antimicrobial agents and low-molecular weight polypeptides affect polyethylene wear in knee simulator testing," *Tribology International,* vol. 65, pp. 97-104, 2013.

[253] J.-M. Brandt, A. Vecherya, L. Guenther, S. Koval, M. Petrak, E. Bohm, and U. Wyss, "Wear testing of crosslinked polyethylene: Wear rate variability and microbial contamination," *Journal of the mechanical behavior of biomedical materials,* vol. 34, pp. 208-216, 2014.

[254] A. L. Galvin, L. Kang, I. Udofia, L. M. Jennings, H. M. McEwen, Z. Jin, and J. Fisher, "Effect of conformity and contact stress on wear in fixed-bearing total knee prostheses," *Journal of biomechanics,* vol. 42, pp. 1898-1902, 2009.

[255] P. S. Walker, "Bearing surface design in total knee replacement," *Engineering in medicine,* vol. 17, pp. 149-156, 1988.

[256] D. L. Bartel, V. Bicknell, and T. Wright, "The effect of conformity, thickness, and material on stresses in ultra-high molecular weight components for total joint replacement," *J Bone Joint Surg Am,* vol. 68, pp. 1041-1051, 1986.

[257] D. L. Bartel, J. J. Rawlinson, A. H. Burstein, C. S. Ranawat, and W. F. J. Flynn, "Stresses in Polyethylene Components of Contemporary Total Knee Replacements," *Clinical Orthopaedics and Related Research,* vol. 317, pp. 76-82, 1995.

[258] Archard J. F. and Hirst W., "The wear of metals under unlubricated conditions," *Proceedings of the Royal Society A,* vol. 236, pp. 397–410, 1956.

[259] S. O'Brien, Y. Luo, C. Wu, M. Petrak, E. Bohm, and J. M. Brandt, "Computational development of a polyethylene wear model for the articular and backside surfaces in modular total knee replacements," *Tribology International,* vol. 59, pp. 284-291, 2012.

[260] B. J. Fregly, W. G. Sawyer, M. K. Harman, and S. A. Banks, "Computational wear prediction of a total knee replacement from in vivo kinematics," *Journal of biomechanics,* vol. 38, pp. 305-314, 2005.

[261] A. Abdelgaied, F. Liu, C. Brockett, L. Jennings, J. Fisher, and Z. Jin, "Computational wear prediction of artificial knee joints based on a new wear law and formulation," *Journal of biomechanics,* vol. 44, pp. 1108-1116, 2011.

[262] K. Hirakawa, T. W. Bauer, M. Yamaguchi, B. N. Stulberg, and A. H. Wilde, "Relationship between wear debris particles and polyethylene surface damage in primary total knee arthroplasty," *The Journal of Arthroplasty,* vol. 14, pp. 165-171, 1999.

[263] S. M. Gabriel, D. A. Dennis, M. J. Honey, and R. D. Scott, "Polyethylene wear on the distal tibial insert surface in total knee arthroplasty," *The Knee,* vol. 5, pp. 221-228, 1998.

[264] S. T. O'Brien, Y. Luo, and J.-M. Brandt, "In-vitro and in-silico investigations on the influence of contact pressure on cross-linked polyethylene wear in total knee replacements," *Wear,* vol. 332, pp. 687-693, 2015.

[265] J. Reinders, R. Sonntag, and J. P. Kretzer, "Synovial fluid replication in knee wear testing: An investigation of the fluid volume," *Journal of Orthopaedic Research,* vol. 33, pp. 92-97, 2015.

[266] S. Palmer, P. Morrison, and A. Ross, "Early catastrophic tibial component wear after unicompartmental knee arthroplasty," *Clinical Orthopaedics and Related Research,* vol. 350, pp. 143-148, 1998.

[267] I. Langmuir, "The adsorption of gases on plane surfaces of glass, mica and platinum," *Journal of the American Chemical Society,* vol. 40, pp. 1361-1403, 1918.

[268] E. R. Valstar, R. Gill, L. Ryd, G. Flivik, N. Börlin, and J. Kärrholm, "Guidelines for standardization of radiostereometry (RSA) of implants," *Acta orthopaedica,* vol. 76, pp. 563-572, 2005.

[269] G. Selvik, "Roentgen stereophotogrammetry: a method for the study of the kinematics of the skeletal system," *Acta Orthopaedica Scandinavica,* vol. 60, pp. 1-51, 1989.

[270] C. Hurschler, F. Seehaus, J. Emmerich, B. L. Kaptein, and H. Windhagen, "Comparison of the model-based and marker-based roentgen stereophotogrammetry methods in a typical clinical setting," *The Journal of arthroplasty,* vol. 24, pp. 594-606, 2009.

[271] B. Kaptein, E. Valstar, B. Stoel, P. Rozing, and J. Reiber, "A new model-based RSA method validated using CAD models and models from reversed engineering," *Journal of biomechanics,* vol. 36, pp. 873-882, 2003.

[272] B. Kaptein, E. Valstar, B. Stoel, P. Rozing, and J. Reiber, "Evaluation of three pose estimation algorithms for model-based roentgen stereophotogrammetric analysis," *Proceedings of the Institution of Mechanical Engineers, Part H: Journal of Engineering in Medicine,* vol. 218, pp. 231-238, 2004.

[273] B. Kaptein, E. Valstar, B. Stoel, P. Rozing, and J. Reiber, "A new type of model-based Roentgen stereophotogrammetric analysis for solving the occluded marker problem," *Journal of biomechanics,* vol. 38, pp. 2330-2334, 2005.

[274] J. Kärrholm, "Roentgen stereophotogrammetry: review of orthopedic applications," *Acta Orthopaedica Scandinavica*, vol. 60, pp. 491-503, 1989.

[275] J. Kärrholm, R. H. Gill, and E. R. Valstar, "The history and future of radiostereometric analysis," *Clinical orthopaedics and related research*, vol. 448, pp. 10-21, 2006.

[276] K. G. Nilsson and T. Dalen, "Inferior performance of Boneloc® bone cement in total knee arthroplasty: A prospective randomized study comparing Boneloc® with Palacos® using radiostereometry (RSA) in 19 patients," *Acta Orthopaedica Scandinavica*, vol. 69, pp. 479-483, 1998.

[277] K. G. Nilsson, J. Kärrholm, L. Carlsson, and T. Dalén, "Hydroxyapatite coating versus cemented fixation of the tibial component in total knee arthroplasty: prospective randomized comparison of hydroxyapatite-coated and cemented tibial components with 5-year follow-up using radiostereometry," *The Journal of arthroplasty*, vol. 14, pp. 9-20, 1999.

[278] K. G. Nilsson, J. Kärrholm, L. Ekelund, and P. Magnusson, "Evaluation of micromotion in cemented vs uncemented knee arthroplasty in osteoarthrosis and rheumatoid arthritis: randomized study using roentgen stereophotogrammetric analysis," *The Journal of arthroplasty*, vol. 6, pp. 265-278, 1991.

[279] I. Önsten, A. Nordqvist, Å. Carlsson, J. Besjakov, and S. Shott, "Hydroxyapatite augmentation of the porous coating improves fixation of tibial components A

RANDOMISED RSA STUDY IN 116 PATIENTS," *Journal of Bone & Joint Surgery, British Volume,* vol. 80, pp. 417-425, 1998.

[280] L. Ryd, B. Albrektsson, L. Carlsson, F. Dansgard, P. Herberts, A. Lindstrand, L. Regner, and S. Toksvig-Larsen, "Roentgen stereophotogrammetric analysis as a predictor of mechanical loosening of knee prostheses," *Journal of Bone & Joint Surgery, British Volume,* vol. 77, pp. 377-383, 1995.

[281] L. Ryd, A. Lindstrand, R. Rosenquist, and G. SELVIK, "Tibial component fixation in knee arthroplasty," *Clinical orthopaedics and related research,* vol. 213, pp. 141-149, 1986.

[282] L. Ryd, A. Lindstrand, R. Rosenquist, and G. Selvik, "Micromotion of conventionally cemented all-polyethylene tibial components in total knee replacements," *Archives of orthopaedic and traumatic surgery,* vol. 106, pp. 82-88, 1987.

[283] L. Ryd and S. Toksvig-Larsen, "Early postoperative fixation of tibial components: an in vivo roentgen stereophotogrammetric analysis," *Journal of orthopaedic research,* vol. 11, pp. 142-148, 1993.

[284] L. Ryd, X. Yuan, and H. Löfgren, "Methods for determining the accuracy of radiostereometric analysis (RSA)," *Acta Orthopaedica Scandinavica,* vol. 71, pp. 403-408, 2000.

[285] F. Seehaus, J. Emmerich, B. L. Kaptein, H. Windhagen, and C. Hurschler, "Experimental analysis of Model-Based Roentgen Stereophotogrammetric Analysis (MBRSA) on four typical prosthesis components," *Journal of biomechanical engineering,* vol. 131, p. 041004, 2009.

[286] J. Uvehammer and J. Kärrholm, "Inducible displacements of cemented tibial components during weight-bearing and knee extension. Observations during dynamic radiostereometry related to joint positions and 2 years history of migration in 16 TKR," *Journal of orthopaedic research,* vol. 19, pp. 1168-1177, 2001.

[287] E. Valstar, F. De Jong, H. Vrooman, P. Rozing, and J. Reiber, "Model-based Roentgen stereophotogrammetry of orthopaedic implants," *Journal of biomechanics,* vol. 34, pp. 715-722, 2001.

[288] E. Valstar, H. Vrooman, S. Toksvig-Larsen, L. Ryd, and R. Nelissen, "Digital automated RSA compared to manually operated RSA," *Journal of biomechanics,* vol. 33, pp. 1593-1599, 2000.

[289] X. Yuan and L. Ryd, "Accuracy analysis for RSA: a computer simulation study on 3D marker reconstruction," *Journal of biomechanics,* vol. 33, pp. 493-498, 2000.

[290] M. Sundberg, L. Lidgren, A. Dahl, and O. Robertsson, "Swedish Knee Arthroplasty Register: Annual Report," 2015.

[291] A. Pearse, G. Hooper, A. Rothwell, and C. Frampton, "Survival and functional outcome after revision of a unicompartmental to a total knee replacement THE NEW ZEALAND NATIONAL JOINT REGISTRY," *Journal of Bone & Joint Surgery, British Volume,* vol. 92, pp. 508-512, 2010.

[292] A. J. Carr, O. Robertsson, S. Graves, A. J. Price, N. K. Arden, A. Judge, and D. J. Beard, "Knee replacement," *The Lancet*, vol. 379, pp. 1331-1340, 2012.

[293] T. J. Gioe, K. K. Killeen, K. Grimm, S. Mehle, and K. Scheltema, "Why are total knee replacements revised?: analysis of early revision in a community knee implant registry," *Clinical Orthopaedics and Related Research,* vol. 428, pp. 100-106, 2004.

[294] T. J. Gioe, C. Novak, P. Sinner, W. Ma, and S. Mehle, "Knee arthroplasty in the young patient: survival in a community registry," *Clinical Orthopaedics and Related Research,* vol. 464, pp. 83-87, 2007.

[295] E. Koskinen, P. Paavolainen, A. Eskelinen, P. Pulkkinen, and V. Remes, "Unicondylar knee replacement for primary osteoarthritis: a prospective follow-up study of 1,819 patients from the Finnish Arthroplasty Register," *Acta orthopaedica,* vol. 78, pp. 128-135, 2007.

[296] A. D. Liddle, A. Judge, H. Pandit, and D. W. Murray, "Adverse outcomes after total and unicompartmental knee replacement in 101 330 matched patients: a

study of data from the National Joint Registry for England and Wales," *The Lancet,* vol. 384, pp. 1437-1445, 2014.

[297] J. Goodfellow, J. O'Connor, and D. Murray, "A critique of revision rate as an outcome measure RE-INTERPRETATION OF KNEE JOINT REGISTRY DATA," *Journal of Bone & Joint Surgery, British Volume,* vol. 92, pp. 1628-1631, 2010.

[298] Ø. Gøthesen, B. Espehaug, L. Havelin, G. Petursson, S. Lygre, P. Ellison, G. Hallan, and O. Furnes, "Survival rates and causes of revision in cemented primary total knee replacement A report from the Norwegian Arthroplasty Register 1994–2009," *Bone & Joint Journal,* vol. 95, pp. 636-642, 2013.

[299] A. W-Dahl, O. Robertsson, L. Lidgren, L. Miller, D. Davidson, and S. Graves, "Unicompartmental knee arthroplasty in patients aged less than 65: combined data from the Australian and Swedish Knee Registries," *Acta orthopaedica,* vol. 81, pp. 90-94, 2010.

[300] M. G. Teeter, J. S. Milner, S. J. MacDonald, and D. D. Naudie, "Manufacturing lot affects polyethylene tibial insert volume, thickness, and surface geometry," *Proceedings of the Institution of Mechanical Engineers, Part H: Journal of Engineering in Medicine,* vol. 227, pp. 884-889, 2013.

[301] R. W. Hood, T. M. Wright, and A. H. Burstein, "Retrieval analysis of total knee prostheses: a method and its application to 48 total condylar prostheses," *Journal of Biomedical Materials Research,* vol. 17, pp. 829-842, 1983.

[302] M. A. Conditt, J. A. Stein, and P. C. Noble, "Factors affecting the severity of backside wear of modular tibial inserts," *J Bone Joint Surg Am,* vol. 86, pp. 305-311, 2004.

[303] R. C. Wasielewski, J. O. Galante, R. M. Leighty, R. N. Natarajan, and A. G. Rosenberg, "Wear patterns on retrieved polyethylene tibial inserts and their relationship to technical considerations during total knee arthroplasty," *Clinical Orthopaedics and Related Research,* vol. 299, pp. 31-43, 1994.

[304] ASTM, "F732-00: Standard Test Method forWear Testing of Polymeric

Materials Used in Total Joint Prostheses," ed, 2000.

[305] V. Saikko, "Wear and friction properties of prosthetic joint materials evaluated on a reciprocating pin-on-flat apparatus," *Wear,* vol. 166, pp. 169-178, 1993.

[306] T. Ahlroos and V. Saikko, "Wear of prosthetic joint materials in various lubricants," *Wear,* vol. 211, pp. 113-119, 1997.

[307] J. Fisher, D. Dowson, H. Hamdzah, and H. L. Lee, "The effect of sliding velocity on the friction and wear of UHMWPE for use in total artificial joints," *Wear,* vol. 175, pp. 219-225, 1994.

[308] C. R. Bragdon, D. O. O'Connor, J. D. Lowenstein, M. Jasty, S. A. Biggs, and W. H. Harris, "A new pin-on-disk wear testing method for simulating wear of polyethylene on cobalt-chrome alloy in total hip arthroplasty," *The Journal of Arthroplasty,* vol. 16, pp. 658-665, 2001.

[309] D. Mazzucco and M. Spector, "Effects of contact area and stress on the volumetric wear of ultrahigh molecular weight polyethylene," *Wear,* vol. 254, pp. 514-522, 2003.

[310] L. Korduba and A. Wang, "The effect of cross-shear on the wear of virgin and highly-crosslinked polyethylene," *Wear,* vol. 271, pp. 1220-1223, 2011.

[311] J. Q. Yao, T. A. Blanchet, D. J. Murphy, and M. P. Laurent, "Effect of fluid absorption on the wear resistance of UHMWPE orthopedic bearing surfaces," *Wear,* vol. 255, pp. 1113-1120, 2003.

[312] V. Saikko, O. Calonius, and J. Keränen, "Effect of slide track shape on the wear of ultra-high molecular weight polyethylene in a pin-on-disk wear simulation of total hip prosthesis," *Journal of Biomedical Materials Research Part B: Applied Biomaterials,* vol. 69, pp. 141-148, 2004.

[313] A. Kilgour and A. Elfick, "Influence of crosslinked polyethylene structure on wear of joint replacements," *Tribology International,* vol. 42, pp. 1582-1594, 2009.

[314] V. Saikko and T. Ahlroos, "Type of motion and lubricant in wear simulation of polyethylene acetabular cup," *Proceedings of the Institution of Mechanical Engineers, Part H: Journal of Engineering in Medicine,* vol. 213, pp. 301-310, 1999.

[315] V. Saikko, "A multidirectional motion pin-on-disk wear test method for prosthetic joint materials," *Journal of Biomedical Materials Research,* vol. 41, pp. 58-64, 1998.

[316] V. Saikko and T. Ahlroos, "Wear simulation of UHMWPE for total hip replacement with a multidirectional motion pin-on-disk device: Effects of counterface material, contact area, and lubricant," *Journal of Biomedical Materials Research,* vol. 49, pp. 147-154, 2000.

[317] H. Marrs, D. Barton, R. Jones, I. Ward, J. Fisher, and C. Doyle, "Comparative wear under four different tribological conditions of acetylene enhanced cross-linked ultra high molecular weight polyethylene," *Journal of Materials Science: Materials in Medicine,* vol. 10, pp. 333-342, 1999.

[318] L. Kang, A. L. Galvin, T. D. Brown, J. Fisher, and Z. M. Jin, "Wear simulation of ultra-high molecular weight polyethylene hip implants by incorporating the effects of cross-shear and contact pressure," *Proceedings of the Institution of Mechanical Engineers, Part H: Journal of Engineering in Medicine,* vol. 222, pp. 1049-1064, 2008 2008.

[319] D. Baykal, R. Siskey, H. Haider, V. Saikko, T. Ahlroos, and S. Kurtz, "Advances in tribological testing of artificial joint biomaterials using multidirectional pin-on-disk testers," *Journal of the mechanical behavior of biomedical materials*, vol. 31, pp. 117-134, 2014.

[320] T. Joyce, D. Monk, S. Scholes, and A. Unsworth, "A multi-directional wear screening device and preliminary results of UHMWPE articulating against stainless steel," *Bio-medical materials and engineering*, vol. 10, pp. 241-249, 2000.

[321] L. Wilches, J. Uribe, and A. Toro, "Wear of materials used for artificial joints in total hip replacements," *Wear*, vol. 265, pp. 143-149, 2008.

[322] M. R. Gevaert, M. LaBerge, J. M. Gordon, and J. D. DesJardins, "The quantification of physiologically relevant cross-shear wear phenomena on orthopaedic bearing materials using the MAX-shear wear testing system," *Journal of Tribology*, vol. 127, pp. 740-749, 2005.

[323] International Organization for Standardization, "Implants for surgery -- Wear of total knee-joint prostheses," in *Loading and displacement parameters for wear testing machines with load control and corresponding environmental conditions for test* vol. 14243-2:2004, ed, 2009.

[324] H. Haider and P. Walker, "Analysis and recommendations for the optimum spring configurations for soft tissue restraint in force-control knee simulator testing," in

TRANSACTIONS OF THE ANNUAL MEETING-ORTHOPAEDIC RESEARCH SOCIETY, 2002, pp. 912-912.

[325] J. P. Kretzer, E. Jakubowitz, R. Sonntag, K. Hofmann, C. Heisel, and M. Thomsen, "Effect of joint laxity on polyethylene wear in total knee replacement," *Journal of biomechanics,* vol. 43, pp. 1092-1096, 2010.

[326] S. T. O'Brien, E. R. Bohm, M. J. Petrak, U. P. Wyss, and J.-M. Brandt, "An Energy Dissipation and Cross Shear Time Dependent Computational Wear Model for the Analysis of Polyethylene Wear in Total Knee Replacements " *Journal of biomechanics,* vol. 47, pp. 1127-1133, 2014.

[327] M. A. Baldwin, C. W. Clary, C. K. Fitzpatrick, J. S. Deacy, L. P. Maletsky, and P. J. Rullkoetter, "Dynamic finite element knee simulation for evaluation of knee replacement mechanics," *Journal of biomechanics,* vol. 45, pp. 474-483, 2012.

[328] J. P. Halloran, S. K. Easley, A. J. Petrella, and P. J. Rullkoetter, "Comparison of deformable and elastic foundation finite element simulations for predicting knee replacement mechanics," *Journal of biomechanical engineering,* vol. 127, pp. 813-818, 2005.

[329] J. P. Halloran, A. J. Petrella, and P. J. Rullkoetter, "Explicit finite element modeling of total knee replacement mechanics," *Journal of biomechanics,* vol. 38, pp. 323-331, 2005.

[330] P. J. Laz, S. Pal, J. P. Halloran, A. J. Petrella, and P. J. Rullkoetter, "Probabilistic finite element prediction of knee wear simulator mechanics," *Journal of biomechanics*, vol. 39, pp. 2303-2310, 2006.

[331] T. K. Kim, C. B. Chang, Y. G. Kang, S. J. Kim, and S. C. Seong, "Causes and predictors of patient's dissatisfaction after uncomplicated total knee arthroplasty," *The Journal of arthroplasty*, vol. 24, pp. 263-271, 2009.

[332] J. M. Weiss, P. C. Noble, M. A. Conditt, H. W. Kohl, S. Roberts, K. F. Cook, M. J. Gordon, and K. B. Mathis, "What functional activities are important to patients with knee replacements?," *Clinical orthopaedics and related research*, vol. 404, pp. 172-188, 2002.

[333] P. C. Noble, M. J. Gordon, J. M. Weiss, R. N. Reddix, M. A. Conditt, and K. B. Mathis, "Does total knee replacement restore normal knee function?," *Clinical orthopaedics and related research*, vol. 431, pp. 157-165, 2005.

[334] R. Willing and I. Y. Kim, "A holistic numerical model to predict strain hardening and damage of UHMWPE under multiple total knee replacement kinematics and experimental validation," *Journal of biomechanics*, vol. 42, pp. 2520-2527, 2009.

[335] S. O'Brien, Y. Luo, C. Wu, M. Petrak, E. Bohm, and J. M. Brandt, "Prediction of backside micromotion in total knee replacements by finite element simulation," *Proceedings of the Institution of Mechanical Engineers, Part H: Journal of Engineering in Medicine*, vol. 226, pp. 235-245, 2012.

[336] A. J. Petrella, J. R. Armstrong, P. J. Laz, and P. J. Rullkoetter, "A novel cross-shear metric for application in computer simulation of ultra-high molecular weight polyethylene wear," *Computer Methods in Biomechanics and Biomedical Engineering,* vol. 15, pp. 1223-1232, 2012.

[337] D. Zhao, H. Sakoda, W. G. Sawyer, S. A. Banks, and B. J. Fregly, "Predicting Knee Replacement Damage in a Simulator Machine Using a Computational Model With a Consistent Wear Factor," *Journal of Biomechanical Engineering,* vol. 130, pp. 011004-10, 2008.

[338] D. Zhao, W. Sawyer, and B. Fregly, "Computational Wear Prediction of UHMWPE in Knee Replacements," *Journal o f ASTM International,* vol. 3, pp. 45-50, 2006.

[339] J. S. Bergström, S. M. Kurtz, C. M. Rimnac, and A. A. Edidin, "Constitutive modeling of ultra-high molecular weight polyethylene under large-deformation and cyclic loading conditions," *Biomaterials,* vol. 23, pp. 2329-2343, 2002.

[340] A. C. Godest, M. Beaugonin, E. Haug, M. Taylor, and P. J. Gregson, "Simulation of a knee joint replacement during a gait cycle using explicit finite element analysis," *Journal of biomechanics,* vol. 35, pp. 267-275, 2002.

[341] J. Lubliner, *Plasticity Theory*: Dover Publications, 2008.

[342] M. R. DiSilvestro, S. W. Swope, T. L. Dietz, and D. E. McNulty, "The design and development of a measurement system for the investigation of dynamic

micromotion in total knee joint replacements," *Instrumentation and Measurement, IEEE Transactions on,* vol. 54, pp. 1126-1132, 2005.

[343] D. McNulty, S. Swope, M. DiSilvestro, T. Dietz, and T. Smith, "Comparison of Static and Dynamic Micromotion Test Methods for Blasted Ti-6-4 and Polished CoCr Modular Tibial Total Knee Components," in *Society for Biomaterials*, 2004.

[344] Y. Bei and B. J. Fregly, "Multibody dynamic simulation of knee contact mechanics," *Medical Engineering & Physics,* vol. 26, pp. 777-789, 2004.

[345] B. J. Fregly, Y. Bei, and M. E. Sylvester, "Experimental evaluation of an elastic foundation model to predict contact pressures in knee replacements," *Journal of biomechanics,* vol. 36, pp. 1659-1668, 2003.

[346] J. A. Thompson, M. W. Hast, J. F. Granger, S. J. Piazza, and R. A. Siston, "Biomechanical effects of total knee arthroplasty component malrotation: a computational simulation," *Journal of Orthopaedic Research,* vol. 29, pp. 969-975, 2011.

[347] S. L. Delp, F. C. Anderson, A. S. Arnold, P. Loan, A. Habib, C. T. John, E. Guendelman, and D. G. Thelen, "OpenSim: open-source software to create and analyze dynamic simulations of movement," *Biomedical Engineering, IEEE Transactions on,* vol. 54, pp. 1940-1950, 2007.

[348] S. Pal, H. Haider, P. J. Laz, L. A. Knight, and P. J. Rullkoetter, "Probabilistic computational modeling of total knee replacement wear," *Wear*, vol. 264, pp. 701-707, 2008.

[349] T. A. Maxian, T. D. Brown, D. R. Pedersen, and J. J. Callaghan, "A sliding-distance-coupled finite element formulation for polyethylene wear in total hip arthroplasty," *Journal of biomechanics*, vol. 29, pp. 687-692, 1996.

[350] B. J. Fregly, C. Marquez-Barrientos, S. A. Banks, and J. D. DesJardins, "Increased conformity offers diminishing returns for reducing total knee replacement wear," *Journal of biomechanical engineering*, vol. 132, p. 021007, 2010.

[351] Y. Bei, B. J. Fregly, W. G. Sawyer, S. A. Banks, and N. H. Kim, "The relationship between contact pressure, insert thickness, and mild wear in total knee replacements," *Computer Modeling in Engineering and Sciences*, vol. 6, pp. 145-152, 2004.

[352] B. J. Fregly, W. G. Sawyer, M. K. Harman, and S. A. Banks, "Computational prediction of in vivo wear in total knee replacements," in *Proc 2003 Summer Bioengineering Conference, American Society of Mechanical Engineers, New York*, 2003.

[353] M. K. Harman, S. A. Banks, B. J. Fregly, W. G. Sawyer, and W. A. Hodge, "Biomechanical mechanisms for damage: Retrieval analysis and computational

wear predictions in total knee replacements," *Journal of Mechanics in Medicine and Biology,* vol. 5, pp. 469-475, 2005.

[354] K. Kawanabe, I. C. Clarke, J. Tamura, M. Akagi, V. D. Good, P. A. Williams, and K. Yamamoto, "Effects of A–P translation and rotation on the wear of UHMWPE in a total knee joint simulator," *Journal of Biomedical Materials Research,* vol. 54, pp. 400-406, 2001.

[355] A. Galvin, L. Kang, J. Tipper, M. Stone, E. Ingham, Z. Jin, and J. Fisher, "Wear of crosslinked polyethylene under different tribological conditions," *Journal of Materials Science: Materials in Medicine,* vol. 17, pp. 235-243, 2006.

[356] M. A. Hamilton, M. C. Sucec, B. J. Fregly, S. A. Banks, and W. G. Sawyer, "Quantifying Multidirectional Sliding Motions in Total Knee Replacements," *Journal of Tribology,* vol. 127, pp. 280-286, 2005.

[357] F. Liu, A. Galvin, Z. Jin, and J. Fisher, "A New Formulation for the Prediction of Polyethylene Wear in Artificial Hip Joints," *Proceedings of the Institution of Mechanical Engineers, Part H: Journal of Engineering in Medicine,* vol. 225, pp. 16-24, January 1, 2011 2011.

[358] D. Van Citters, M. Dressler, R. Levine, X. Wu, M. Mayor, and J. Currier, "A Comparison of Wear Simulator Results with Dimensional Changes of Retrieved Tibial Inserts: An Extended Duration Study," in *Orthopedic Research Society 2013 Annual Meeting,* San Antonio, Texas, 2013.

[359] E. K. Burke and G. Kendall, *Search Methodologies: Introductory Tutorials in Optimization and Decision Support Techniques*: Springer, 2006.

[360] M. B. Collier, C. A. EnghJr, J. P. McAuley, and G. A. Engh, "Factors associated with the loss of thickness of polyethylene tibial bearings after knee arthroplasty," *The Journal of Bone & Joint Surgery,* vol. 89, pp. 1306-1314, 2007.

[361] A. Wang, A. Essner, and G. Schmidig, "The effects of lubricant composition on in vitro wear testing of polymeric acetabular components," *Journal of Biomedical Materials Research Part B: Applied Biomaterials*, vol. 68, pp. 45-52, 2004.

[362] W. L. Oberkampf and T. G. Trucano, "Verification and validation in computational fluid dynamics," *Progress in Aerospace Sciences,* vol. 38, pp. 209-272, 2002.

[363] J. P. Collier, L. C. Sutula, B. H. Currier, J. H. Currier, R. E. Wooding, I. R. Williams, K. B. Farber, and M. B. Mayor, "Overview of Polyethylene as a Bearing Material Comparison of Sterilization Methods," *Clinical Orthopaedics and Related Research,* vol. 333, pp. 76-86, 1996.

[364] T. M. Wright, C. M. Rimnac, S. D. Stulberg, L. Mintz, A. K. Tsao, R. W. Klein, and C. McCrae, "Wear of polyethylene in total joint replacements: observations from retrieved PCA knee implants," *Clinical Orthopaedics and Related Research,* vol. 276, pp. 126-134, 1992.

[365] A. A. Edidin, C. W. Jewett, A. Kalinowski, K. Kwarteng, and S. M. Kurtz, "Degradation of mechanical behavior in UHMWPE after natural and accelerated aging," *Biomaterials,* vol. 21, pp. 1451-1460, 2000.

[366] P. S. M. Barbour, D. C. Barton, and J. Fisher, "The influence of stress conditions on the wear of UHMWPE for total joint replacements," *Journal of Materials Science: Materials in Medicine,* vol. 8, pp. 603-611, 1997.

[367] A. Wang, A. Essner, V. K. Polineni, C. Stark, and J. H. Dumbleton, "Lubrication and wear of ultra-high molecular weight polyethylene in total joint replacements," *Tribology International,* vol. 31, pp. 17-33, 1998.

[368] C. L. Brockett, L. M. Jennings, C. Hardaker, and J. Fisher, "Wear of moderately cross-linked polyethylene in fixed-bearing total knee replacements," *Proceedings of the Institution of Mechanical Engineers, Part H: Journal of Engineering in Medicine,* p. 0954411912445265, 2012.

[369] Y. S. Liao, H. McKellop, Z. Lu, P. Campbell, and P. Benya, "The effect of frictional heating and forced cooling on the serum lubricant and wear of UHMW polyethylene cups against cobalt-chromium and zirconia balls," *Biomaterials,* vol. 24, pp. 3047-3059, 2003.

[370] A. Ogston and J. Stanier, "The physiological function of hyaluronic acid in synovial fluid; viscous, elastic and lubricant properties," *The Journal of physiology,* vol. 119, p. 244, 1953.

[371] P. A. Costigan, K. J. Deluzio, and U. P. Wyss, "Knee and hip kinetics during normal stair climbing," *Gait & posture,* vol. 16, pp. 31-37, 2002.

[372] D. D. D'Lima, J. C. Hermida, P. C. Chen, and C. W. Colwell Jr, "Polyethylene wear and variations in knee kinematics," *Clinical Orthopaedics and Related Research,* vol. 392, pp. 124-130, 2001.

[373] D. D. D'Lima, S. Patil, N. Steklov, J. E. Slamin, and C. W. Colwell, "Tibial forces measured in vivo after total knee arthroplasty," *The Journal of Arthroplasty,* vol. 21, pp. 255-262, 2006.

[374] J. L. Astephen, K. J. Deluzio, G. E. Caldwell, and M. J. Dunbar, "Biomechanical changes at the hip, knee, and ankle joints during gait are associated with knee osteoarthritis severity," *Journal of Orthopaedic Research,* vol. 26, pp. 332-341, 2008.

[375] K. J. Deluzio, U. P. Wyss, B. Zee, P. A. Costigan, and C. Serbie, "Principal component models of knee kinematics and kinetics: normal vs. pathological gait patterns," *Human Movement Science,* vol. 16, pp. 201-217, 1997.

[376] K. J. Deluzio, U. P. Wyss, P. A. Costigan, C. Sorbie, and B. Zee, "Gait assessment in unicompartmental knee arthroplasty patients: Principal component modelling of gait waveforms and clinical status," *Human Movement Science,* vol. 18, pp. 701-711, 1999.